



International Committee for Future Accelerators

Sponsored by the Particles and Fields Commission of IUPAP

Beam Dynamics Newsletter

No. 70

**Issue Editor:
M. A. Palmer**

**Editor in Chief:
Y. H. Chin**

May 2017

Contents

1	FOREWORD.....	7
1.1	FROM THE CHAIR.....	7
1.2	FROM THE EDITOR.....	8
2	THE 2017 WILSON PRIZE	9
2.1	APS ROBERT R. WILSON PRIZE PRESENTATION	9
	2.1.1 Introduction	9
	2.1.2 Appendix 1	29
	2.1.3 Appendix 2	30
	2.1.4 Appendix 3	30
	2.1.5 References	31
2.2	INTRABEAM SCATTERING AND TOUSCHEK EFFECT	32
3	STATUS AND PLANS FOR MAJOR U.S. LIGHT SOURCE FACILITIES	37
3.1	STATUS OF THE ADVANCED LIGHT SOURCE.....	37
	3.1.1 Introduction	37
	3.1.1.1 1993-2006.....	38
	3.1.1.2 2006-2016.....	38
	3.1.1.3 2016 and beyond	39
	3.1.2 ALS Brightness Upgrade.....	40
	3.1.2.1 Lattice Design.....	40
	3.1.2.2 Magnet Design and Production	41
	3.1.2.3 Installation.....	41
	3.1.2.4 Commissioning.....	41
	3.1.3 ALS-U 42	
	3.1.3.1 Motivation	42
	3.1.3.2 ALS-U R&D progress.....	45
	3.1.3.2.1 Magnets and Radiation Production	46
	3.1.3.2.2 Coherence Preserving X-ray Optics	47
	3.1.3.2.3 On-axis Swap-out Injection.....	47
	3.1.3.2.4 Vacuum System - NEG Coating	48
	3.1.3.2.5 Intrabeam Scattering and Harmonic Cavities.....	48
	3.1.4 Summary.....	49
	3.1.5 Acknowledgments	49
	3.1.6 References	49
3.2	ADVANCED PHOTON SOURCE STATUS REPORT.....	52
	3.2.1 Introduction	52

3.2.2	APS Accelerators.....	52
3.2.2.1	<i>Main parameters and modes of operation</i>	52
3.2.2.2	<i>Reliability and availability</i>	54
3.2.2.3	<i>Insertion Devices and brightness plots</i>	55
3.2.3	Storage Ring Modeling.....	56
3.2.3.1	<i>Lattice</i>	56
3.2.3.2	<i>Collective effects</i>	57
3.2.3.3	<i>Lifetime benchmarking</i>	59
3.2.4	Beam Stability Improvements.....	60
3.2.4.1	<i>Orbit stabilization developments</i>	60
3.2.4.2	<i>Automated user steering</i>	63
3.2.5	Accelerator Improvements and Recent and Future Developments.....	63
3.2.5.1	<i>Superconducting undulators</i>	63
3.2.5.2	<i>Abort system</i>	64
3.2.5.3	<i>Helical undulator</i>	65
3.2.6	Conclusion.....	66
3.2.7	Acknowledgements.....	66
3.2.8	References.....	66
3.3	LCLS FEL OPERATIONS.....	69
3.3.1	Abstract 69.....	
3.3.2	Introduction.....	69
3.3.2.1	<i>Hard and Soft X-ray Self Seeding</i>	69
3.3.2.2	<i>Polarized X-ray Beams</i>	70
3.3.2.3	<i>X-Band Transverse Deflecting Cavity</i>	72
3.3.2.4	<i>Extending the energy envelope</i>	73
3.3.2.5	<i>Dual Color and Dual Bunches at LCLS</i>	74
3.3.2.6	<i>Dechirper for energy spread and bandwidth control</i>	76
3.3.3	Operation of the LCLS.....	77
3.3.3.1	<i>Schedules</i>	77
3.3.4	LCLS Availability.....	78
3.3.5	Facility Upgrades and Research & Development at LCLS.....	79
3.3.6	Conclusions.....	81
3.3.7	Acknowledgments.....	81
3.3.8	References.....	81
3.4	LCLS-II: A CW X-RAY FEL UPGRADE TO THE SLAC LCLS FACILITY.....	82
3.4.1	<i>Abstract</i> 82.....	
3.4.2	Introduction.....	82
3.4.3	Configuration and Challenges.....	85
3.4.3.1	<i>SCRF Linac</i>	85
3.4.3.2	<i>High brightness CW injector</i>	88
3.4.3.3	<i>Variable gap undulators</i>	89
3.4.3.4	<i>High Beam Power</i>	92
3.4.3.1	<i>Beam Dynamics</i>	93

3.4.4	Performance Simulations.....	94
3.4.4.1	<i>Simulation Strategy and Computational Setup</i>	94
3.4.4.2	<i>Electron Beam Properties</i>	95
3.4.4.3	<i>20 pC</i>	95
3.4.4.4	<i>100 pC</i>	96
3.4.4.5	<i>300 pC</i>	96
3.4.4.1	<i>SASE Tapering Optimization and Performance Study</i>	97
3.4.4.2	<i>Self-Seeded Simulation Strategy and Performance Study</i>	99
3.4.5	Conclusion.....	101
3.4.6	Acknowledgments	101
3.4.7	References	101
3.5	COMMISSIONING AND START-UP OF NSLS-II	103
3.5.1	Abstract	103
3.5.2	Introduction	103
3.5.3	General Layout	104
3.5.4	Accelerator Lattice	106
3.5.5	Accelerator Subsystems.....	108
3.5.6	Injector System	111
3.5.7	NSLS-II Commissioning.....	112
3.5.7.1	<i>Commissioning Sequence</i>	112
3.5.7.2	<i>Lattice Commissioning</i>	112
3.5.7.3	<i>Orbit Stabilization</i>	116
3.5.7.4	<i>Dynamic Aperture Commissioning</i>	117
3.5.7.5	<i>High Intensity Commissioning</i>	121
3.5.8	Insertion Devices and Integration in Accelerator Operations	122
3.5.9	Present Performance	124
3.5.10	Conclusion.....	126
3.5.11	Acknowledgments	126
3.5.12	References	126
4	WORKSHOP AND CONFERENCE REPORTS	129
4.1	EUCARD2 WORKSHOP ON “STATUS OF ACCELERATOR DRIVEN SYSTEMS RESEARCH AND TECHNOLOGY DEVELOPMENT”	129
4.2	THE COMPACT LINEAR COLLIDER (CLIC) WORKSHOP 2017	132
4.2.1	References:	133
4.3	THE ICFA MINIWORKSHOP BEAM DYNAMICS MEETS VACUUM, COLLIMATION, AND SURFACES	135
5	RECENT DOCTORIAL THESES	138
5.1	STUDY ON THE KEY PHYSICS PROBLEMS OF SPPC/CEPC ACCELERATOR DESIGN.....	138

6	FORTHCOMING BEAM DYNAMICS EVENTS	140
6.1	INTERNATIONAL WORKSHOP ON NONLINEAR DYNAMICS AND COLLECTIVE EFFECTS IN PARTICLE BEAM PHYSICS (NOCE 2017).....	140
6.2	THE 13 TH INTERNATIONAL TOPICAL MEETING ON THE APPLICATIONS OF ACCELERATORS	141
6.3	INTERNATIONAL WORKSHOP ON BEAM-BEAM EFFECTS IN CIRCULAR COLLIDERS.....	142
6.4	VHEE17 MINI ICFA BEAM DYNAMICS WORKSHOP	143
6.5	A SUMMARY OF UPCOMING WORKSHOPS AND CONFERENCES.....	145
7	ANNOUNCEMENTS OF THE BEAM DYNAMICS PANEL	146
7.1	ICFA BEAM DYNAMICS NEWSLETTER.....	146
	7.1.1 Aim of the Newsletter.....	146
	7.1.2 Categories of Articles	146
	7.1.3 How to Prepare a Manuscript	146
	7.1.4 Distribution	147
	7.1.5 Regular Correspondents.....	147
7.2	ICFA BEAM DYNAMICS PANEL MEMBERS	149

1 Foreword

1.1 From the Chair

Yong Ho Chin, KEK
Mail to: yongho.chin@kek.jp

Since I was appointed by ICFA as the new chair of the ICFA Beam Dynamics Panel (BDP) last November, I have tried to reorganize and reboot some of the panel activities that have been inactive for some time. For this end, we have invited Zhentang Zhao of SINAP and Peter Ostroumov of MSU to the new panel members. Both of them are world renowned scientists and I am sure that they will bring new energy and enthusiasm to the panel activities. We have proposed two Advanced Beam Dynamics workshops, HB (Hadron Beams) 2018 workshop (June 17-22, 2018 in Daejeon, Korea), and FLS (Future Light Sources) 2018 workshop (March 4-9, 2018, in SINAP, Shanghai, China) to ICFA during the ICFA meeting that was held in February in Valencia, Spain, and both were approved. Zhentang Zhao was appointed to the new chair of the Future Light Sources sub-panel of the ICFA BDP and he will chair the FLS2018 workshop as well. I will preside over the FLS workshop IOC (International Organizing Committee) as an acting chair (from the next FLS workshop, Zhentang Zhao will preside over the FLS IOC as the chair). The new membership of Zhentang Zhao and Peter Ostroumov was officially approved by ICFA at the same meeting. You can find information on forthcoming events (workshops, conferences, etc.) on the the ICFA BDP website:

<http://icfa-bd.kek.jp>

We have also approved six new ICFA mini-workshops since the last Newsletter:

1. ICFA Mini-Workshop on Very High Energy Electron (VHEE) Radiotherapy: Medical and Accelerator Physics Aspects Towards Machine Realisation, July 24-26, 2017, at Cockcroft Institute, Daresbury, UK.
2. ICFA Mini-Workshop on Non-linear Dynamics and Collective Effects, September 19-22, 2017 in Arcidosso, Italy.
3. ICFA Mini-Workshop on Beam-Beam Effects in Circular Colliders, September 27-29, 2017 in Berkeley, CA, USA.
4. ICFA Mini-Workshop, "Space Charge 2017", October 4-6, 2017, at TU Darmstadt, Germany.
5. ICFA Mini-Workshop on Slow Extraction, November 9-10, 2017, at CERN
6. ICFA Mini-Workshop on Slow Extraction, November 2018, at FNAL, USA.

Their information and workshop URLs can be found on the ICFA BDP webpage.

During the ICFA meeting in Valencia, there was intense discussion on the future of ILC. It is still far from clear, but one clear understanding may be that the next year, 2018, will be a critical and decision-making year for fate of ILC. I will keep informing you,

The editor of this issue is Dr. Mark Palmer, a panel member and a senior scientist at BNL, New York. The theme is "Status and Plans for Major U.S. Light Source Facilities." He collected 5 well-written review articles, and they provide very good and comprehensive reviews of the light source facilities in US. The 2017 Robert R. Wilson Prize presentations are also included. I want to thank Mark for editing a valuable newsletter of high quality for the accelerator community.

1.2 From the Editor

Mark Palmer, Brookhaven National Laboratory
Mail to: mpalmer@bnl.gov

When I was considering topics for this Newsletter, I kept returning to the rapid advances in light source technology that have taken place over the past decade. While undertaking a complete survey of the field would be quite daunting, I felt that some selected updates, looking at where a few of these machines are and where they are headed, would provide a useful snapshot of key recent developments for our readers. Thus, the primary topic for this issue focuses on the status of some of the major light sources in the U.S. as well as their plans for upgrades in the near future. This issue includes some very nice articles from David Robin and Christoph Steier on the Advanced Light Source and its proposed upgrade path, from Vadim Sajaev and other members of the Advanced Photon Source team, from Axel Brachmann on LCLS status and performance, from Gabriel Marcus and Tor Raubenheimer on the LCLS-II upgrade, and from Ferdinand Willeke on the status and plans of the NSLS-II.

This issue also includes two articles on the topic of Intrabeam Scattering (IBS). It was my privilege to chair the American Physical Society Committee for the 2017 Robert R. Wilson Prize for Achievement in the Physics of Particle Accelerators. After reviewing a number of outstanding nominations, the selection committee reached the unanimous conclusion that the work carried out by James Bjorken, Sekazi Mtingwa and Anton Piwinski in this area deserved recognition with the award named for one of the most prolific American accelerator builders. Their work has contributed fundamentally to the performance achieved with most proton, anti-proton and ion machines as well as very low emittance electron machines. Details on the award can be found at: <https://www.aps.org/programs/honors/prizes/wilson.cfm>. Sekazi Mtingwa accepted the prize for the group at this year's April Meeting of the American Physical Society (held January 28-31, 2017 in Washington DC, USA; <http://www.aps.org/meetings/april/>). His materials for that meeting are reproduced here along with a separate contribution on the topic from Anton Piwinski. I would like to point out that this topic ties in wonderfully with the previously mentioned updates on high brightness electron storage rings. Our understanding of this key piece of beam dynamics has played a critical role in the development of 4th generation storage ring designs with their very low emittance and high brightness beams.

There are three conference reports in this issue. These are from the EuCARD2 Workshop on the "Status of Accelerator Driven System Research and Technology Development;" from the 2017 CLIC Workshop; and from the ICFA mini-workshop "Beam Dynamics Meets Vacuum, Collimation, and Surfaces." Many thanks to the workshop organizers who provided these reports.

This issue also has announcements for:

- NOCE 2017: The International Workshop on Nonlinear Dynamics and Collective Effects in Particle Beam Physics;
- AccApp`17: The 13th International Topical Meeting on the Applications of Accelerators; and
- BeamBeam2017: The International Workshop on Beam-Beam Effects in Circular Colliders
- VHEE17 Mini ICFA Beam Dynamics Workshop

Each of these meetings promise to be of significant interest to our community.

In closing, I am sure our readership will find the articles included in this issue informative and enlightening. I would like to thank the authors again for their thoughtful contributions. I expect that we will see further updates on this general topic in future Newsletters. Enjoy!

2 The 2017 Wilson Prize

Each year, the American Physical Society awards the Wilson Prize for Achievement in the Physics of Particle Accelerators. This year the prize was awarded to James Bjorken (SLAC), Sekazi Mtingwa (MIT), and Anton Piwinski (DESY) with the citation:

“For the detailed, theoretical description of intrabeam scattering, which has empowered major discoveries in a broad range of disciplines by a wide variety of accelerators, including hadron colliders, damping rings/linear colliders, and low emittance synchrotron light sources.”

Dr. Mtingwa presented the acceptance lecture for the group at this year’s “April Meeting” of the American Physical Society. The contents of that lecture are reproduced here. We also include a short essay from Anton Piwinski on this topic.

2.1 APS Robert R. Wilson Prize Presentation

Reflections on Our Experiences with the Touschek Effect and Intrabeam Scattering

Anton Piwinski (DESY)
James D. Bjorken (Stanford)
Sekazi K. Mtingwa (MIT)

Mail to: sekazi.mtingwa@gmail.com
Presented by Sekazi K. Mtingwa

2.1.1 Introduction

It is a great pleasure and privilege for me to be here representing Anton Piwinski; James Bjorken, known as Bj to his friends and colleagues; and myself in receiving the prestigious APS Robert R. Wilson Prize. Both Anton and Bj send their regrets that they are not able to enjoy this moment in person with us due to health concerns. I am sure that I speak for all of us in wishing each of them a full and quick recovery.

First, I would like to take the opportunity to talk about Anton’s reflections on the beginning of the investigations of intrabeam scattering. He first heard about this phenomenon in 1973 while attending a workshop in Italy. He recalls learning that intrabeam scattering could be a serious problem in proton accelerators. Since DESY in Hamburg was discussing at that time a new proton storage ring, he decided to investigate this problem.

In the literature, he found several reports on the Touschek effect, but little about intrabeam scattering. The Touschek effect and intrabeam scattering are two different aspects of the same phenomenon, namely Coulomb scattering within a charged particle beam. For the Touschek effect, only large scattering angles are taken into account. On the other hand, for intrabeam scattering, small scattering angles are considered and it is assumed that all changes of coordinates due to the scattering are small compared to the beam dimensions. For the Touschek effect, sufficient theoretical investigations existed that allowed for a reasonable calculation of the beam lifetime due to the effect. However for intrabeam scattering, there were only a few attempts to estimate the

transfer of oscillation energy from one direction to another, mainly from transverse to longitudinal, i.e. from betatron oscillations to synchrotron oscillations, but not vice versa, which is necessary for a realistic description. Indeed, intrabeam scattering is a mutual exchange of oscillation energies among all three directions and only by taking into account all energy transfers can one obtain a complete description.

Table 1 shows the main characteristics and differences between intrabeam scattering and the Touschek effect. Fig. 1 shows the first measurement of the Touschek effect in 1963. The inverse of the lifetime is plotted as a function of the number of electrons stored in the beam. As seen, the lifetime varies from 6 to 50 hours. The measurements were done in the small storage ring Anello Di Accumulazione (AdA), which is the Italian word for storage ring, at an energy of 188 MeV. In the figure, there is a small displacement above zero, which is caused by the scattering of the electrons off the residual gas. In order to explain this measurement, Bruno Touschek found the relativistic mechanism for the longitudinal momentum change. To simplify the calculation, he made some approximations, e.g. he assumed non-relativistic particle velocities in the center-of-mass system of the beam and he assumed a flat beam, i.e. no vertical betatron oscillations of the electrons.

Table 1: Coulomb Scattering of Particles within a Beam

Touschek effect	Intrabeam scattering
1) single scattering	multiple scattering
2) only energy transfer from transverse to longitudinal oscillations is considered	exchange of oscillation energies between all 3 directions is considered
3) a small transverse momentum is transformed into a large change of longitudinal momentum (multiplied by the Lorentzfactor γ)	all changes are assumed to be small as compared to the beam dimension
4) no change of particle distribution but loss of both colliding particles	diffusion in all 3 directions leads to a change of particle distribution, increase and decrease of dimension are possible

Appendix 1 shows the successive improvements of the theory of the Touschek effect. After the first measurements and explanation by Touschek and others in 1963, the lifetime was determined for ultra-relativistic energies, i.e. for relativistic energies in the center-of-system, by B. Gittelmann and D. Ritson at SLAC. In 1965, U. Voelkel of DESY finally generalized the theory for arbitrary energies. Then, in 1998, Piwinski finally extended the theory to arbitrary beam sizes, removing the restriction to flat beams, thereby taking into account vertical betatron oscillations. Moreover, he

included nonzero derivatives of the accelerator lattice functions that describe the effect of the magnets that guide and focus the beam.

Turning next to intrabeam scattering, Fig. 2 shows a typical example of a measurement of this effect that was performed in 1984 at CERN's Super Proton Synchrotron (SPS) at an energy of 300 GeV. It depicts the longitudinal distribution of a proton bunch on the left side and an antiproton bunch on the right side at different times. The time difference between successive curves is a quarter of an hour. The main difference between the two sets of curves is the particle density, or number of particles in a bunch, with the density of the proton bunch being an order of magnitude larger than that of the antiproton bunch. Consequently, the growth of the proton bunch length is clearly stronger than that of the antiproton bunch. Similar measurements also were made for the bunch width and for the bunch height. All such measurements in various storage rings show such a slow change of the beam dimensions.

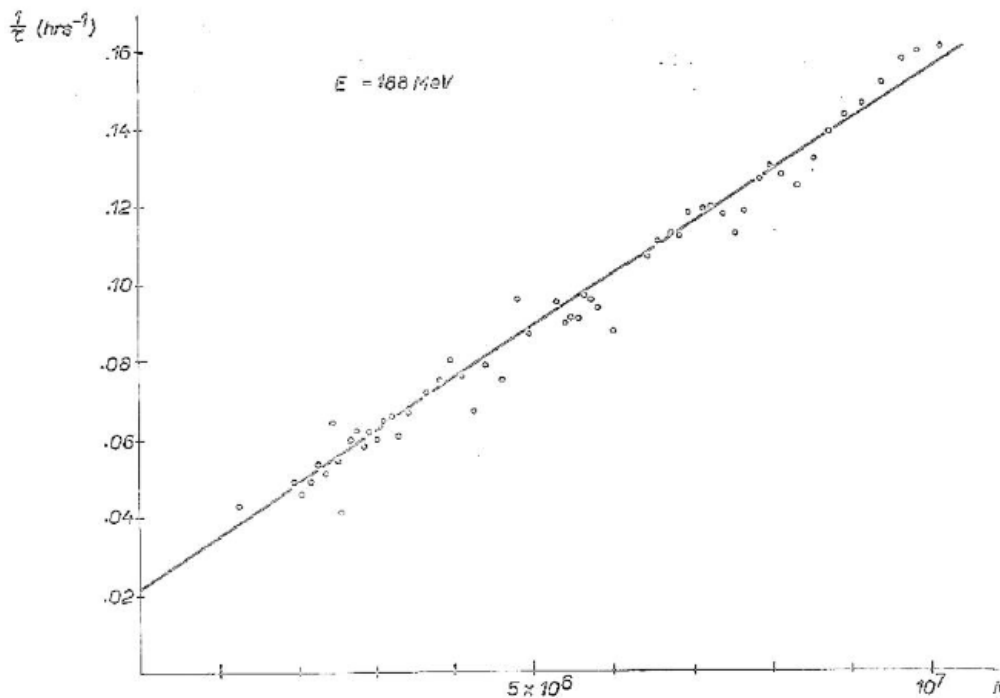


Figure 1: Touschek Effect: 1st Measurement in 1963. Inverse Lifetime $1/\tau$ as a Function of the Number of Stored Particles in the Beam

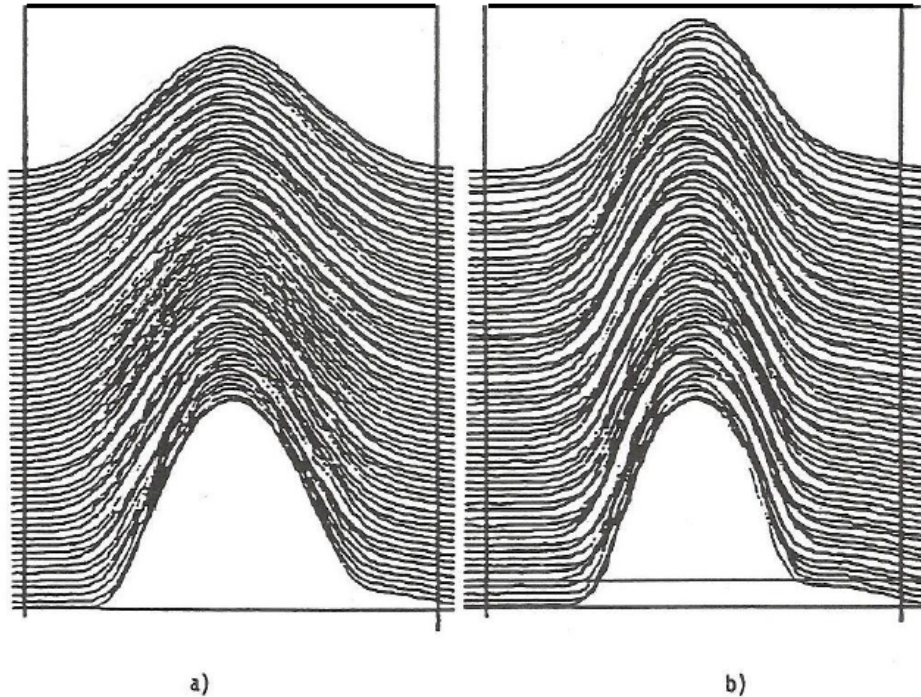


Figure 2: Measurements Made at 15 min Intervals in the CERN SPS of the Longitudinal Distribution of: a) A Proton Bunch ($N^+ = 1.5 \times 10^{11}$); b) An Antiproton Bunch ($N^- = 1.2 \times 10^{10}$).

Appendix 2 shows a brief review of early investigations on intrabeam scattering. Bruck and Le Duff in 1964 and Pellegrini in 1966 performed the first investigations, where they calculated the transfer of oscillation energy from one direction to another. In 1974, Piwinski published his classic paper in which he included, for the first time, energy exchanges among all three directions, including energy losses due to transfers from one direction to the other. Thus at last, Piwinski's work allowed one to calculate the development of the beam dimensions over a long time.

In 1977, Simon van der Meer was working on his new idea about the stochastic cooling of beams, for which he would later receive the Nobel Prize. He asked for the most precise calculation of the rise times due to intrabeam scattering, because stochastic cooling would have to compete with intrabeam scattering. Then Sacherer and Piwinski independently derived formulae, including the derivatives of the lattice functions. Huebner, Möhl and Sacherer incorporated this work into a computer program, which researchers used at a number of accelerator facilities. Then in 1983, Bj and I used quantum field theory to develop a completely new description of intrabeam scattering that included the full set of lattice parameters and their derivatives [1].

Most of you present today, as well as many others, are completely unaware that Bj ever had anything to do with the theory of particle accelerators. But for a long time, he has been extremely proud to have earned a membership card in the union of accelerator theorists. However, he related me that he never dreamed that it would come to this.

Bj's interest in the subject began in the 1970's at SLAC, thanks in large part to his close association and friendship with Burton Richter. Burt put into his hands the classic Matt Sands tutorial on electron storage rings [2]. When he moved to Fermilab in 1979, he vowed to learn about proton machines as well. By 1981, he recalls that he had progressed enough that he became something of a groupie within the community of Fermilab accelerator theorists. Then, in the summer of 1981, Alvin Tollestrup introduced him to the intrabeam scattering problem, which he had been working

on himself. As mentioned earlier, there had been a lot of prior work, the most important being by Anton [3]. But the most general case of a strong-focusing machine lattice was not yet fully understood. And at Fermilab, this case needed to be understood in the context of the design of the Antiproton Accumulator, in which stochastic beam cooling was being implemented, and of the Tevatron.

Bj informed me that his recollection of the details, not to mention his comprehension of the subject matter, has greatly deteriorated in the more than three decades since that time. But since he is a packrat, he found a fat file full of notes from that period. From them, it appears that he rather quickly got up to speed on the problem. He related to me that, in retrospect, the reason for this lay in his experiences in the world of particle-physics theory. A bunch of 10 billion protons traveling down a beampipe at nearly the speed of light is not totally dissimilar from an ion containing a hundred nucleons doing the same thing, or even a single relativistic nucleon containing all those quarks and gluons, also doing the same thing. So, now in hindsight, it appears to Bj that from the start, he was in something of a comfort zone, and could apply the manifestly-relativistically-invariant formalisms developed for particle theory, especially by Feynman, to this problem.

Evidence for this exists in his own handwritten notes, dated August 1981, which are in particle physics language, and which exhibit for sure a fresh approach to the problem. Evidently, the first problem facing him was whether he could reproduce what Piwinski had already done. On page 8 of his first note appears the sentence “Translate into ordinary lingo.” By page 9, he had moved into the accelerator physics language: there is a line “We follow Piwinski in defining the following variable...” And by page 11, the conclusion was “This agrees with Piwinski’s formula, although it may still be accidental.” Two days after this first note, Bj created a second one, which rephrased and streamlined the computations present in the first one. The key mathematical tactic was a famous identity used by Feynman and Schwinger to evaluate integrals associated with Feynman diagrams. It is not clear to Bj whether there was a genuine “aha” moment in that two day interim. And this is about the time in late August 1981 that I, who had just completed a postdoctoral position in the Fermilab theoretical physics group, and was transitioning to a new position, went to Bj looking for a problem. Bj recalls that intrabeam scattering was all that he could offer. But despite having to start from scratch in learning the trade, I signed on. So it is possible that the reason Bj wrote those two notes was to provide me with something better than the chaotic scribbling, barely intelligible to Bj himself, that he used when working alone.

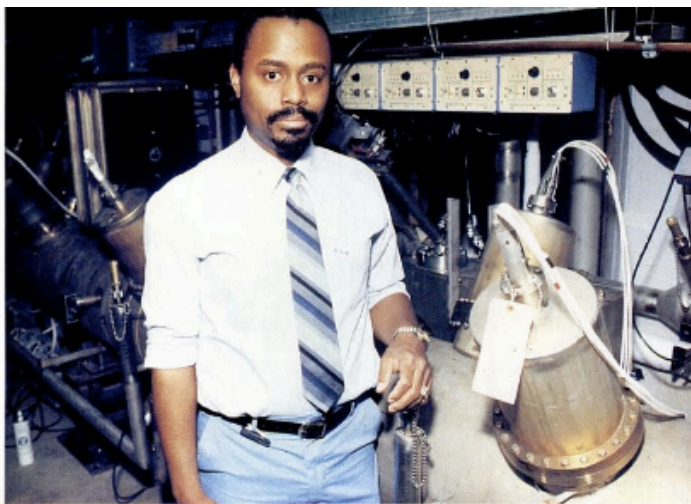
Between the fall of 1981 and the spring of 1982, I was rapidly riding up the learning curve, and more and more of the problem landed in my hands. I also would like to credit the excellent Matt Sands tutorial on electron storage rings for providing me with my first introduction to the basic theory of particle accelerators. There was all through this period a close working relationship with Alessandro Ruggiero, the resident Fermilab accelerator theorist most deeply involved in the intrabeam scattering problem. He produced several internal notes during this period, and is acknowledged in our paper as well. And in Bj’s file is a short message from Piwinski, indicating that he was during this period also up to speed. We found ourselves in agreement on the results, although there was a pesky overall factor of two that had to be negotiated amongst us. In a nutshell, the physics idea expressed in our paper is that, viewed in the rest frame of the bunch, intrabeam scattering tends to make the bunch grow in size, and to evolve toward isotropy in momentum space. On the other hand, accelerator designers impose strong, time-dependent electromagnetic fields that squeeze and stretch the bunch in ways designed to inhibit such behavior. The formulae that we derived exhibit this physics somewhat more transparently than what had been

done before. Finally, by the summer of 1982, Bj and I had created a draft of our paper, which we subsequently published in the journal, *Particle Accelerators* [4].

It was about this time that I actually made a foray into experimental work. Fred Mills, who was in charge of magnet design and construction at the Antiproton Source, asked me to help him to develop an analytic approach for designing the endpacks to be installed on either end of each magnet so that the integrated field through each magnet would meet the design specifications.

We succeeded in this important task. Each prototype magnet that was fabricated would have its integrated field measured and we would calculate how to design the endpack. Fortunately, we were spot on for each magnet, greatly reducing the time required to produce the Antiproton Source dipoles and quadrupoles. It turns out that our colleagues at Michigan State University were constructing a much smaller accelerator during the early 1980s and Fred shared our approach with them to speed their process along.

With two accelerator victories under my belt, I formally joined the Antiproton Source Stochastic Beam Cooling Group in 1983. Since Bj and I had just published our paper on intrabeam scattering, stochastic cooling was a natural fit for me to further my interest in accelerator physics. There I worked closely with John Marriner in finalizing the vacuum and beam sensitivity designs of the pickup and kicker electrodes. Glen Lambertson and his colleagues performed much of the early work at Lawrence Berkeley National Laboratory (LBNL), where they designed and constructed the prototype devices. I was detailed to Fermilab's technical staff that fabricated the pickups and kickers, where I performed quality assurance tests to ensure their microwave performance, collaborated with James Simpson and colleagues at Argonne National Laboratory's 20 MeV electron linac in performing beam tests on LBNL prototype electrodes, and oversaw the installation of the pickups and kickers into the Debuncher and Accumulator Accelerators in the Antiproton Source tunnel. As shown in Fig. 3, I even had the good fortune to be featured in the August 1985 issue of **Ebony Magazine**. The caption states that I was standing next to a superconducting magnet. In fact, it was one of our stochastic cooling tanks, but I think the public has forgiven the editors.



Dr. Sekazi Mtingwa, shown near a superconducting magnet, is a physicist at Fermi National Accelerator in Batavia, Ill. He's currently working on what may be the most powerful accelerator in the U.S.

DR. SEKAZI MTINGWA's key to the future could lay in unlocking the very origin of the universe. "High-energy physics is really the area of physics that deals with the simplest particles in nature," says Dr. Mtingwa, 35, a physicist at the Fermi National Accelerator Laboratory in Batavia, Ill. "The substances around us are composed of molecules; molecules are composed of atoms, and atoms are sort of the basic building blocks of nature. But even

atoms have a nucleus (made up of protons and neutrons) and electrons that travel around them," Dr. Mtingwa says. His mission is to smash those atoms by stripping them of electrons, then circulating the protons at high speeds around a special "accelerator," striking them against targets and then studying the new combinations that result. It is the curiosity about what lies beyond even the smallest particle combination uncovered to date that is

spurring a debate in the physics world about the need to build a Superconducting Supercollider (SSC), an atom-smasher with power currently unattainable. Physicists argue the SSC could uncover the link for understanding the origin of the universe through the new particles it would reveal. The price tag of \$6 billion is slowing government approval for building the giant accelerator. Dr. Mtingwa is working on Fermilab's Tevatron I (scheduled to be operational in August), which now is considered the most powerful accelerator in the U.S. The Tevatron I has 1,000 superconducting magnets in a 20-foot-deep tunnel and is considered a forerunner of the SSC. The Tevatron I will collide protons and artificially created antiprotons at energy levels equivalent to one trillion electron volts. What does all this mean? Dr. Mtingwa and other physicists are not sure yet. "This is really the frontier of physics," says the Princeton Ph.D. and former Ford Fellow. "The more you probe into this particular subatomic world, the more building blocks you find." One thing he is sure of, however, is that fans of the futuristic television show *Star Trek* won't be seeing anyone reduced to particles and "beamed" through space anytime soon.

Figure 3: Sekazi Mtingwa Featured in Ebony Magazine (Correction to Caption: Mtingwa is standing next to a stochastic cooling tank.).

As depicted in Fig. 4, the Antiproton Source consisted of a target station, beam transport lines, and two small accelerators called the Debuncher and Accumulator, which were both contained in the same tunnel. Protons were extracted from the Main Ring at 120 GeV and impinged upon a tungsten-rhenium target, whereby a Li lens would focus secondary particles off the target, and a pulsed dipole magnet would steer 8.9 GeV antiprotons toward the Debuncher. This accelerator converted the antiproton bunches into a continuous beam and began the process of cooling it, namely reducing its momentum spread and transverse phase space. The final cooling and accumulation of the antiprotons into a high-density core in momentum space occurred in the Accumulator. In our work, Bj and I wanted to ensure that intrabeam scattering in the Accumulator would not prevent the goal of stacking 4×10^{11} antiprotons in the core every 4 hours. Our theoretical analyses and numerical simulations showed that intrabeam scattering would not be a problem, so we were all relieved.

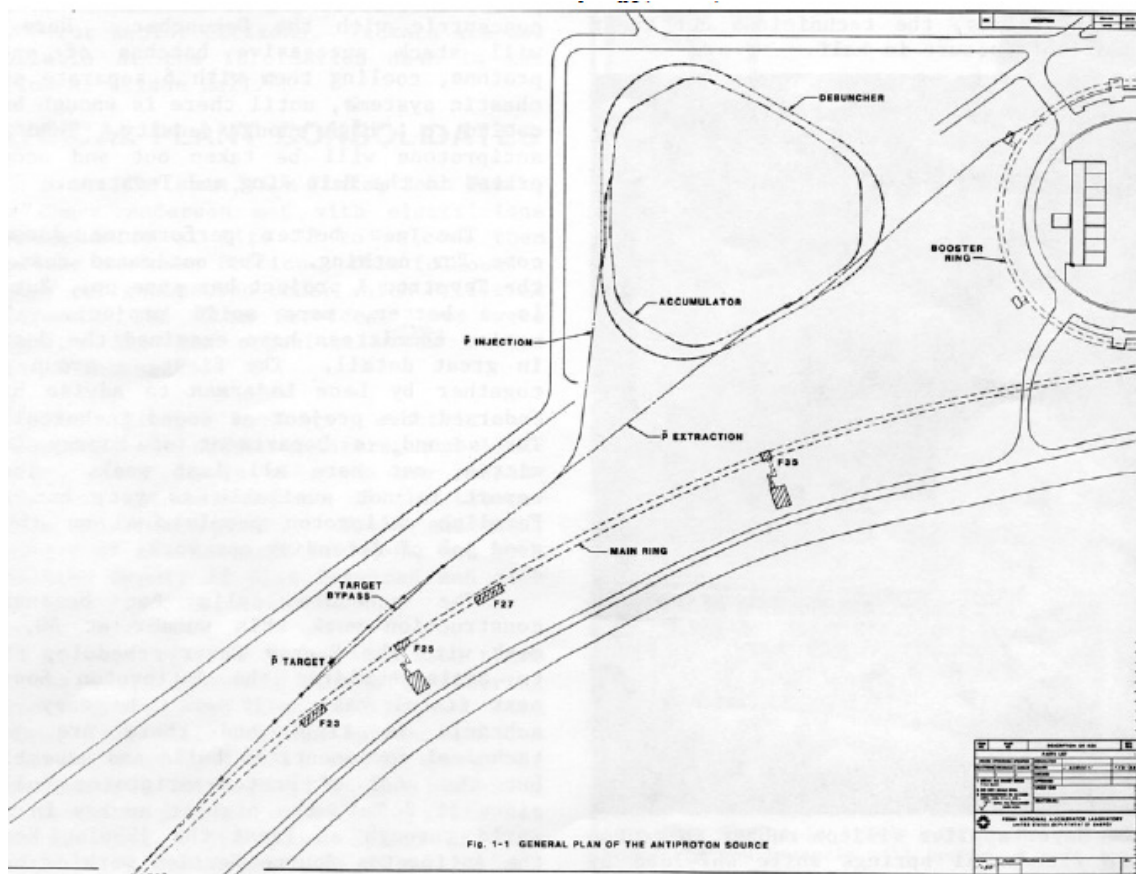


Figure 4: Antiproton Source (figure courtesy of Fermilab).

Since I have gotten my hands both full of chalk dust as a theorist and grime as an experimentalist, I would like to pause for a moment to reflect on a method for determining for which career one is better suited. First of all, I think that we can all agree that a particle accelerator is one of the most complex scientific devices to design, construct and operate. There are many systems that must work in tandem and to high precision. At the Tevatron complex, I was involved in the construction of the two systems already mentioned: magnet and stochastic cooling. Relative to the latter, there were 23 large tanks like the one shown in Fig. 3, 12 in the Debuncher and 11 in the Accumulator, each containing numerous delicate, even brittle, pickup and kicker electrodes. John Marriner and I were responsible for ensuring that those intricate devices worked once commissioning commenced. While we were constructing and installing them, I cannot tell you how many powers-of-ten times I prayed that they would indeed work. On the other hand, John was so sure that all was well, even when some major glitches had to be resolved. So, all the time, I was busy praying and he was busy smiling. From that experience, I surmised that if you spend more time praying than smiling, then you are really a theorist and should probably stick to your pen and pad. As for the entire Antiproton Source, when all systems were turned on during the commissioning and things started working, I'm sure John felt that it was indeed a job well done, while I felt that it was truly one of the greatest miracles in human history. Indeed the Antiproton Source worked well over the following decade, being a crucial element in the 1995 discovery of the top quark. Somehow I feel that I and all my accelerator colleagues at the Antiproton Source and Tevatron should be counted as co-discoverers of the top quark, given the extreme sweat and tears that it took to put those accelerator systems into place for the detectors. I think that our high energy community should take a serious look at devising a system to reward those on the accelerator end with co-authorship of papers involving major discoveries.

Since those early years of the Antiproton Source, many improvements and upgrades were made, including to the stochastic cooling systems. Around the year 2000, a decade after Bj and I had left, intrabeam scattering finally caught up with Fermilab. The magazine, *Science*, featured a story on the lab's problems [5]. I quote:

“A year and a half ago, the Tevatron, which smashes protons and antiprotons together at enormous energies, began operating again after a \$260 million refit. Despite months of tinkering, however, scientists and engineers couldn't boost the beam's luminosity – its “brightness” – high enough to begin the bulk of the accelerator's research program.....

A major problem with the accelerator lies in the system that accumulates, accelerates, and stores antiprotons – which, unlike protons, are hard to produce. Fully 80% of the antiprotons were supposed to survive the trip from the accumulator system to the collider, but in January, a mere 30% made the journey intact. “Really, until April we had no idea what the physical cause of this problem was,” says [Stephen] Holmes [Head of Fermilab's Beams Division]. So, despite Fermilab's best efforts, “we topped out at about 40%. We were pretty much stuck.”

In April, however, scientists at Fermilab figured out that the antiproton problem was caused by intrabeam scattering. “When the antiprotons are going around and around in the antiproton accumulator, they are confined to a very small space, and they are bouncing off each other,” says Holmes. “This tends to heat the beam, making it get bigger. It wants to blow up.” Scientists had anticipated problems, but this effect was worse than expected.

“Now a 2-week shutdown in June might have solved the antiproton problem,” Holmes says. While the accelerator was turned off, engineers improved the beam cooling system and refocused the magnetic optics that keeps the beam tight. Now about 50% to 60% of the antiprotons survive the trip to the accelerator, and the number is rising. With that roadblock removed, last week the Tevatron's luminosity surged to a record-setting 2.64×10^{31} inverse square centimeters per second.....”

Not long after Bj and I completed our work, Alvin Tollestrup informed me that he was looking for ways to simplify Piwinski's scattering function so that he could use it for studying upgrades to the Tevatron lattice. Aside from phase space factors, Piwinski's scattering function gives the rise times for the three beam dimensions and involves taking an integral of trigonometric functions times the exponential of trigonometric functions. Alvin is one of those rare physicists who can design both detectors and accelerator lattices. As he tinkered with lattice designs for the first Tevatron upgrade, he wanted to know the effects of intrabeam scattering on luminosity lifetime for changes to the lattice, without waiting long periods of time running computer programs. He asked if I would be interested in collaborating with him to obtain simple analytic expressions for the Piwinski scattering function, since that would greatly reduce the computer time required. Given the 1 TeV energy of the protons and antiprotons at the Tevatron, we had the advantage of using the Month-Weng discussion [6] of the Piwinski formalism and applying it to asymptotically large energies. Indeed, we did achieve success in completely integrating the Piwinski scattering function to arrive at a simplified new high energy scattering function useful for predicting the evolution of luminosity with time for the Tevatron and future generations of hadron colliders [7]. One of our Fermilab colleagues, David Finley, used our results and my paper with Bj to study the effects of intrabeam scattering on the proposed Tevatron upgrade's integrated luminosity and demonstrated that, while

intrabeam scattering effects were visible, they did not negate gains made by adjusting other accelerator parameters [8].

Approximately 15 years passed before I engaged with intrabeam scattering again. I became interested in the next generation electron-positron collider and joined the team that led to the International Linear Collider (ILC) collaboration. My LBNL colleagues, William Barletta, Miguel Furman and Andy Wolski invited me to spend some time with Andy working on intrabeam scattering for the ILC damping rings. KEK had already begun studies in their prototype damping ring called the Accelerator Test Facility (ATF). Karl Bane at SLAC had spent some time there and had proposed an elegant ansatz for connecting the Piwinski formalism to Bj's and my formulae at high energies, which is quite applicable to the 1.28 GeV electron beams at the ATF damping ring [9]. Bane called it the *Modified Piwinski* solution. Kiyoshi Kubo, one of the lead researchers at the ATF, Andy and I succeeded in combining my work with Tollestrup with Bane's ansatz to arrive at a *Completely Integrated Modified Piwinski* solution to intrabeam scattering [10]. We then used it to obtain excellent numerical analyses for the ATF data.

The work by Bj and me, using a quantum field theory approach to intrabeam scattering, is an excellent example of the importance of cross-fertilization. Bj recalls that, in those days, it was especially easy for him to cross over from particle physics to accelerator physics. He did not have to go through an annual performance review, demonstrating how his activities were contributing to the goals of the elementary particle physics theory group, as defined by some set of oversight committees. Nowadays it is harder to engage in crossover research or in research topics outside of the mainstream.

Presently, Bj is interested in the dark energy problem, which places him again as an amateur, this time within the world of general relativity. And he sees again opportunities for crossover activity. One has to do with gravitational lensing. The standard methodology uses the language of ray-tracing optics. He does not see any significant use of the Hamiltonian language of Courant, Livingston, and Snyder, an approach that has revolutionized the field of particle-beam optics for more than a half century. He cannot help but wonder whether this approach could be productive when applied to gravitation.

Another such area is in the formalism of general relativity itself. The predominant choice of language is that of the century-old Einstein-Hilbert description, where the basic degrees of freedom are the 10 independent components of the metric tensor. Almost as old is the description advocated by Cartan, often called "gauge gravity," where the degrees of freedom are the 24 components of an $O(3,1)$ gauge potential called the spin connection, supplemented by 16 more called the "vierbein," out of which the standard metric tensor is constructed. The Einstein-Cartan language is distinctly different from the Einstein-Hilbert language, although the physics consequences are nearly, but not totally, identical. In particular, if one wants to incorporate Dirac particles as gravitational sources, one is obliged to utilize the Einstein-Cartan language. For sure, this gauge-gravity language is familiar to essentially all general relativity theorists. But, as Bj sees it, it is in the bones of only a minority of them, and he wishes that there were more of a balance.

The distinction between Einstein-Hilbert and Einstein-Cartan gravity is a more grandiose version of what occurs in Higgs physics. The language of the nonlinear sigma model, with its three degrees of freedom, is enough to describe the Higgs mechanism, which gives the electroweak gauge bosons their mass. But one needs the linear sigma model, with its four degrees of freedom, to account for the famous Higgs particle itself.

For the last set of comments, I would like to reflect on the role that accelerator physics has had on my desire to improve the state of science and technology in Africa and other parts of the developing world. In 1988, the late Nobelist, Abdus Salam, brought a group of scientists and mathematicians from Africa and the United States together at the International Centre for Theoretical Physics (ICTP) in Trieste to foster collaborations between the two communities. Fig. 5 contains a photo of the participants of the *1st Edward Bouchet Conference*, named for Bouchet, the first African American to receive

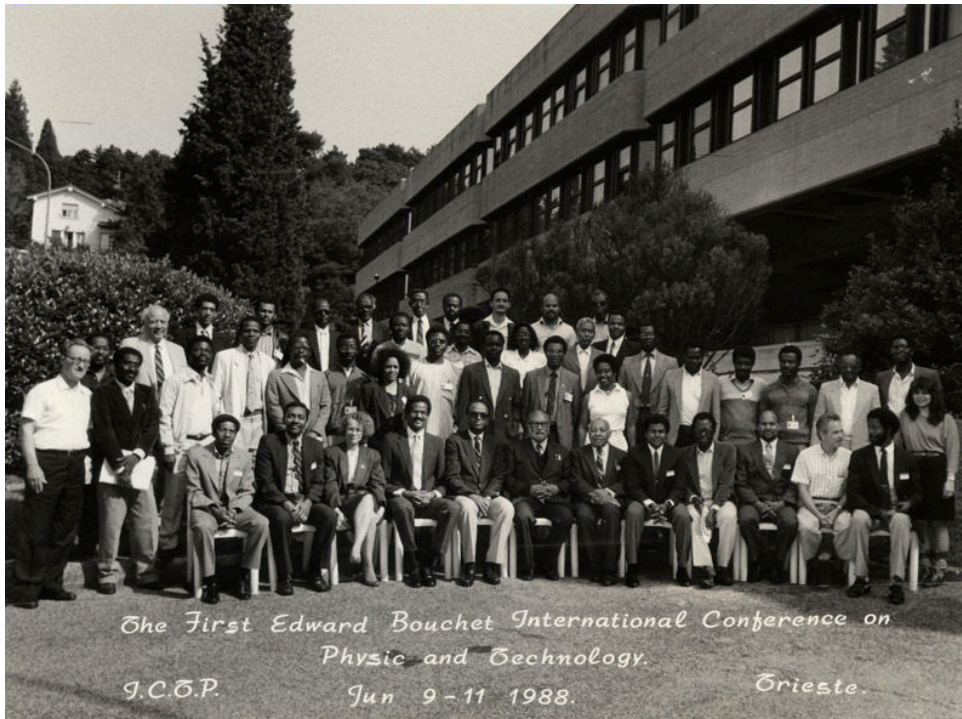


Figure 5: Group Photo of the 1st Edward Bouchet Conference (Figure Courtesy of ICTP).

a Ph.D. in physics and it was from Yale University in 1876. After the passing of Salam, we renamed ourselves the *Edward Bouchet - Abdus Salam Institute (EBASI)*. While the U.S. was in the middle of sorting out the controversial 2000 Presidential election, we were meeting at ICTP. At that meeting, I proposed that we undertake a major effort to bring a synchrotron light source to Africa. We decided that that may be a bit too ambitious, but that as a first step we should do something to improve laser science and technology in Africa. With that mandate, I connected with major science and technology proponents in Africa, most notably Philemon Mjwara, who at the time was Centre Manager of South Africa's National Laser Centre (NLC) and is presently Director General of South Africa's Department of Science and Technology. He led South Africa's co-winning bid with Australia to host the Square Kilometre Array (SKA), which will become the world's largest radio telescope. With our colleagues, we established the *African Laser Centre (ALC)* to enhance laser research and training in Africa. The ALC is headquartered at the NLC in Pretoria and consists of over 30 laser laboratories in many African countries as depicted in Fig. 6. I chaired the writing of the 2002 document, *A Strategy and Business Plan for an African Laser Centre*, wherein we included an African synchrotron light source as a long-term goal, making this the first call for an international synchrotron light source in Africa. The official launch of the ALC occurred during November 2003 in Johannesburg during a meeting of the New Partnership for Africa's Development (NEPAD) Conference on Science and Technology for Development. NEPAD

declared the ALC to be one of its Centres of Excellence. Fig. 7 is a group photo of the ALC organizers. Figs. 8-10 contain photos of various ALC workshops and conferences. Fig. 11 provides a number of ALC accomplishments during the 2006-2015 period.



Figure 6: Counties with ALC Member Institutions (Figure Courtesy of the African Laser Centre).



Figure 7: Organizers of the African Laser Centre, Pretoria, South Africa, November 2003.



Figure 8: 5th Annual ALC Student Workshop, Namibia 2012.



Figure 9: 2nd US-Africa Advanced Studies Institute, iThemba LABS, outside Cape Town, South Africa, November 2007.



Figure 10: 3rd US-Africa Advanced Studies Institute, Cairo, Egypt, November 2008.

Output	Quantity	Comments
Projects supported	87	A total of 87 research collaborations between a South African team and other African research teams elsewhere on the African continent have been supported up to. This represents 87 grants.
Publications in refereed journals	151	Annual Report for period 2006 – 2013
Popular journal articles	13	Annual Report for period 2006 - 2013
Publications in conference proceedings	210	Annual Report for period 2006 - 2013
Chapters in books	12	Annual Report for period 2006 - 2013
Theses completed	59	Annual Report for period 2006 - 2013
Masters scholarships awarded	38	This represents total the number of scholarship grants that were awarded within the period 2007-2013.
PhD scholarships awarded	78	This represents the total number of scholarship grants that were awarded within the period 2007-2013.
Training events (workshops/conferences/symposia, short courses) supported	33	2005-2013
Number of students trained at workshops, symposia and short courses	1249	Number of beneficiaries to ALC training since inception to 2013
Masters Students supported	141	This represents the total number of MSc students working within the supported collaboration projects.
PhD Students supported	165	This represents the total number of PhD students working within the supported collaboration projects.

Figure 11: ALC Accomplishments during 2006-2015.

When my colleagues in Africa inquire as to the kind of laser work that I do, I must tell them that I know little about them. They look really confused. To resurrect their respect for me, I always point to my ambition to see a synchrotron light source in Africa. That seems to satisfy most. South Africa is the furthest along in using advanced light sources, mostly at the European Synchrotron Radiation Facility (ESRF) in Grenoble. Herman Winick and I attended a synchrotron science workshop during December 2011 in Pretoria convened by the South African Institute of Physics and South Africa's Synchrotron Research Roadmap Implementation Committee. Fig. 12 is a group photo of attendees. The Director General of the ESRF, Francesco Sette, attended and urged South Africa to become a formal member of the ESRF. After the meeting, I chaired the writing of the document, *Strategic Plan for Synchrotron Science in South Africa*. One of the proposals was for South Africa to adopt Sette's request, which it did, and on May 21, 2013, South Africa officially became the 20th dues-paying member country of the ESRF. Fig. 13 is a photo of the signing ceremony.



Figure 12: Synchrotron Science Workshop, Pretoria, South Africa, December 1-2, 2011 (Photo courtesy of the South African Institute of Physics).



Figure 13: South Africa Joins the ESRF, Grenoble, France, May 21, 2013. Front row (l to r): Francesco Sette, ESRF Director General; Nithaya Chetty, Group Executive for Astronomy, South Africa's National Research Foundation; Luis Sanchez Ortiz, ESRF Director of Administration. Back row (l to r): Bauke Djikstra, ESRF Director of Research; Thomas Auf der Heyde, Deputy Director General, South Africa's Department of Science and Technology; Itziar Echeverria, ESRF DG Office; Tshepo Ntsoane, Chairman of South Africa's Synchrotron Research Roadmap Implementation Committee (SSRIC); Simon H. Connell, University of Johannesburg. (Photo courtesy of the ESRF)

Fig. 14 depicts the locations of light sources in the world and shows that Africa is the only habitable continent in the world without one. To spur the effort on for a light source in Africa, Herman Winick and I wrote a paper entitled, *A Synchrotron Radiation Research Facility for Africa* [11], which gave a foundation to the effort that convened the first *African Light Source (AfLS) Conference and Workshop* at the ESRF during November 16-20, 2015. Led by Simon Connell from the University of Johannesburg, the meeting had approximately 100 participants and Fig. 15 shows a few of them. The meeting generated short-, medium- and long-term goals, as well as adopted a set of resolutions, dubbed the Grenoble Resolutions, that provide the *WHY* for an AfLS [12].



Figure 14: Locations of World Synchrotron Light Sources (figure courtesy of lightsources.org).

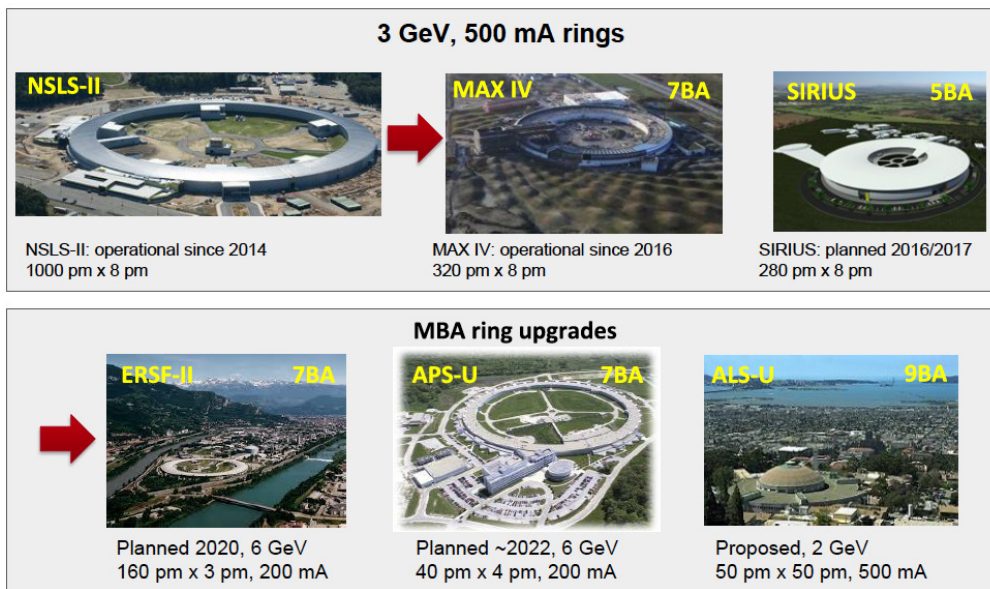


Figure 15: Several Researcher & Student Participants at the 1st African Light Source Conference & Workshop, ESRF, Grenoble, November 2015 (photo courtesy of ESRF).

A final initiative that I have had the honor of chairing, with considerable input from Herman Winick and my prior Antiproton Source colleague, Ernie Malamud, is called *Lightsources for Africa, the Americas, and Middle East Project (LAAMP)*, which is led by the International Union of Pure and Applied Physics (IUPAP) C13 Commission on Physics for Development on which I serve and the International Union of Crystallography. The Americas part of the project focuses on Mexico and the Caribbean. The goal is to enhance advanced light source science in more regions of the world. Some 25 institutions and organizations have agreed to collaborate, including light sources, ICTP, UNESCO, and international physics societies. Currently, we are in the fundraising phase and hope to formally kick off our programs later this year, with perhaps the two most important being sending students and researchers to various light sources for training and developing *Strategy and Business Plans* for each region, leading to the possibility of constructing light sources in regions that do not already have one.

These initiatives have brought me full circle back to intrabeam scattering. The new 4th generation synchrotron light sources make use of a new magnet design called the *multiband achromat (MBA)*, which was invented by researchers in Sweden and implemented at their new MAX IV light source. That and other light sources implementing this new technology are shown in Fig. 16. Vertical electron beam emittances, which are the product of beam size and divergence, are naturally quite small. In comparison, horizontal emittances tend to be many times larger. The smaller the horizontal electron emittance, the brighter photon beams tend to be that they generate. See the horizontal beam emittances in Fig. 17 and the resultant photon brightness in Fig. 18. Operating at horizontal and vertical emittances of 320 and 8 picometers, respectively, Fig. 19 shows the Max IV % horizontal beam emittance growth with and without devices called Landau Cavities (LCs), which help to mitigate intrabeam scattering effects.

Fig. 19 shows that, more and more, intrabeam scattering will be a stringent limitation that must be overcome in future light sources. It is a dominant heating mechanism for all high intensity beams, constraining luminosity lifetimes in hadron colliders and determining equilibrium emittances in antiproton accumulators, electron and positron damping rings, and synchrotron light sources. When my colleagues in Africa ask me what laser science I do, I have to say none. When they ask me what synchrotron light source beamline technique I use, I still have to say none. However, because of my work on intrabeam scattering, I can now say that I do not use the synchrotron light source beamlines, but I do work on squeezing the last photons out of them. And that seems to satisfy them.



Other international implementations: Japan (SPRing8-2, 6 GeV), China (HEPS, 5-6 GeV), Germany (PETRA-IV), France (SOLEIL), Switzerland (SLS, 2.4 GeV), Italy (ELETTRA) and others are developing plans

Figure 16: World Light Sources Implementing the New Multibend Achromat Technology [13] (figure courtesy of the MAX IV Laboratory).

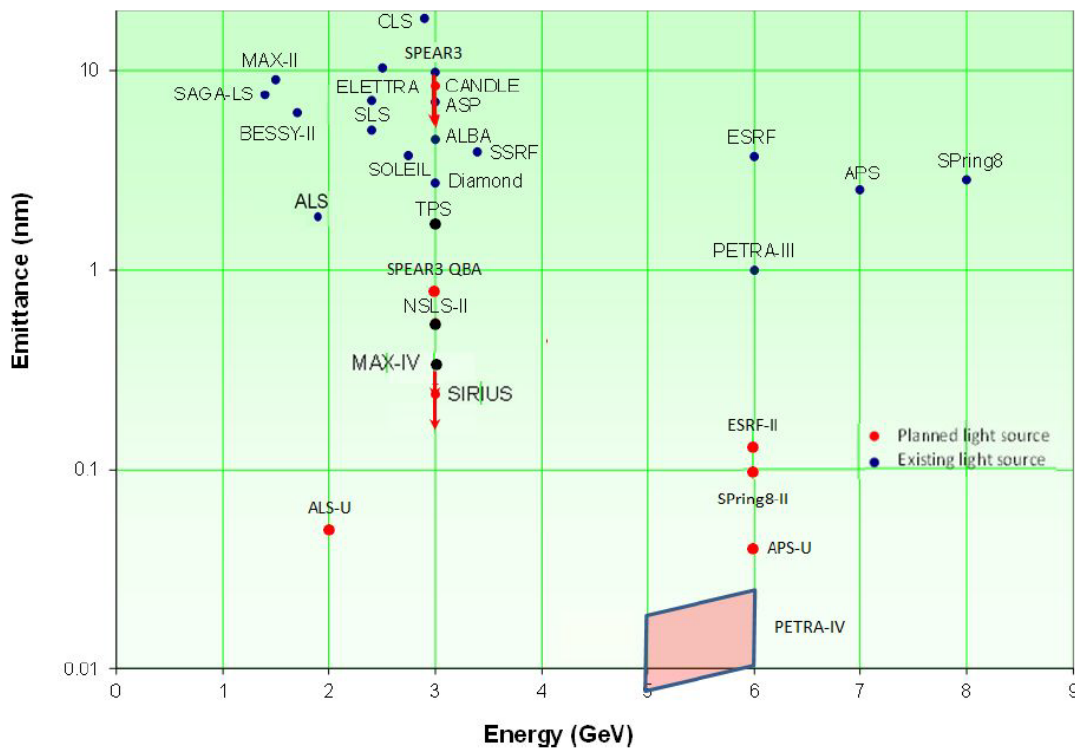
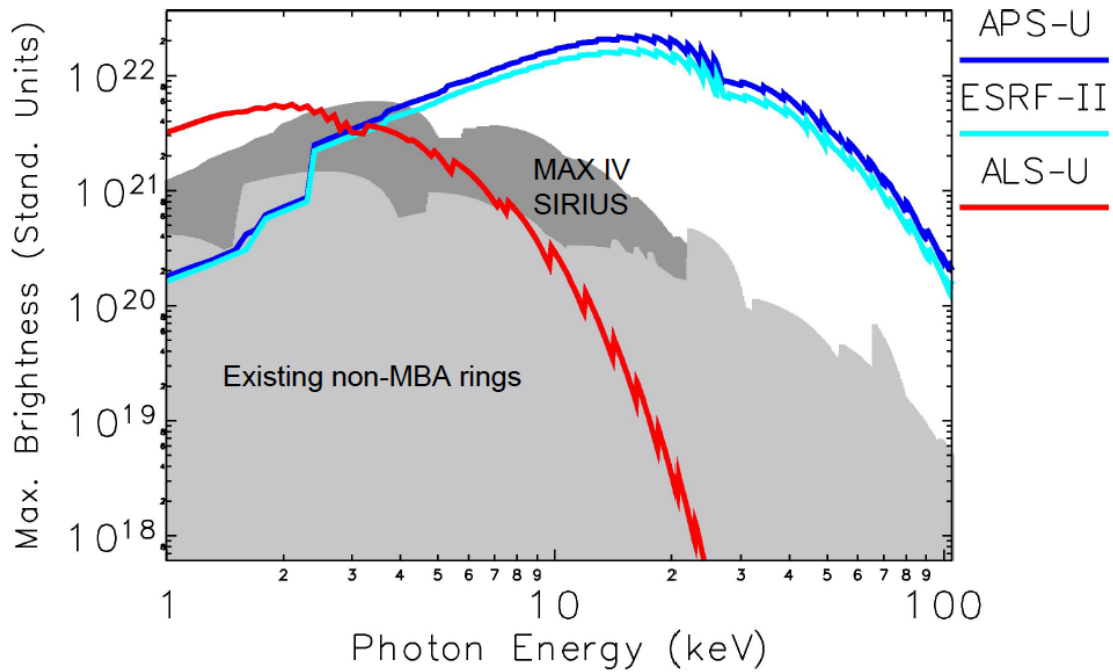


Figure 17: Horizontal Beam Emittances at World Light Sources [13] (figure courtesy of the MAX IV Laboratory).



Based on data supplied by O. Chubar (BNL), R. Hettel (SLAC), A. Kling (DESY), S. Krinsky (BNL), S. Leemann (MAX IV), T. Rabedeau (SLAC), P. Raimondi (ESRF), C. Steier (ALS), T. Watanabe (SPRING-8)

Figure 18: An incomplete snapshot of the SR light source brightness landscape [13] (figure courtesy of the MAX IV Laboratory).

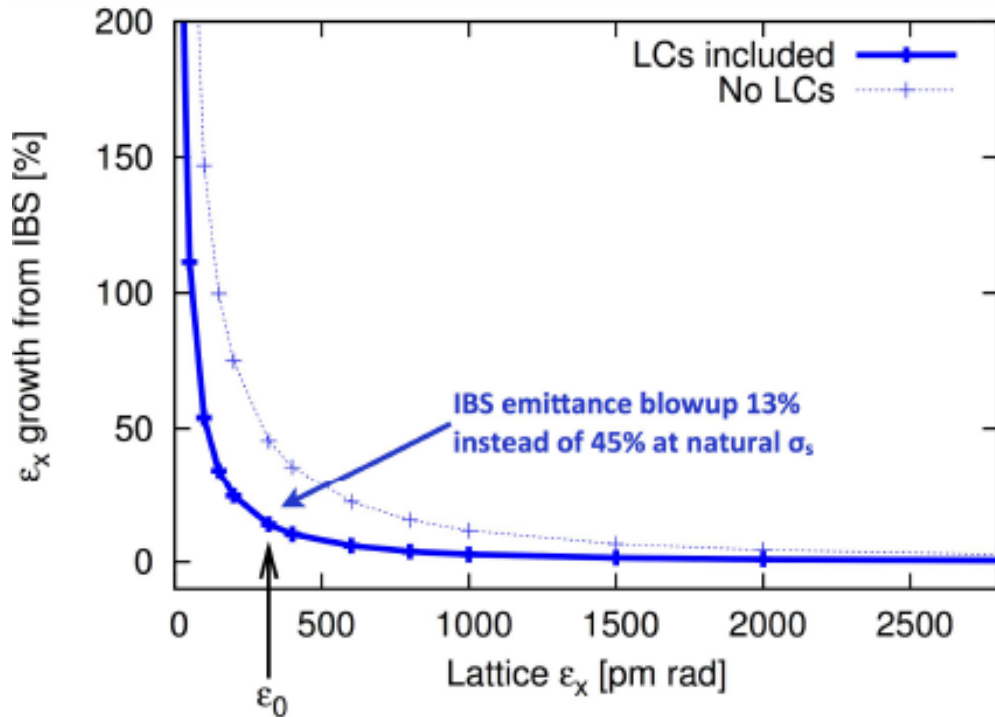


Figure 19: % Horizontal Beam Emittance Growth due to Intrabeam Scattering (LCs=Landau Cavities) [13] (figure courtesy of the MAX IV Laboratory).

As a high energy physicist, I am proud that our community has invented the synchrotrons used at light sources. They are revolutionizing so many disciplines, from biology, drug discovery, materials science, physics, chemistry to paleontology and cultural heritage studies. As a community, we need to add this to our list of technological breakthroughs that have changed the way we live, along with the World Wide Web and various imaging techniques. We need to shout it to the heavens. I try to promote them and the advanced free-electron lasers in the U.S. by serving as President of an organization called the *Interdisciplinary Consortium for Research & Educational Access in Science and Engineering (INCREASE)*. We host workshops at the national laboratories centered at the light sources, for faculty and students principally but not exclusively from Minority-Serving Institutions, to enhance their use of these large national user facilities. The INCREASE leadership is based at TriSEED Consultants in the Research Triangle, Hampton University and Brookhaven National Laboratory. Much work is yet to be done.

In conclusion, when Bj and I undertook our work on intrabeam scattering, we were simply trying to understand its effect on the Antiproton Source's ability to accumulate antiprotons. Little did we know that over the years intrabeam scattering would become so crucial for the operation of so wide a class of accelerators, even assisting in the discovery of the top quark and Higg's particle and helping to revolutionize so many disciplines at synchrotron light sources.

Anton, Bj and I would like to extend our heartfelt thanks to Herman Winick for his enthusiastic support and others who supported us for the Wilson Prize.

On a personal note, I would like to thank all those who have played an important role in supporting and promoting my career over these many years, starting with my dear wife Estella, daughters, Bj, Alvin Tollestrup, Leon Lederman, Abdus Salam, James Young, Victor Weisskopf and Curtis Callan.

2.1.2 Appendix 1

Historical Notes for the Touschek Effect

- 1) C. Bernadini, G. F. Corazza, G. Di Giugno, G. Ghiago, J. Haissinski, P. Marin, R. Querzoli, and B. Touschek, Phys. Rev. Lett. 10, 407 (1963)

First measurement of the effect and explanation by B. Touschek

- 2) B. Gittelmann, D. M. Ritson, HELP-291, Stanford Univers., Stanford, 1963

Calculation of the rise time for ultra-relativistic energies

- 3) U. U. Voelkel, DESY 67/5 March 1965

Calculation for arbitrary energies

- 4) A. Piwinski, DESY 98-179, November 1998

Consideration of the vertical betatron oscillations and a variation of the beam envelopes

2.1.3 Appendix 2

Historical Notes for IBS

- 1) H. Bruck, J. Le Duff, Lab. Acell. Lin., Orsay, Rap. Techn (1964)
- 2) C. Pellegrini, Proc. Int. Symposium on Elec. Pos. Storage Rings (1966)
Investigation of the transfer of oscillation energy from one direction to another
- 3) A. Piwinski, Proc. 9th Int. Conf. on High Energy Acc. SLAC (1974)
Investigation of energy transfer between all three directions taking into account the corresponding energy losses
- 4) K. Huebner, D. Moehl, F. Sacherer, CERN, computer code (1977)
Calculation of rise time due to IBS including the derivations of amplitude function and dispersion (A. Piwinski, F. Sacherer)
- 5) J. D. Bjorken, S. K. Mtingwa, Particle Acc. 13, 115 (1983)
A completely new and elegant method for the calculation of the rise times

2.1.4 Appendix 3

Grenoble Resolutions

1. *Advanced light sources are the most transformative scientific instruments similar to the invention of conventional lasers and computers.*
2. *Advanced light sources are revolutionizing a myriad of fundamental and applied sciences, including agriculture, biology, biomedicine, chemistry, climate and environmental ecosystems science, cultural heritage studies, energy, engineering, geology, materials science, nanotechnology, palaeontology, pharmaceutical discoveries, and physics, with an accompanying impact on sustainable industry.*
3. *The community of researchers around the world are striving collaboratively to construct ever more intense sources of electromagnetic radiation, specifically derived from synchrotron light sources and X-ray free-electron lasers (XFELs), to address the most challenging questions in living and condensed matter sciences.*
4. *The African Light Source is expected to contribute significantly to the African Science Renaissance, the return of the African Science Diaspora, the enhancement of University Education, the training of a new generation of young researchers, the growth of competitive African industries, and the advancement of research that addresses issues, challenges and concerns relevant to Africa.*

5. *For African countries to take control of their destinies and become major players in the international community, it is inevitable that a light source must begin construction somewhere on the African continent in the near future, which will promote peace and collaborations among African nations and the wider global community.*

2.1.5 References

1. J. Bjorken and S. Mtingwa, Particle Accelerators, Vol. 13, p. 115 (1983).
2. M. Sands, SLAC Report 121 (1970).
3. A. Piwinski, Proc. 9th Int. Conf. on High Energy Accelerators, p. 405 (1974).
4. Ibid.
5. C. Seife, *Science*, Vol. 297, p. 757 (2002).
6. M. Month and W.-T. Weng, AIP Conf. Proc. No. 105, p. 124, AIP, New York, NY (1983).
7. S. Mtingwa and A. Tollestrup, Fermilab-Pub-89/224 (1987).
8. D. Finley, Fermilab-TM-1646 (1989).
9. K. Bane, Proc. of the 8th EPAC, p. 1443, Paris (2002).
10. K. Kubo, S. Mtingwa and A. Wolski, Phys. Rev. Spec. Topics – Accel. and Beams , **8**, 081001 (2005).
11. S. Mtingwa and H. Winick, <http://www.lightsources.org/news/2014/09/05/synchrotron-radiation-research-facility-africa> (2014).
12. See Appendix 3.
13. M. Borland, *et al.*, “Accelerator Physics Challenges in the Design of Multi-Bend-Achromat-Based Storage Rings,” contribution to NAPAC 2016, Chicago, IL, USA, October 2016.

2.2 Intrabeam Scattering and Touschek Effect

Anton Piwinski (DESY)
Mail to: anton.piwinski@desy.de

I would like to talk about the beginning of the investigations of the intrabeam scattering (IBS). I heard the first time about of the IBS in 1973 on a workshop in Italy, and I learned that IBS could be a serious problem in proton accelerators. Since DESY in Hamburg was discussing at that time a new proton storage ring, I decided to investigate this problem.

In the literature I found several reports for the Touschek effect (TE) but I found very little about IBS. Here I should mention that IBS and TE are two different aspects of the same effect, namely Coulomb scattering within a particle beam. For the TE only large scattering angles are taken into account. For IBS, on the other hand, the small scattering angles are considered and it is assumed that all changes of coordinates due to the scattering are small as compared to the beam dimensions.

For the TE enough investigations existed which allowed a reasonable calculation of the beam life time due to the TE. For IBS, however, there were only a few attempts to estimate the transfer of oscillation energy from one direction to another, mainly from transverse to longitudinal, i.e. from betatron oscillations to synchrotron oscillations.

There was no attempt to take into account the losses of oscillation energy in one direction when the energy is transformed into another direction. These losses are important for a realistic description of the IBS. Indeed, IBS is a mutual exchange of oscillation energies between all three directions and only by taking into account all energy transfers in all directions one can calculate the rise times for the three dimensions.

Table 1 shows the main characteristics and differences between IBS and TE.

Figure 1 shows the first measurement of the TE in 1963. The inverse of the life- time is plotted as a function of the number of electrons or as a function of the electron density. The life time varies from 6 to 50 hours. The measurements were done in the small storage ring AdA (AdA is the Italian abbreviation for storage ring) at an energy of 188 MeV. There is a small displacement above zero, which is caused by the scattering of the electrons on the residual gas.

Table 1: Coulomb Scattering of Particles within a Beam

<i>Touschek effect</i>	<i>Intrabeam scattering</i>
Single scattering	Multiple scattering
Only energy transfer from transverse to longitudinal oscillations is considered	Exchange of oscillation energies between all 3 directions is considered
A small transverse momentum is transformed into a large change of longitudinal momentum (multiplied by the Lorentz factor γ)	All changes are assumed to be small as compared to the beam dimension
No change of particle distribution but loss of both colliding particles	Diffusion in all 3 directions leads to a change of particle distribution, increase and decrease of dimension are possible

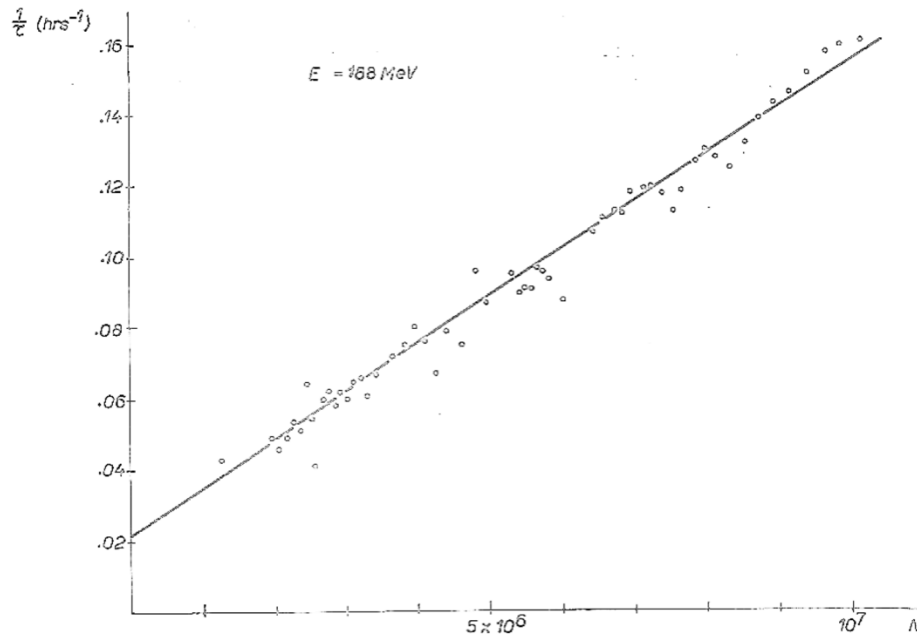


Figure 1: First measurement of the Touschek effect in 1963. Inverse lifetime $1/\tau$ as a function of the number of particles in the beam.

In order to explain this measurement Bruno Touschek found the relativistic mechanism for the longitudinal momentum change. To simplify the calculation he made some approximations, e.g. he assumed non-relativistic particle velocities in the center-of-mass system of the beam and he assumed a flat beam, i.e. no vertical betatron oscillations of the electrons.

Table 2 shows the successive improvements of the theory of the TE. After the first measurements and explanation by B. Touschek and others in 1963 the life time was determined for ultra-relativistic energies, i.e. for relativistic energies in the center-of-mass system, by B. Gittelmann and D. Ritson at SLAC. In 1965 the theory was finally generalized by U. Voelkel of DESY for arbitrary energies. In 1998 the theory was extended for arbitrary beam size, i.e. instead of a flat beam vertical betatron oscillations were taken into account. The derivations of the amplitude functions and the dispersion were also included.

Table 2: Historical notes for the Touschek Effect

<i>Reference</i>	<i>Comments</i>
<i>C. Bernadini, G. F. Corazza, G. Di Giugno, G. Ghiago, J. Haissinski, P. Marin, R. Querzoli, and B. Touschek, Phys. Rev. Lett. 10, 407 (1963)</i>	First measurement of this effect and explanation by B. Touschek
<i>B. Gittelmann, D. M. Ritson, HELP-291, Stanford University, 1963</i>	Calculation of the rise time for ultra-relativistic energies
<i>U. Voelkel, DESY 67/5 March 1965</i>	Calculation for arbitrary energies
<i>A. Piwinski, DESY 98-179, November 1998</i>	Consideration of the vertical betatron oscillations and a variation of the beam envelopes

Figure 2 shows a typical example of a measurement of the IBS. It shows the longitudinal distribution of a proton bunch on the left side and of an antiproton bunch on the right side at different times. The time difference between successive curves is a quarter of an hour. The main difference between the two sets of curves is the density. For the proton bunch it is larger by an order of magnitude than the density of the antiproton bunch. Consequently, the growth of the proton bunch length is clearly stronger than for the antiproton bunch. The measurements were done 1984 in the SPS at CERN with an energy of 300 GeV.

Similar measurements were also made for the bunch width and for the bunch height. All the measurements in various storage rings show such a slow change of the dimensions.

Table 3 shows a brief review of the investigations on IBS. The first investigations were done by Bruck and Le Duff in 1964 and by Pellegrini in 1966. They calculated the transfer of oscillation energy from one direction to another. In 1974 the total energy exchange among all three directions was considered. Also the oscillation energy losses due to transfer into another direction were taken into account so that the development of the beam dimensions over a long time could be calculated.

In 1977 Simon van der Meer was working on his stochastic cooling for which he later received the Nobel Prize. He asked for the most precise calculation of the rise times due to IBS because this cooling would have to compete with the IBS. Then F. Sacherer and I independently derived formulae including the derivations of the amplitude function β and of the dispersion D . A computer program was then written by Huebner, Moehl and Sacherer including these additional parameters. This program was used by researchers in several institutes. In 1983 BJ and Sekazi developed a completely new and elegant theory for the IBS. We will hear more about this theory in the next talks.

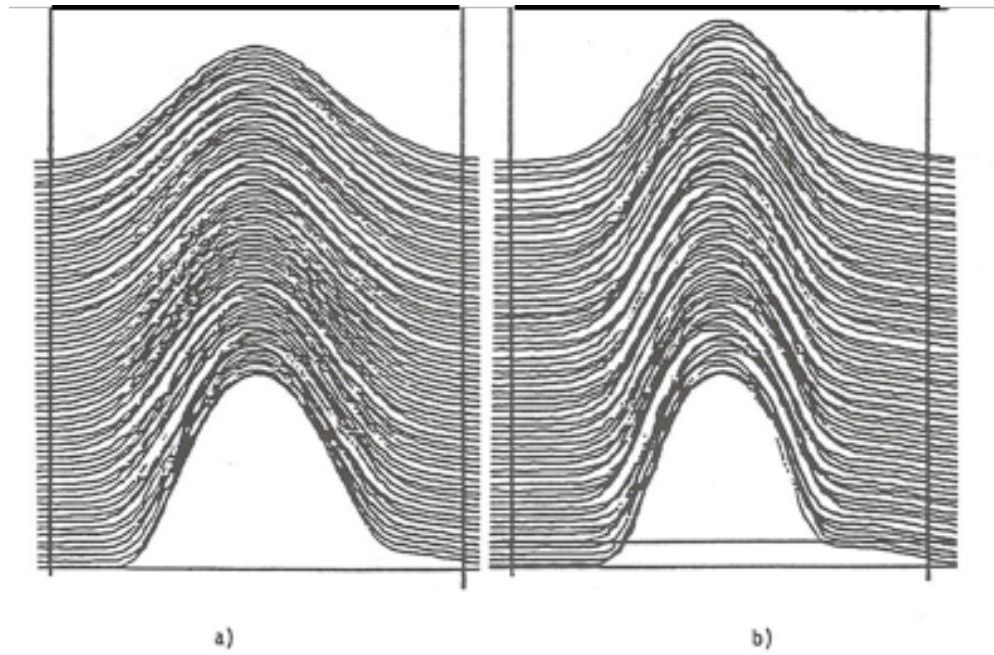


Figure 2: Measurements made in the CERN SPS of the longitudinal distribution of a) a proton bunch ($N^+ = 1.5 \cdot 10^{11}$) and b) an antiproton bunch ($N^- = 1.2 \cdot 10^{10}$).

Table 3: Historical notes for the Touschek Effect

<i>Reference</i>	<i>Comments</i>
<i>H. Bruck, J. Le Duff, Lab. Acell. Lin., Orsay, Rap.Techn. (1964)</i>	
<i>C. Pellegrini, Proc. Int. Symposium on Elec. Pos. Storage Rings (1966)</i>	Investigation of the transfer of oscillation energy from one direction to another
<i>A. Piwinski, Proc. 9th Int. Conf. on High Energy Acc. SLAC (1974)</i>	Investigation of energy transfer between all three directions taking into account the corresponding energy losses
<i>K. Huebner, D. Moehl, F. Sacherer, CERN, computer code (1977)</i>	Calculation of rise time due to IBS including the derivations of amplitude function and dispersion (A. Piwinski, F. Sacherer)
<i>J. D. Bjorken, S. K. Mtingwa, Particle Acc. 13, 115 (1983)</i>	A completely new and elegant method for the calculation of the rise times

The rise times $\tau_{s,x,z}$ for the three dimensions can be written in the following form:

$$\frac{1}{\tau_{s,x,z}} = d \cdot F(a_{s,x,z}, b_{s,x,z})/\gamma^4$$

Here d is the particle density in phase space

$$d = \frac{N}{\sigma_s \sigma_p \sigma_x \sigma_{x'} \sigma_z \sigma_{z'}}$$

γ is the Lorentz factor, and the function F considers the imbalance of the oscillation energies for the three direction or, with other words, the imbalance of the temperatures for the three directions since it depends only on $a_{s,x,z}$ and $b_{s,x,z}$, which are the ratios of bunch dimensions. I will not show the explicit form of the function F . It is complicated and it contains an integral which must be solved numerically. F can be positive or negative or zero. It can be zero for all three directions at the same time only at energies below transition energy. Above transition energy at least one of the three rise times must be different from zero.

This behavior can be seen with help of the following invariant which can be derived from the three rise times:

$$\left(\frac{1}{\gamma^2} - \alpha_M\right) \left\langle \frac{\Delta^2 p}{p^2} \right\rangle_{av.} + \langle x'^2 \rangle_{av.} + \langle z'^2 \rangle_{av.} = \text{const.}$$

$p, \Delta p$ = momentum and momentum deviation

x', z' = horizontal and vertical betatron angles

The momentum compaction factor α_M is the ratio of the relative orbit lengthening to the corresponding relative energy change. The average has to be taken over all particles and the whole circumference. Below transition energy ($\gamma_{tr} = 1/\sqrt{\alpha_M}$) the first bracket is positive and all oscillation amplitudes are limited. Here an equilibrium distribution can exist. Above transition energy the first bracket is negative and all oscillation amplitudes can grow as far as they do not exceed other limitations, e.g. the chamber wall.

This invariant is correct only if the derivatives of β and dispersion D are neglected. If they are taken into account, the above mentioned expression is not constant but increases slowly. The derivatives appear always in the combination $D'\beta - \beta'D/2$. Therefore, the contributions from large β' in the interaction regions (>100) vanishes since the dispersion in interaction regions is usually zero. The invariant can be considered as an approximation which shows in principle the different behavior below and above transition energy.

3 Status and Plans for Major U.S. Light Source Facilities

3.1 Status of the Advanced Light Source

David Robin and Christoph Steier
Mail to: DSRobin@lbl.gov
Lawrence Berkeley National Laboratory, 1 Cyclotron Road,
MS15R0217, Berkeley, CA94720, USA

3.1.1 Introduction

The Advanced Light Source (ALS) is a storage-ring-based synchrotron radiation source at Lawrence Berkeley National Laboratory (LBNL). The ALS was commissioned in 1993 and is one of the first members of the 3rd generation synchrotron light sources.



Figure 1: The Advanced Light Source at Lawrence Berkeley National Laboratory.

The ALS produces light from the far infrared to the harder x-ray region of the photon spectrum and is optimized for the production of vacuum ultraviolet (VUV) and soft x-ray radiation. Soft x-rays are ideally suited for revealing the chemical, electronic, and magnetic properties of materials, as well as the chemical reactions that underpin these properties. This knowledge is crucial for the design and control of new advanced materials. The ALS continues to enable breakthrough science and multiple discoveries by a user community of nearly 2,600 unique annual users that continues to grow, with an exceptional publication record that includes more than 10,000 refereed journal articles to date (see Fig. 2).

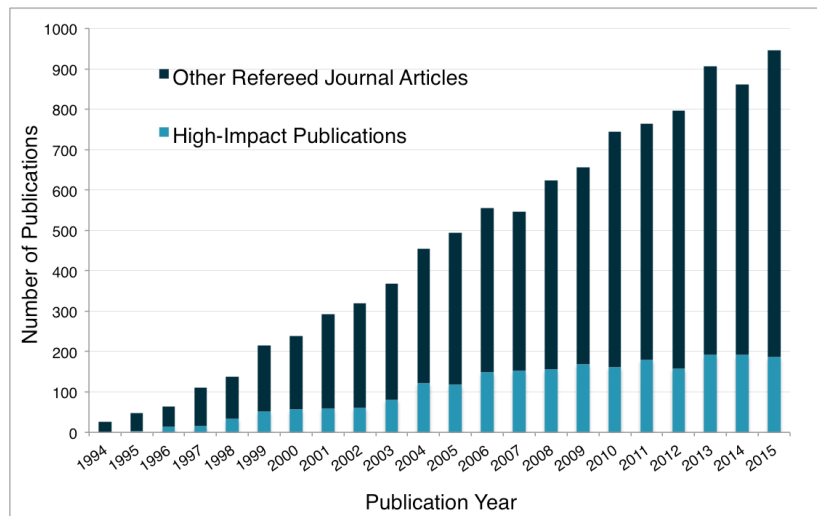


Figure 2: Number of refereed journal articles by year.

Since the ALS was commissioned in 1993 there have been many additional 3rd generation light sources built and commissioned. Nevertheless the ALS has been able to maintain its position at the leading edge of soft x-ray science. An important reason for this is that the ALS has been continuously upgraded through a sequence of important and at times pioneering improvements in technical performance.

3.1.1.1 *1993-2006*

The first of those important upgrades as well as developments of new accelerator physics techniques started very quickly after ALS user operations began in 1993. This included pioneering the development of multi-bunch feedback systems to control collective instabilities [Barry93, Fox93]. The introduction of high-field (~ 5 T) superconducting bending magnets (“superbends”) as an integral part of the storage ring lattice to provide high brightness harder x-ray dipole sources [Robin05]. Introduction and development of femtosecond slicing for short (~ 200 fs) pump probe experiments [Steier03]. The development of lattice optimization and beam dynamics techniques such as frequency map analysis [Robin00, Steier02], global analysis of stable solutions [Robin08], and multi-objective genetic algorithms [Yang09] for improved lattice optimization. During this time, there also were extensive studies to develop compensation techniques for the effects of insertion devices on the electron beam, particularly elliptically polarizing insertion devices [Steier08]. Also worth mentioning is the development of the understanding and limitations of the production and use of coherent synchrotron radiation [Byrd02] in storage rings.

3.1.1.2 *2006-2016*

Over the last decade, the developments continued. This included both performance improvements as well as addressing obsolescence of equipment. In terms of performance improvements one of the major accomplishments has been the increase in the storage ring brightness through a succession of several upgrades. The brightness of the ALS using both insertion device as well as dipole sources has increased more than 30 times resulting from using top-off injection to double the time averaged current from 250 mA to 500 mA [Steier09], reducing the vertical emittance by a factor of five from 150 pm-rad to 30 pm-rad [Steier03b], and reducing the horizontal emittance by a factor of >3 from 6.75 nm-rad to 2.0 nm-rad [Steier14, Madur14], as well as the introduction of advanced insertion devices.

Some other performance and capability improvements that occurred during the last decade have been the introduction of a novel mode of operation named pseudo single bunch operation [Sun13, Hertlein15] that allows some users to select pulses of light on demand while the remainder of the users continues operation in high brightness multi-bunch mode. Improvements to bunch fill patterns were achieved using FPGA based parasitic bunch cleaning [Sannibale06], and bunch equalizing with a bunch-by-bunch current monitoring [Weber14].

As the ALS was nearing its third decade of operation, there has been a campaign to address obsolescence of equipment with new equipment with improved capabilities. This included upgrades of the Booster and Storage Ring RF systems and main magnet power supplies [Baptiste08] as well as upgrading of the accelerator controls and instrumentation system including development and installation of very high resolution beam position monitors [Vetter12] and upgrades to the orbit feedback systems.

Finally, there are exciting plans for continued further upgrades of the capability of the ALS both in the near term and in the longer term. In the near term (next few years) the plan is to install a number of new insertion devices including the first hard x-ray producing undulator [BCSB14] together with a new form of injection using using a nonlinear injection kicker [Pappas15] and to continue improvements of beam stability by further upgrades to the beam diagnostics and orbit feedbacks. The longer term plans are detailed in the next section.

3.1.1.3 2016 and beyond

In the longer term there is a much more ambitious proposal for a major upgrade of the ALS, called ALS-U [Steier16, Steier14, Tarawneh14]. This upgrade would significantly increase the brightness and coherent flux by up to 3 orders of magnitude over what the ALS produces today. In Figure 3 one can see the evolution in brightness beginning in 1993, 2008, 2014, and what it will be after ALS-U.

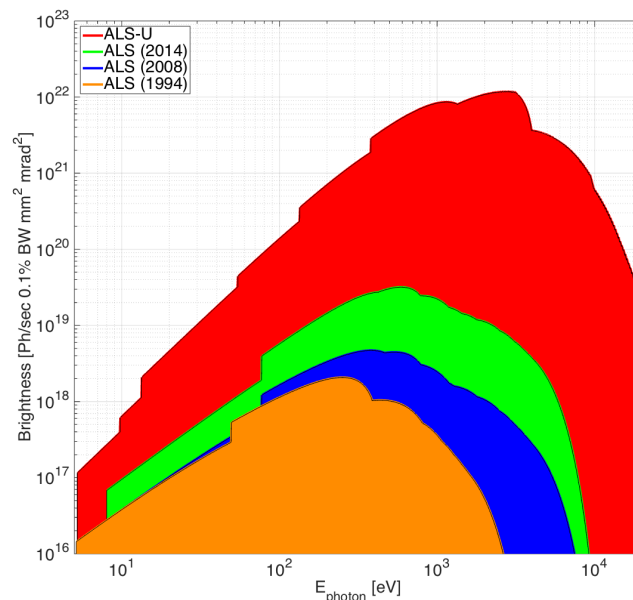


Figure 3: Comparison of ALS brightness at the start of user operations (1993), before the top-off upgrade (2008), after the top-off and brightness upgrade (2014) as well as the predicted brightness after ALS-U.

In the following sections we will expand on one recently completed upgrade (the brightness upgrade completed in 2014) and the ALS-U proposal

3.1.2 ALS Brightness Upgrade

To remain competitive with the newest synchrotron radiation sources in the core soft x-ray region (relevant to life science, chemistry, catalysis, surface science, nanoscience, and complex materials) a major lattice upgrade of the ALS was started [Steier11] and successfully completed in 2013 reducing the horizontal emittance from 6.75 nm to 2.0 nm. Combined with the earlier top-off upgrade, it provided a brightness improvement of more than a factor of 30.

3.1.2.1 Lattice Design

The ALS lattice has a triple bend achromat structure, with a fixed, large defocusing gradient in the bending magnets. Originally, there were only two families of sextupoles, with four sextupole magnets in each arc. An attractive set of possible upgrade lattices was found with higher straight section dispersion and an integer tune two units higher than the old lattice [Nishimura07] (see Fig. 4). Those lattices have natural emittances of just above 2 nm (compared to the more than 6 nm of the old lattice). Later on, more systematic techniques [Robin08, Yang09, Steier11] were used to find the global optimal lattices in terms of emittance and brightness. In those studies an additional family of low emittance lattices was found with very small horizontal beta function (order of 0.5 m) in the straights at much higher phase advance, which would increase the brightness further by better matching to the photon diffraction ellipse. The high-beta lattices were within the range of the existing quadrupole magnets. However, the original sextupoles were too weak and the dynamic aperture would have been very poor. Both challenges were overcome with the addition of sextupoles in the straight sections.

With this addition of new magnets and the changed strength of existing interlocked magnets, parts of the safety analysis for top-off operation needed to be redone. The analysis was completed in time for the installation shutdown and no hardware changes were necessary.

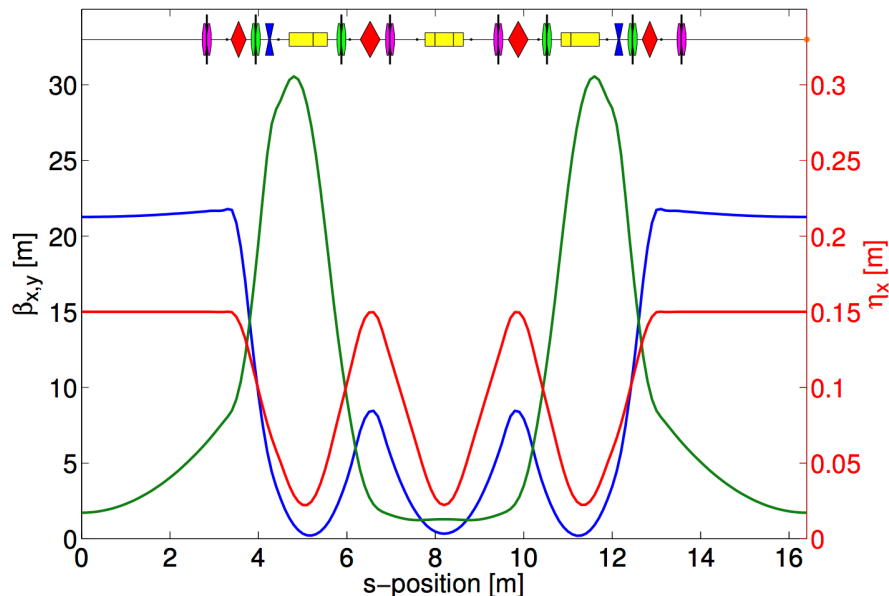


Figure 4: Lattice functions of ALS lattice with 2.0 nm natural emittance (1.9 GeV).

3.1.2.2 *Magnet Design and Production*

The design [Madur12] of the new sextupoles was performed in a collaboration by LBNL and SINAP and was finished in 2011. Because of space constraints, three different sextupole magnet designs are used. One of the families is optimized for small hysteresis and fast time response and has a closed yoke. It is also used as primary correctors in the fast orbit feedback. All new sextupoles also contain skew quadrupole coils (half of them are currently connected to power supplies). This allows to improve the vertical beamsize stability in the ALS by providing an effective correction of the small but relevant skew quadrupole errors of the planar insertion devices.

Magnet production, carried out at SINAP, started with prototype magnets just after the design reviews in early 2011. The pole shapes were manufactured by wire-edm on fully assembled magnet cores to achieve excellent field quality. Manufacturing was completed in summer 2012, on time to achieve the project installation milestones. During construction there was a detailed quality assurance program and all magnets were fully qualified by electrical, mechanical, and magnetic measurements. Precise fiducialization was carried out both mechanically and with the help of magnetic measurements. All magnets exceeded the necessary field quality requirements.

3.1.2.3 *Installation*

In order to create sufficient space in all locations where new magnets were going to be installed, several modifications of vacuum chambers and stands were completed in 2012. The installation started late in 2012 during short maintenance shutdowns, with 13 of the new sextupoles being installed ahead of the main installation shutdown. This allowed to test their corrector functionality (time response, hysteresis) and to incorporate them into slow and fast orbit feedback. The remainder of the 48 magnets were installed during the 2013 spring shutdown (see photos in Fig. 5). At the same time, all new power supplies and equipment protection systems were installed, the top-off interlock ranges enlarged and the interlocks retested.



Figure 5: Left: SHD magnet installed between two of the QF and QD quadrupoles. Right: Ribbon cutting celebration after successful installation.

3.1.2.4 *Commissioning*

Migration to the new lattices was quick (few hours), after all magnet polarities and magnet transfer functions had been verified in a beam based way in the old lattice. Simulations had predicted excellent dynamic and momentum aperture as well as lifetime for the optimized upgrade lattices [Steier11, Sun12]. These predictions were quickly confirmed. Further commissioning included optimizing the harmonic sextupole settings, updating the ID feed-forward algorithms (tune, beta beating, coupling)

for the new lattice, implementing the new dispersion bump [Sun12b] (see Fig. 6) for the fs-slicing facility and retesting the top-off interlocks with the new interlock ranges.

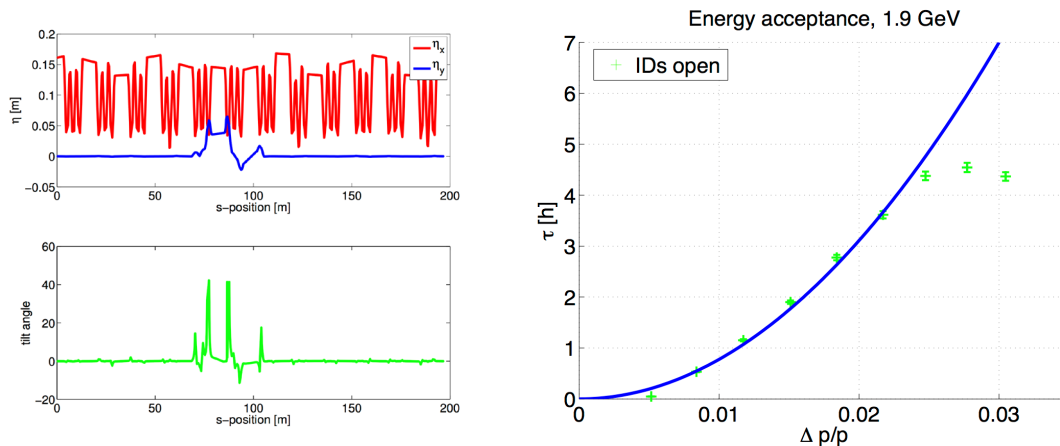


Figure 6: Left: New fs-slicing optics that provides the spatial separation of the energy sliced beam in the new upgrade lattices. Right: Lifetime vs. RF amplitude scan for the upgrade lattice confirming improved momentum acceptance compared to operation before the upgrade.

The dispersion bump was refined after final lattice optimizations. The dynamic aperture and momentum aperture (see Fig. 6) including the fs-slicing lattice insertion are similar to the bare lattice results and commissioning continued on a fast pace. The new lattices also provide a larger, intrinsic horizontal separation of the sliced electron beam.

Optimizing the photon beamlines for the new beam dimensions progressed quickly and user beamlines were able to resolve the brightness increase (see Fig. 7). The Touschek beam lifetime after the upgrade, despite the smaller horizontal and slightly smaller vertical emittance is larger than before the upgrade, due to the larger dynamic momentum aperture, as predicted.

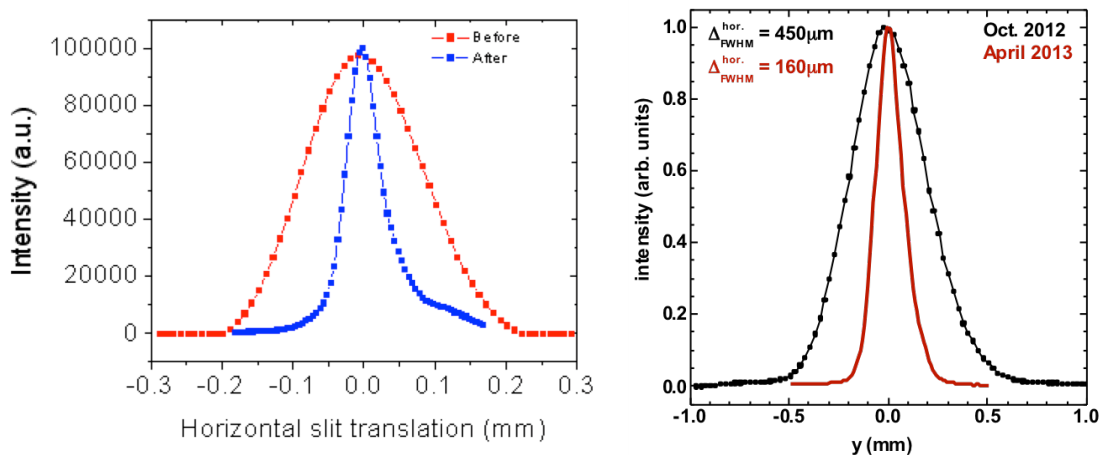


Figure 7: Comparison of the horizontal beam profile before and after the upgrade measured at beamlines 12.3.2 and 6.3.1 showing the factor of three improvement in brightness (vertical scale is renormalized, both beamlines have different magnification factors).

3.1.3 ALS-U

3.1.3.1 Motivation

Today's third-generation storage-ring-based light sources offer stable, nearly continuous, soft x-ray

beams. These beams are excellent for studying the properties of homogeneous and simply organized solids, but, with today's performance, are inadequate to elucidate the vast majority of functional complex materials, which are heterogeneous and can exhibit multiple phases and key structural features at the nanoscale. With the exception of heroic experiments, experiments on today's light sources have been limited to imaging 2D static systems at 30-nm resolution. This hampers our ability to obtain the knowledge needed to understand, design, and synthesize complex nanoscale structures, and to measure and optimize the nanoscale and larger-scale processes that make materials functional and useful.

Crucially missing from current soft x-ray ring-based light sources is high transverse coherent flux—a capability critical to novel ways of probing material structures and properties. In a beam with transverse coherence, the phase of the light field is fixed in a direction perpendicular to the propagation direction of the beam. The direct consequence is that all of the intensity of the beam can be focused into the smallest possible size defined by the wavelength. In addition, high transverse coherent flux allows the light field to be split and recombined, enabling the observation of interference phenomena and precise measurement of the phase of a beam with respect to a reference. High coherent flux and nearly continuous soft x-ray beams can resolve nanometer-scale features and interactions, and follow real-time (from nanoseconds to minutes) kinetics, which reveal the nature of chemical transformations and the origin of functional behavior of complex materials.

To meet the high transverse coherent flux challenge, an upgrade of the ALS (ALS-U) has been proposed that will take full advantage of state-of-the-art accelerator technology while leveraging the existing ALS infrastructure. ALS-U will have nearly full transverse coherence in its core photon energy range. ALS-U is possible due to recent breakthroughs in accelerator technology allowing storage rings to be built or modified to deliver much higher coherent x-ray flux than current machines. The key to producing high coherent flux in storage-ring-based sources is the multibend achromat (MBA) lattice, a magnetic structure which, when combined with other modifications to the electron accelerator, can reduce the beam emittance and dramatically increase its coherent fraction.

In 2015, the era of MBA light sources was ushered in at Sweden's MAX IV facility, the world's first MBA light source [Eriksson08]. MAX IV is the forerunner of many MBA storage-ring-based light sources to come, including upgrades, such as DOE's Advanced Photon Source (APS-U) just outside Chicago and the European Synchrotron Radiation Facility (ESRF-II) in France, and greenfield projects, such as Sirius in Brazil. Most of these projects use higher-energy electron rings than ALS and are optimized for producing hard x-rays.

The proposed ALS-U is an MBA-enabled upgrade of the ALS, optimized to generate nearly continuous soft x-rays with the highest coherent flux and brightness. To maximize the performance of the MBA-based electron storage ring, ALS-U will employ a new, concentric accumulator ring and an electron bunch-train exchange process. With these advanced technologies, ALS-U will produce up to 1,000 times more coherent flux than today's ALS and well beyond the coherent soft x-ray flux at any storage-ring-based light source operating, under construction, or planned.

The scope of work for ALS-U is as follows:

- Replacement of the existing triple-bend achromat storage ring with a new, high-performance storage ring based on a nine-bend achromat (see Fig. 8) [Tarawneh14, Sun16]. The new ring will have the same straight section length, location, and symmetry as the original ring.
- Addition of a low-emittance, full-energy accumulator ring in the existing storage-ring tunnel to enable on-axis, swap-out injection.

- Upgrade of the optics on existing beamlines, and realignment or relocation of the beamlines where necessary
- Addition of several new undulator beamlines whose world-class capabilities are optimized for novel science and made possible by the beam's high transverse coherent flux.
- Upgrade of some utilities for better electron and photon beam stability.

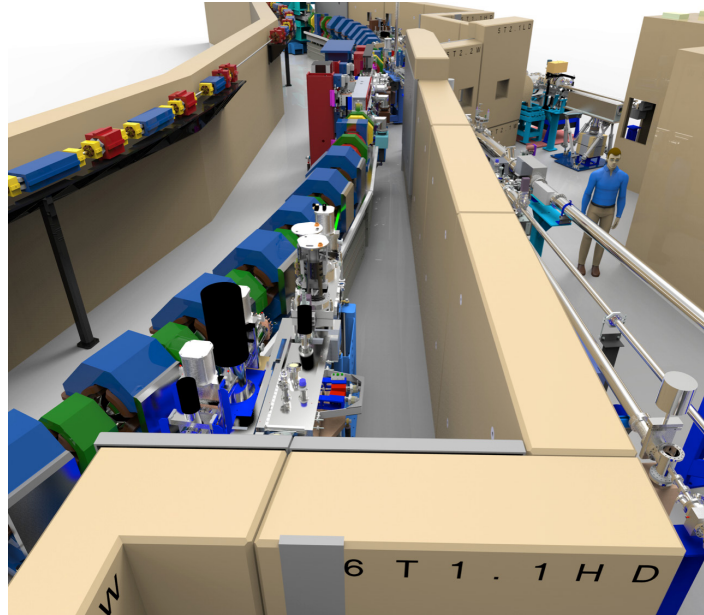


Figure 8: CAD model of ALS-U showing the existing accelerator tunnel with the new storage and accumulator rings.

A comparison of transverse beam profiles (Figure 9) shows that the ALS-U beams will be round and approximately $10\ \mu\text{m}$ in diameter, about 25 times more narrow than the ALS beam in the horizontal direction. The bunch lengths of ALS-U will be more than two times longer to mitigate the impact of intrabeam scattering, making the source more continuous and enabling an almost 10% duty cycle.

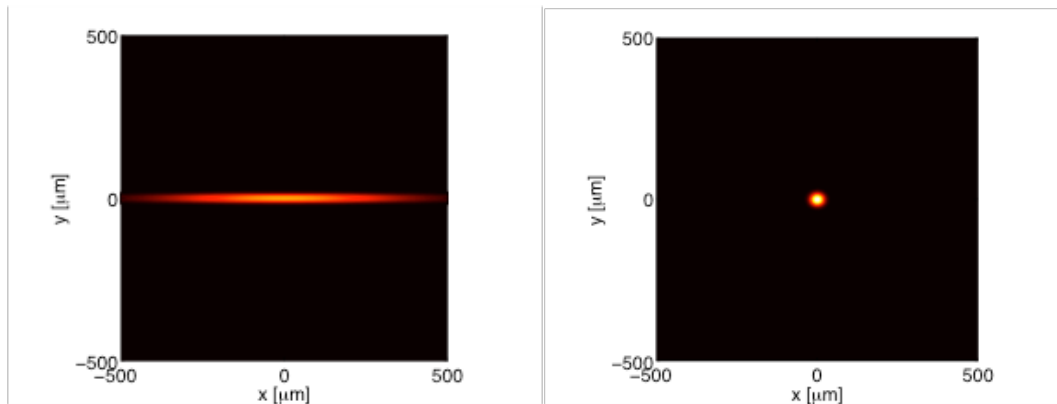


Figure 9: Comparison of the beam profiles of ALS (left) and ALS-U (right).

The coherent flux at several existing and planned storage-ring-based x-ray facilities are shown in Figure 10. NSLS-II currently produces the highest soft x-ray flux in the United States, although it is somewhat lower than MAX IV. SLS-2 in Switzerland will surpass both NSLS-II and MAX IV. ALS-U will provide the highest soft x-ray coherent flux of any existing or planned storage ring up to a photon energy of 3.5 keV, which covers the entire soft x-ray regime.

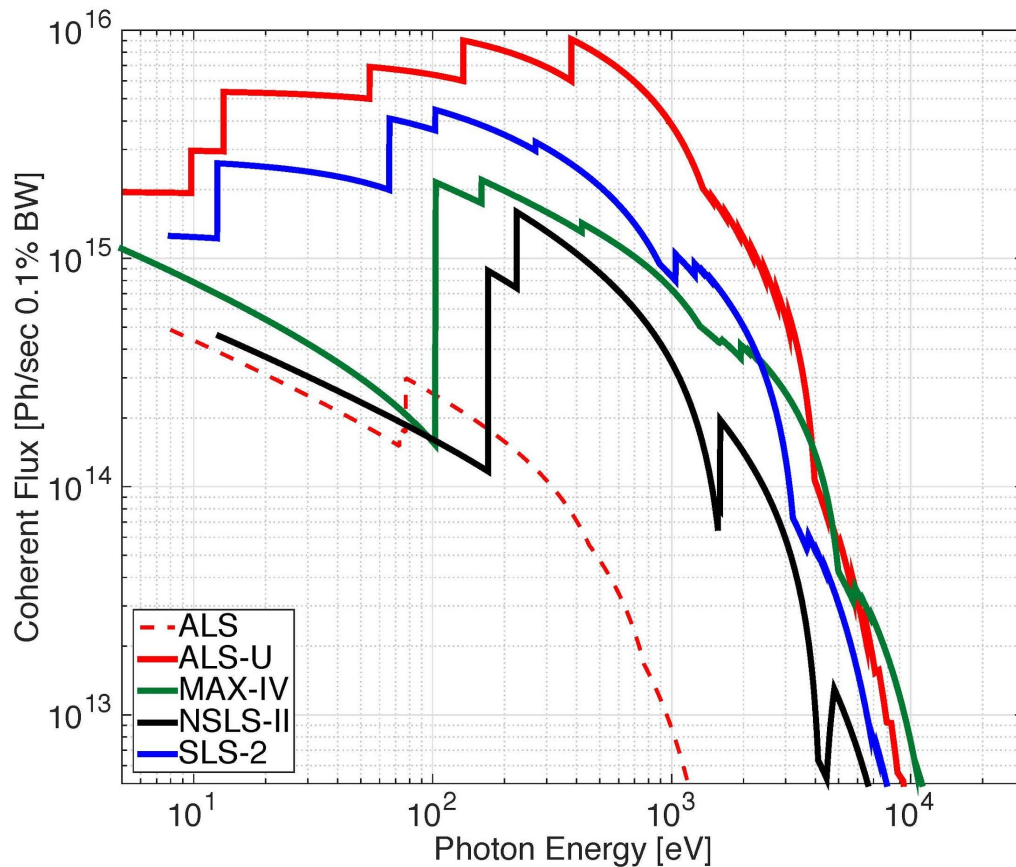


Figure 10: Coherent flux produced by selected storage-ring-based x-ray facilities.

3.1.3.2 *ALS-U R&D progress*

One of the consequences of producing the extremely small emittances in ALS-U is that there is a reduction in the dynamic aperture, which makes traditional off-axis injection difficult, although the momentum acceptance will remain large enough to support good beam lifetime. To overcome this challenge, ALS-U will use on-axis swap-out injection to exchange beam bunch trains between the storage ring and a low-emittance, full-energy accumulator ring. The swap-out mechanism will enable a generational leap in performance. Not only does it allow operating with ultralow emittance, it also makes it possible to employ very small, round chambers in the insertion-device straight sections. These small chambers, in turn, enable higher-performance undulators.

To reduce technical risks and explore new technologies that could provide a large performance advantage, a research and development program was started at the beginning of FY14. The program concentrates on the areas with the highest technical risk or opportunity and is well aligned with the community consensus of remaining challenges of MBA lattices, as well as the special needs of a soft x-ray DLSR [Bei10, Steier14]. In the accelerator area, the R&D includes development programs to demonstrate pulser and kicker technology for swap-out injection, vacuum technology to enable ultimate performance of polarized undulators, harmonic rf systems for bunch lengthening, highly integrated and high-stability magnet and vacuum assemblies, advanced radiation-production sources, and optimization of algorithms and tools for fast commissioning. In the area of beamlines, optical fabrication technology has advanced in the last few years to the point that surfaces can be made with

sufficient accuracy to transport coherent soft x-rays. However, R&D is needed in high-power mirror technology. The current cooling schemes employed are inadequate for wavefront preservation, and a new generation of cooled optics is required.

3.1.3.2.1 Magnets and Radiation Production

To achieve diffraction-limited emittances, quadrupole gradients on the order of 100 T/m are necessary, which is feasible but challenging for high-precision iron-dominated magnets. Other design goals are to provide sufficient space for the vacuum system, low power consumption, reliability, field quality, and ability to align accurately and efficiently, to name a few. Another challenge is the very high packing density, which brings magnets into close proximity. In the case of ALS-U, the typical pole-to-pole distance between adjacent magnets is 75 mm, three times the typical pole gap of 24 mm.

Pre-conceptual designs have been finished for all magnets that are used in the baseline lattice. The magnets are all feasible; however, some of them require special materials or other design features to fit with the vacuum system and achieve sufficient field quality. Figure 11 shows the CAD drawing of the transverse-gradient dipole, a radially offset, C-shaped quadrupole magnet used for the inner seven dipoles of the nine-bend achromat and one option for superbend magnets.

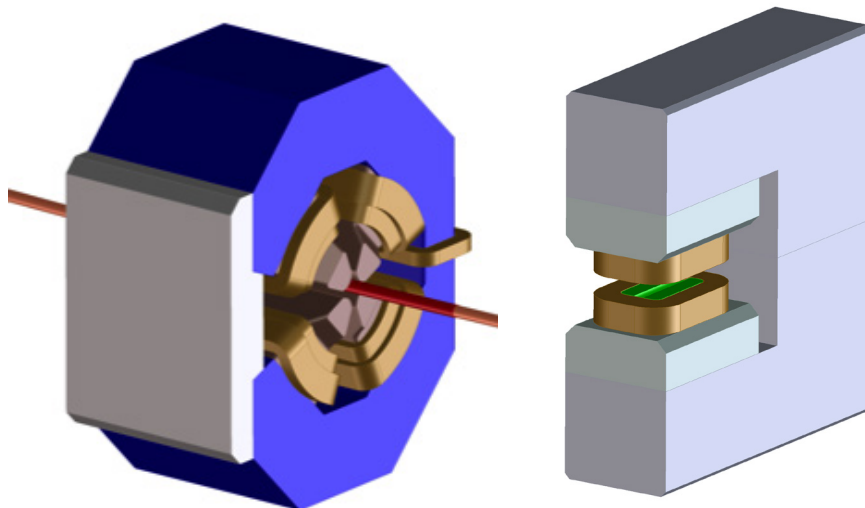


Figure 11: (Left) Conceptual design of an ALS-U transverse-gradient dipole. (Right) Compact s/c magnet with longitudinally shaped field profile to provide hard x-ray radiation.

Multiple design options are being pursued for radiation-producing devices, with the possible options under investigation as part of the ongoing R&D program. The smaller vertical apertures in the ALS-U design present a new opportunity, and even more importantly, equally small horizontal apertures in some straights will enable new undulator technologies with superior performance, especially for experiments requiring polarization control. The current plan for the four new undulators includes the use of devices with polarization control, with two of them being small-gap elliptically polarizing undulators (EPUs) and two of them using more advanced technologies, such as Delta undulators or bifilar helical superconducting undulators.

The ALS experimental program makes extensive use of bending-magnet and superbend source points in addition to undulator sources. Therefore, ALS-U will have to maintain a large number of superbend beamlines, in addition to the insertion-device straights. Engineering studies have shown that superconducting magnets could be built small enough to fit together with two additional quadrupoles

into the slot of one transverse-gradient dipole (see Fig. 11). The field at the source points would be similar to the current ALS.

3.1.3.2.2 Coherence Preserving X-ray Optics

At ALS-U, the source size will be around 25 times smaller in the horizontal direction and will demand surface slope errors of x-ray optics approximately 25 times smaller than today's values. The present internally cooled copper solution reaches the required tolerances for ALS with the present beam size but is far short of the performance needed for ALS-U. To address this problem, we have studied internally water-cooled silicon, side-water-cooled silicon, internally liquid nitrogen (LN2)-cooled silicon, and side LN2-cooled silicon. Figure 12 illustrates one case, that of side-water-cooled silicon. The simulation prediction for optimally side-cooled silicon is $0.1 \mu\text{rads RMS}$, which is well inside the tolerance required. Several avenues are being pursued to validate these simulation results and study practical implementation challenges, especially for the LN2 cooled solutions.

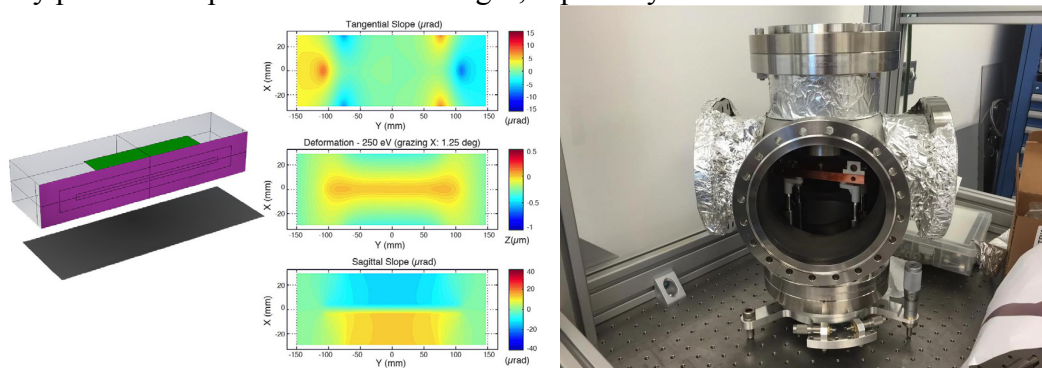


Figure 12: (Left) CAD model of a side-cooled silicon block and resulting deformation for the maximum power load. (Right) interferometric test setup for LN2 cooled Si optics.

3.1.3.2.3 On-axis Swap-out Injection

It is planned to use on-axis injection [Borland09, Steier15] with bunch train swap-out and an accumulator ring. The new accumulator will be housed in the storage ring tunnel. It will act as a damping ring where its lattice will allow for off-axis injection from the current ALS booster and the extracted low emittance beam is injected on-axis into the small dynamic aperture of ALS-U.

On-axis swap-out injection requires special fast pulsers and state-of-the-art stripline kicker magnets (see Fig. 13). Prototype high-voltage pulsers, based on inductive and transmission-line adder technology, are being developed and tested [Steier14] to meet the requirements of ALS-U. Excellent progress has been made and we have demonstrated pulses with the necessary very short rise and fall times, as well as the required flat-top length and flatness for an inductive adder. We are also pursuing industrial partnerships as well as a collaboration with APS-U.

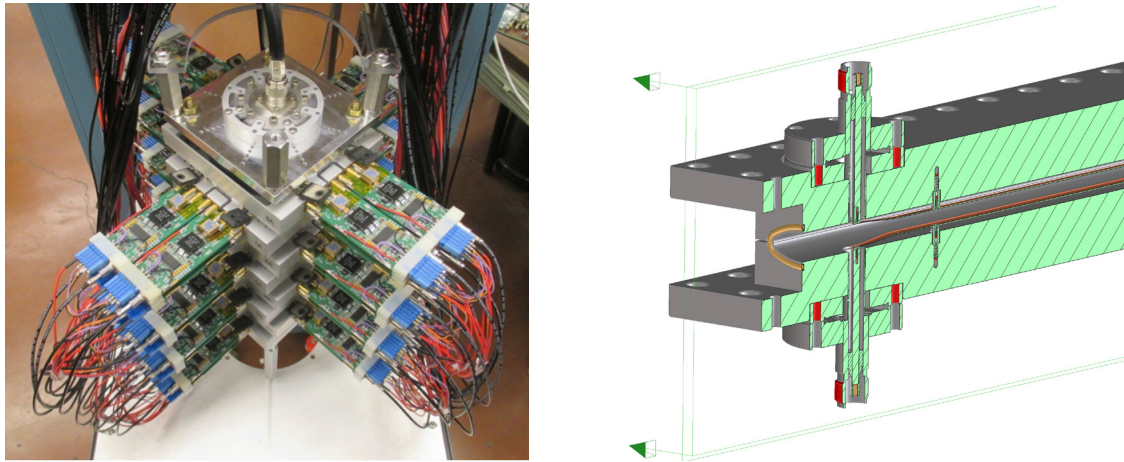


Figure 13: (Left) Full assembly (8 stages) of inductive adder. (Right) CAD model of stripline kicker with small gap and tapered electrodes.

The most effective and direct way to minimize the risks of the interaction of the storage ring beam with the small gap stripline kicker structures [Santis14] is to build, install, and test fully functional kicker/pulsor systems at facilities such as the ALS that have the necessary beam diagnostics and space and that can closely approximate the relevant beam parameters. We have finished the design of such a kicker and are currently manufacturing it. It will be installed later in 2016 for beam tests.

3.1.3.2.4 Vacuum System - NEG Coating

The most promising technology to achieve good vacuum pressures with the small apertures necessary are Non Evaporable Getter (NEG) coated vacuum chambers. Substantial progress has been made, both in industry, and within this R&D program, bringing NEG coated chambers with less than 6 mm diameter within reach [Anders15]. One recent advance at LBNL was the use of Ti-Zr-V alloy wires to improve the chemical uniformity of coatings at small apertures. Challenges remain, including miniaturization of photon extraction chambers.

We have performed detailed simulations of the performance of vacuum-chamber layouts with synchrotron radiation (see Fig. 14). Power densities and the resulting mechanical stresses on the chambers are acceptable. The simulations predict that the average pressure, despite the small vacuum apertures and correspondingly poor conductance, will be similar or better than for the current ALS (i.e. <0.5 nTorr).

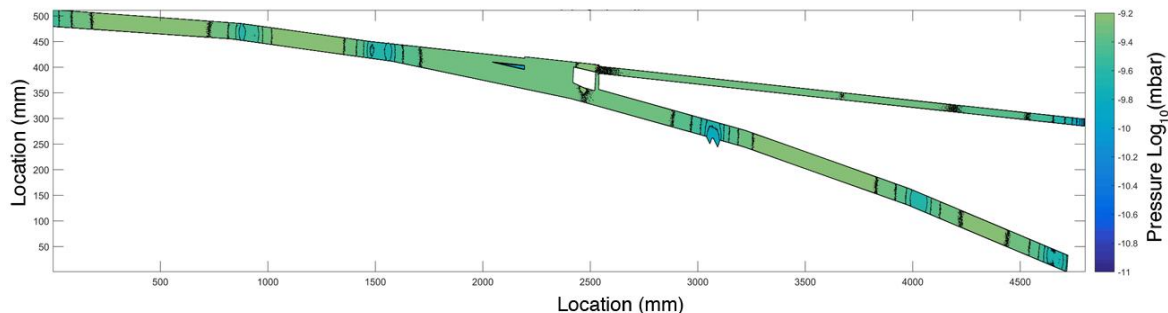


Figure 14: Synrad and Molflow simulation of an undulator photon-extraction chamber geometry with a round Cu chamber. The example chamber shown here spans about the first quarter of one ALS-U arc.

3.1.3.2.5 Intrabeam Scattering and Harmonic Cavities

Intra Beam Scattering leads to emittance increase at larger bunch charge and is a very rapid function of the beam energy. It is more severe at 2 GeV compared to higher energy rings. Therefore, it is

necessary to fill as many buckets as possible, operate with the largest vertical emittance possible, and stretch the bunch length by factors of 3-4 with harmonic RF systems. However, bunch lengthening factors at this level have not been routinely achieved so far. The main reason are transient effects due to inhomogeneities in the fill pattern. Those inhomogeneities can have different reasons. For ALS-U, swap-out injection requires short gaps in the fill pattern. The demonstrated performance of the inductive adder allows gaps as small as 10 ns, i.e. four unfilled buckets. We have replicated this fill pattern in the ALS and have demonstrated lengthening factors of about four, using three normal conducting, passive 3rd harmonic cavities (see Figure 15).

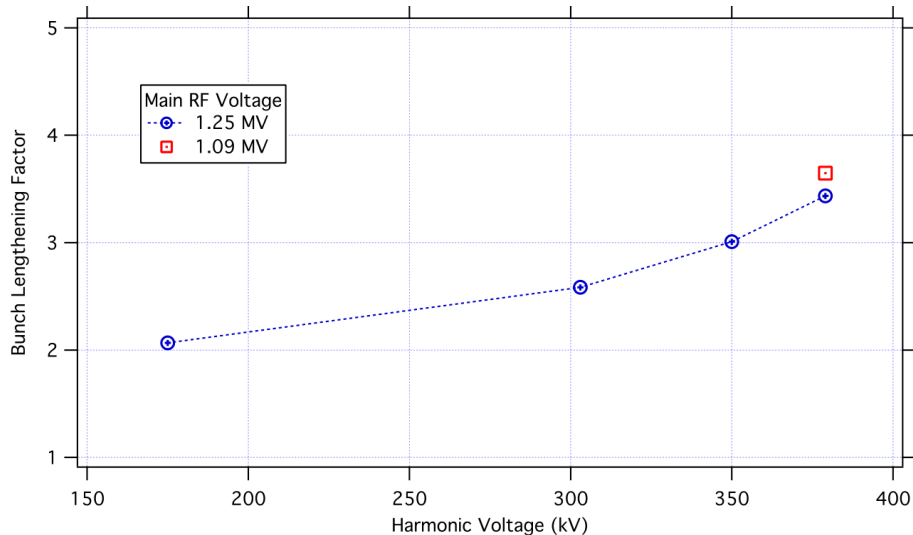


Figure 14: Measured bunch lengths with ALS-U fill pattern in the ALS for various harmonic and main RF voltages.

3.1.4 Summary

The Advanced Light Source (ALS) at Berkeley Lab is one of the first 3rd generation light sources. It has been updated many times with several of those upgrades breaking new grounds in accelerator physics and technology. The ALS remains one of the brightest sources for soft x-rays worldwide and the user program continues to expand. Recent developments in technology, accelerator physics and simulation techniques open the door to even larger future brightness improvements. Similar to proposals at several other 3rd generation sources, this can be achieved by reducing the horizontal emittance with a new ring based on a multi-bend achromat lattice, reusing the existing tunnel, as well as much of the infrastructure and beamlines.

3.1.5 Acknowledgments

The work discussed here is on behalf of the Advanced Light Source and Advanced Light Source Upgrade Development Teams and is based on the efforts of many individuals from the Lawrence Berkeley National Laboratory's Advanced Light Source, Accelerator Technology and Applied Physics, and Engineering Divisions. This work was supported by the Laboratory Directed Research and Development Program of Lawrence Berkeley National Laboratory under U.S. Department of Energy Contract No. DE-AC02-05CH11231.

3.1.6 References

[Barry93] W. Barry, et al., Design of the ALS Transverse Coupled Bunch Feedback System,

- PAC1993, Washington DC, p. 2109
- [Fox93] J. Fox, et al., Feedback Control of Coupled Bunch Instabilities, PAC1993, Washington DC, p. 2076
- [Robin05] D. Robin, J. Krupnick, R. Schlueter, C. Steier, S. Marks, B. Wang, J. Zbasnik, et al., Superbend upgrade of the Advanced Light Source, Nucl. Instrum. Meth. A 538, 1-3 (11 February 2005), 65-92
- [Steier03] C. Steier, et al., Accelerator Physics Challenges of the fs-Slicing Upgrade at the ALS, Proceedings of the Particle Accelerator Conference 2003, Portland, Oregon, May 2003
- [Robin00] D. Robin, C. Steier, J. Laskar, L. Nadolski, Global dynamics of the Advanced Light Source revealed through experimental frequency map analysis, Phys. Rev. Lett., 85, 3, 558 (2000)
- [Steier02] C. Steier, et al., Measuring and Optimizing the Momentum Aperture in a Particle Accelerator, Phys. Rev. E 65, 056506 (2002)
- [Robin08] David S Robin, Weishi Wan, Fernando Sannibale, and Victor P. Suller, Global analysis of all linear stable settings of a storage ring lattice, Phys. Rev. ST Accel. Beams 11, 024002 (28 February 2008)
- [Yang09] L. Yang, D. Robin, F. Sannibale, C. Steier, Weishi Wan, Global optimization of an accelerator lattice using multiobjective genetic algorithms, Nucl. Instr. & Meth. A, 609, 1 (2009) 50-57, doi:10.1016/j.nima.2009.08.027.
- [Steier08] Christoph Steier, et al., Shimming Correction of Dynamic Multipole Effects on Apple-II Type EPU's at the ALS, Proceedings of EPAC 2008, Genova, Italy, June 2008
- [Byrd02] J. Byrd, W. P. Leemans, A. Loftsdottir, B. Marcellis, Michael C. Martin, W. R. McKinney, F. Sannibale, T. Scarvie, and C. Steier, Observation of broadband self-amplified spontaneous coherent terahertz synchrotron radiation in a storage ring, Phys. Rev. Lett. 89, 22, 224801 (2002)
- [Steier09] C. Steier, et al., Successful Completion of the ALS Top-off Upgrade, AIP conference proceedings of SRI 2009, 10th International Conference on Radiation Instrumentation, Melbourne, Australia (2009)
- [Steier03b] C. Steier, et al., Coupling Correction and Beam Dynamics at Ultralow Vertical Emittance in the ALS, Proceedings of the Particle Accelerator Conference 2003, Portland, Oregon, May 2003
- [Steier14] C. Steier, et al., 2014 J. Phys.: Conf. Ser. 493 012030 doi:10.1088/1742-6596/493/1/012030, "Completion of the Brightness Upgrade of the ALS"
- [Madur14] A. Madur, et al., "The Installation and Commissioning of the Advanced Light Source Combined-Function Harmonic Sextupoles for the Low Emittance Upgrade," IEEE Transactions on Applied Superconductivity 24(3), 4100404 (2014). (doi:10.1109/TASC.2013.2283014)
- [Hertlein15] Hertlein, M. P., Scholl, A., Cordones, A. A., Lee, J. H., Engelhorn, K., Glover, T. E., Barbrel, B., Sun, C., Steier, C., Portmann, G. and Robin, D. S. X-rays only when you want them: optimized pump-probe experiments using pseudo-single-bunch operation, J. Synchrotron Rad. 22, 729-735 (2015)
- [Sun13] C. Sun, et al., "Pseudo-Single-Bunch with Adjustable Frequency," Synchrotron Radiation News 26(3), 9-13 (2013). (doi:10.1080/08940886.2013.791209)
- [Sannibale06] F. Sannibale, et al., Tests of a New Bunch Cleaning Technique for the Advanced Light Source, 10th European Particle Accelerator Conference, Edinburgh, UK, 26 - 30 Jun 2006, pp.3463
- [Weber14] J. Weber, C. Lionberger, E. Norum, G. Portmann, C. Serrano, E. Williams, ALS Timing System Upgrade, Proceedings of IBIC2014, Monterey, CA, USA (MOPD18), p. 187
- [Bapiste08] K. Baptiste, J. Julian, S. Kwiatkowski, ALS STORAGE RING RF SYSTEM UPGRADE, Proceedings of EPAC08, Genoa, Italy (MOPD016), p. 478
- [Vetter12] Vetter, K.; Penna, A. J. D.; DeLong, J.; Kosciuk, B.; Mead, J.; Pinayev, I.; Singh, O.;

- Tian, Y.; Ha, K.; Portmann, G.; Sebek, J. NSLS-II Rf Beam Position Monitor Update, in *Beam Instrumentation Workshop (BIW2012)*, Newport News, VA, USA, 238.
- [BCSB14] Berkeley Center for Structural Biology to Receive \$5M from HHMI to Build a New Microfocus Crystallography Beamline, <http://biosciences.lbl.gov/2014/10/24/berkeley-center-for-structural-biology-to-receive-5m-from-hhmi-to-build-a-new-microfocus-crystallography-beamline/>
- [Pappas15] Chris Pappas, et al., DEVELOPMENT OF NONLINEAR INJECTION KICKER MAGNET FOR ALS ACCELERATOR Proceedings of IPAC2015, Richmond, VA, USA (TUPJE084), p. 1837
- [Steier16] C. Steier, J. Byrd, H. Nishimura, D. Robin, S. De Santis, F. Sannibale, C. Sun, M. Venturini, W. Wan, PHYSICS DESIGN PROGRESS TOWARDS A DIFFRACTION LIMITED UPGRADE OF THE ALS, Proceedings of IPAC2016, Busan, Korea. ISBN 978-3-95450-147-2, <http://www.ipac16.org/proceedings/papers/wepow049.pdf>
- [Steier14] Steier, C. Possibilities for a Diffraction-Limited Upgrade of a Soft X-Ray Light Source. *Synchrotron Radiation News* 2014, 27, 18.
- [Tarawneh14] Tarawneh, H.; Steier, C.; Falcone, R.; Robin, D.; Nishimura, H.; Sun, C.; Wan, W. Als-li, a Potential Soft X-Ray, Diffraction Limited Upgrade of the Advanced Light Source. *Journal of Physics: Conference Series* 2014, 493, 012020.
- [Steier11] C. Steier, et al., NIM A, DOI: 10.1016/j.nima.2010.11.077
- [Nishimura07] H. Nishimura, et al., PAC 2007, Albuquerque, p. 1970.
- [Madur12] A. Madur, C. Steier, et al., Magnetic Design of the Advanced Light Source Harmonic Sextupole, *IEEE Trans. Appl. Supercond.* 22, 3 (10.1109/TASC.2012.2184514)
- [Sun12] C. Sun, et al., Small-emittance and low-beta lattice designs and optimizations, *Phys. Rev. ST Accel. Beams* 15, 054001 (2012)
- [Sun12b] C. Sun, et al., New fs-slicing optics, IPAC2012
- [Eriksson08] Eriksson, M.; Hansson, A.; Leemann, S. C.; Lindgren, L. J.; Sjoström, M.; Wallen, E. J.; Rivkin, L.; Streun, A. Using Multi-Bend Achromats in Synchrotron Radiation Sources, in *European Particle Accelerator Conference (EPAC2008)*, Genoa, Italy, 2007.
- [Bei10] M. Bei et al., NIM A (2010), doi:10.1016/j.nima.2010.01.045.
- [Sun16] C. Sun, et al., WEPOW050, Proceedings IPAC 2016.
- [Borland09] M. Borland, AIP Conf Proc 1234, 2009.
- [Steier15] C. Steier, et al., Proceedings of IPAC2015, 1840 (2015).
- [Santis14] S. De Santis, et al., Proceedings of IPAC2014, 1977 (2014).
- [Anders15] A. Anders, et al., AVS 62nd Inter. Symp., San Jose, CA.

3.2 Advanced Photon Source Status Report

V. Sajaev, M. Borland, L. Emery, K. Harkay, Y. Ivanyushenkov, R. Lindberg, N. Sereno,
A. Xiao, A. Zholents

Mail to: sajaev@aps.anl.gov

Argonne National Laboratory, 9700 South Cass Ave, Argonne, IL 60439

3.2.1 Introduction

The Advanced Photon Source is a 7-GeV, third-generation synchrotron light source that provides x-rays in a wide range of spectra from a few keV to a hundred of keV to 48 insertion device and 23 bending magnet beamlines for about 5000 hours per year. APS has been in operation since 1995 [1]. During that period, APS has achieved excellent operational availability, pioneered top-up operation (beam injection with open beamline shutters) [2], introduced high precision x-ray beam position monitors and superconducting undulators. Currently, the storage ring upgrade based on a multi-bend achromat lattice is pursued for APS that will increase the x-ray brightness by more than a factor of 100. This is described in [3], and this article only describes the status of the existing machine.

3.2.2 APS Accelerators

3.2.2.1 *Main parameters and modes of operation*

The Advanced Photon Source is a 7-GeV, 1104-m circumference electron storage ring. The ring consists of 40 nearly identical sectors, each sector has a 6-m-long straight section. Five of those straight sections are occupied by RF cavities and injection magnets, leaving 35 straight sections available for installation of up to 4.8-m-long insertion devices. In many cases two insertion devices share the straight section and in 8 cases a canted assembly is used to support independent operation of two beamlines. Figure 1 shows beta functions for a typical sector. Main APS storage ring parameters are given in Table 1.

Table 1. Main parameters of the APS storage ring

<i>Parameter</i>	<i>Value</i>
Energy	7 GeV
Circumference	1104 m
Nominal beam current	100 mA
Natural chromaticity	-90; -43
Betatron tunes	36.2; 19.27
Momentum compaction factor	2.82×10^{-4}
RF harmonic number	1296
RF voltage	9.5 MV
Energy loss per turn (dipoles)	5.4 MV
Natural emittance	2.5×10^{-9} m
Natural energy spread	9.6×10^{-3}

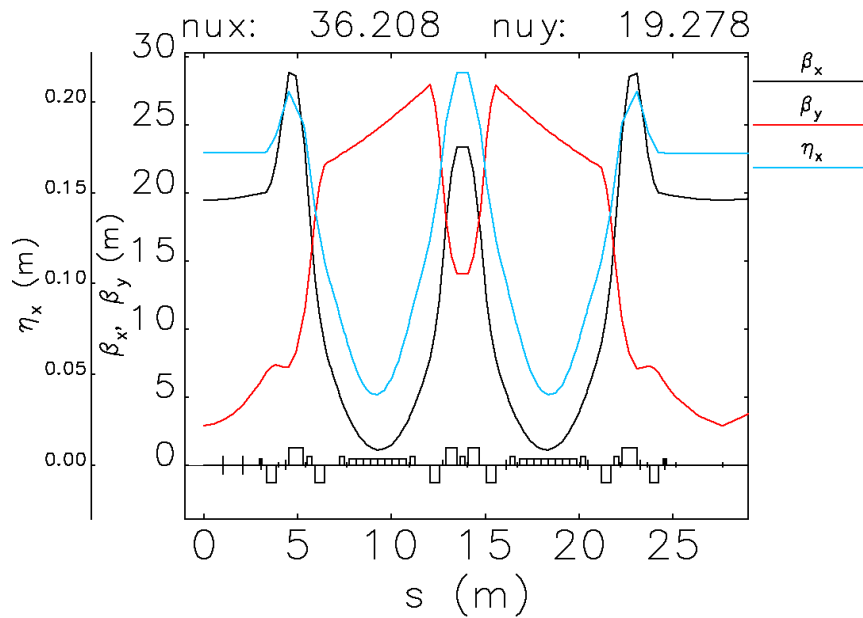


Figure 1. Beta functions of the nominal APS sector

All 400 quadrupoles and all 280 sextupoles are powered separately. This allows for independent tuning of beta functions in different sectors to satisfy user requirements if needed and as allowed by the nonlinear dynamics. For past few years, APS has been providing reduced horizontal beam size to users in sector 32. By reducing horizontal beta function at that location from 20 m to 3 m, the beam size is reduced from 270 μm to 120 μm . Figure 2 shows the beta functions of two sectors around the sector 32 insertion device straight section.

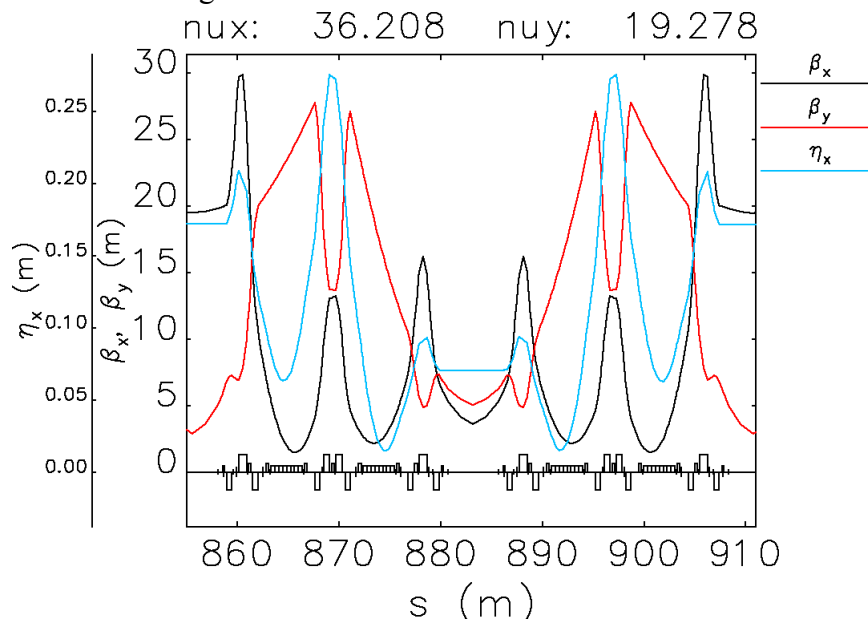


Figure 2. Beta functions of the two sectors with the reduced horizontal beam size straight section in the middle.

APS operates in three fill patterns: 24 equally-spaced bunches, 324 equally-spaced bunches, and the so called “hybrid” fill pattern consisting of one high charge and 56 small charge bunches, with the high charge bunch separated from the “train” of small charge bunches by a 1.5- μs interval on both sides. The 24-bunch fill pattern is the main operation mode, being used about 60% of the time. The

rest of the time is equally split between the other two modes. Table 2 shows the main parameters of these fill patterns.

Table 2. Main parameters of APS operational fill patterns. For hybrid fill pattern, two numbers correspond to high- and small-charge bunches.

	<i>24 bunches</i>	<i>324 bunches</i>	<i>Hybrid</i>
Total current (mA)	100	100	100
Bunch charge (nC)	16	1.1	60 (5.6)
Interval between bunches (ns)	150	11	1500
Bunch length (ps)	33	22	50 (27)
Top-up injection	On	Off	On
Top-up injection interval (min)	2	---	1
Chromaticity	+4; +4	+4; +4	+10; +10
Bunch-by-bunch feedback	ON	OFF	ON
Lifetime (hours)	10	60	5

The APS injector consists of a thermionic RF gun, a 400-MeV pulsed S-band normal-conducting linear accelerator, a 375-MeV Particle Accumulator Ring (PAR), and a booster synchrotron that accelerates beam to 7 GeV. The unique feature of the APS injector is the presence of the PAR that can accumulate several bunches from the linac into a single bunch and allows a high-charge single bunch injection up to 8 nC when needed. This feature is important for a swap-out injection planned for the APS upgrade [3].

3.2.2.2 *Reliability and availability*

Since X-ray experimenters prefer an uninterrupted and constant photon beam, an operational goal is to prevent failures during a running period and to reduce duration of the downtimes required to fix a failure. The high reliability is achieved by: 1) tracking and analysing the downtime statistics, 2) availability of critical “ready to go” spares like a second thermionic gun, power supplies, and klystrons, 3) preventive maintenance, 4) timely replacement of aging equipment, 5) and continuous accelerator improvement program.

The two main reporting parameters are percentage of up-time with photon shutters open (availability) and the mean time between failures (MTBF). The availability is the ratio of the time that the beam is delivered to the users to the scheduled time, with very short up-time periods not counted (see below). In general, the downtime period starts when the beam is not delivered (e.g., beam is stored but withheld from users for some reason) or when the beam current is below 50 mA. The MTFB calculation is the total number of hours scheduled divided by the number of faults, ignoring scheduled maintenance periods. If there are two faults spaced by up to an hour, then only one fault is counted and the downtime duration covers the whole time interval. This rule reflects the minimum useful beam time for x-ray experiments.

The minimum acceptable level for availability is 97% and for MTBF is 70 hours, which are often exceeded. Because we run a fixed number of hours per year (5000), the number of faults per year is an equivalent statistic, with the goal being 71 or fewer faults per year. Figure 3 shows these statistics over many years.

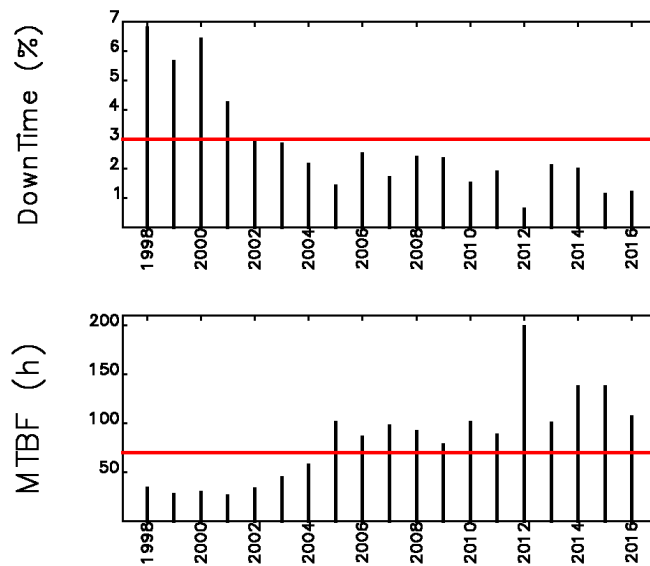


Figure 3. APS downtime percentage and mean time between failures.

During top-up operation we also track the time the stored current is inside and outside the ± 2 mA requirement. Injector downtime -- the cause for the stored current falling out of range -- is recorded as well. A minimum of 8 minutes is given for any injector downtime. The injector availability will therefore necessarily be lower than the current-in-range figure. In 2015 calendar year we were in range 99.0% of the delivered beam time and the injector availability was 98.9% of the delivered beam time.

The next level of reporting is the assignment of down time to a technical group. Each group is allocated a fault rate budget determined by the history of distribution of faults (2005-2007 baseline) and a requirement of more than 70 hours total MTBF with less than 3% total downtime. The data is generated over three time bases: week-by-week, run-by-run, and fiscal year-by-fiscal year. A reliability summary for each technical group is given with group name, unavailability hours, number of faults, mean time to beam loss, and fault per day. These data and reports keep the technical groups accountable for downtime, and provide an incentive to improve performance.

The identification of the cause of downtime (and technical group) can sometimes be difficult. We use a large set of high-level tools to view minor and major EPICS alarms near the time of the beam loss, review and process various EPICS data (i.e. orbit motion movies), and analyze the orbit history to track down the perturbation source location.

After the source of downtime has been determined and assigned, the responsible technical groups address the issue through proper maintenance or design improvement, which then go through an Accelerator Improvement Management System that assigns priority to projects based on their cost and impact. As a result, beam losses of the same type/cause tend not to repeat throughout the years since the underlying problem is resolved through equipment improvement.

3.2.2.3 *Insertion Devices and brightness plots*

As mentioned above, APS has 35 insertion device straight sections that can accommodate devices with a total length of 4.8 m. 53 insertion devices are presently installed including two superconducting planar devices (see below), one double-period revolver [4], and two devices designed to emit variably-polarized radiation [5, 6]. Eight straight sections feature canted insertion devices, with a

canting angle of 1 mrad in all but one case. Others feature dual in-line devices, some of which are used in tandem. Examples of the latter configuration include dual in-line devices with periods of 17.2, 27, and 33 mm, among others. The three most popular periods are 33 mm (29 instances), 30 mm (9 instances), and 27 mm (5 instances). The 33-mm-period device gives continuous tuning starting from 3 keV.

The two installed SCUs have periods of 16 and 18 mm. The 18-mm-period device has a length of 60 periods and is a second-generation device. The 16-mm-period device is only 21 periods in length and was originally a prototype that provided sufficient performance to justify long-term use. It is slated to be replaced by a new device with an 18-mm period.

Figure 4 shows brightness tuning curves for each unique device installed in the APS at present. Each curve is labelled by the number of periods and the period length in mm. The two long-period devices (periods of 125 and 128 mm) are designed for production of variably polarized radiation and are represented by two curves, with the upper, single-harmonic curve being for circular polarization and the lower, multi-harmonic curve for horizontal linear polarization.

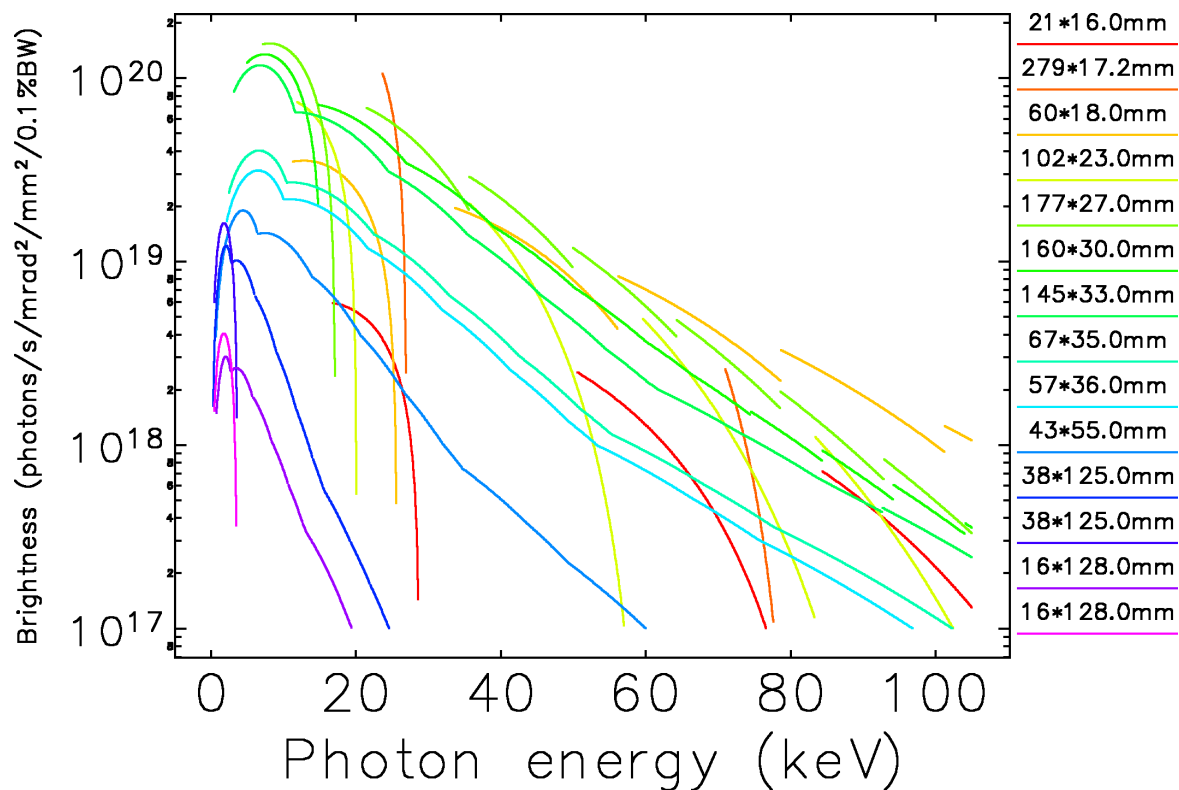


Figure 4. Brightness plots for each unique device. Each plot is labeled by the number of periods of the period length in mm.

3.2.3 Storage Ring Modeling

3.2.3.1 *Lattice*

Almost any storage ring simulation starts with the need to have the correct model of the storage ring lattice. As for most storage rings in the world, APS uses a response matrix fit [7] to derive the lattice model. The response matrix measurement and processing software [8] is written in Tcl/Tk scripting language and uses `elegant` [24] and the SDDS data processing toolkit [9]. A typical response

matrix measurement uses 20 correctors in each plane and takes about 12 minutes to complete. The lattice measurement and correction for operational lattices is generally done once before every three-month run. The required corrections are usually rather small, and the resulting rms beta function beat is normally close to 1%.

APS was one of the early adaptors of the multi-objective genetic algorithm (MOGA) optimization approach [10], which provides tracking-based optimization of lattice performance. One of the early applications of MOGA optimization was improvement of the lifetime for the high-chromaticity hybrid lattice by breaking mirror symmetry of sextupoles within sectors [11].

Another example of the MOGA application is the increase of the dynamic aperture for the high-chromaticity lattice by breaking symmetry around the sector with the smallest aperture vacuum chamber. It is well known that lattices with highly symmetric beta functions are beneficial for the nonlinear dynamics. However, if the physical aperture does not follow the same symmetry as the beta functions, one might imagine a case where breaking symmetry could actually improve the dynamics by better tailoring the local phase space to the physical aperture. At APS, every user sector has small-gap insertion device vacuum chamber with the full horizontal/vertical gaps of 18x7 or 20x8 mm, with one notable exception: sector 4 has vacuum chamber with 15x5 mm gaps. This vacuum chamber is the smallest aperture in the ring, and most of the losses during injection happen at this location. Using MOGA optimization, we were able to arrange sextupoles around this vacuum chamber in such a way that the normally triangular horizontal phase space was changed to a more compressed shape, which increased the dynamic aperture. Figure 5 (left) shows comparison of sextupole strengths in two sectors around the small-gap chamber and two nominal sectors, and Figure 5 (right) shows the improvement of the dynamic aperture measured with a fast kicker.

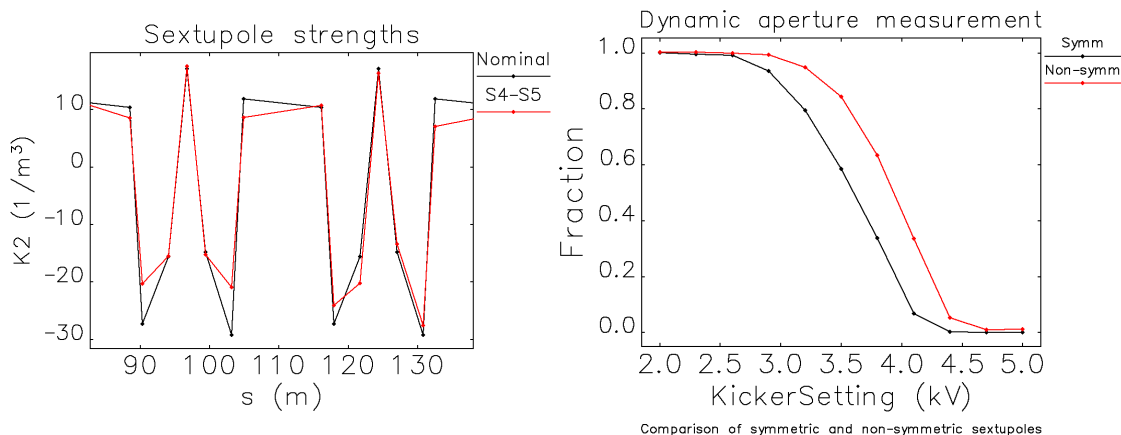


Figure 5. Left: Comparison of sextupole strengths in two sectors around the ID4 small-gap vacuum chamber and two nominal sectors. Right: Dynamic aperture improvement as measured by the fast kicker – about 10% improvement.

3.2.3.2 Collective effects

APS operation must contend with various collective effects that may drive instabilities, as these may lead to an increase in energy spread and/or emittance, or may even result in loss of beam. While many deleterious collective effects can plague electron storage rings, in typical operation the APS does not observe instabilities due to ion or multi-bunch effects; rather, most collective effects at the APS are caused by single-bunch wakefields that are driven by the resistive wall and by changes in the vacuum chamber geometry. Over the past decade there has been considerable progress in identifying sources

of such wakefields, in calculating the associated wakes, and in using these wakes in particle tracking studies to predict various collective effects. In this section we outline our methods for simulating the effects of wakefields on the beam, and how these simulations compare with measurements. More details are available in [12, 13, 14].

The first step in simulating collective effects is identifying sources of impedance and calculating the associated wakefields. We have found that important sources of geometric impedance include the 360 arc BPMs, the 76 narrow-gap ID BPMs, the 240 bellows, the 480 flange gaps, and the 34 ID transition pairs. To determine the associated impedance, we have performed time-domain simulations using a Gaussian bunch of rms length $\sigma_b = 1$ mm in the 3D code GdfidL [15]. This is equivalent to filtering the point particle impedance by a Gaussian filter of frequency width $\sigma_f = c/(2\pi\sigma_b) \sim 48$ GHz. In addition to the geometric impedance, we also calculate the resistive wall impedance associated with the vacuum chamber walls using analytic formulas for an elliptical chamber [16]. We have found that the APS transverse impedance can be roughly divided into three equal contributions coming from the ID transitions, the resistive wall, and the rest of the ring.

The next step is to form a single “impedance element” for the entire ring. For the longitudinal impedance this is determined by simply summing the longitudinal impedance contributions from each element, while in the transverse plane the ring impedance is found by weighting with the local beta-function and summing. We note that this procedure is followed both for the usual dipolar impedance, in which the force on the test particle is proportional to the displacement of the source electron, and also for the quadrupolar impedance whose strength scales with the displacement of the test electron itself.

Once we have calculated the ring impedance, we apply it in the tracking code elegant [24] as a ZLONGIT and ZTRANSVERSE element to make predictions of various collective effects. We track particles through the APS ring using the ILMATRIX element in elegant, which allows for fast, symplectic particle tracking through a periodic cell including chromatic and amplitude-dependent tunes, beta functions, and dispersion. ILMATRIX does this by computing a linear matrix for each particle that is determined both by user-supplied parameters and the particle coordinates. The user-supplied quantities include the Twiss parameters, tunes, dispersion, etc., and how these quantities depend on the particle energy and on the transverse action. Nevertheless, we have found numerically that the predicted collective effects do not depend on higher-order nonlinear effects, so that simulations of the APS that only include the linear optics and chromaticity are sufficient. In addition, we typically employ 200,000 particles in our tracking studies, and track for tens of thousands of turns to predict both equilibrium properties and the current at which single-bunch instability occurs.

We show comparisons of tracking predictions using the impedance model with measurements in Figure 6. First, we find that the predicted longitudinal collective effects agree quite well with measurements; the predicted level of bunch lengthening with current closely follows the measured fit, and the simulation accurately predicts the onset of the microwave instability at ~ 7 mA and the subsequent rise in energy spread. Second, our tracking successfully models the single-bunch instability threshold over a wide range of chromaticity. We use this model prior to the installation of any new components to determine whether they are compatible with high-charge operations.

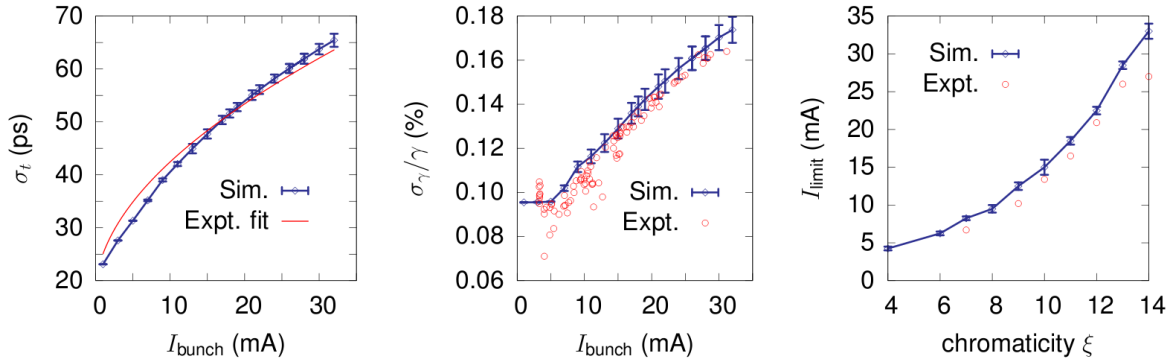


Figure 6. Comparison of APS impedance model predictions to measurements. Left: bunch length as a function of bunch current. Middle: energy spread as a function of current. Right: single bunch current limit as a function of chromaticity. These plots show that both longitudinal and transverse effects are well-predicted.

3.2.3.3 Lifetime benchmarking

For a modern storage-ring-based synchrotron light source, the beam lifetime is mainly limited by the Touschek scattering effect, due to the combination of small beam emittance and moderate beam energy. This effect becomes much more severe for a next-generation light source, for example the planned APS upgrade, particularly in the higher bunch current operation mode. To understand how well the beam lifetime can be predicted, we performed a benchmarking study to compare the analytical beam lifetime formula [17] with measurements.

The formula indicates that the Touschek lifetime is determined by the bunch charge, the local 6D beam size, and the local momentum acceptance. Our measurements were performed with various values of bunch charge, coupling (different transverse beam size), and rf voltage (different bunch length and momentum acceptance). The bunch lengthening effect due to impedance has also been included through measuring bunch length at different bunch current and rf voltage. The local momentum acceptance is calculated using calibrated lattice model (obtained from the response matrix fit). The comparison of measured and calculated (using measured bunch current, rf voltage, coupling and bunch length) beam lifetime is shown in Figure 7. Good agreement ($\sim 5\%$) for most of the cases is achieved. Higher-than-predicted beam lifetime (by about 10%) at lower rf voltage may result from a slight transverse emittance blow up and/or from rf voltage calibration error.

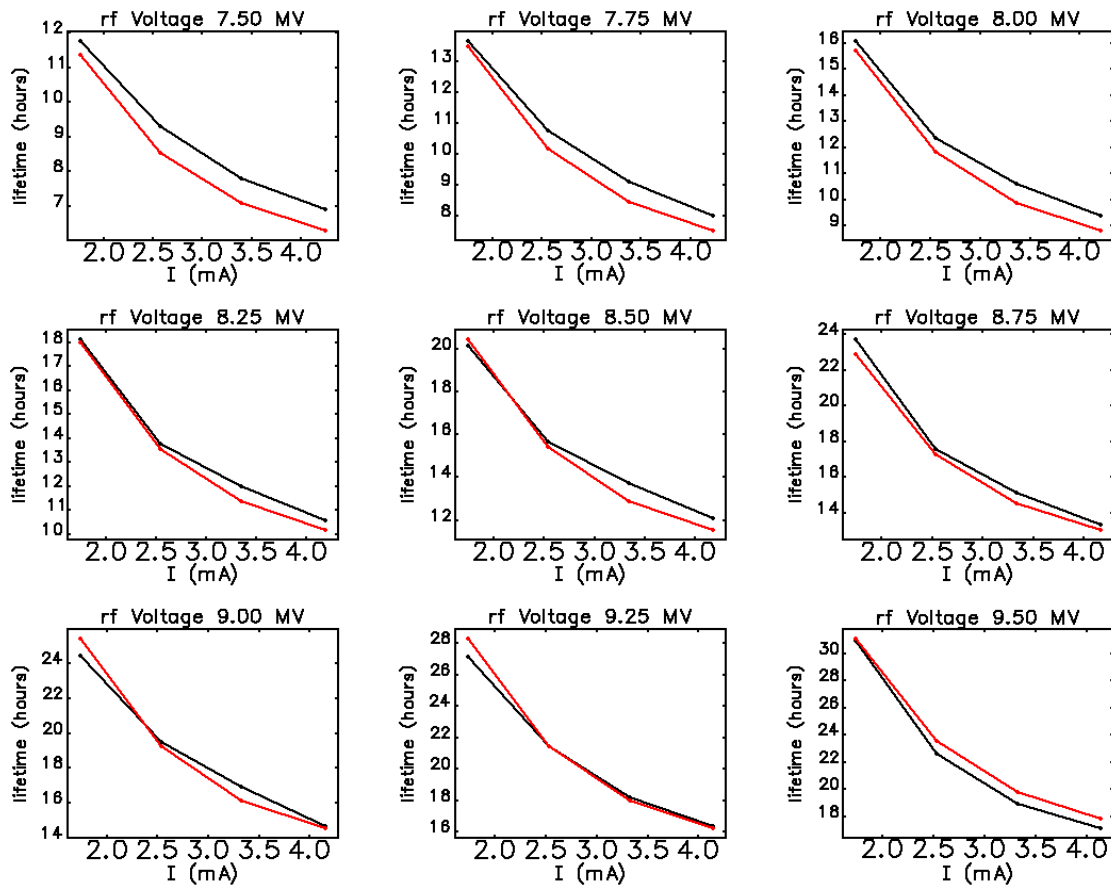


Figure 7. Measured (black) and calculated (red) beam lifetime vs bunch current at different rf voltages.

3.2.4 Beam Stability Improvements

3.2.4.1 *Orbit stabilization developments*

The Advanced Photon Source (APS) monopulse beam position monitor (BPM) system, designed to measure single- and multi-turn beam positions, is one of two BPM systems currently in use to measure and control both AC and DC orbit motions. Recently, all the BPMs in this system were upgraded by replacing its 1992-era 12-bit signal conditioning and digitizing unit (SCDU) with a field-programmable gate array (FPGA)-based system for signal processing [18, 19]. The upgrade, referred to as the BPM Signal Processor-100 (BSP-100) consists of repackaging the broadband rf receiver modules together with a VME Extensions for Instrumentation (VXI) form factor housing eight 14-bit ADCs, an embedded “Coldfire” processor IOC and one Stratix® II FPGA. It can acquire and process data for four monopulse receiver units for both horizontal and vertical planes. Key features of the BSP-100 are the ability to acquire buffers of data at the ADC rate (oscilloscope mode), short and long buffers for turn-by-turn acquisition, and a single-turn buffer to study storage ring injection events. All three acquisition modes are used routinely to improve and monitor storage ring performance. Continuous data processing streams are also available for slow data archiving and a fast data output for use by the real-time feedback system. In storage ring beam measurements, the system achieved good noise floor performance of $\sim 5\text{nm}/\sqrt{\text{Hz}}$ and compared favorably in other aspects with a commercial BPM solution called Libera Brilliance from Instrumentation Technologies [20].

Present short-term orbit stability during user operations with orbit correction running is shown in Table 3.

Table 3. Present short-term rms orbit stability during user operation on BPMs closest to insertion devices.

	<i>0.1 – 30 Hz</i>	<i>0.1 – 100 Hz</i>	<i>Full bandwidth</i>
Horizontal	1.2 μm	3.5 μm	5.5 μm
Vertical	0.5 μm	1.4 μm	3.2 μm

For X-ray BPMs the APS has developed, as part of the APS upgrade (APS-U) project R&D, a next-generation Grazing Incidence Insertion Device (GRID) X-ray BPM [26, 27]. This upgrade is a significant improvement over the existing photoemission BPMs. APS-U beam position stability requirement is several micrometers and require X-ray beam directional stability in 100 nrad range for undulator power exceeding 20 kW. The GRID design is based on hard X-ray fluorescence from copper absorbers in the beamline front-ends. Beam tests in the present APS storage ring demonstrated a 30-fold improvement in signal-to-background ratio over existing photoemission-based (PE) XBPMs. Figure 8 shows the signal to background improvement of the GRID XBPM over the existing PE XBPMs. Stray bending magnet background radiation from the dipole source upstream of the undulators is a primary background, and is nearly eliminated by the GRID design.

In summer of 2015, we included the GRID XBPM located in storage ring sector 27 into the orbit feedback system and demonstrated its use during operations. In the vertical plane, the GRID calibration factor is simply a constant due to pin-hole type imaging. Horizontally, however, the calibration factor depends on gap due to the large variation of horizontal beam size with gap since the white beam angular divergence varies as K/γ . We implemented a lookup table in the control system to automatically change the horizontal calibration depending on the gap settings of upstream and downstream undulators. During weekly operation periods the beam position at the GRID is routinely held to less than 5 microns (which is 20 m away and is equivalent to 300 nrad angular variation at the undulator source) and frequently much less. Operational experience with the GRIDs also demonstrated that the design meets APS-U performance specifications. Two more GRID XBPMs have been installed in sectors 6 and 35 and are being commissioned.

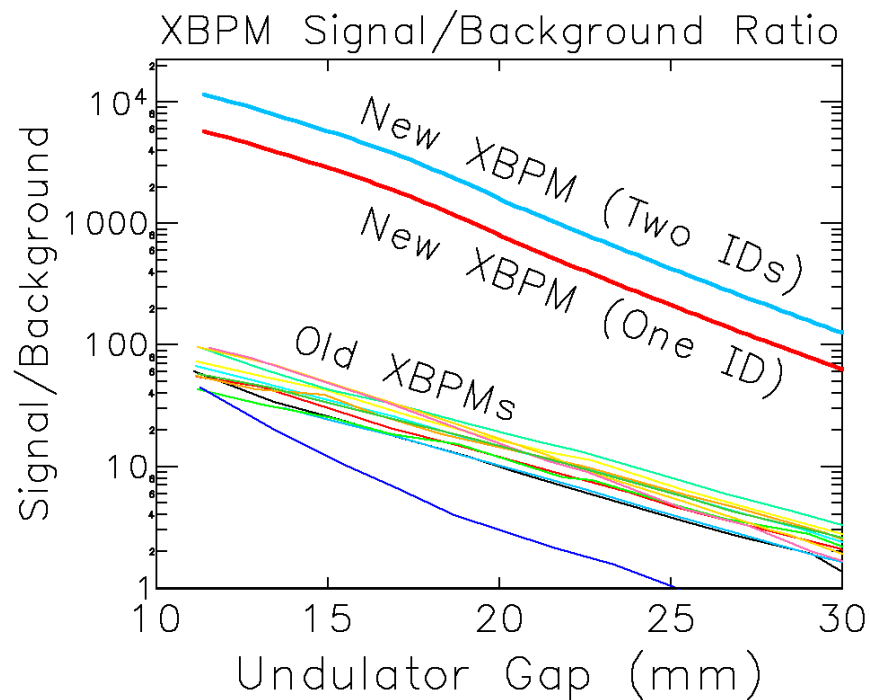


Figure 8. Comparison of the signal to background noise ratio for new and old X-ray BPMs.

As part of long-term beam stability improvements to the existing APS storage ring as well as to identify modifications required to meet stringent APS-U specifications, we have begun an effort to improve insertion device water and storage ring tunnel air temperature stability. The improvements in both areas begin with understanding the legacy systems already in place since 1994, then proposing and implementing improvements. For water systems, better tuning of feedback loops as well as implementing new valve hardware, actuators, temperature sensors, and higher resolution temperature measurement electronics resulted in an improvement by a factor of ten in water temperature regulation, as shown in Figure 9 (left).

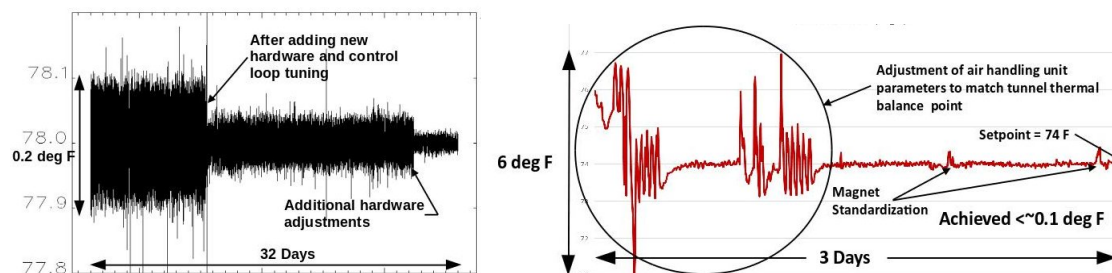


Figure 9. Left: Improvement in water temperature regulation. Right: Improvement in tunnel air temperature stability.

To increase tunnel air temperature stability, various improvements have been made to reduce the impact of outside environmental changes on the tunnel air temperature. The original air handling system design had intake and exhaust vents to the outside and it was found that by simply sealing these vents, tunnel air temperature was no longer driven by large changes in outside air temperature and wind from warm and cold fronts. With the air handling system closed off from the outside, tuning of feedback loops and implementation of more precise control of the fans that distribute air in the tunnel resulted in a factor of ten improvement in air temperature stability, as shown in Figure 9 (right)

in two sectors of the storage ring. We now plan to upgrade the other five air handling units (AHU) around the ring to maintain improved air temperature stability all around the ring.

3.2.4.2 *Automated user steering*

From the start of the APS operations in 1995, if the beamline scientists needed to steer the electron beam to move the radiation source, they were required to communicate with a floor coordinator to make steering requests, who, in turn, communicated with a main control room (MCR) operator to have the steering done using control room software. Then in January 2016, a new steering request protocol was implemented, in which the beamlines communicated with the control room operator directly using a web page form, reducing the turn-around time for steering requests.

In order to give beamlines more convenient (and fast) control of their source points, APS has implemented in June 2016 direct source-point angle steering using EPICS in concert with a workstation-based server script. Now, the beamline scientists enter their request directly into a local workstation window and the effect appears in about 5 seconds (while the old steering request protocols may still be used).

Insertion device (ID) sources, including the canted sectors, and dipole sources can be controlled by their respective users using the same EPICS access security as for ID gap control. We allow only source angle steering and not source position steering (if a position steering is really required for some reason, then the MCR operators will perform it from the control room). Only one source point steering is handled at a time for now, thus a steering lock-out mechanism is implemented to prevent simultaneous steering. This one-steering-at-a-time policy is not an important limitation since the steering action is of short duration. The beamline steering system may be disabled by MCR operators at any time when any operational problem occurs.

These steering events are occurring while the global orbit correction is running continuously at a 10 Hz interval on the 1.5 kHz real-time orbit feedback network. The steering commands are integrated with the global orbit correction by applying a feed-forward bump for the array of beam position monitor setpoints and corrector setpoints. The workstation steering server calculates the appropriate EPICS "delta waveforms" and sends them to the global orbit correction controller which applies these local bump changes asynchronously with and in between the 10-Hz uniform interval orbit correction. The server limits the orbit setpoint change to about 2 μm in one feedforward step, thus several changes are sent by the server at an interval of 1 second until the steering angle is achieved. Since we are feed-forwarding both the BPM and corrector setpoints, there is no interruption of global correction at any time. The complete storage-ring configuration is saved automatically after each steering with a description of the steering in case the storage ring needs to recover from a later fault.

3.2.5 **Accelerator Improvements and Recent and Future Developments**

3.2.5.1 *Superconducting undulators*

APS has been developing in-house superconducting undulator technology since early 2000s. Presently, the APS operates two superconducting undulators – SCU0 in Sector 6 (in operation since January 2013) and SCU1 in Sector 1 (since May 2015) [21]. Their parameters are summarized in Table 4.

Table 4. Main parameters of two operational superconducting undulators at APS

<i>Parameter</i>	<i>Units</i>	<i>SCU0</i>	<i>SCU1</i>
Photon energy at fundamental	keV	17-25	12-25
Period length	mm	16	18
Magnetic length	m	0.33	1.08
Magnetic gap	mm	9.5	9.5
Max undulator field	T	0.8	0.96
Max undulator parameter K		1.20	1.56

Table 5 gives a summary of the operational experience with the SCUs. Operating hours accumulate when the main coil current is above 50 A, and down hours accumulate when the device cannot be operated, in each case while user beam is delivered. Downtime typically occurs when the LHe cooling tank pressure is above a specified operating limit, such as after a quench. Both SCUs exhibited high availability and usage starting in the first years of their operation, a reflection of both their reliability and performance. The ID6 SCU developed a LHe leak in November 2014, which contributed 149 h of downtime, but has since operated with no downtime. The SCUs have self-quenched only a few times over many thousands of operating hours – once for ID1 SCU and six times for ID6 SCU – and these quenches have not caused any beam trips. Both SCUs meet the field quality specifications during a self-quench, which is designed to limit beam orbit perturbations below the Machine Protection System (MPS) trip limit. Self-quenches only produce brief orbit motion of about ± 0.1 mm, which is well within the MPS trip limit of ± 0.5 mm.

Table 5. APS SCU operational statistics.

Calendar year	APS delivered hrs	ID6 SCU operating hrs	ID6 SCU down hrs	ID6 SCU avail.%	ID1 SCU operating hrs	ID1 SCU down hrs	ID1 SCU avail.%
2013	4871	4189	20	99.6	-	-	-
2014	4926	4391	174	96.5	-	-	-
2015	4940	4834	0	100	-	-	-
May-Dec, 2015	3241	-	-	-	3059	0.1	99.997
Jan-Jul, 2016	2871	2797	0	100	2695	0.3	99.99

3.2.5.2 *Abort system*

Protection against beam-loss-induced quenches is a well-known issue in high-energy proton accelerators that use superconducting magnets. Superconducting wigglers and SCUs employed at synchrotron light sources have quench-detection interlocks to protect the magnet; however, characterizing and mitigating beam-loss-induced quenches is reported only at APS and Canadian Light Source [22]. At APS, both SCUs were found to quench often during beam dumps triggered by the Personnel Safety or Machine Protection Systems, with ID6 SCU quenching more often (SCUs are powered off prior to manual beam dumps). Quenches can occur when less than 1 nC is lost in the coils, which is less than 0.3% of the total stored beam. For both SCUs, quench recovery is typically fast enough to allow them to be operated once the beam is restored; however, such quenches are best minimized.

In January 2016, a new beam abort system was implemented at APS that works in tandem with the existing beam dump system [23]. Its purpose is to control the beam loss location and, thereby, minimize beam loss-induced quenches at the two SCUs. The abort system consists of a dedicated horizontal kicker designed to kick out all bunches in a few turns after being triggered by MPS. The abort system concept was developed on the basis of single- and multi-particle tracking simulations using *elegant* [24] and bench measurements of the kicker pulse. The design loss location is the injection straight section vacuum chamber. Performance of the abort system – kick amplitudes and bunch loss distributions – was analysed using beam position monitor turn histories and found to agree reasonably well with the model. BPM loss distributions are consistent with fast fiber-optic beam loss diagnostics installed at the SCUs [25].

When the beam is dumped by the Machine Protection system (MPS), the rf power is turned off, and the beam spirals in for about 60 turns before it gets lost on vacuum chamber walls. When the beam is dumped by the Personnel Safety System (PSS), the dipole is turned off in addition to the rf, and beam losses occur before MPS detects beam centroid motion. Most beam dumps are triggered by MPS, with only about 10% being triggered by PSS. The abort kicker is ineffective for PSS dumps because beam is lost before the kicker is triggered. We accept this inconvenience since PSS dumps are typically a rare occurrence.

To avoid beam losses on the ID1 SCU upstream photon absorber, the abort kicker pulse is delayed by 25 turns relative to the MPS trigger to allow the beam to move closer to the inboard wall. This improves the ID1 SCU protection during MPS dumps. The ID6 SCU photon absorber does not intercept aborted-beam losses, and the abort system protects ID6 SCU with or without delay.

The abort system has worked reliably so far. As designed, the kicker remains charged during user operations and discharges consistently on MPS events. Between January and July, 2016, the ID6 SCU quench rate decreased dramatically from 80% to 18% of beam dumps, while the ID1 SCU quench rate actually increased slightly from 23% to 27% of beam dumps. The increase of quenches in ID1 SCU is attributed to an unusually high rate of PSS-related dumps during first three months of 2016 – 40% of all dumps – and the abort kicker system is known to be ineffective with PSS beam dumps.

3.2.5.3 *Helical undulator*

Following successful installation and operation in the APS storage ring of two planar superconducting undulators (SCUs), the APS SCU team has expanded its scope of work to include a superconducting helical undulator (HSCU). The goal of this project is to design, fabricate and install in Sector 7 of the APS a circular polarizing superconducting undulator that would provide photons in 6-12 keV range. The expected spectrum of HSCU radiation is shown in the Figure 10.

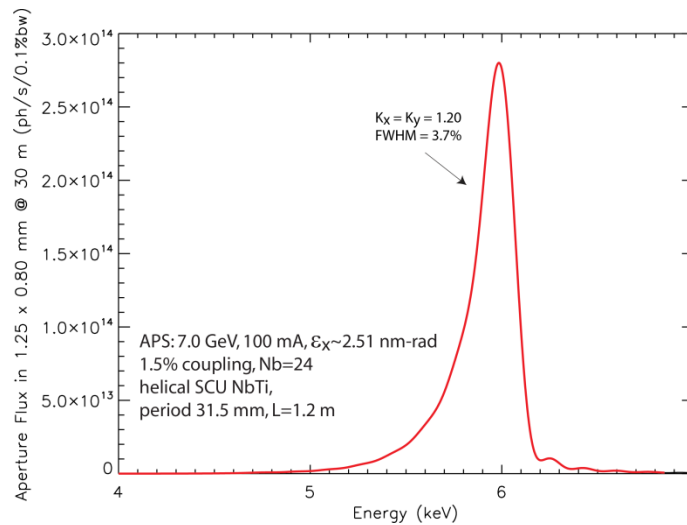


Figure 10. Design spectrum of the helical SCU being designed at APS

The challenging task of fabricating a precise helical core is currently being addressed. We have developed a novel scheme of continuous winding of the helical undulator magnet that has been tested on two short 2-cm-period prototypes wound with NbTi superconductor. These test magnets (one with an aluminum core and the other with an iron core) required almost no training during cold testing in a liquid He bath, as the first quenches occurred above the design currents. This work is now expanding to fabrication of 3.15-cm period cores. In parallel, a cryostat for HSCU is being designed. It will use a smaller and cheaper vacuum vessel compared to SCU0/SCU1 cryostat, and it has already been ordered. A prototype of the HSCU beam chamber is being fabricated as well.

Due to its small horizontal aperture, the installation of the helical undulator will require the local change of beta functions to increase the acceptance of the chamber. A lattice with horizontal beta function reduced from nominal 20 m to 10 m has been developed and successfully tested.

3.2.6 Conclusion

After more than 20 years of operation, the Advanced Photon Source remains one of the brightest synchrotron radiation sources in the world, as well as one of the most reliable. APS provides light to thousands of users annually using its 48 insertion device and 23 bending magnet beamlines. The exceptional performance of APS owes much to the foresight of the designers and to the continued creativity and diligence of APS staff. At the same time, there is rapid progress towards the APS upgrade, which will ensure that APS continues to drive scientific progress in the years to come.

3.2.7 Acknowledgements

This work is supported the U.S. Department of Energy, Office of Science, Office of Basic Energy Sciences, under Contract No. DE-AC02-06CH11357.

3.2.8 References

1. J. Galayda, "The Advanced Photon Source," Proceedings of the PAC 1995, 4-8 (1995)
2. L. Emery and M. Borland, "Top-up Operation Experience at Advanced Photon Source," Proceedings of the PAC 1999, 200 (1999)
3. S. Henderson, "Status of the APS Upgrade Project," Proceedings of the IPAC 2015, 1791

- (2015)
4. B. Stillwell, J. H. Grimmer, D. Pasholk, E. Trakhtenberg, M. Patil, “New concepts for revolver undulator designs,” Proceedings of 2015 IPAC, 750-752 (2015).
 5. M. Jaski, M. Abliz, R. Dejus, B. Deriy, E. Moog, I. Vasserman, A. Xiao, and E. Gluskin, “An electromagnetic variably-polarizing quasis-periodic undulator,” Proceedings of the 2013 PAC, 1064-1066 (2013).
 6. E. Gluskin, N. Vinokurov, V. Tcheskidov, A. Medvedko, Yu. Evtushenko, V. Kolmogorov, P. Vobly, E. Antokhin, P. Ivanov, I. B. Vasserman, E. M. Trakhtenberg, P. K. Den Hartog, B. Deriy, M. Erdmann, O. Makarov, E. R. Moog, AIP Conf. Proc. 521, 344-347 (2000).
 7. J. Safranek, “Experimental determination of storage ring optics using orbit response measurements,” NIMA 388, 27-36 (1997)
 8. V. Sajaev, L. Emery, “Determination and Correction of the Linear Lattice of the APS Storage Ring,” Proceedings of the EPAC 2002, 742-744 (2002)
 9. R. Soliday, M. Borland, L. Emery, H. Shang, “New features in SDDS toolkit,” Proc. of the PAC 2003, 3473-3475 (2003)
 10. I. Bazarov and C. Sinclair, “Multivariate optimization of a high-brightness DC gun photoinjector,” PRST-AB 8, 034202 (2005)
 11. M. Borland, L. Emery, V. Sajaev, A. Xiao, “Application of Direct Methods of Optimizing Storage Ring Dynamic and Momentum Apertures,” Proceedings of the ICAP 2009, 255-258 (2009)
 12. Y. C. Chae, “The impedance database and its application to the APS storage ring,” Proceedings of the 2003 PAC, 3017-3019 (2003)
 13. Y. C. Chae and Y. Wang, “Impedance database II for the Advanced Photon Source storage ring,” Proceedings of the 2007 PAC, 4336-4338 (2007)
 14. R. R. Lindberg and A. Blednykh, “Instability thresholds for the Advanced Photon Source multi-bend achromat upgrade,” Proceedings of the 2015 International Particle Accelerator Conference, 1822-1824 (2015)
 15. W. Bruns, <http://www.gdfidl.de>
 16. A. Piwinski, DESY-94-068 (1994)
 17. A. Piwinski, “The Touschek effect in strong focusing storage rings,” DESY Report No. DESY 98-179, 1998
 18. R. Lill, A. Pietryla, E. Norum, F. Lenkszus, “Design of the APS RF BPM Data Acquisition Upgrade,” Proceedings of the 2005 PAC, 2005
 19. H. Bui, G. Decker, R. Lill, A. Pietryla, W. E. Norum, “Performance of FPGA-based Data Acquisition for the APS Broadband Beam Position Monitor System,” Proceedings of BIW08, 2008
 20. S. Xu, G. Decker, H. Bui, H. Shang, F.R. Lenkszus, R. Laird, C. Yao, “Comparative Measurements of Libera Brilliance and BSP-100,” Proceedings of IPAC’10, Kyoto, Japan, 2010
 21. Y. Ivanyushenkov et al, “Development and operating experience of a short-period superconducting undulator at the Advanced Photon Source,” Phys. Rev. ST Accel Beams 18, 040703 (2015)
 22. W.A. Wurtz et al, Proc. 2014 IPAC, p. 1992 (2014)
 23. K.C. Harkay et al., “Development of an abort kicker at APS to mitigate beam loss-induced quenches of the superconducting undulator,” Proceedings of the 2015 IPAC, p 1787 (2015)
 24. M. Borland, “elegant: A Flexible SDDS-Compliant Code for Accelerator Simulation,” Technical Report ANL/APS LS-287, Advanced Photon Source (2000)
 25. J.C. Dooling, K.C. Harkay, Y. Ivanyushenkov, “Fast beam loss diagnostic to quantify charge deposition in APS superconducting undulators,” ICFA Beam Dynamics Newsletter 66, p. 24

(2015)

26. D. Shu, B. Rodricks, J. Barraza, T. Sanchez, T. Kuzay, NIMA 319, 56 (1992)

27. B. X. Yang, et. al., Proceedings of the BIW 2012, 235-237 (2012)

3.3 LCLS FEL Operations

Axel Brachmann for the LCLS team
 Mail to: brachman@slac.stanford.edu
 SLAC, Menlo Park, CA 94025, USA

3.3.1 Abstract

The LCLS has operated as a user facility since October 2009 [1, 2] and has continually delivered X-ray beams to the LCLS users. After initial commissioning, many upgrades took place, extending the operating range of available X-ray photon energies, X-ray pulse energies, pulse lengths and also adding new capabilities such as polarized beams and advanced diagnostics. This paper will describe the most significant upgrades, new capabilities, performance and future plans.

3.3.2 Introduction

Many LCLS experiments are enabled by techniques that are based on manipulating the electron beam or the photon beam as it is generated and amplified by the LCLS undulator system. The development of these capabilities began immediately after establishing the LCLS facility. In all cases, the conception of a new delivery capability is driven by the needs of the LCLS science program and strives to provide the often challenging X-ray beam conditions needed by LCLS users to successfully complete experiments conducted at LCLS. Often, this work results in unexpected new modes, for example the dechirper project's main goal was to gain independent control of the electron bunch energy spread but in addition led to a new bunch length diagnostic tool suitable for atto-second timescales. Furthermore, the device allows the generation of dual bunch separated by several eV's, which can serve as a new tool for pump-probe experiments. New diagnostics such as the X-band transverse deflecting cavity (XTCAV) are important to understand in detail the physics of the FEL process. Often, new diagnostics are not only used for optimizing the electron and photon beams but also provide means to measure additional beam parameters that can be used by LCLS experiments to resolve intricacies of the physical processes under investigation.

The capabilities of LCLS are constantly evolving. The most significant accomplishments for the last several years are Hard and Soft X-ray self-seeding, polarized X-ray beams, XTCAV bunch length diagnostic, extensions of the beam energy envelope, dual-pulse and dual-energy bunches and the dechirper for energy spread control using wake-fields. We will briefly describe these new capabilities and provide references for more detailed information

3.3.2.1 *Hard and Soft X-ray Self Seeding*

Systems for Self-Seeded X-ray beams have been implemented at LCLS, both for hard (HXRSS) [3] and soft X-rays (SXRSS) [4]. Hard X-ray Self-Seeding is based on diffraction of the X-rays using a diamond crystal (figure 1), there as for soft X-rays a ruled diffraction grating is used. Seeded beam provide near Fourier transform limited beams (e.g. 0.16 eV at 530 eV, 0.5 eV at 8 keV) maintaining very high peak power (10's of GW) but with 2 to 5 times higher spectral brightness. Figure 2 shows a typical spectrum and comparison to normal SASE operation.

Seeded beams became available to users in 2013 (HXRSS) and 2015 (SXRSS). Many experiments have been carried out using these advanced capabilities, an example is the investigation of X-ray scattering dynamics in warm dense matter (Fletcher et al., Nature Photonics, 9 274, 2015).

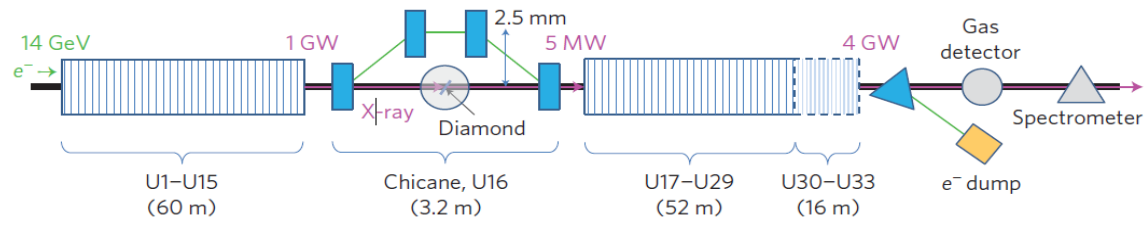
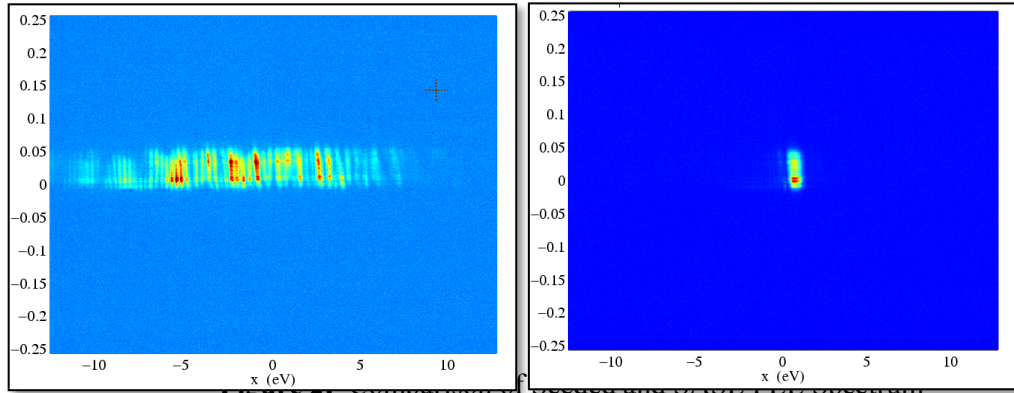


Figure 1:
LCLS
Hard X-
ray Self-
Seeding
System



3.3.2.2 Polarized X-ray Beams

Since 2015, LCLS provides polarized X-rays in the soft energy spectrum (500 eV – 1200 eV) [5]. A photon beam with $\sim 99\%$ degree circularly polarized photon beam can be delivered to users with up to 200 μJ pulse energy. This has been achieved by the development, installation and commissioning of new type of undulator, consisting of 4 independently movable rows of undulator magnets. Based on the shape of the undulator magnets, the device has been named the ‘DELTA’ undulator. An on-axis view is depicted in figure 3. Figure 4 shows the full ~ 3 m long undulator installed at the end of the ~ 100 m long LCLS undulator beam line. It is possible to control the degree of circular, vertical, horizontal and any non-rotated elliptical. Reverse taper of the regular undulator system and diversion of the linearly polarized beam aids in achieving high degrees of helical polarization. This technique is illustrated in figure 5 and described in detail in reference [5]. Polarized beams have been used to demonstrate the magnetic circular dichroism in GdFeCo films. In comparison with similar experiments at a conventional synchrotron light source, using a high brightness polarized FEL beam accomplishment such an experiment in minutes compared to hours or days.

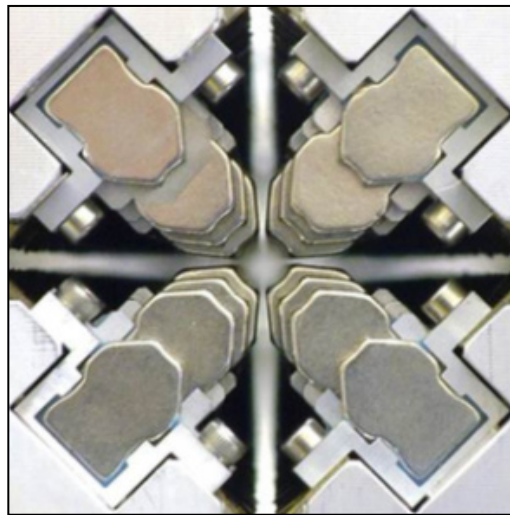


Figure 3: On axis view of the DELTA undulator

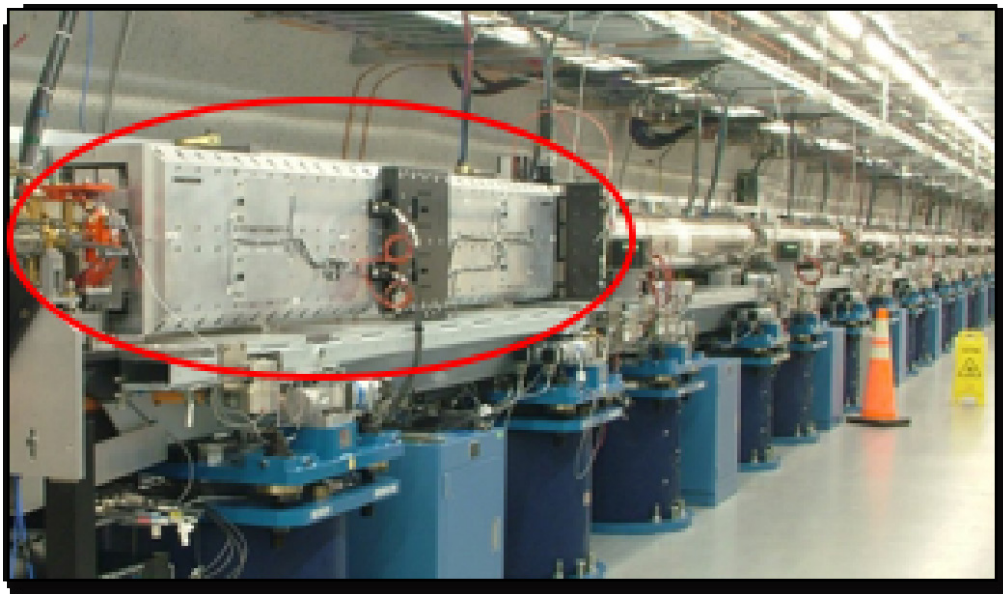


Figure 4: DELTA undulator installed at LCLS at the end of the undulator beamline.

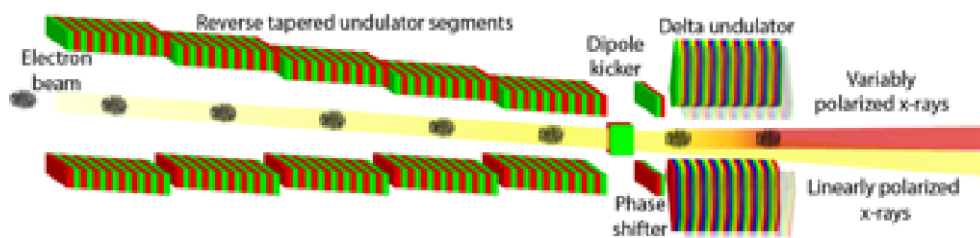


Figure 5: Reverse taper and beam diverting [5]

3.3.2.3 X-Band Transverse Deflecting Cavity

Since 2014, an X-band RF transverse deflector cavity (XTCAV) is available at LCLS [6]. It enables the measurement of electron beam bunch lengths with femtosecond resolution. In addition, data analysis allows the derivation of the corresponding photon pulse **structure and energy distribution**. The arrangement of the deflecting RF structure with respect to the FEL systems is shown in Figure 6. Figure 7 is an image of the actual device installed downstream of the undulator. This device is analyzing the electron bunch after the FEL process took place and therefore can be used as a non-invasive diagnostic.

This measurement enables us to resolve intricate details of the FEL lasing process and consequently improve the accelerator tuning procedures. An example is shown in figure 8. The data are available to the X-ray instruments and provide detailed time resolved information of X-ray photon pulse structure used to conduct the LCLS experiment. More recently, a compact, X-band SLAC Linac Energy Doubler cavity (SLED) has been designed and installed providing a factor of two time resolution improvement for high-energy, hard x-ray operation.

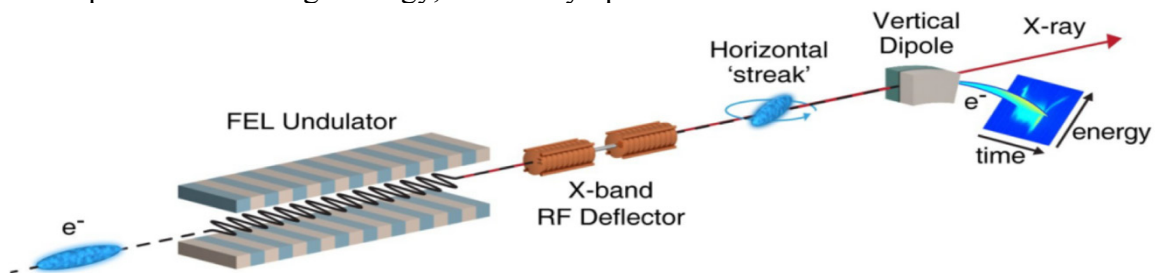


Figure 6: X-band transverse deflecting cavity (XTCAV) diagnostic for bunch length measurements.

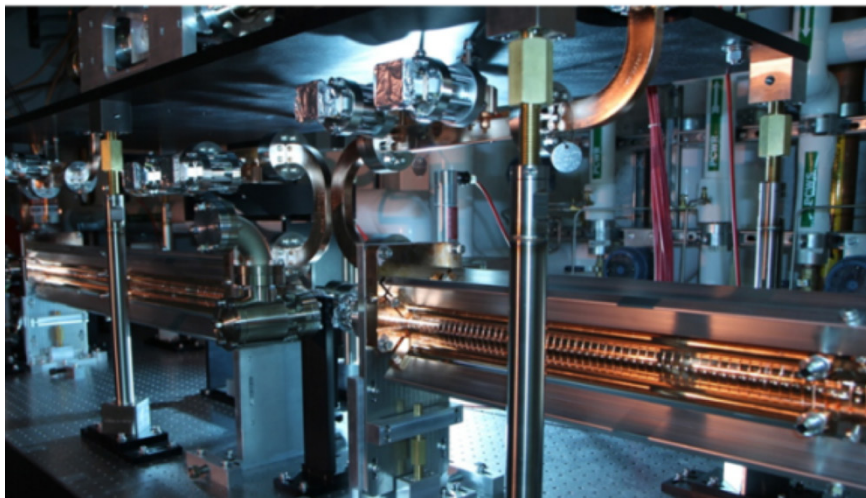


Figure 7: XTCAV installed at LCLS.

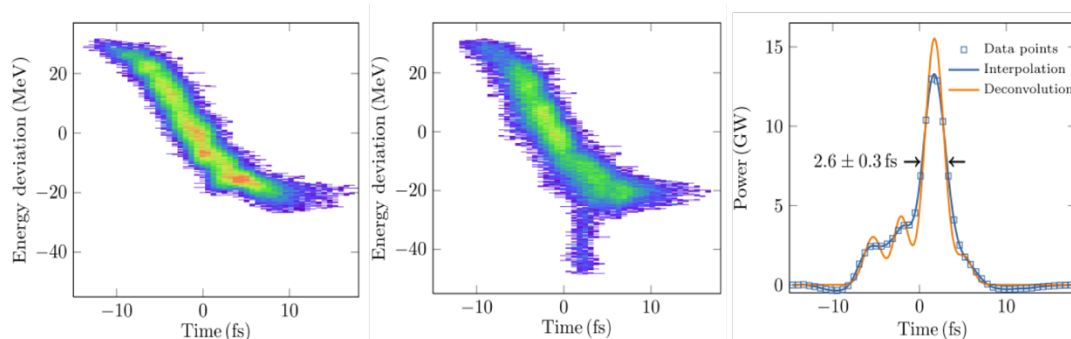


Figure 8: XTCAV measurements. Left – Electron bunch distribution without FEL lasing; Middle – Electrons that contribute to the FEL lasing process lose energy; Right – derived X-ray bunch profile.

3.3.2.4 *Extending the energy envelope*

During the last 2 years, the energy range of the LCLS FEL has been extended both beyond the low and high energy limits. The motivation for extending the energy range up to 12.9 keV is the reach of the Se K-edge at 12.7 keV. High photon energy is also desirable to increase the resolution of X-ray protein crystal structure determination. After initial demonstration of feasibility in 2015, we further developed the accelerator setup to be able to routinely deliver a photon beam at this energy. It requires utilization of the full currently installed high power RF complement of the LCLS linac.

Earlier in 2015, the accelerator was set-up to deliver X-rays to a photon energy of 280 eV, extending beyond the LCLS design baseline of the 500 eV. The extension into this energy region allows science using the nitrogen and carbon absorption energies (at 400 eV and 280 eV, respectively). For example, we delivered 400 eV photons to the experiment LH97 (‘Direct verification of the role of short-lived intermediates in catalytic N₂ fixation’). The entire energy reach of LCLS including pulse energies recently delivered to LCLS experiments is shown in figure 9.

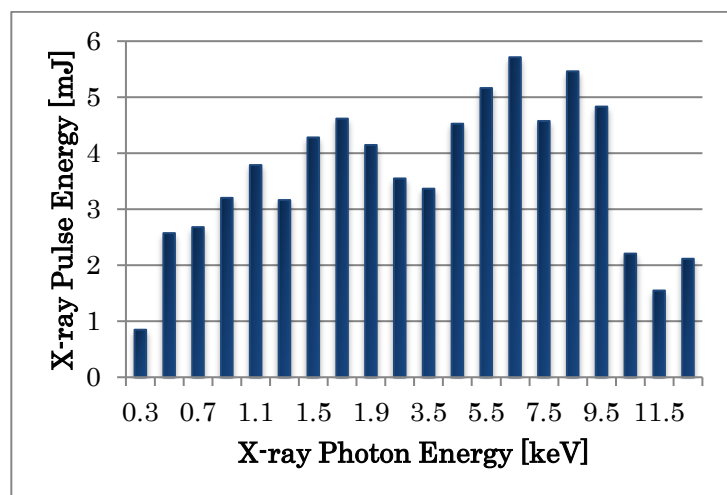


Figure 9: LCLS X-ray energy range and delivered pulse energies to LCLS users for Soft and Hard X-rays.

3.3.2.5 Dual Color and Dual Bunches at LCLS

Two color x-FELs have received considerable attention at fourth generation light sources, since they enable a wide range of applications from bio-imaging to time-resolved studies of atomic physics. Many accelerator based schemes have been developed to achieve two-color operation [7-11]. Table 1 summarized the dual bunch modes currently available at LCLS. While no individual scheme can meet all the requirements set by the large X-ray user community, each scheme can meet a set of requirements for some specific applications. Techniques include the split undulator scheme (Fig. 10), the generation of dual pulses by using a pulse stacker as part of the photo-injector laser system (Fig. 10), the generation of dual pulses by using a pulse stacker as part of the photo-injector laser system (Fig. 11), dual slotted emittance spoilers (foils) integrated into the dispersive region of the second bunch compressor [12], and fresh-slice by using the dechirper [13]. Dual pulses can be delivered in seeded and SASE FEL operational modes (figure 12) [10].

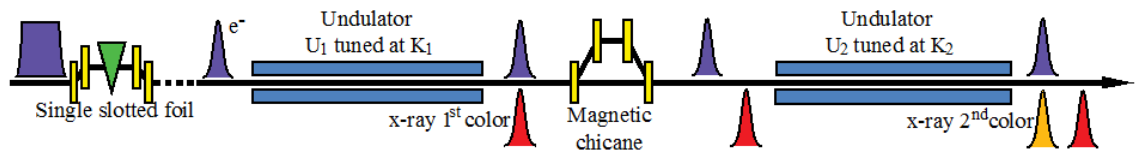


Figure 10: Generation of dual-pulses of femtosecond to picosecond separation with the split undulator scheme.

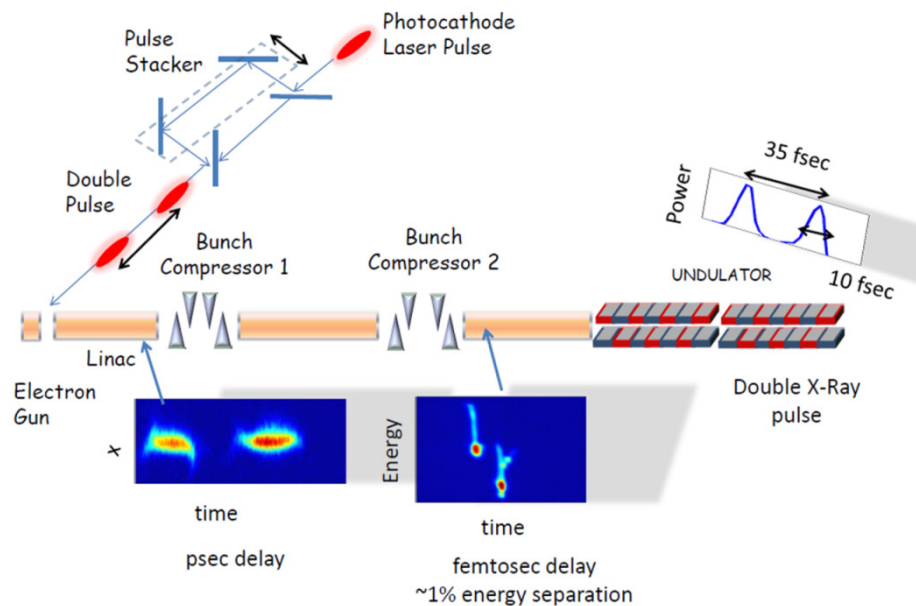


Figure 11: Generation of dual-pulses of femtosecond separation by beam splitting the cathode drive laser pulse.

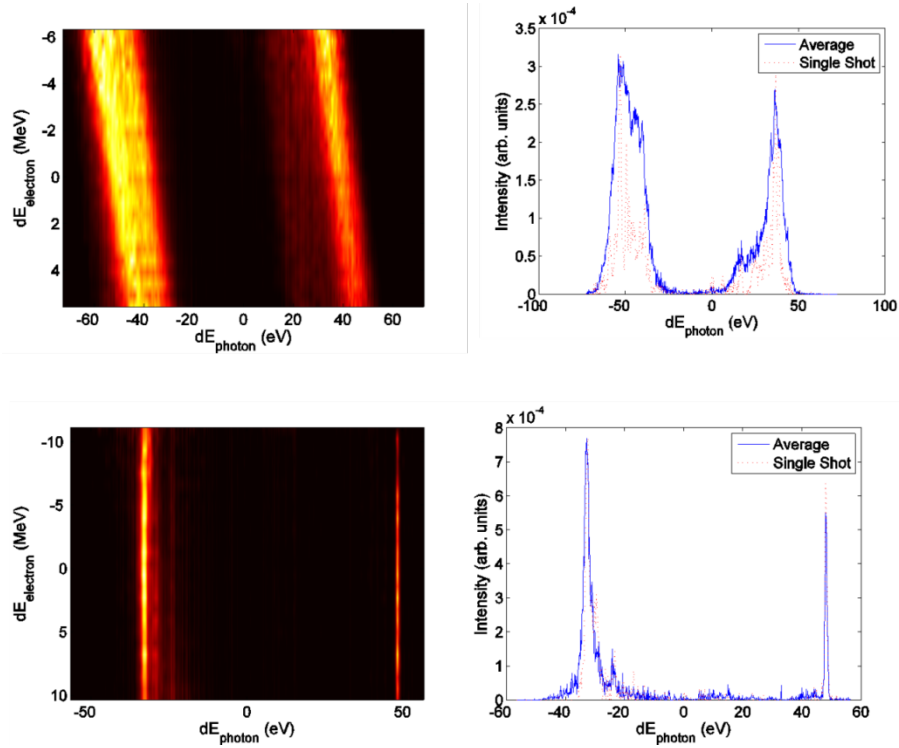


Figure 12: Dual energy pulses both for SASE and Seeded FEL Operation.

Table 1: Dual pulse, dual energy parameters.

<i>Technique</i>	<i>Dual Pulse</i>	<i>Dual Energy</i>	<i>Same Energy</i>	<i>Pulse Separation</i>	<i>Min Bunch Length</i>	<i>Energy Range</i>	<i>Energy Separation</i>	<i>Max Pulse Energy</i>	<i>Mode</i>
Laser Stacker (TWIN BUNCHES)	yes	yes	No	0 – 100 fs	~ 10 fs	HXR, SXR	~ 1%, ~ 3%	1.2 mJ @SXR (70-100fs) 2 mJ @HXR (30fs)	SASE
Twin bunches + V slotted foil	yes	yes	No	0 – 50 fs	~ 5 – 10 fs	SXR	~ 3 %	50 uJ	SASE
Twin bunches + HXR Self-Seeding	yes	yes	No	0 – 100 fs	~ 10 fs	HXR	~ 1 %	150 uJ per pulse	SEEDED
Single bunch SASE	yes	yes	yes	~>0 - 900 fs or ~>0-50 fs	~ 10 fs	HXR, SXR	~ 2.5 %	75 uJ, 150 uJ	SASE
One pulse seeded	yes	yes	yes	~>0 -50 fs	~ 20 fs	SXR	~ 2.5 %	150 uJ total	SASE SEEDED
Two Polarization, Two Color, Two Pointing	yes	yes	yes	~>0 - 900 fs or ~>0-50 fs	~ 20 fs	SXR	~ 2.5 %	30 uJ per pulse	SASE
Fresh –slice Two-Color	yes	yes	yes	~ -15 - +885 fs or ~ -15 - +35 fs	~ 5 – 8 fs	SXR	~ 2.5 %	700 uJ total, max 250 uJ on pump for zero delay feature	SASE
Fresh-slice Two-Polarization, Two Color, Two Pointing	yes	yes	yes	~ -15 - +885 fs or ~ -15 - +35 fs	~ 5 – 8 fs	SXR	~ 2.5 %	300 uJ	SASE
Double Slotted Foil	yes	yes	yes	15 - 70 fs (SXR); 7-20 fs (HXR)	10 fs	HXR, SXR	~ 1.5 %	100-300 uJ	SASE
Two laser/two bucket (ns Double bunch)	yes	yes	yes	350 ps increments, +/- 38 ns	10 fs	HXR, SXR	~ 2 %	1-2 mJ	SASE SEEDED

3.3.2.6 *Dechirper for energy spread and bandwidth control*

A ‘dechirping’ device was installed at LCLS in the summer of 2015 [14]. Two sets of jaws constructed of corrugated aluminum rails, in the horizontal and vertical dimension, provide independent energy chirp control for the LCLS electron beam. The device has been installed in the transport line between linac and undulator section. Figure 13 shows the dechirper installed at LCLS. The main purpose is to use the wake fields generated by the head of the electron bunch to control the energy distribution along the remaining length of the bunch to correct the undesired time-energy correlation (‘chirp’) introduced by magnetic compression devices, which undesirably increase the photon bunch bandwidth. The amount of ‘chirp control’ is illustrated in figure 14. As a result, the bandwidth of the photon bunch can be reduced by up to 50% (illustrated in figure 15). The use of a pair of crossed dechirper devices reduces emittance degradation observed elsewhere. Additionally the device can provide means for passive atto-second bunch length measurement [15] and is being used as an alternate method to generate multi-energy FEL pulses [13].

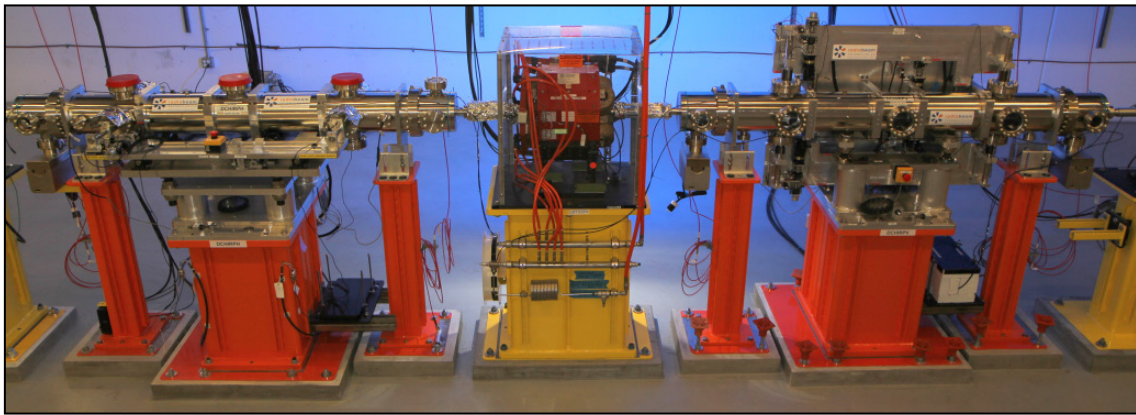


Figure 13: De-chirper installed at LCLS.

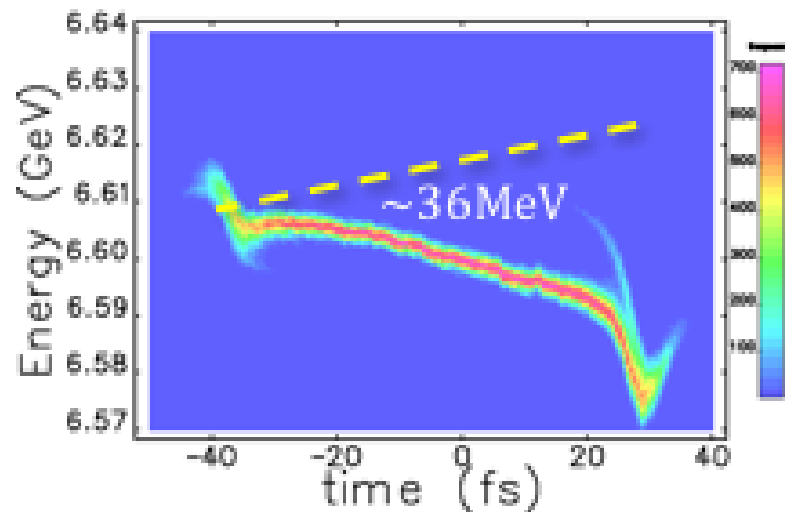


Figure 14: Typical energy distribution control using the LCLS de-chirper.

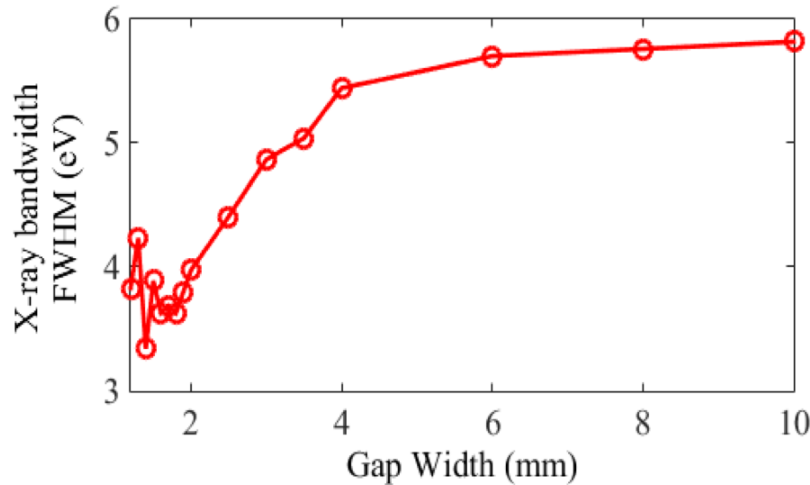


Figure 15: Photon bunch bandwidth as a function of dechirper jaw gap.

3.3.3 Operation of the LCLS

3.3.3.1 Schedules

The LCLS accelerator typically operates for approximately 9.5 months per year. Operation is interrupted for 6-8 weeks during the summer and 3 weeks during the winter when maintenance activities occur. Beams are delivered to users for about 5000 hours per year. From 2017 – 2019, this schedule will be interrupted by a 5 month period early 2017 and a 12 month period in 2018 and 2019. These long down times are necessary to allow the installation of the LCLS-II superconducting accelerator and new undulator systems, both for LCLS-I and II. The historical, current and anticipated operating schedule is shown in figure 16.

	January	February	March	April	May	June	July	August	September	October	November	December	
2009											Run 1 Oct. 1-Dec. 17		
2010					Run 2 May 6 - Sep. 13				Run 3 Oct. 7 - Dec. 17				
2011	Run 3 Jan. 13 - Mar. 8						Run 4 Jan. 18 - Oct. 24				Run 5 Nov.17-Dec.1		
2012	Run 5 Jan. 19 - May 29				Run 6 May 31 - July 31			Run 6 Oct. 5 - Dec. 19					
2013	Run 7 Jan. 16 - Jul. 16						Run 8 Aug. 6		Run 8 Oct. 17 - Dec. 20				
2014	Run 8 Jan. 16 - Mar. 24		Run 9 Mar. 26 - Aug. 4						Run 10 Oct. 15 - Dec. 19				
2015	Run 10 Jan. 15 - Mar. 23		Run 11 Mar. 27 - Aug. 11						Run 12 Oct. 15 - Dec. 18				
2016	Run 12 Jan. 12 - Mar. 22		Run 13 Mar. 24 - Aug. 9		Run 13 Mar. 24 - Aug. 9			Run 14 Proposals due Jan.11; PRP meets Mar.17-18; Aug.11 - Dec.16					
2017						Run 15 Proposals due Nov. 5; PRP meets Jan. 19-20; Jun. 15 - Nov. 27						Run 16 Dec.22	
2018	Run 16 Proposals due May. 1; PRP meets Jul. 20-21; Jan. 11 - Jun. 4												

Figure 16: Historical, current and future LCLS operating schedule.

A typical LCLS experiment is planned for five 12 hour shifts. Until recently, two experiments were running during a 5 day period. Currently, for many experiments beams are multiplexed by X-ray optics, which allows conducting more than one experiment to be executed at a time. Also, streamlining of X-ray operations, standardization of experimental conditions and setup procedures facilitate shorter experiments and thus increase access to the LCLS facilities.

During a one or two day period in-between X-ray experiments we conduct maintenance activities, accelerator physics and machine development programs, support accelerator R&D projects, implement new capabilities and prepare accelerator configurations for upcoming X-ray experiments. Figure 17 illustrates a typical run schedule.

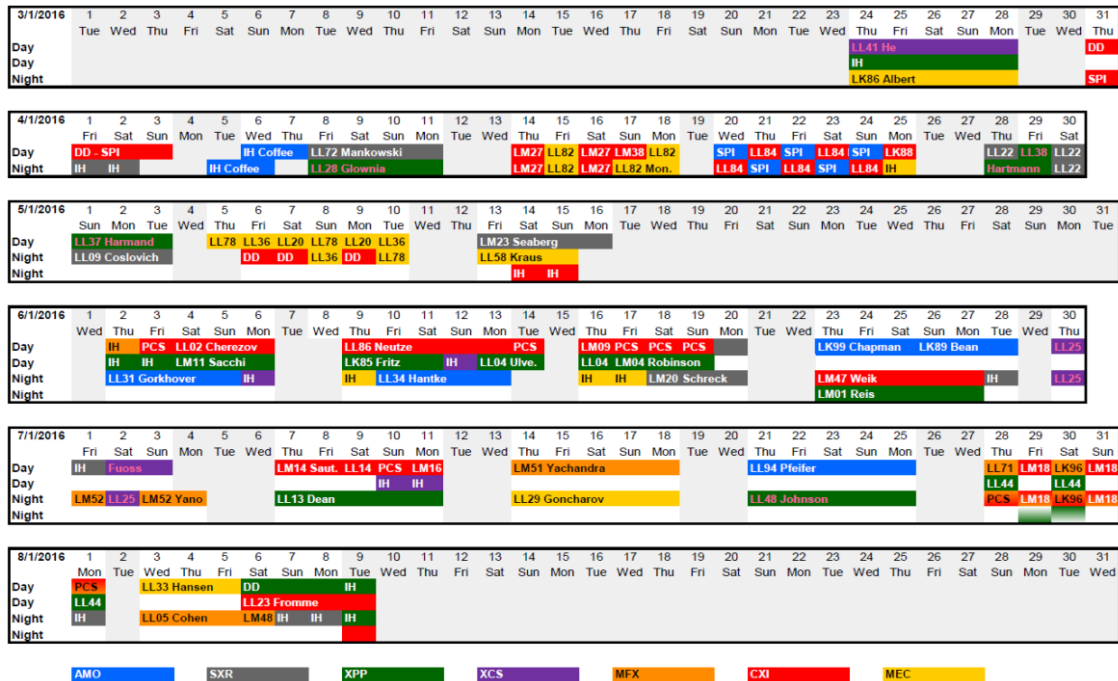


Figure 17: Run 13 operating schedule.

3.3.4 LCLS Availability

The goal for LCLS beam delivery is 95 percent X-ray beam availability. Since the beginning of LCLS user operation, achieved beam availability ranges from 91.8-97.1 % (figure 18). Typical beam availability data for an individual run is shown in figure 19. Statistical tools such MTBF and MTTR are used to manage subsystem performance and strategic investments are implemented accordingly. In most cases, the major downtimes extending for several hours to days are caused by the facility infrastructure systems such as cooling water or high voltage power distribution.

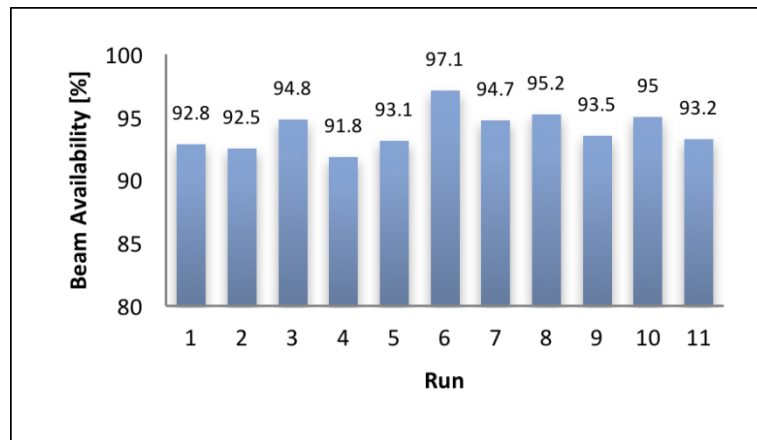


Figure 18: X-ray beam availability by run (from 2009 to 2016).

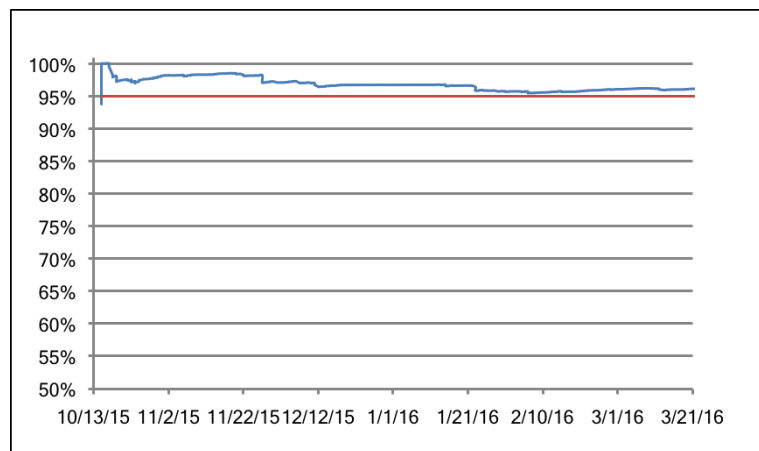


Figure 19: X-ray beam availability during run 12 (indicating goal of 95 %).

3.3.5 Facility Upgrades and Research & Development at LCLS

The main thrust of future developments includes improving the overall efficiency and reliability of LCLS operations. Many projects are underway to upgrade technical systems, which in some cases date back to the early days of SLAC and are more than 50 years old. A significant effort is underway to upgrade all aspects of the accelerator control systems, including the safety systems, to modern industrial standards. An important aspect is to achieve compatibility of LCLS-I and II systems with the goal to design and implement a unified control system with common hardware and software solutions. This effort is coordinated with the LCLS-II project, which is close to finalizing the design of all systems supporting the new superconducting LCLS-II accelerator. Other areas of attention are the high power RF systems. Significant performance and reliability improvements are anticipated by upgrading klystron modulators, adding tools for diagnostics and remote PFN optimization.

During normal accelerator operation, a significant amount of time is spent to tune the accelerator to deliver the FEL performance required by the experimental programs. Although sophisticated machine tuning tools have been developed during the past years, further standardization, streamlining and automation of basic tuning procedures has the potential to increase available beam time for user or accelerator physics programs. A set of new techniques is currently emerging and a coordinated effort for their further development is underway. Examples are the automation of High Level Applications with the goal to minimize human intervention, ‘mine’ the vast set of accelerator systems and performance data to extract correlations of performance and system data and the implementation of ‘machine learning’ techniques. Results have been achieved using Robust Conjugate Direction Search algorithms [16] and implementation of statistical optimization techniques developed at DESY [17]. Figures 20 and 21 illustrate recently achieved improvements of the LCLS accelerator performance using these techniques.

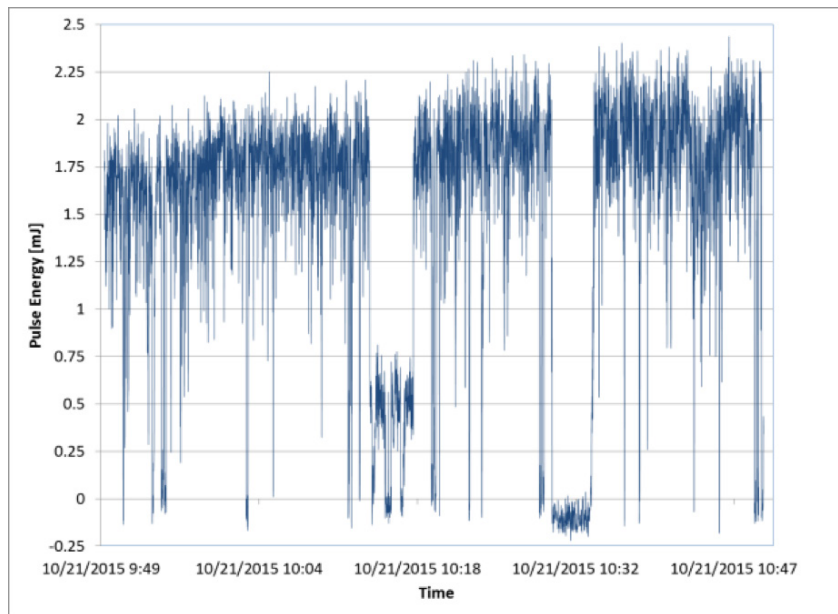


Figure 20: Automatic FEL pulse energy maximization by using RCDS algorithms on matching quadrupole magnets.

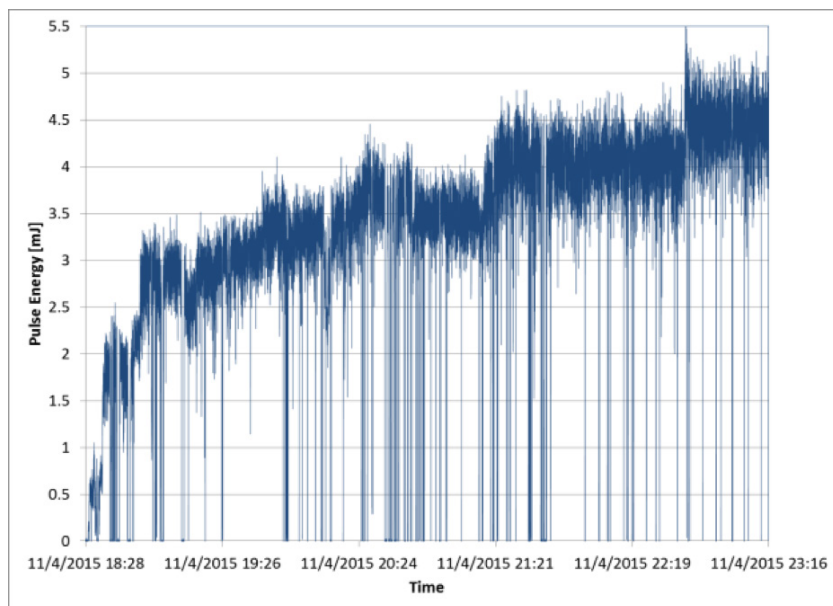


Figure 21: Automatic FEL pulse energy maximization by using ‘OCELOT’ algorithms on lattice tuning.

To maintain the performance of the accelerator, effective and efficient diagnostics tools are important. Daily operation heavily relies on emittance measurements, which are mainly done using wire scanners. Traditionally, scans take several minutes for a full measurement. At LCLS, we are implementing a new design using fast continuous motors to replace the current stepper motor based technology [18], achieving a scan time of a few seconds for a complete measurement.

The LCLS Facility continues to conduct a vibrant R&D program to support LCLS operations and to enable new capabilities in many areas of science conducted using the LCLS FEL. Examples of R&D program results are the seeding capabilities in the Hard and Soft X-ray regions, polarized X-ray beams and new diagnostics such the transverse deflecting cavity for bunch length measurements with femtosecond resolution. A focus for the coming years to develop a multi-bunch capability,

increasing the peak power of X-ray pulses into the terra-watt regime using tapered undulators and the development of atto-second & mode-locked X-rays. Strategic efforts are being planned to advance photo-injector technology, including the development of superconducting RF gun technology for the LCLS. A task force is being formed to evaluate and develop external seeding techniques for LCLS.

3.3.6 Conclusions

LCLS has successfully operated as a user facility since 2009. A key to its success is the constant development of new capabilities and performance improvements. FEL science is still an emerging area and relies heavily on continues advancements of accelerator technology, providing many opportunities for Research and Development. This trend will continue for the foreseeable future. However, many aspects of FEL operation have reached maturity and attention moves towards streamlining and automation of processes and operation with the ultimate goal to increase the scientific output of the FEL facility.

3.3.7 Acknowledgments

The operation of the LCLS is made possible by a SLAC's dedicated community of physicists, engineers and technicians and a variety of support staff. The main contributions are provided by SLAC's Accelerator and LCLS directorate. In addition, for many aspects, LCLS benefits from international collaborations. Work supported by DOE Contract: DE-AC02-76-SF00515.

3.3.8 References

1. P. Emma, et al., Nat. Photonics 4, 641 (2010).
2. Special Issue on X-ray Free-Electron Lasers, J. Synchrotron Rad., 22, 471 (2015).
3. Amann et al., Nature Photonics 6 693 (2012).
4. Ratner et al., PRL 114, 054801 (2015).
5. Lutman et al., Nat Photonics DOI: 10.1038/NPHOTON.2016.79 (2016).
6. Behrens et al., Nature Comm. 5, 3762 (2014).
7. Lutman et al., Phys Rev. Lett. 110, 134801 (2013)
8. Marinelli et al., Phys Rev. Lett. 111, 134801 (2013)
9. Marinelli et al., Nature Comm. 6, 6369 (2014).
10. Ding et al., Phys. Rev. ST Accel. Beams 18, 090701 (2015).
11. Lutman et al., Phys. Rev. Lett. 113, 254801 (2014).
12. Emma et al., Phys. Rev. Lett. 92, 074801 (2004).
13. Lutman et al. Private communication
14. Zhang et al., Phys. Rev. ST Accel. Beams 18, 010702 (2015).
15. Novokhatski, Phys.Rev. ST Accel. Beams 18, 104402 (2016)
16. Huang et al., SLAC-PUB-15414, (2015).
17. Agapov et al., Proceedings of IPAC 2015, TUPWA037, (2015).
18. D'Ewart et al., Proceedings of ICALEPC, MOPGF015, (2015).

3.4 LCLS-II: A CW X-ray FEL Upgrade to the SLAC LCLS Facility

Gabriel Marcus and Tor Raubenheimer for the LCLS-II Collaboration

Mail to: gmarcus@slac.stanford.edu

SLAC, Menlo Park, CA 94025, USA

3.4.1 Abstract

The LCLS-II is an X-ray FEL upgrade to the existing Linac Coherent Light Source X-ray FEL at the SLAC National Accelerator Laboratory (SLAC). The facility will be based on a new 4 GeV CW superconducting RF (SCRF) linac which is being constructed by a collaboration of Argonne National Laboratory, Cornell University, Fermi National Accelerator Laboratory, Lawrence Berkeley National Laboratory, Thomas Jefferson National Accelerator Facility, and SLAC. This paper will describe the overall layout and expected performance of the project.

3.4.2 Introduction

The LCLS-II is an X-ray Free-Electron Laser (FEL) which is an upgrade of the Linac Coherent Light Source (LCLS) FEL [1] at SLAC. The LCLS was commissioned in 2009 [2] and has been very productive; a summary of the accelerator performance and highlights of the photon science program can be found in Ref. [3]. The LCLS-II upgrade is designed to deliver photons between 200 eV and 5 keV at repetition rates as high as 1 MHz (929 kHz) using a superconducting RF linac (SCRF) linac while still providing pulses at short wavelengths and high X-ray pulse energy over the photon range of 1 to 25 keV using the existing 120 Hz copper RF (CuRF) LCLS linac. The project consists of a new 4 GeV SCRF linac, extensive beam transport systems, and two new variable gap undulators.

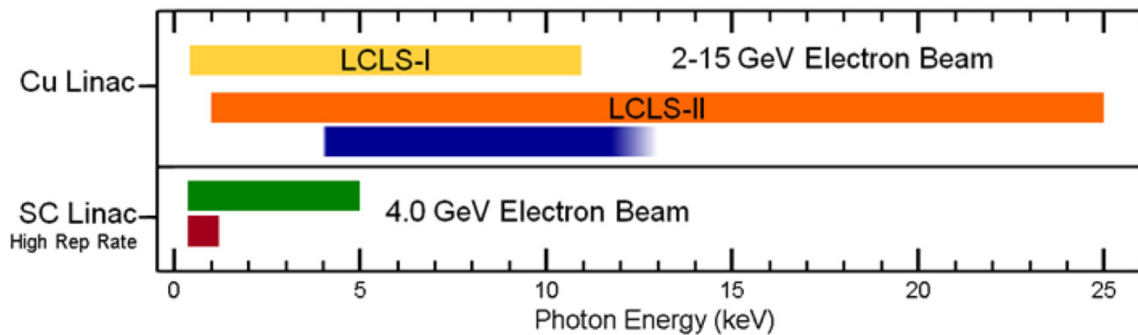


Figure 1: Schematic illustrating performance of the LCLS and the LCLS-II upgrade where yellow represents SASE at 120 Hz, blue represents Self-Seeding at 120 Hz; green represents SASE at high rate; and red represents Self-Seeding at high rate.

The LCLS-II will extend the high peak brightness capability and flexibility of LCLS while also having the ability to provide MHz rate beams from a CW SCRF linac. The operating regimes are illustrated in Figure 1 and listed below:

1. Soft X-ray photons from SASE and self-seeding between 0.2 and 1.3 keV at MHz rates, with an average X-ray power in excess of 20 Watts;
2. Hard X-ray photons from SASE between 1.0 and 5.0 keV at MHz rates with an average X-ray power in excess of 20 Watts and with the possibility of a future upgrade to self-seeding operation at energies between 1 and 4 keV;

implementation of additional feedback systems that are possible due to the high repetition rates of the linac.

Table 1: LCLS-II electron and x-ray parameters.

SCRF Parameter	nominal	range	CuRF Parameter	nominal	range	units
Electron Energy	4.0	2.0 - 4.5	Electron Energy	15	2.5 - 15.0	GeV
Bunch Charge	100	10 - 300	Bunch Charge	100	10 - 250	pC
Bunch Repetition Rate in Linac	6.2e5	0 - 9.3e5	Bunch Repetition Rate in Linac	120	0 - 120	Hz
Average e^- current in linac	0.062	0.0 - 0.3	Average e^- current in linac	2.7e-4	0 - 5e-4	μ A
Max. beam power at linac end	0.25	0 - 1.2	Avg. e^- beam power at linac end	0.25	0 - 1.2	MW
Rms slice emittance at undulator	0.40	0.2 - 0.7	Norm. rms slice emittance at undulator	0.40	0.2 - 0.7	μ m
Final peak current (at undulator)	800	300 - 1200	Final peak current (at undulator)	3000	1000 - 4000	A
Final slice E-spread (rms, w/heater)	500	125 - 1500	Final slice E-spread (rms, w/heater)	1500	500 - 3000	keV
RF frequency	1.3	-	RF frequency	2.8	-	GHz
Avg. CW RF gradient	16	8 - 19	Avg. CW RF gradient	~20	-	MV/m
Avg. Cavity Q0	2.70E+10	1.5 - 5e10	Avg. Cavity Q0	1.3e4	-	-
Photon energy range of SXR	-	0.2 - 1.3	Photon energy range of SXR	-	N/A	keV
Photon energy range of HXR	-	1 - 5	Photon energy range of HXR	-	1 - 25	keV
Typical photon pulse energy	0.2	0.01 - 5	Typical photon pulse energy	2	1 - 5	mJ

The LCLS-II will be flexible in its operating modes consistent with the maximum x-ray beam power, the maximum electron beam power to the BSY and undulator dumps, the maximum repetition rate and the range of bunch charges. As noted above, the HXR can be fed from either the SCRF linac or the CuRF linac while, in the baseline design, the SXR can be fed only from the SCRF linac. The BSY Beam Spreader can direct the SCRF linac beam arbitrarily toward either undulator or to the BSY dump. The design does not presently include the capability of delivering different bunch charges or peak currents to the two undulators simultaneously, however that capability may also be developed in the future.

The beams from the CuRF linac at 120 Hz will retain all of the flexible operating modes that are being developed at LCLS [3, 6-10]. These include pulse-length control, two-color pulses and two pulses with delay at the 100 fs scale [8, 9]. New techniques are being developed as well which may allow pulse-by-pulse bunch length control and limited shaping of the x-ray pulses. Many of these techniques will be implemented on the SCRF linac as well however these capabilities are beyond the baseline project and will take time after initial operation to develop the full capability.

In the following, we will describe the overall facility layout and primary challenges and then we will summarize the current state of the FEL performance simulations. Much of the material for the paper is taken from Refs. [11] and [12]. Given the rapid pace of the LCLS-II project much of the material is not yet documented in peer-reviewed articles and can only be found in conference proceedings, in particular, those of the IPAC and FEL meetings.

3.4.3 Configuration and Challenges

The LCLS-II will consist of a new CW injector and SCRF linac, extensive transport line, and two new variable gap undulators. The layout of the new systems is similar to the design of the LCLS. The primary differences are also related to the technical challenges the project faces:

1. The CW SCRF linac
2. High brightness CW injector
3. Variable gap undulators
4. High power beams
5. Beam dynamics of high brightness low energy beams

These issues will be described further in the sections below.

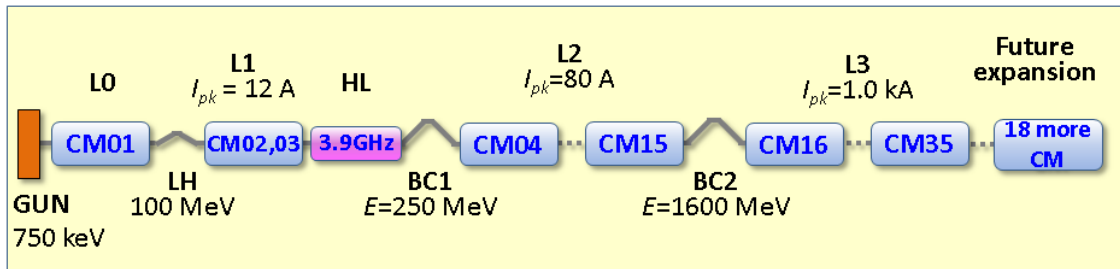


Figure 3: Schematic of LCLS-II SCRF linac.

3.4.3.1 SCRF Linac

The LCLS-II SCRF linac will be constructed from 35 1.3 GHz cryomodules (CM), each containing eight 9-cell cavities. Like the LCLS linac, the linac will contain a Laser Heater at roughly 100 MeV to suppress the micro-bunching instability and two bunch compressors, BC1 at 250 MeV and BC2 at 1.6 GeV as illustrated in Figure 3. In addition, two 3.9 GHz CM with eight 9-cell cavities will be installed upstream of BC1 to linearize the longitudinal phase space.

The linac parameters are listed in Table 2.

Table 2: SCRF 1.3 GHz Linac Parameters

Gradient	16 MV/m
Average Q₀	2.7x10 ¹⁰
Num. Cavities	280 (35 CM)
Total voltage at 16 MV/m	4.65 GV
Max. Beam Energy	4.5 GeV
Max. bunch rep. rate	929 kHz
Max. bunch charge	300 pC

The SCRF cavities are based on the TESLA design pioneered at DESY and the CM's are similar to those developed for the ILC and EuXFEL program but modified for CW operation.

In a CW SCRF linac, the heat load is dominated by the RF losses in the cavities which scale quadratically with gradient as Grad^2/Q_0 . The state-of-art at 1.3 GHz is the EuXFEL cavities which achieve Q_0 's of roughly 1.5×10^{10} and gradient's in excess of 25 MV/m. The dynamic heat load due to these cavities is fine at the low duty-cycle of the EuXFEL but would be expensive to cool in the CW LCLS-II. To minimize the RF losses, the LCLS-II project supported R&D aimed at developing Q_0 's in excess of 2.7×10^{10} at a gradient >16 MV/m.

This challenge has been met using the Nitrogen-doping technique that has been developed at FNAL [13]. This technique has improved the Q 's of the 1.3 GHz 9-cell cavities by roughly a factor of two as illustrated in Figure 4. The set of dressed cavities illustrated in Figure 4 have an average $Q \sim 3 \times 10^{10}$ and a maximum gradient of >22 MV/m. While the cavity processing has proceeded very well, there are still challenges in translating these benefits to a full CM and the LCLS-II will be designed with additional cryogenic overhead to ensure success in meeting the design goal of a 4 GeV electron beam. An excellent summary of the present high-Q SCRF cavity status can be found in Ref. [14].

The cavity processing procedure is being developed at FNAL, JLab, and CU. FNAL and JLab will each build one prototype 8-cavity CM and these will be verified during 2016. The construction of the rest of the CM's for the LCLS-II will be shared between FNAL and JLAB.

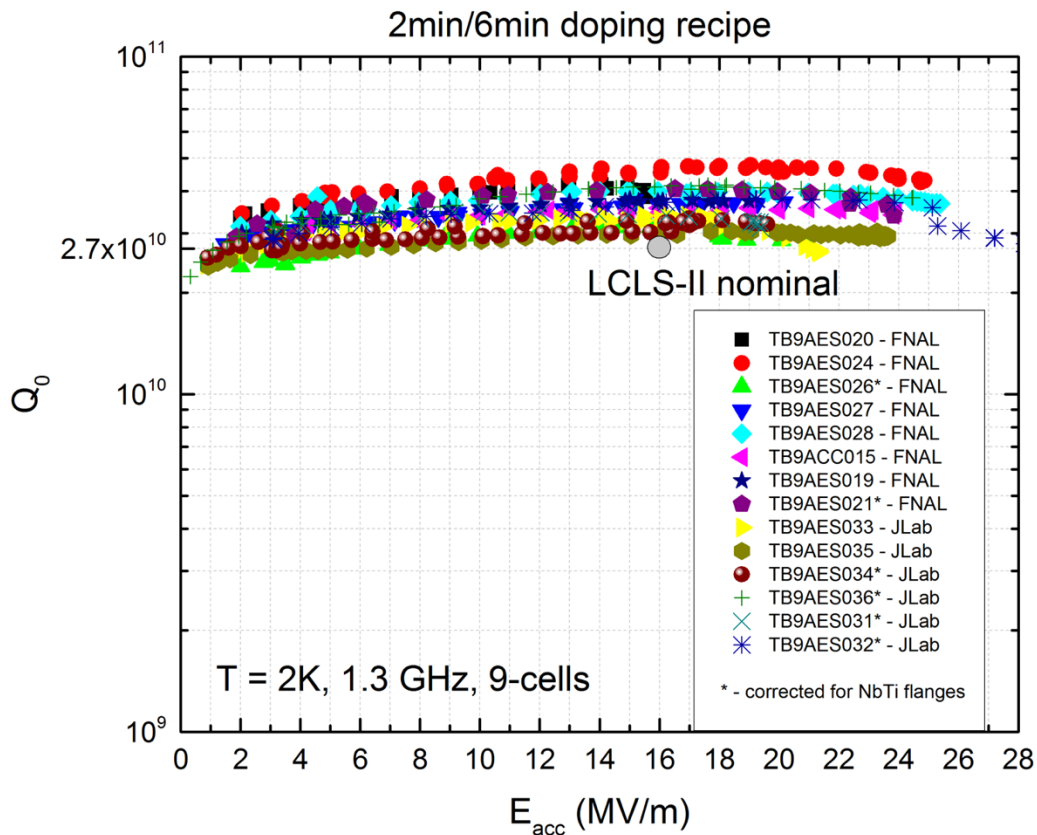


Figure 4: Q_0 versus gradient for N-doped 9-cell cavities tested at FNAL and JLab.

The SCRF linac will be cooled with two large cryoplants. The cryoplants will be similar to that built for the JLab 12 GeV upgrade [15] and each will provide cooling for 4 kW of heat dissipation at 2°K. The plant is being designed by JLab while FNAL is designing the cryo-distribution

systems. The plants will be located roughly halfway along the linac (adjacent to BC2) and will feed cryogenics both upstream toward the injector and downstream. The layout for one of the plants is illustrated in Figure 5.

The SCRF linac is being designed to accelerate $300\ \mu\text{A}$ up to $>4\text{GeV}$ for 1.2 MW of beam power, which is sufficient to ultimately generate more than 100 Watts of X-rays in up to 10 individual undulator beamlines. The initial LCLS-II configuration will be limited to a maximum power of 250 kW, supplying beam to only the first two undulators. It only includes sufficient RF power to accelerate $100\ \mu\text{A}$ up to 4 GeV at 16 MV/m with 10 Hz detuning of the cavities or, as illustrated in Figure 6, $50\ \mu\text{A}$ up to 4.5 GeV at 17.5 MV/m with 10 Hz detuning. The specification of 10 Hz detuning is expected to be conservative in which case higher current beams could be accelerated. The project will be based on a single-source, single cavity RF configuration to have necessary control of the cavity fields. The RF power will be supplied by 3.8 kW solid-state amplifiers and the LLRF system for the LCLS-II is described in Ref. [17].

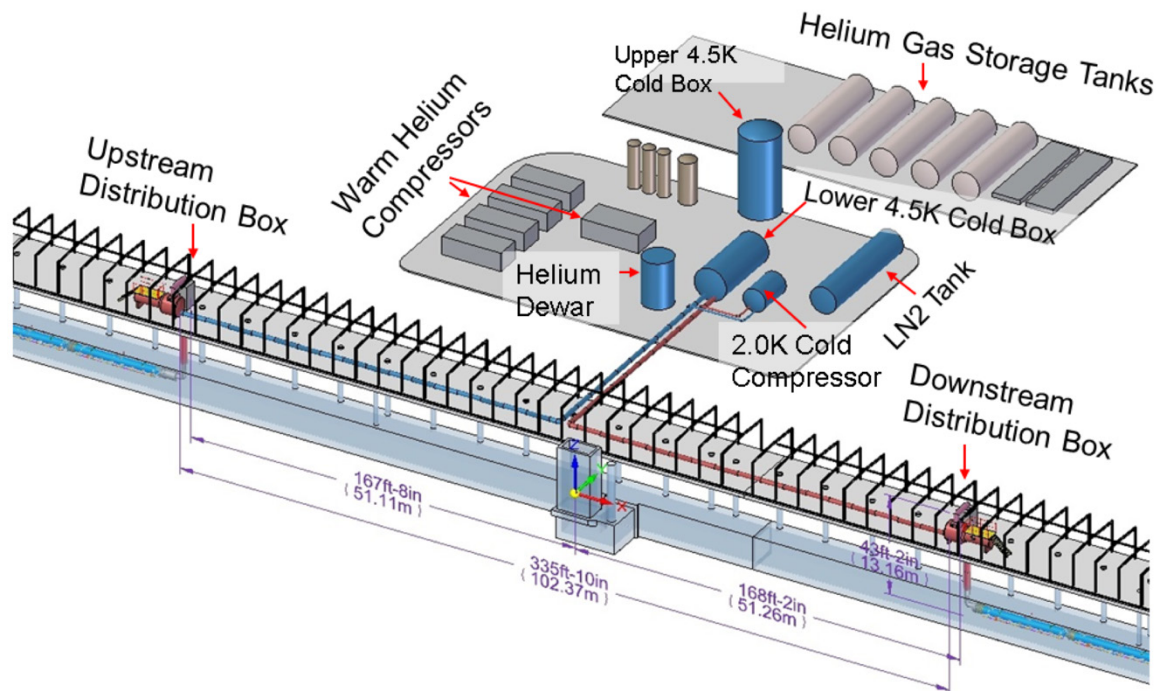


Figure 5: Schematic of a single cryoplant for the LCLS-II SCRF linac.

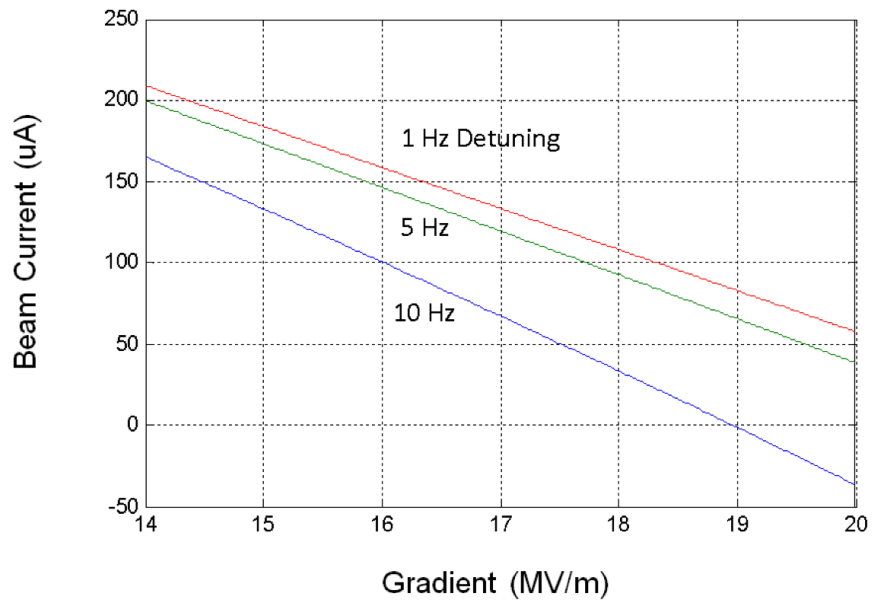


Figure 6: Beam current versus cavity gradient for the initial RF system for various detuning values from Ref. [16].

3.4.3.2 *High brightness CW injector*

The performance of an FEL depends critically on the incoming electron beam brightness. For CW operation, a normal-conducting high gradient RF gun is not possible and, while lots of potential exists, superconducting RF guns have not yet demonstrated the desired brightness.

Instead, the LCLS-II will use an RF gun very similar to the 186 MHz RF gun being developed as part of the APEX project at LBNL [18]. The normal-conducting photo-cathode gun will provide a beam of 750 keV which is then bunched with a 1.3 GHz normal-conducting buncher cavity before being injected into a standard 1.3 GHz SCRF CM where it is captured and accelerated to 100 MeV. It is expected that the relatively high voltage and gradient of the RF gun will provide higher beam brightness than a DC gun operating at 400 to 500 kV.

The APEX project has demonstrated the operation of the RF gun at 800 kV and has operated the system with the 1.3 GHz buncher cavity and downstream accelerator structures which accelerate the beam to 20 MeV to verify the beam brightness [19]. Brightness measurements of 20 pC bunches were made during winter 2016 and these meet the LCLS-II specifications [20].

In parallel, the Cornell DC gun which was developed for an Energy Recovery Linac [21], has been operated at 400 kV and the beam brightness has been measured for bunch charges across the LCLS-II operating range of 10 – 300 pC using a new NaKSb cathode [22]. The gun was optimized to meet the LCLS-II emittance and peak current requirements and the studies are an excellent benchmark of the ASTRA and GPT gun simulation codes, providing confidence in the LCLS-II injector design. These codes are being used to optimize the detailed implementation at LCLS-II to increase the beam aperture and improve the emittance performance of the injector design [23, 24].

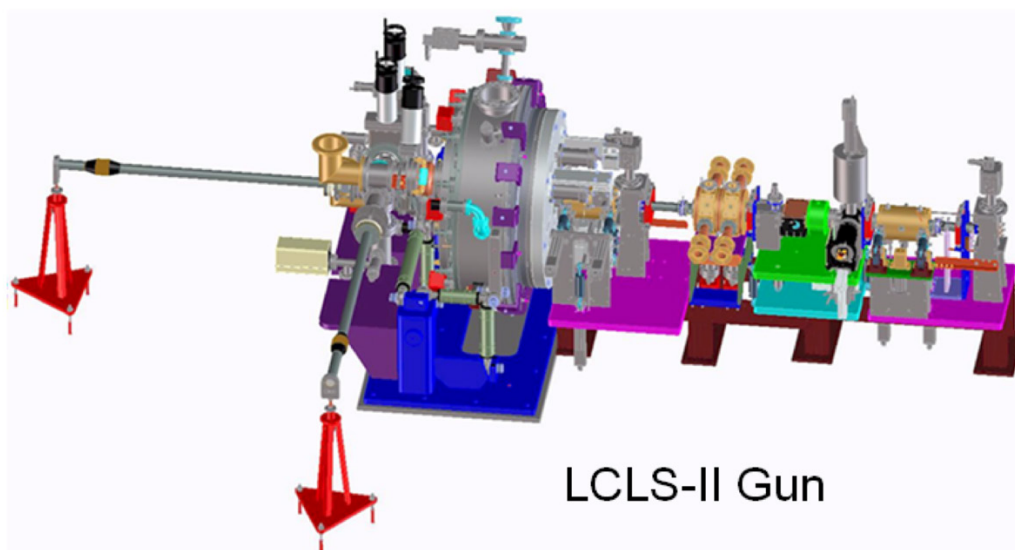


Figure 7: Schematic of the LCLS-II injector, based on the LBNL APEX RF gun [18].

The baseline cathode will be Cs_2Te illuminated in the UV. The laser system has been sized for a 0.5% QE and the emittance performance is based on a 1 mm-mrad per mm thermal emittance. Measurements at the APEX RF gun of the thermal emittance and QE are better than the design specifications.

In addition, alkali-antimonide cathodes are being developed at LBNL and around the world. Tests of LBNL-produced examples have demonstrated good results in APEX and, if proven robust, will be adopted by the LCLS-II project to improve the beam emittance and simplify the gun laser system. As noted, measurements on the Cornell DC gun were made using a NaKSb cathode with a thermal emittance $\sim 30\%$ smaller than the typical Cs_2Te cathodes of 0.8 mm-mrad/mm.

3.4.3.3 *Variable gap undulators*

As noted, the SXR undulator can be fed from the SCRF linac, while the HXR undulator can be fed from either the SCRF or the CuRF linacs, although not from both simultaneously. The undulators will be installed side-by-side in the existing LCLS Undulator Hall. A schematic of the undulator layout appears in Figure 8.

Both undulators are variable-gap hybrid permanent-magnet undulators; the existing fixed gap LCLS undulators will be removed. The HXR undulator has a period of 26 mm, close to that of the existing LCLS undulator, while the SXR undulator has a period of 39 mm. The maximum length of the existing LCLS Undulator Hall is roughly 150 meters. As illustrated in Figure 9, this will allow for the installation of up to 38 segments for the HXR, with each segment being 3.4 meters long followed by an interspace of ~ 0.65 meters for a quadrupole, phase shifter, RF BPM, and x and y steering coils. To support self-seeding, two of these undulator slots will be reserved for self-seeding monochromators. The baseline will include 32 HXR segments plus two self-seeding slots, one of which contains the existing LCLS HXR self-seeding monochromator [25]; the other is reserved for a future upgrade.

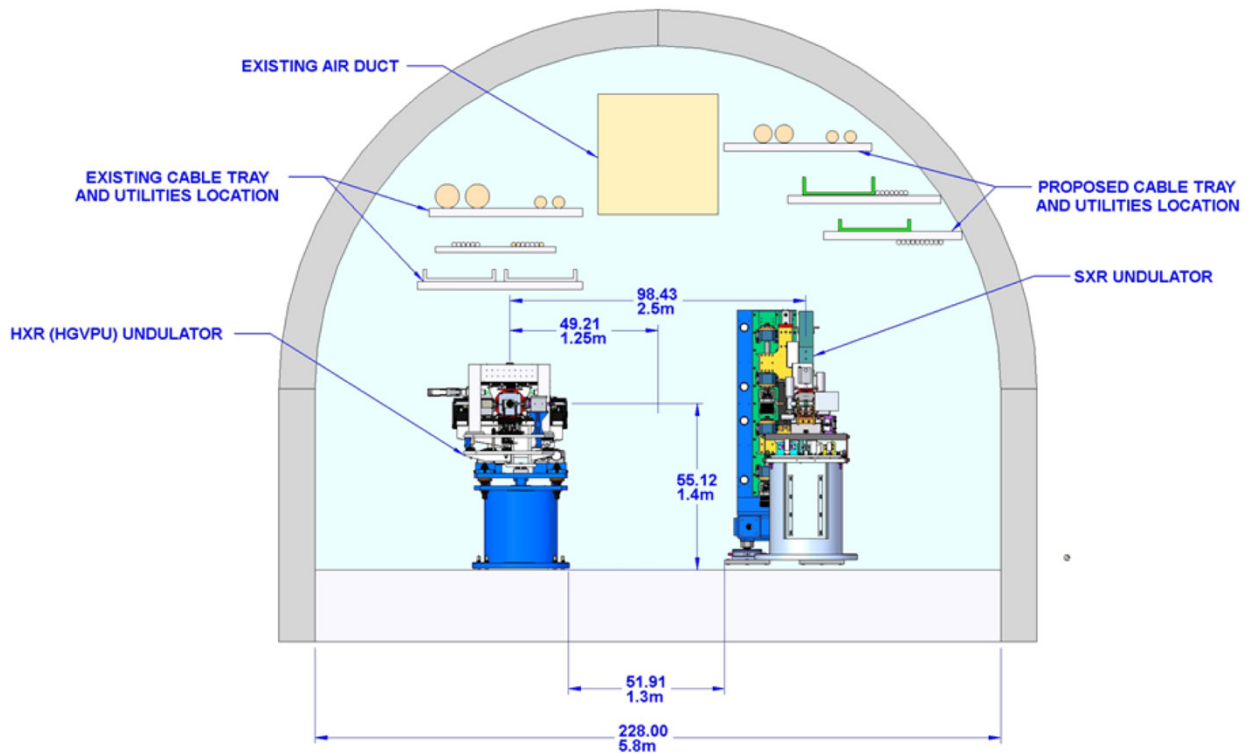


Figure 8: Schematic of HXR and SXR undulators in the LCLS Undulator Hall.

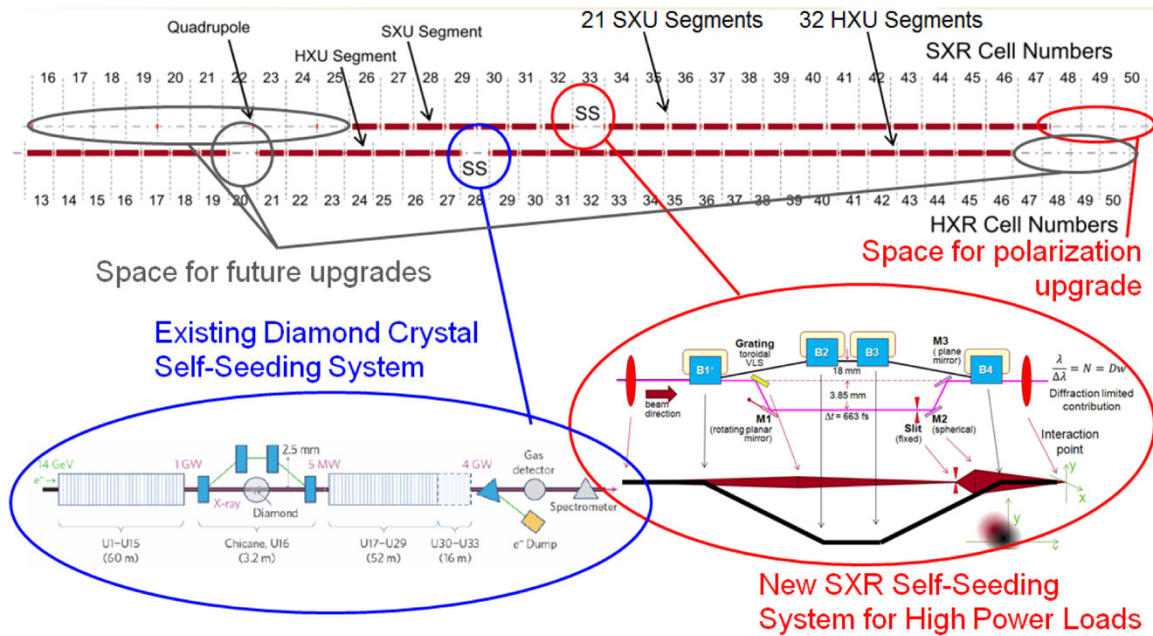


Figure 9: LCLS-II undulator layout.

The SXR undulator can be shorter, and there will be 21 SXR undulator segments plus one empty slot for the self-seeding monochromator which will be based on the LCLS SXRSS monochromator but modified for higher average power with a resolving power $>10,000$. Development of the SXRSS monochromator is ongoing. The last three SXR undulator slots are reserved for the future installation of polarization control undulators such as DELTA undulators [26, 27], and the space upstream of the SXR undulator may be used for future seeding installations or additional undulators for two-color X-ray generation or other upgrades.

The LCLS-II undulators are being provided by LBNL [27]. The undulator parameters are listed in Table 3. The SXR is based on the well-established vertical-variable-gap hybrid undulator technology. A 3.4-meter prototype of an SXR undulator segment has been constructed and is shown in Figure 10. To reduce transmission losses in the horizontally deflecting optics downstream of the HXR undulator at photon energies about a few keV, the HXR will be based on the newly developed horizontal-gap vertically-polarizing undulator technology that was developed at ANL [28, 29]; a prototype is shown in Figure 11.

Table 3: Parameters for the HXR and SXR Undulators.

	<i>HXR</i>	<i>SXR</i>
Period	26 mm	39 mm
Mag. Material	Nd ₂ Fe ₁₄ B	Nd ₂ Fe ₁₄ B
Max. K	2.44	5.48
Min. gap	7.2 mm	7.2 mm
Gap orientation	Horizontal	Vertical
Seg. Length	3.4 m	3.4 m
Num. Segments	32	21
Interspace Len.	~0.65 m	1 m
Total Length	130 m	92 m

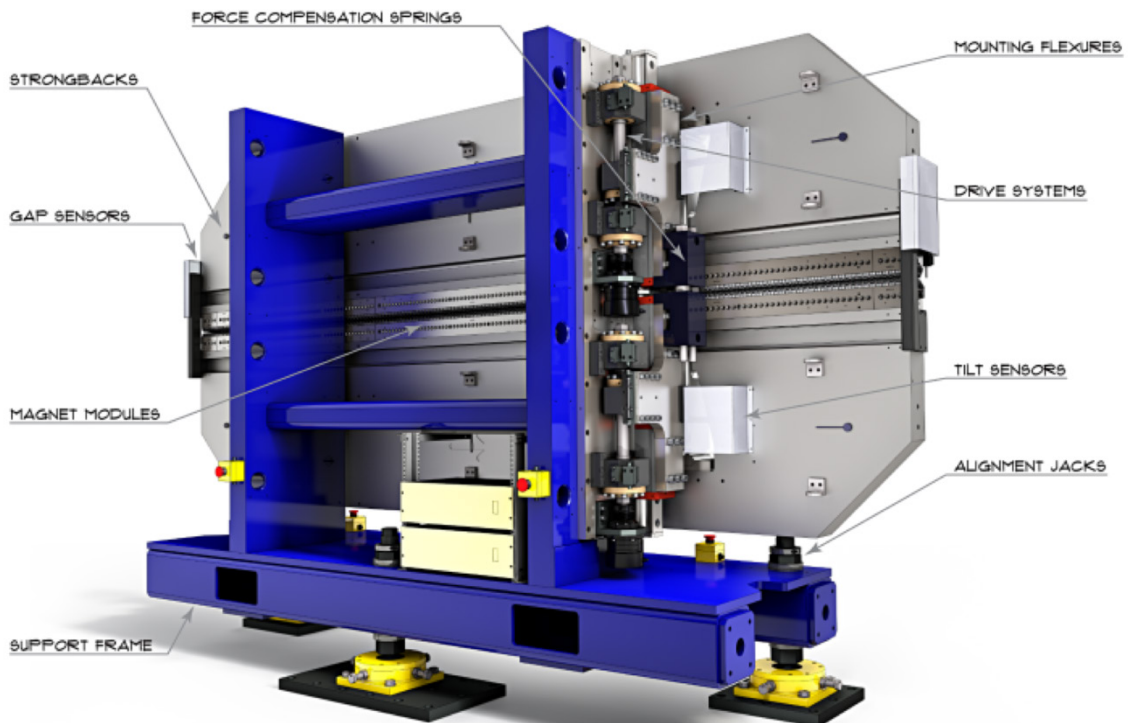


Figure 10: Prototype LCLS-II variable gap SXR undulator (LBNL).



Figure 11: Prototype LCLS-II variable horizontal gap HXR undulator (ANL).

3.4.3.4 *High Beam Power*

The LCLS-II SCRF linac is being designed to deliver 1.2 MW at 4 GeV of electron beam power although the initial RF system will only support a maximum of 400 kW at 4 GeV. Each of the two undulator systems (SXR and HXR) is designed to operate with up to 120 kW of electron beam power which can generate as much as 1 kW of X-rays. The X-ray transport systems are designed for a maximum of 200 W across the operating spectrum however many components are challenged by the intense x-ray beam. The collimators and stoppers need additional attention [30] and, in gas-

based attenuators or diagnostics, the x-ray beam can create a hollow channel [31] reducing their effectiveness and possibly amplifying intensity jitter effects.

Furthermore, to ensure a 10-year operating lifetime, beam loss in the hybrid permanent magnet undulator systems must be limited to an average of 12 mW, i.e. 1×10^{-7} of the maximum beam power. Control of the electron and X-ray beam power requires careful design of passive and active systems.

SLAC has operating experience with high power beams and the beam dumps and operating systems are being designed with this experience. The beam dumps are water-cooled dumps based on previous designs and the collimation system to limit the beam losses in the undulators is a four-stage design in which each stage will collimate in $(x, x', y, y'$ and $\Delta E)$. Additional collimation of parasitical (off-time) buckets may also be implemented.

Because of transients induced when changing the beam current profile and timing in the SCRF linac, the time required to change the rate is limited by the damping time of the feedback systems. When operating with a high-repetition-rate beam in the linac, we expect that this time will be a fraction of a second. The time needed to switch between the SCRF linac and the CuRF linac will be dominated by the time required to change out the DC magnets and re-establish the electron beam. This should take less than one hour. To simplify operations, the beam power in the undulators is controlled using a magnetic kicker located at the end of the SCRF linac. This will allow the full power linac beam to be tuned up onto a high power dump before beam is taken to and through the undulators. Using the kicker, the rate to each of the undulators can be rapidly controlled from single-shot to maximum rate.

The very high average power of the accelerated CW electron beam can damage components within a few 100 μ s. For this reason, several accelerator operating modes are envisioned for initial low-power commissioning, recovery from RF trips, recovery from beam-loss trips, and startup from shut-down periods. The Machine Protection System (MPS) is being designed to achieve better than a 100 μ s trip response time which is facilitated using the segmented design; if a fault arises near the undulator systems, beam can first be put onto the high power linac beam dump and then stopped at the electron source.

3.4.3.1 *Beam Dynamics*

The LCLS-II beam from the CuRF linac is very similar to that of the operating LCLS and thus is well quantified however understanding the beam from the SCRF linac has a new set of challenges. As noted, the design of the linac is similar to that of the LCLS with a laser heater and two-stage bunch compressor.

To ensure the performance of the LCLS-II analytic studies and detailed Start-to-End (S2E) simulations of the LCLS-II are being performed using the IMPACT [32-34] and Elegant [35] tracking codes and the Genesis FEL simulation code [36]. The low energy of the beam from the SCRF linac and the long transport makes the space charge and micro-bunching effects much more significant than in LCLS. A number of new effects driven by space charge have been observed including micro-bunching effects driven by transverse space charge in dispersive regions and the impact of longitudinal nonlinearities [37-39].

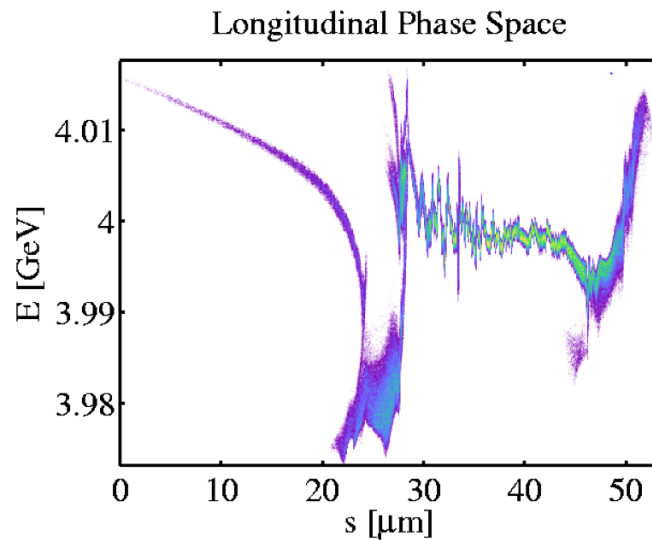


Figure 12: Longitudinal phase space illustrating micro-bunching instability.

These new effects have led to design modifications to moderate their impact. For example, seven additional small chicanes have been added along the beamline to locally compensate the longitudinal dispersion (R56) of bending regions and thereby mitigate the microbunching instability [40]. With these changes, it is believed that the high-rate HXR and SXR FEL's will exceed specification of >20 W across the parameter range as described in the following section. In parallel, experimental studies are being performed on the LCLS to verify the simulation codes in a parameter regime similar to that expected for the LCLS-II operation [41, 42]. When complete, this confirmation is expected to provide significant confidence in the LCLS-II accelerator and FEL design.

3.4.4 Performance Simulations

High fidelity numerical particle simulations that leverage a number of accelerator and FEL codes have been used to analyze the LCLS-II FEL performance. Together, the physics models that are included in these codes have been crucial in identifying, understanding, and mitigating a number of potential hazards that can adversely affect the FEL performance some of which have been discussed above. Here, we present a brief overview of the LCLS-II FEL performance, based on these start-to-end simulations, for both the soft X-ray and hard X-ray undulators including both SASE and self-seeded operational modes as of July 2015, the date of the most recent complete global optimization study.

3.4.4.1 Simulation Strategy and Computational Setup

As noted, the simulation results reported here are based on the suite of codes IMPACT and GENESIS. These simulations include the effects of three-dimensional space-charge, coherent and incoherent synchrotron radiation, RF cavity wakefields and resistive wall wakefields in the generation, acceleration and transport of the electron beam from the cathode to the undulator for three charge distributions: 20 pC, 100 pC, and 300 pC. To model the initial shot-noise of the electron beam, which may act as the seed for the space-charge driven microbunching instability, the number of macro-particles tracked from the cathode were equal to the real number of electrons. The various charge distributions were then used to define the electron beams in GENESIS, where resistive wall wakefield effects are also included in the FEL simulations. Self-amplified-spontaneous-emission (SASE) has been studied across the tuning ranges for each of the individual

charge distributions for both the HXR and SXR undulators; these studies include fully time-dependent taper optimizations.

3.4.4.2 *Electron Beam Properties*

A detailed start-to-end simulation study of the accelerator beam delivery system can be found elsewhere [43, 44]. Below, we present the electron beam longitudinal phase space and critical slice parameters for each of the three charge distributions discussed above at the entrance to the SXR undulator and then we will discuss the FEL simulations. As noted, optimization of the electron beam and FEL pulses is ongoing and the results presented below provide a snap-shot as of summer, 2015.

3.4.4.3 *20 pC*

Figure 13 shows the longitudinal phase space along with various slice properties of the 20 pC electron beam that has been tracked to the SXR undulator.

The core of the distribution is roughly 8 μm long, is slightly chirped with the head of the beam having a lower energy, and has a $\sim 300 \mu\text{A}$ current; the energy chirp is removed using the resistive wakefield of the long transport line and a small adjustment of parameters should allow the residual chirp to be compensated. The normalized slice emittance is less than $\sim 0.2 \text{ mm-mrad}$ in both transverse planes, so while the current is rather low, the beam is sufficiently bright such that it can produce greater than 20 μJ of energy per pulse at the high end of the tuning range in the HXR undulator (5 keV). The rms slice energy spread in the core of the beam is about 0.45 MeV if one neglects the filamentation seen in the longitudinal phase space.

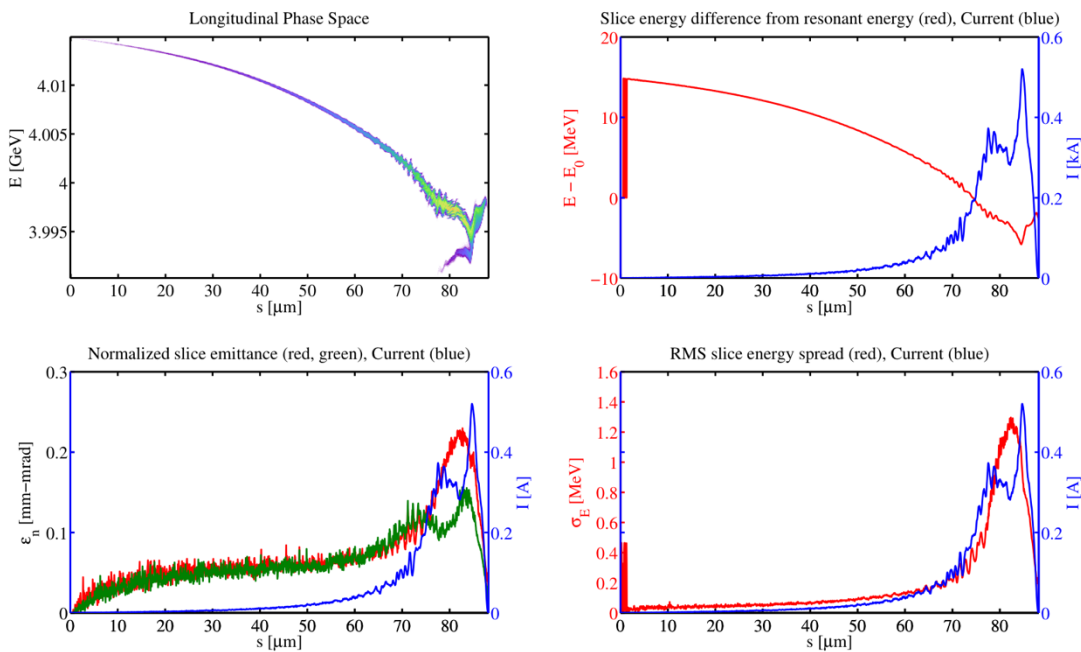


Figure 13: Slice properties of the 20 pC electron beam.

3.4.4.4 100 pC

Figure 14 shows the longitudinal phase space along with various slice properties of the 100 pC electron beam that has been tracked to the SXR undulator.

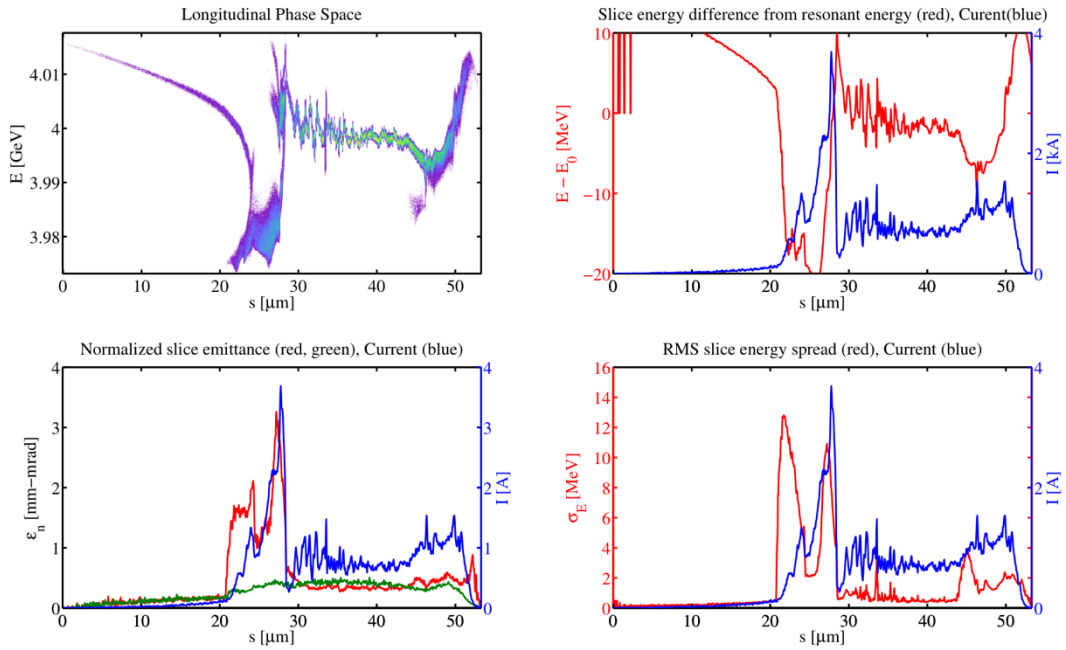


Figure 14: Slice properties of the 100 pC electron beam.

3.4.4.5 300 pC

Figure 15 shows the longitudinal phase space along with various slice properties of the 300 pC electron beam that has been tracked to the SXR undulator.

The core of this distribution, which is less impacted by the space-charge induced micro-bunching instability than the 100 pC electron beam, is roughly 50 μm long and has a current of 900 A. The normalized slice emittance is less than 0.70 mm-mrad in both transverse planes while the rms slice energy spread is roughly 0.40 MeV. While the larger transverse emittance for this charge distribution will negatively impact the performance at the high end of the tuning range of the HXR undulator, the relatively flat longitudinal phase space in the core may be useful for self-seeded or externally seeded applications [45].

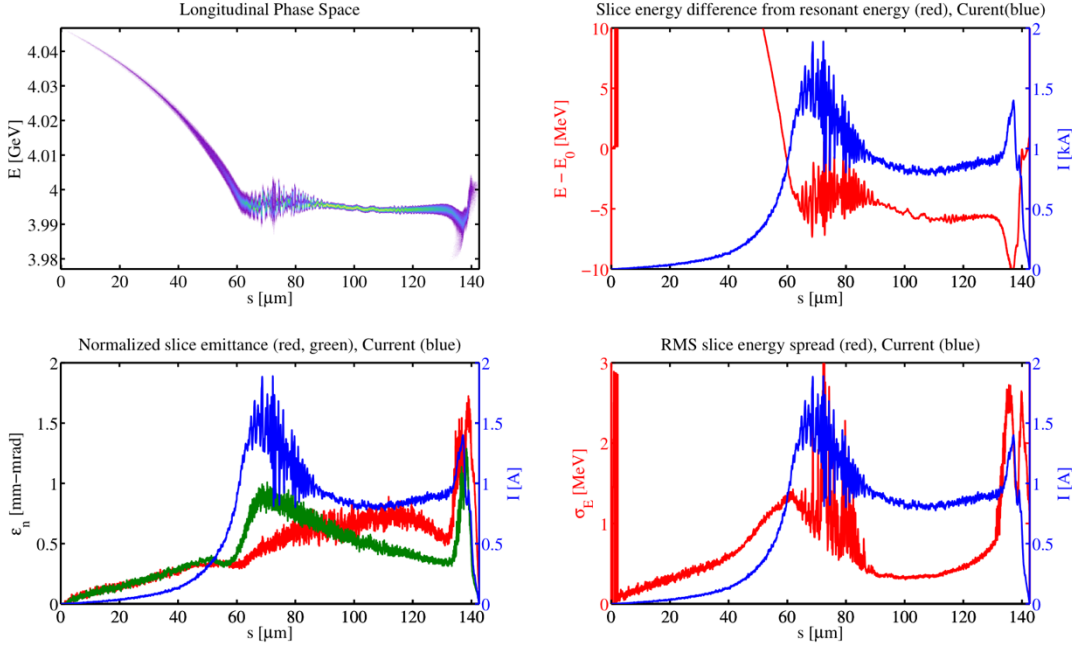


Figure 15: Slice properties of the 300 pC electron beam.

3.4.4.1 *SASE Tapering Optimization and Performance Study*

The tapering scheme employed here follows the strategy laid out in [46] and is based on a three-parameter optimization of the final FEL pulse energy. Fully time-dependent (not single-slice or monochromatic) FEL taper optimizations are needed in order to accurately capture the dynamics of SASE in the post-saturation regime. The optimal taper that is nominally given by single-slice optimization scans is more appropriate for seeded FELs. This is because particles in distinct coherence regions (SASE spikes) tend to have uncorrelated ponderomotive phases [47]. We have found that the optimal taper found from a single-slice parameter scan often produces less than half the energy that could be achieved by a full time-dependent parameter scan. This is a significant result as the accurate characterization of the pulse energy, along with the effective source size and divergence, are needed to ensure optimal x-ray transport to the various end stations.

A summary of the LCLS-II SASE performance with post-saturation tapering can be found in Table 4 and illustrated in Figure 16 for the charge distributions and tuning ranges that span the relevant parameter spaces. The SASE FEL seems to be insensitive to the microbunching induced energy and current modulations at all but highest photon energies in the HXR undulator, where the beam is more sensitive to slice energy spread. In many cases, the maximum expected average X-ray power is higher than the power limit of the X-ray transport design of 200 Watts and, to stay within the power limits, either the FEL repetition rate could be reduced or the X-ray pulse energy could be reduced by not tapering fully.

Table 4: LCLS-II SASE Performance. Black: E (μJ) after taper, () - at saturation; Green: Δt_{FWHM} (fs); Cyan: ΔE_{γ} (eV); Purple: P_{Pk} (GW); Red: P_{Avg} (W); Pink: z_0 (m); Blue: σ_{rms} (x,y) (μm); Brown: Θ_{rms} (x,y) (μrad); at 5 keV, lasing requires very bright beams.

	SXR			HXR		
	250eV	750eV	1.25keV	1.5keV	3.25keV	5keV
20pC (1.5 MHz)	267 (42), 35, 3, 8, 400, 32, (297, 307), (16.5, 16.9)	239 (43), 32, 6.5, 8, 360, 26, (104, 105), (7.10, 7.31)	168 (41), 38, 8, 4, 250, 20, (59, 57), (4.52, 4.55)	206 (27), 34, 4.5, 6, 310, 72, (79, 83), (4.11, 4.20)	147 (22), 39, 7, 4, 220, 50, (51, 49), (1.71, 1.72)	25 (7), 17, -, 1.5, 38, 24, (29, 29), (1.49, 1.52)
100pC (300 kHz)	1205 (260), 52, 3, 23, 360, 34, (290, 245), (13.74, 11.60)	795 (135), 50, 6, 16, 240, 28, (95, 77), (5.61, 5.30)	527 (76), 43, 6, 12, 160, 22, (57, 54), (3.59, 3.40)	1136 (111), 45, 5, 25, 340, 62, (79, 78), (2.94, 2.86)	469 (46), 46, 8, 10, 140, 40, (51, 51), (1.54, 1.56)	10 (6), 25, 10, 0.5, 3, 14, (52, 53), (2.49, 2.54)
300pC (100 kHz)	5482 (1013), 252, 4, 22, 550, 40, (178, 164), (9.76, 9.10)	3844 (519), 215, 4, 18, 380, 20, (62, 65), (4.83, 4.68)	1897 (422), 150, 4, 13, 190, 16, (42, 39), (3.56, 3.62)	2364 (300), 130, 3, 18, 240, 62, (70, 65), (2.93, 2.66)	642 (147), 120, 3.5, 5, 64, 40, (45, 43), (1.65, 1.56)	-(0.4), -, -, -, -, -, -, -, -

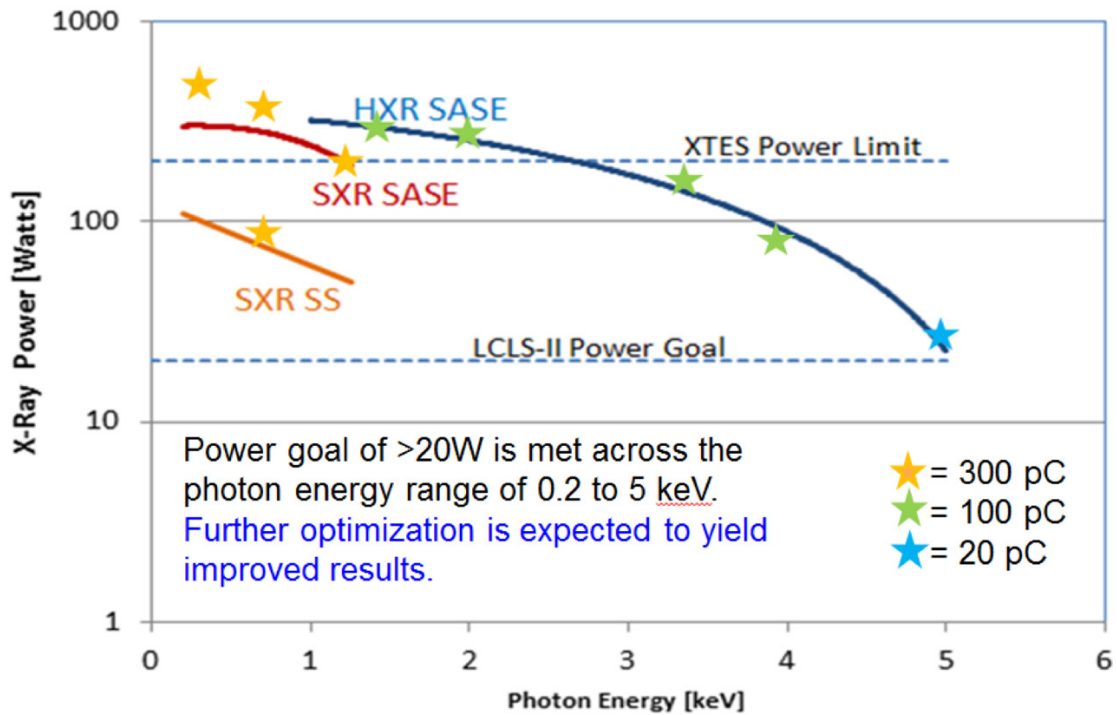


Figure 16: SASE X-ray average power from LCLS-II high-rate beam.

3.4.4.2 *Self-Seeded Simulation Strategy and Performance Study*

The SXR beamline will incorporate a self-seeding system (SXRSS) to produce longitudinally coherent soft X-ray FEL pulses. It will consist of two sections of undulator that are separated by a monochromator and a magnetic chicane. The first undulator will consist of 7-8 independent segments while the second undulator consists of 13-14 independent segments. The monochromator design will be based on the existing LCLS SXRSS monochromator [48] with additional flexibility built in. It will have a compact footprint that is designed to allow both the chicane and monochromator to occupy the equivalent space of a single undulator segment along the strong focusing quadrupole FODO cell strongback. The resolving power is nominally specified to be $R = 15,000$, but upgrade paths to $R \sim 30,000$ are being explored.

The specification of the individual components of both the monochromator and chicane are not yet established. As such, a phenomenological approach is used to model the bandwidth reduction of the seed numerically. The nominal monochromator design relative bandwidth ($1/R$) and overall efficiency ($\sim 5\%$) are used to specify the amplitude of a Gaussian frequency filter function. The phase of the filter function is defined through Kramers-Kronig relations such that causality is not violated when the filter is applied to the fully three-dimensional FEL pulse exiting the seventh or eighth undulator section. The fields exiting the monochromator are then used to specify the seed into the next undulator. Diffraction through the actual monochromator setup is not modeled. This is, however, a small effect at these photon energies. In addition, a new and simple optical propagation theory has been developed to track the full three-dimensional field through the optical lattice and will be explored when the monochromator design has matured [49].

The magnetic chicane serves the dual role of compensating for the delay introduced by the monochromator and destroying any residual electron beam microbunching from the first undulator. This is modeled in a very simple way by using the dumped particle distribution and re-initializing the shot-noise.

The nominal performance for the SXRSS system using the 100 pC electron beam distribution tuned to produce 750 eV photons (no taper) is illustrated in Figure 17.

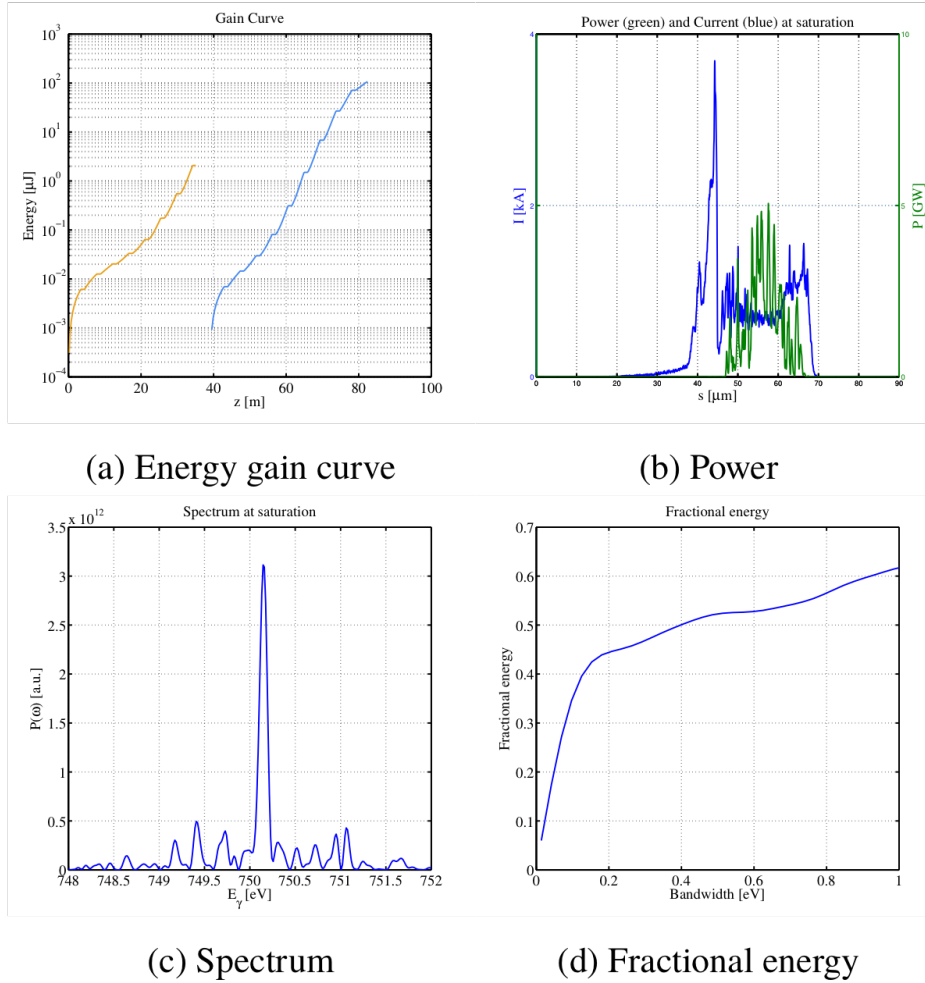


Figure 17: (a) Energy gain curve for the SASE undulator (orange) which generates the seed to be monochromatized and amplified downstream (blue); (b) Power (green) and current (blue) at saturation; (c) On-axis spectrum at saturation; (d) Fractional energy within a given bandwidth at saturation.

The first undulator terminates the field growth well before saturation after 8 undulator sections (orange, Figure 4a). Here, the FEL energy is roughly $2 \mu\text{J}$ while the longitudinal profile in both the spectral and temporal domain display the typical SASE spiking. The field is then frequency filtered while the electron beam shot-noise is re-initialized according to the description above. The field is amplified to saturation in a downstream undulator (blue, Figure 4a). The temporal duration at this point is roughly $\Delta t = 36$ fs (green, Figure 4b), which is consistent with the resolving power of $R=15,000$ at this photon energy. Some spiking due to the fluctuating electron beam slice properties is evident.

The spectrum achieved in simulation thus far (Figure 4c) has a dominant spike with a spectral width $\Delta E_\gamma \sim 100$ meV, which is roughly twice as large as the initial bandwidth defined by the monochromator resolving power. This is partly a result of the longer wavelength energy and density modulations [50, 51] present along the longitudinal phase space of the electron beam as well as long wavelength resistive wall wakefield induced energy modulations. Additionally, the higher frequency modulations produce the additional frequency content shown in the figure. These effects conspire to lower the fractional energy that is stored within the primary bandwidth of the FEL pulse, which in turn lowers the overall peak spectral brightness. We expect improved

performance using the 300 pC beam which has reduced longitudinal phase space distortion. Optimization of the self-seeded spectrum is ongoing.

3.4.5 Conclusion

The LCLS-II project is developing an upgrade to the LCLS X-ray FEL at SLAC that is based on a 4 GeV SCRF linac and two variable-gap undulators. The project is being constructed by a collaboration of six institutions from across the US. The design of the accelerator and required hardware is well advanced with prototypes of the injector and undulators complete and prototypes of the cryomodules in fabrication. The simulated performance achieves the baseline project goals and performance optimizations are ongoing with further improvement expected. The project is rapidly proceeding toward first X-rays at the end of 2019.

3.4.6 Acknowledgments

The LCLS-II project is a huge undertaking which is the result of a strong national collaboration and international support. In particular, the authors would like to thank members of the LCLS-II beam physics group for their support and editing of this document. As noted in the Introduction, much of the material for the paper is taken from Refs. [11] and [12]. Given the rapid pace of the LCLS-II project much of the material is not yet documented in peer-reviewed articles and can only be found in the conference proceedings of the IPAC and FEL meetings. Work supported by DOE Contract: DE-AC02-76-SF00515 and the LCLS-II Project.

3.4.7 References

1. Linac Coherent Light Source (LCLS) Conceptual Design Report, SLAC-R-593 (2002).
2. P. Emma, et al., *Nat. Photonics* **4**, 641 (2010).
3. C. Boestedt, et al., *Rev. Mod. Phys.* **88**, 015007 (2016); and references within.
4. Science Driven Instrumentation for LCLS-II, https://portal.slac.stanford.edu/sites/lcls_public/Instrument_Document_Repository/LCLS-II_Instrumentation_Whitepaper_DOE.pdf (2015).
5. Y. Nosochkov, et al., MOPOW048, IPAC'16, Busan, South Korea (2016).
6. Z. Huang, MOB02, FEL'15, Daejeon, South Korea (2015).
7. Y. Ding, TUA01, FEL'15, Daejeon, South Korea (2015).
8. A. Marinelli, et al., WEP080, FEL'15, Daejeon, South Korea (2015).
9. Z. Zhang, et al., WEP059, FEL'15, Daejeon, South Korea (2015).
10. J. MacArthur, et al., WEP004, FEL'15, South Korea (2015).
11. G. Marcus, et al., TUP007, FEL'15, Daejeon, South Korea (2015).
12. T.O. Raubenheimer, WEP014, FEL'15, Daejeon, South Korea (2015).
13. A. Grassellino et al., *Supercond. Sci. Technol.*, **26**, 102001 (2013).
14. A. Grassellino, MOYGB2 IPAC'15, Richmond, VA (2015) and references within.
15. A. Freyberger, MOXGB2 IPAC'15, Richmond, VA (2015) and references within.
16. C. Nantista and C. Adolphsen, LCLSII-TN-15-29, unpublished (2015).
17. C. Hovater, MOPWI021 IPAC'15, Richmond, VA (2015).
18. F. Sannibale et al., *Phys. Rev. STAB* **15**, 103501 (2012).
19. R. Huang, et al., *Phys. Rev. STAB* **18**, 013401 (2015).
20. F. Sannibale, et al., TUOCA02, IPAC'16, Busan, South Korea (2016).
21. C. Gulliford et al., *Phys. Rev. STAB* **16**, 073401 (2013).
22. C. Gulliford, et al, *Phys. Rev. STAB* **18**, 083401 (2015).

23. F. Zhou, et al., MOP021, FEL'15, Daejeon, South Korea (2015).
24. C. Mitchell, et al., TUP073, FEL'15, Daejeon, South Korea (2015).
25. J. Amann, et al., Nature Photonics **6**, 693 (2012).
26. A. Temnykh, Phys. Rev. STAB, **11**, 120702 (2008).
27. H.D. Nuhn, et al., WED01, FEL'15, these proceedings.
28. E. Gluskin, TUXC1 IPAC'15, Richmond, VA (2015) and references within.
29. http://journals.iucr.org/s/facilities/current_aps.pdf (2016).
30. Y. Feng, et al., TUP056, FEL'15, Daejeon, South Korea (2015).
31. Y. Feng, et al., Proc. of SPIE, **9589**, 958910 (2015).
32. J. Qiang et al., Phys. Rev. STAB, **9**, 044204 (2006).
33. J. Qiang et al., J. of Comp. Phys., **163**, 434 (2000).
34. J. Qiang et al., Phys. Rev. STAB, **12**, 100702 (2009).
35. M. Borland, APS LS-287, unpublished (2000).
36. S. Reiche, Nucl. Instr. & Meth. **A429**, 243 (1999).
37. Y. Ding, et al., TUPMA003, IPAC'15, Richmond, VA (2015) and references within.
38. M. Venturini, et al, TUC01, FEL'15, Daejeon, South Korea (2015).
39. M. Venturini and J. Qiang, Phys. Rev. STAB, **18**, 054401 (2015).
40. J. Qiang, et al., TUPOR018, IPAC'16, Busan, South Korea (2016).
41. D. Ratner et al., PRSTAB **18**, 030704 (2015).
42. D. Ratner et al., MOP058, FEL'15, Daejeon, South Korea (2015).
43. M. Venturini et al., TUC01, FEL'15, Daejeon, South Korea (2015).
44. J. Qiang et al., WEP070, FEL'15, Daejeon, South Korea (2015).
45. G. Penn et al., WEP025, FEL'15, Daejeon, South Korea (2015).
46. Y. Jiao et al., Phys. Rev. STAB, **15**, 050704 (2012).
47. W. M. Fawley, Nucl. Instr. Meth. Phys. Res. Sec. A **483**, 537 (2002).
48. D. Ratner, et al., Phys. Rev. Lett., **114**, 054801 (2015).
49. G. Marcus, Opt. Express, **24**, 7 (2016).
50. S. Serkez, et al., Phys. Rev. STAB, **18**, 030708 (2015).
51. Z. Zhang et al., Phys. Rev. STAB, **19**, 050701 (2016).

3.5 Commissioning and Start-up of NSLS-II*

F. Willeke for the NSLS-II Design-, Construction- and Commissioning Team†

Mail to: willeke@bnl.gov
BNL, Upton, NY 11973, USA



Figure 1 : Aerial view of NSLS-II.

3.5.1 Abstract

This report describes the design and performance of the NSLS-II, the new 3rd generation light source at Brookhaven National Laboratory. The 3 GeV NSLS-II storage ring with 792 m circumference is designed for a peak brightness of 10^{22} photons $\text{sec}^{-1}\text{mm}^{-2}\text{mrad}^{-2}$ ($0.1\%BW$)⁻¹ enabled by a beam energy of 3 GeV, a maximum design beam current of 500 mA and a horizontal beam emittance of 0.9 nm rad. Orbital stabilization systems are designed to maintain the beam position within 300 nm ($< 10\%$ of the vertical beam size). These performance parameters allow extending the investigation of the structure of matter by X-ray imaging to a spatial resolution of 1 nm and an energy resolution of 0.1 meV. The accelerator complex was constructed between 2009 and 2014 and was commissioned in 2014. The storage ring started to deliver photons to the first of the six project beamlines in October 2014. The NSLS-II project was completed in 2015 and NSLS-II is now in its 2nd year of operations. All design parameters have been demonstrated and are achieved in routine operation except for total beam current which is presently (May 2016) at 80% of the design value.

3.5.2 Introduction

An era came to an end on 30 September 2014, when the National Synchrotron Light Source (NSLS) ended its last run and dumped its last beam after more than 30 years of operation at Brookhaven National Laboratory. NSLS was the first of the modern synchrotron light sources and had an enormous impact on synchrotron-light-based science over the past decades. It contributed a wealth

* Work supported by DOE under contract No. DE-AC02-98CH10886

† Gabriele Bassi, Johan Bengtsson, Alexei Blednykh, Eric Blum, Weixing Chen, Jinhyuk Choi, Leo Dalesio, Michael Davidsaver, Lewis Doom, Ray Flliller, Gregory Fries, George Ganetis, John Gosman, Wei Ming Guo, Richard Heese, Yoshiteru Hidaka, Hsiao Chaun Hseuh, Stephen Kramer, Samuel Krinsky[deceased], Yongjun Li, Satoshi Ozaki, Boris Podobedov, James Rose, Sergey Seletskiy, Om Singh, John Skaritka, Sushil Sharma, Timur Shaftan, Toshiya Tanabe, Yuke Tian, William Wahl, Gui Mei Wang, Lingyun Yang, Xi Yang, Li Hua Yu, and Emil Zitvogel

of pioneering scientific results, including work that resulted in two Nobel prizes [1, 2]. The following day, 1 October 2014, a new era began for Brookhaven, with the start-up of the new facility, NSLS-II, which is designed to provide the brightest beams ever produced by a synchrotron light source.

The mission of the new facility which was to replace NSLS was to provide a factor of 10 more flux and up to four orders of magnitude more brightness relative to the earlier machine (where brightness is defined as the number of photons per second divided by the beam cross-section at the source and the divergence at the emission point, integrated over a narrow bandwidth of 0.1% at 12 keV). It was to be capable of achieving energy resolution of a fraction of a milli-electron-volt and spatial resolution on the nano-meter scale. This ambition was acknowledged in 2005, when the NSLS-II received CD-0, the first of five “critical decisions” for the construction of any new science facility funded by the US Department of Energy (DOE). The new light source was to enable novel science opportunities in all fields of synchrotron-radiation-based science and would allow experiments that were not possible at any of the other facilities at that time. The project went swiftly through the design and R&D phase documented in the preliminary design report PDR [3] with critical decisions CD-1 and CD-2, and in June 2009, CD-3 was approved, allowing construction of the facility to begin. Construction proceeded smoothly so that the accelerator commissioning could be completed in the fiscal year 2014 (FY14) as originally planned. The NSLS-II project included in addition to the accelerators also the civil construction and six initial, state-of-the-art synchrotron radiation beamlines. It was completed in the spring of 2015 with the critical decision 4 (CD-4) which was obtained three month before the originally scheduled date. First light was delivered to the Coherent Soft X-ray Beamline (CSX) in October 2014.

Operation of the NSLS-II accelerators started on October 1st 2014 with commissioning of the insertion devices, the beam line fronts end and the six beam lines which were funded by the NSLS-II project. This was completed by the end of 2014. Operation for beam lines started in February 2015. During machine studies, the performance of the accelerator complex was steadily improved. By the end of April 2016, 400 mA of beam current was demonstrated and all other design parameters of NSLS-II had been achieved.

This report will focus on the accelerator part of NSLS-II. The basic design considerations and decisions are described in sections 2 and 3. This is followed by the technical description of the accelerator components in section 4. The on-energy injector (3 GeV) is described in section 5. Section 6 discusses commissioning and section 7 describes the NSLS-II insertion devices. The report concludes with the description of the present performance of the accelerator.

3.5.3 General Layout

The design goal of a synchrotron light source is to maximize the effective brightness (emitted photons per unit of time divided by the area of the source and the beam divergence within a certain bandwidth around the photon energy of interest) for a maximum number of beamlines in a desired range of photon energy and for an affordable cost. Furthermore, the facility needs to be designed for reliable and stable operation in support of a large and diverse user community.

These requirements translate into a number of conflicting design choices which needed to be optimized. The most basic ones are the beam energy, the beam current, and the emittance which is closely related to the choice of the storage ring circumference.

The beam energy of 3 GeV was chosen as it is close to the minimum beam energy that allows achieving high brightness photon beams with energies in the range of 10 keV with state-of-the-art of insertion devices. The brightness versus photon energy (see Figure 15) emitted by various in-vacuum undulators versus photon energy exceeds values of

$$B = 10^{21} \text{ photons } s^{-1} \text{ mm}^{-2} \text{ mrad}^{-2} (0.1\% BW)^{-1}$$

(assuming a beam current of 500 mA and a horizontal beam emittance of $\epsilon_x = 1 \pi \text{ nrad m}$).

The considerations for choosing the NSLS-II circumference are discussed in the following paragraph.

A large circumference allows for a small emittance since it accommodates a large number of accelerator cells (a repetitive structure of bending and focusing magnets) and the emittance scales like one over the third power in the number of cells. This follows directly from inspecting the canonical expression for the emittance given in reference [4]. It offers sufficient space for long insertion devices (wigglers and undulator magnets). It also provides sufficient space on the experimental floor for a large number of state-of-the-art beam lines. With sufficiently large circumference, there is space for long bending magnets with relatively low bending field. The total synchrotron radiation power emitted in the dipole magnets is therefore low as it scales with one over bending radius and the beam current is less likely to be limited by synchrotron radiation power loss. Moreover, the radiation loss in the dipole magnets is so low that we can afford to double the synchrotron radiation losses by installing strong wiggler fields in the straight sections (damping wigglers DW). This increases radiation and reduces the emittance by a factor of two. Low bending fields also create a margin in the beam energy spread which is important to achieve high brightness in higher harmonic undulator radiation. The obvious disadvantage is higher cost which scales almost linearly with circumference. Another disadvantage of the weak bending magnet is that the soft synchrotron radiation from the dipole magnets is only of limited use for synchrotron radiation beam lines.

These considerations led to the choice of the NSLS-II storage ring circumference of 792 m . This circumference is divided in five pentants and accommodates 30 achromatic cells and provides room for 30 straight sections alternating between long (9.3 m) and short (6.6 m). Twenty seven straight sections are for insertion devices. There is one long straight section for injection, and two long ones for RF cavities. The ratchet-shaped outer shield wall is laid out for 57 beam ports, 27 for insertion device radiation and 30 for bending magnet radiation. The facility can host at least 57 beamlines. Figure 2 shows the overall layout of the NSLS-II facility.

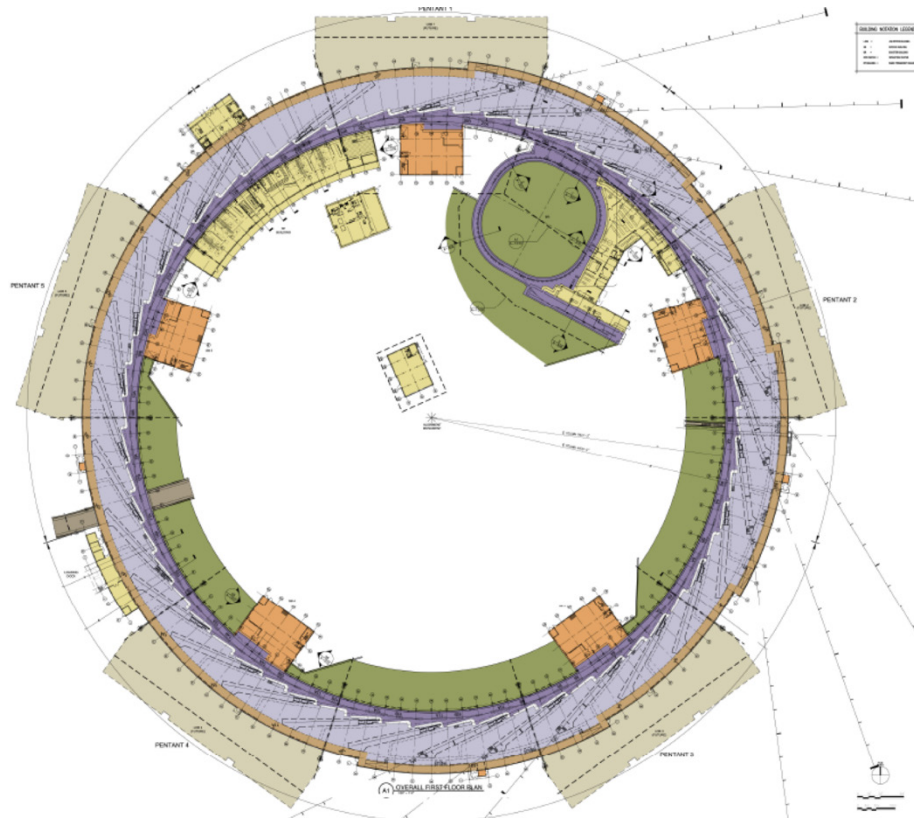


Figure 2: Layout of the NSLS-II Facility. The drawing shows the accelerator tunnel (width x height = 3.2 m x 3.8 m) composed of five pentants surrounded by the experimental floor of 15 m width (not counting a walkway) which accommodates 65 m long beamlines. The compact injector complex consisting of the 200 MeV LINAC and the 3 GeV booster synchrotron with 158 m circumference is placed the inside of the ring-building (at 1 o'clock). There are five service buildings inside the ring which accommodate mechanical utilities and HVAC equipment. A cooling tower is located in the center of the ring. The service building at 11 o'clock is for RF transmitters and for the liquid He plant. On the outside of the ring there are five laboratory office buildings with 144 seats each and a small entrance lobby. Areas shown in green around the inner wall of the storage ring and the injector complex indicate earth berms for radiation shielding.

3.5.4 Accelerator Lattice

NSLS-II has a double bend achromat lattice (DBA) with 30 cells on a 792 m circumference. The achromat is mirror-symmetric around the central horizontally focussing quadrupole magnet. The dipole magnets are rather long and weak ($l = 2.62 \text{ m}$, $B = 0.4 \text{ tesla}$) which allows obtaining close to DBA minimum beam emittance with moderate peak beta-values and a horizontal chromaticity of -3.3 per cell. The horizontal emittance depends on the number of cells, the beam energy and the parameter $X = \beta_{\xi\text{-min}}/L_B$, the minimum horizontal beta in the dipole magnets in units of the dipole length (assumed to occur at the optimum position in the dipole)

$$\varepsilon_x = \frac{C_q \gamma^2}{J_x} \cdot \left(\frac{\pi}{N}\right)^3 \cdot \left(\frac{1}{320 \cdot X} + \frac{1}{3}X\right)$$

($C_q = 3.84 \cdot 10^{-13} \text{ m}$ is the radiation-constant; $\gamma = 5871$ is the relativistic factor; $J_x \approx 1$ is the damping partition number; $N = 30$ is the number of DBA cells; note that weak focussing and edge effects are neglected).

The minimum emittance would be achieved with $X = 0.1$ yielding $\varepsilon_x = 1 \text{ nm rad}$, but this requires unreasonably large beta functions of 80 m around the dipole. The value chosen for NSLS-II is $X = 0.37$ which yields an emittance of 2 nm rad . This choice limits the maximum beta to less than 30 m and provides sufficient dynamic aperture and a manageable sensitivity to imperfections and errors. The lattice functions of NSLS-II are depicted in Figure 3. The photograph in Figure 4 shows the accelerator tunnel with a complete DBA-cell.

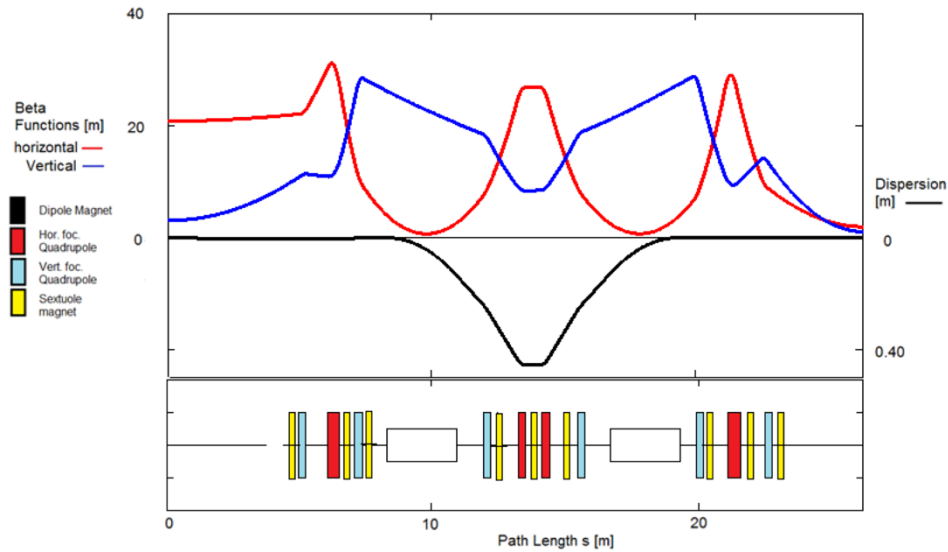


Figure 3: Lattice function of a NSLS-II DBA cell. Adjacent cells are mirror-symmetric to the one shown. The horizontal and vertical beta functions are the red and the blue lines respectively, and the dispersion function is plotted in black (note that the positive direction for the dispersion is pointing downwards).

The soft bending fields of 0.4 Tesla imply low energy loss per turn (286 keV per electron per turn). These are favorable conditions for increasing radiation damping by adding six 3.4 m long damping wigglers, with a peak field of 1.85 Tesla . They increase the radiation damping and reduce emittance by more than a factor of two. The design value of the horizontal beam emittance obtained this way is only $\varepsilon_x = 0.9 \text{ nm rad}$. The straight sections for insertion devices alternate between long (9.3 m , minimum vertical beta is 3 m) and short (6.6 m , minimum vertical beta is 1 m). The optical distortion from the edge effects of the damping wigglers are strong and require local compensation by quadrupole magnets. This breaks the 15-fold super-symmetry weakly to 3-fold super-symmetry. Three of the long straight sections are needed for injection and the four 500 MHz superconducting RF cavities.



Figure 4: View of one NSLS-II DBA cell

The achromat focusing is provided by a quadrupole triplet. Two additional quadrupole triplets on both sides of the achromat match the beam to the straight sections.

Strong sextupoles are required to compensate the chromaticity in the NSLS-II lattice ($m \cdot l = \frac{ec}{E} \int ds \frac{\partial^2 B_y}{\partial x^2}$ is in the order of $5-8 \text{ m}^{-2}$, B_y is the magnetic field in the vertical direction, E is the beam energy, c is the speed of light and e is the elementary charge). The chromaticities are $\xi_{x,y} = \frac{\partial}{\partial \delta} Q_{x,y} = -93, -46$ ($Q_{x,y}$ are the betatron tunes, $\delta = \Delta p/p$ is the relative momentum deviation from the nominal value) in the horizontal and the vertical plane respectively. Chromaticity is compensated by a strong horizontally focussing sextupole in the center of the achromat where the dispersion function reaches a value of 45 cm and by two adjacent defocusing sextupoles which constitutes a two-family chromatic correction. The strong quadrupoles and the sextupoles lead to significant chromatic distortions of the beta function and the dispersion function which gives rise to significant 2nd and higher order tune shift with momentum. The corresponding chromatic tune footprint is quite large and barely fits between the major resonances for ten times the rms energy spread ($10 \cdot \delta_{rms} = 0.36 \%$). Higher order chromatic corrections are thus necessary. This is achieved by breaking the mirror symmetry of the achromat and moving the downstream defocussing sextupole 15 cm closer to the center of the achromat. The strength of the two defocusing sextupoles is optimized individually. This reduces the tune footprint sufficiently to ensure good off momentum dynamic aperture (this is further discussed below). The main parameters of the NSLS-II storage ring are summarized in Table 1.

3.5.5 Accelerator Subsystems

The accelerator magnets of NSLS-II are conventional electro-magnets. All 300 quadrupole magnets are individually powered by switched mode power supplies. Sextupole magnets are powered in 9 circuits in each of the five pentants. Correctors include 180 iron yoke dipole correctors (1 mrad strength) in each plane for slow orbit corrections. There are correction windings on the dipole coils (for a 3 mrad correction). Each cell has an air coil- skew quadrupole mounted on the corrector magnet. There are 90 air-coil dipole correctors in each plane which can generate a $15 \mu\text{rad}$ correction kick each. The quadrupole and sextupole magnets are built to small tolerances of the magnetic field. Quadrupole fields have relative deviations from the ideal field of less than 10^{-4} (10^{-3} for sextupoles) within a 25 mm radius around the center. To achieve this high field quality, advanced manufacturing techniques (two stage high precision machining, a combination of

stamping and fine blanking of the laminations as well as wire erosion techniques) were applied to shape the magnetic poles and yokes with a precision of $10 \mu\text{m}$ and to position the poles with respect to each other with the same precision. As the magnets need to be separated to insert the vacuum chamber, high mechanical stability of the iron yokes to maintain the high field quality are required. The reinforced yokes deform by less than $10 \mu\text{m}$ when separated and reassembled.

The residual orbit distortions after correction and system optimizations (such as BPM offset compensation) are mainly due to limitations of the non-local dipole corrector system and the residual orbit errors are proportional to the uncorrected distortion.

Table 1: Main NSLS-II Storage Ring Design Parameters

Parameter		Design Value
Beam Energy	[GeV]	3
Circumference	[m]	792
Lattice Type		DBA
Number of DBA cells/straight sections		30
Length of the short straight section	[m]	6.6
Length of the long straight section	[m]	9.3
Horizontal Beam Emittance with/without DW	[nm-rad]	2, 0.9
Vertical Beam Emittance	[pm-rad]	8
Betatron Tunes / DBA cell		1.107, 0.541
Natural Chromaticities in x and y per DBA cell		-3.2, -1.05
Dynamic Aperture, horizontal, vertical	[mm]	16, 3
Dynamic Relative Momentum Aperture		0.03
Touscheck Lifetime at 0.5 mA Bunch current	[h]	3
Dipole field, length, bend angle	[T,m,mrad]	0.4, 2.62, 104.7
Quadrupole length, strength	[m, T/m]	0.25, 14-22
Number of quadrupole magnets per achromat		10
Number of Sextupoles per DBA cell		9
Sextupole Length, Strength	[m, T/m ²]	0.20, 400
Number of hor. and vert. dipole correctors per cell		6
Number of Skew quadrupoles per cell		1
Number of fast (air-coil) correctors per cell		3
Number of damping wigglers, length, peak field	[,m, T]	6, 3.4, 1.85
Energy loss per turn per electron with/without DW	[keV]	286, 676
Damping Times: Horizontal, Vertical, Longitudinal	[ms]	55.6, 55.5, 27.7
RMS Relative Energy Spread		$3.4 \cdot 10^{-4}$
Momentum Compaction Factor		$3.6 \cdot 10^{-4}$
RF Frequency	[MHz]	500

This consideration is the motivation for tight tolerances on quadrupole alignment errors of $30 \mu\text{m}$. Similar arguments hold for the alignment of sextupole magnets which cause beam optics distortions. The key factor in meeting this alignment tolerance is the knowledge of the magnetic center with at least the same precision, which has been achieved by a stretched wire method [6]. A wire which carries an AC current of the frequency of one of its mechanical oscillation modes is stretched through the magnet apertures. The wire will oscillate if it is not in the magnetic centre of the quadrupole and sextupole magnets. The wire automatically scans the vertical and horizontal apertures to detect the point of zero excitation. A procedure has been developed to measure the magnet centers of all 6 multipole (4 and 6 pole) magnets mounted on their girder. The loaded girder is placed in a temperature controlled room. After the magnetic centers have been found by exciting the appropriate wire modes, the magnets were adjusted manually so that their magnetic centers are aligned along on a common straight line. After locking the magnet into these positions, the positions of fiducials on the magnets and on the surface of the support with respect to the wire fiducials are measured with (5-10) micron precision girder with laser trackers. This allowed transporting the girder to the accelerator tunnel and restoring the magnet alignment by adjusting the girder supports. This method was thoroughly tested thereby exceeding the specified alignment tolerance (rms value of about 15 microns) which was confirmed later during commissioning with beam. This method worked well with girders fabricated with only normal manufacturing tolerances (100 microns). Figure five illustrates the high precision alignment of quadrupole and sextupole magnets.

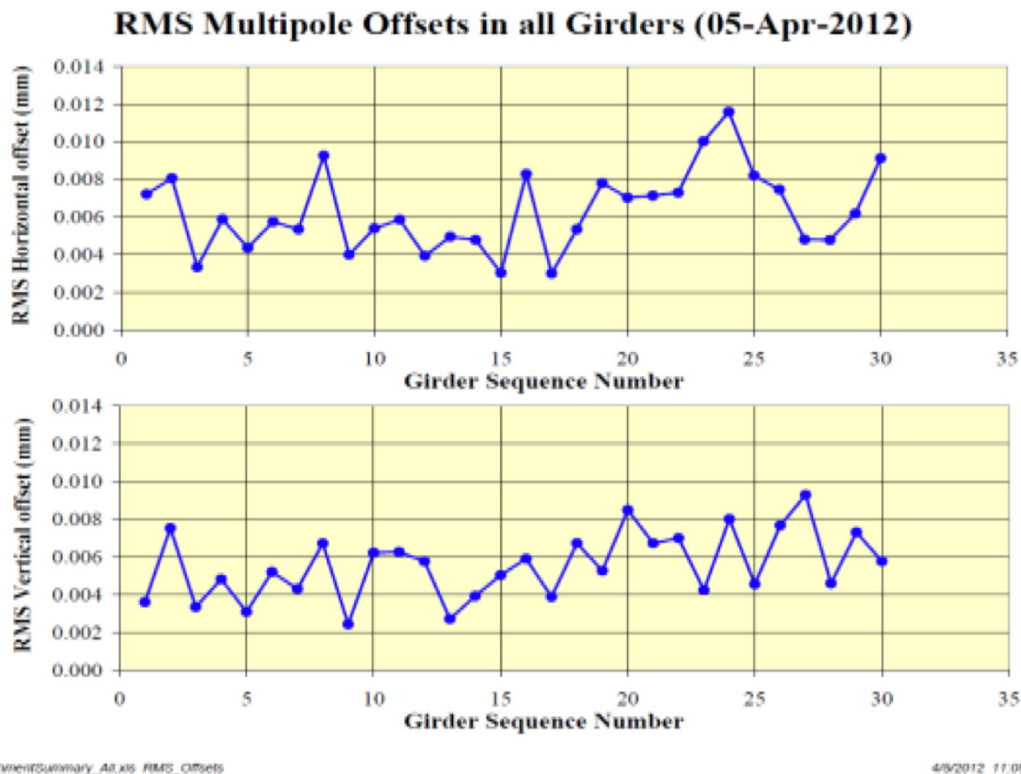


Figure 5: Quadrupole- and sextupole magnet alignment errors w.r.t. to a common straight line on the multipole magnet girders. Plotted are the rms values of the alignment error of the six or seven magnets for the first 35 (out of 90) multipole girders.

Magnets are all powered by switched mode supplies with IGBT switching elements. The precision of the set values corresponds to a 20-bit ADC and the power supplies all achieve stability in the order of 10 ppm in the frequency range from 0.01 Hz to 1 kHz. All power supplies and their electronics are installed in sealed equipment enclosures with circulating chilled air for cooling.

The vacuum system is made of extruded, keyhole-shaped Al and has distributed NEG strip pumps in the antechambers. Explosion bonded bi-metal flanges (Al-steel) are attached to the chamber by robotic electron beam welding. NEG coated vacuum chambers are used inside insertion devices (damping wigglers and elliptical polarizing undulators) as well as in a short vacuum chamber next to the photon exit ports where there is no space for a keyhole chamber. The 0.2 mm thick vacuum chambers inside the 90 air-coil (no iron yoke) corrector magnets are made of INCONEL[®], an austenitic Nickel-Chromium alloy which combines high strength and reduced resistivity.

The power is delivered to the beam by up to four (two at present) superconducting single cell 500 MHz cavities (CESR-B type [7]). The original CESR-B cavity design has been revised to comply with BNL pressure safety requirements and the waveguide coupler has been re-optimized for the NSLS-II parameters with 500 mA of beam current, a beam power loss of 0.80 MW and a cavity voltage of 8 MV . The coupling is adjusted to a Q_{ext} of 97000. In the present configuration with two superconducting cavities which deliver (at the present stage of conditioning) a voltage of about $(3\text{--}3.5)\text{ MV}$, the detuning of the cavity for beam loading compensation $\Delta\omega$ is with $\Delta\omega/\omega_0 = 10\%$ small compared to the revolution frequency of $\omega_0 = 440\text{ kHz}$. The RF power is generated by 310 kW klystron transmitters, one for each cavity system. The layout of each RF straight section includes the space for a 3rd harmonic cavity (1.5 GHz) for bunch lengthening. One two-cell superconducting resonator which was designed in-house has been built but it is not yet installed.

The full suite of beam diagnostics includes the in-house developed BPM system with 200 nm resolution and stability. The pick-up is a four button design with a Boron-Nitride heat sink around the button shaft. The analogue electronic provides band pass filtered 500 MHz signals to the FPGA based digital electronics. The system includes the option to modulate the BPM signals with a “pilot tone” which if demodulated in the digital part of the electronics provides continuous relative calibration of the analogue-digital-converter channels. As the electronics is installed in temperature controlled equipment enclosures, the required stability is achieved without this feature.

The control system is based on EPICS. Special features are the high-level-application platform which allows convenient access to all control variables and which is well integrated in the middle-layer as well as the deterministic serial 10 kHz data link for real time orbit feedback and for time critical equipment protection.

3.5.6 Injector System

The NSLS-II injector consists of a 200 MeV s-band linac and a 3 GeV combined function booster synchrotron. The linac beam is generated in a thermionic gun which can deliver 20 nC in 300 ns long pulses. The DC beam is pre-bunched at 500 MHz before it is injected into the 3 GHz bunching and acceleration system. The linac has three solid state modulators (including the hot spare) two of which drive the four accelerating units. The linac is operated with a maximum beam current of 15 nC/s . There are two beam dumps, one place in line with the linac and another one after the energy spectrometer in the linac-to-booster transfer line. The linac, which was procured as a turn-key system (RI is the commercial supplier), was commissioned in April 2012.

The 3 GeV booster synchrotron is a combined function machine with 60 focusing and defocusing dipoles forming four symmetric arc sections. The circumference is 158 m . The cycle time is 1 sec . With additional quadrupole magnets at both ends of the four arc sections, a horizontal emittance of 35 nm is achieved. RF power is delivered to the beam by a PETRA 7-cell 500 MHz Cu-cavity driven by a 90 kW IOT based transmitter system. Injection is accomplished by a two kicker magnets. The two extraction kickers are supported by a slow extraction bump system. A high energy transfer line with a 3 GeV beam dump connects to the storage ring injection straight. The booster has very flexible EPICs based control system and has a full suite of instrumentation (BPMs with turn by turn capacity, tune monitor, optical monitor, intensity monitors) which enabled a very fast commissioning. The booster synchrotron was constructed in collaboration with the Budker Institute of Nuclear Physics [8]. BINP designed and built most of the accelerator hardware system. Within three weeks acceleration of a beam to 3 GeV could be demonstrated and only two weeks later, a transmission of close to 100% was achieved routinely [9,10]. The injector complex is very robust. After a break or shutdown, full performance is re-established after only a few hours. Operation is fairly reliable and re-tuning is required only rarely [9, 10].

3.5.7 NSLS-II Commissioning

3.5.7.1 Commissioning Sequence

NSLS-II Storage ring commissioning started on March 26, 2014. Beam was stored after a few days. The excellent alignment of quadrupole magnets (see figure 5) as well as the initial on-axis injection were important factors in the fast first commissioning. Accumulation of 25 mA was achieved easily after orbit and chromaticity correction. Up to this point, commissioning was performed with a PETRA 7-cell 500 MHz Cu-cavity. In a shutdown in May/June 2014 the first superconducting cavity was installed and 50 mA of beam current was demonstrated with the superconducting cavity shortly after restart of commissioning. Commissioning was concluded by July 10th after less than 50 days of commissioning. It should be mentioned that the fully functioning instrumentation and the fact that high level applications were fully integrated into the control system at the start of commissioning were important factors in this quick success. Operation of NSLS-II started on October 1, 2014 with the commissioning of insertion devices, beam line front ends and beam lines. For all eight insertion devices and six beam line frontends commissioning was completed by the end of 2014 and all six initial beam lines received “first light” within this period.

3.5.7.2 Lattice Commissioning

The results of lattice commissioning are documented in great detail in the NSLS-II commissioning report [11].

Due to the small alignment error of the quadrupole positions of $\delta x_{\text{rms}} < 30\text{ }\mu\text{m}$ and the small relative errors in the integrated bending fields of 0.05% , the uncorrected closed orbit values were found to be within 10 mm peak to peak. Consequently, the first injected beam circulated for several turns and after slight tune corrections several tens of turns. Residual orbit errors after corrections are about $30\text{-}50\text{ }\mu\text{m}$ as predicted by simulations.

The rms quadrupole magnet gradient errors in NSLS-II are $[\int \Delta G ds / \int G ds]_{\text{rms}} < 0.035\%$ according to the magnetic measurements. Each quadrupole can be individually adjusted. The sextupole rms alignment error is better than $30\text{ }\mu\text{m}$ as well. The uncorrected beta beat was found within $(15\text{-}20)\%$ as expected which is mainly due to gradient errors. If the lattice is calculated using

measured values of the quadrupole gradients, one finds good agreement (within a few percent) with the measure beta functions in the uncorrected machine.

The most important tool for the lattice commissioning is the BPM system. The NSLS-II BPM system has turn-by-turn (TbT) capability with an rms noise of $\sim 2 \mu m$. BPM readings (averaged over 38 turns) have a 200 nm resolution and stability and are provided with 10 kHz data rate.

The beam optics functions have been measured with various response matrix techniques ($R = \Delta z_j / \Delta \theta_i$, z_j are the beam coordinates and θ_i are the correction magnet kicks) and the program “LOCO” (see [12]) and have been corrected by least square minimization techniques to better than $\Delta\beta/\beta = 3\%$. Similar results are obtained if TbT data are used to measure the betatron phase advance between the BPMs and the corrections are based on these measurements. Figure 6 shows the measured vertical beta functions after correction with a residual measured beta beat of $\Delta\beta/\beta_{rms} = 3\%$. However this value is dominated by the BPM gain error and the beta beat should be as small as 3% peak to peak.

The dispersion functions after correction differ by less than 5 mm (peak-to-peak) from the design values. Optics corrections indicate that gradient errors are randomly distributed. If the lattice functions are calculated using the quadrupole strengths obtained by the magnetic measurements one finds good agreement with the measurements (within a few percent).

Due to the strong sextupoles, closed orbit errors have a large impact on beta-beats and linear coupling between horizontal and vertical plane. Iterative orbit and optics corrections were needed. Thorough cycling of the magnets (including correctors) in a consistent way is important to maintain good orbit, beam optics, and reproducibility.

Global and local x-y coupling is determined by TbT BPM measurements and by deriving the mode-II horizontal and the mode-I vertical beta functions which are the consequence of coupling [13, 14, 15] from the measured revolution matrices. There is one skew quadrupole corrector in each cell which allows an almost perfect correction of the coupling by minimizing the the coupled beta functions β_{xII} and β_{yI} as well as driving terms of the coupling resonances $Q_x - Q_y = \text{integer}$, $Q_x + Q_y = \text{integer}$. Figure 7 shows the coupled beta-functions before and after the skew quadrupole corrections, which indicates that the global and local coupling is reduced significantly.

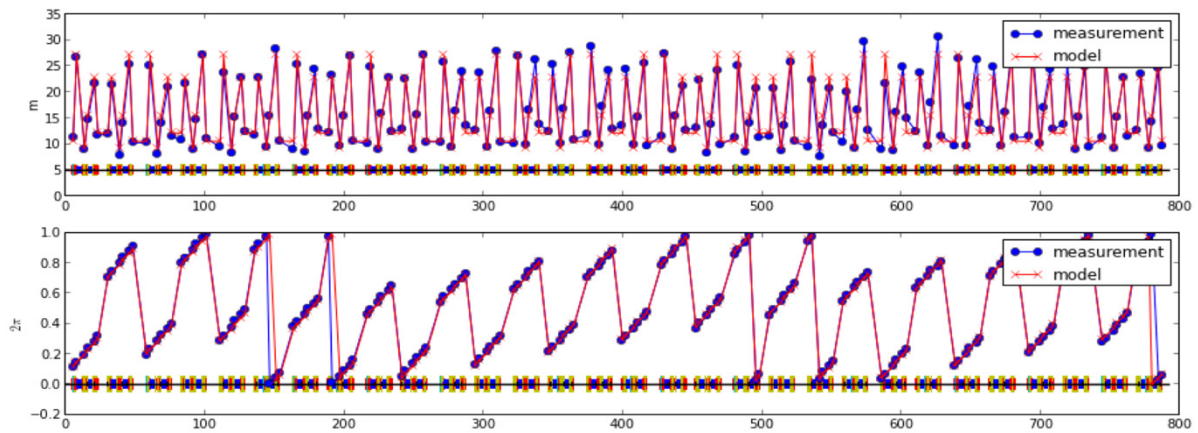


Figure 6: Measurement of vertical beta functions (top) and vertical betatron phase advance (bottom) after corrections with residual beta beat $\Delta\beta/\beta$ of 3% (rms).

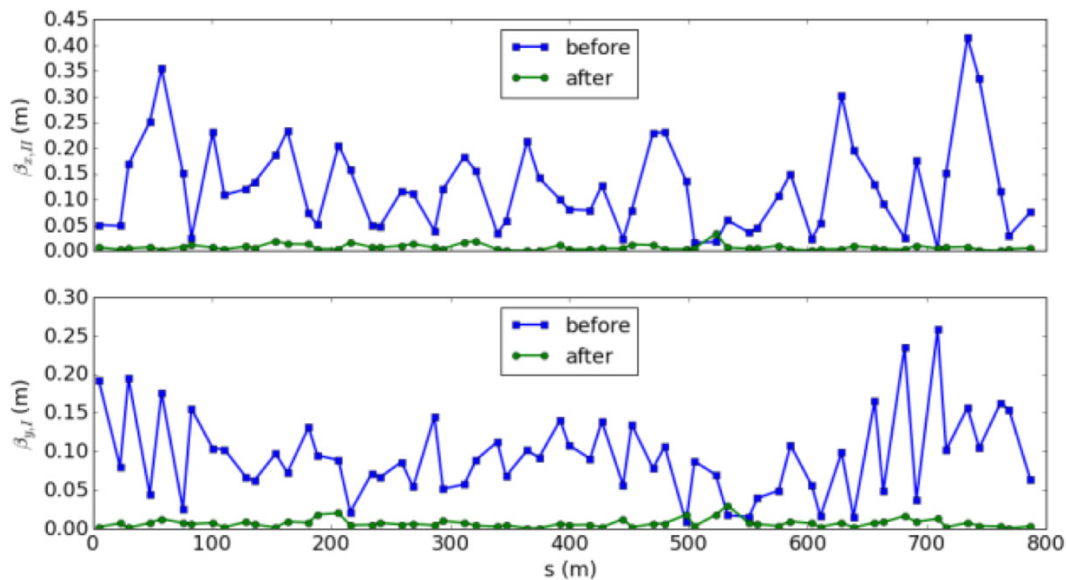


Figure 7: Local and global coupling correction: the mode-II β_{xII} and mode-I β_{yI} which represent the off diagonal blocks of the 4x4 revolution matrices at each element of the accelerator before (blue dots) and after (green dots) correction.

After correction of vertical dispersion and coupling to the level of a few millimeters, the vertical emittance as measured with the pin-hole X-ray monitor is as low as $6 \pi \text{ pm rad}$ ($\varepsilon_y/\varepsilon_x = 0.6\%$) which is well below the diffraction limited design value (for 12 keV photons).

The high degree of control of the lattice function results in a fairly narrow half integer stop band width which is estimated to $\Delta = 0.01$. In a demonstration experiment, the vertical half integer stop band could be crossed during large amplitude coherent synchrotron oscillations without beam loss. Figure 8 shows the synchrotron light emitted from a beam on the half integer resonance with two stable islands.

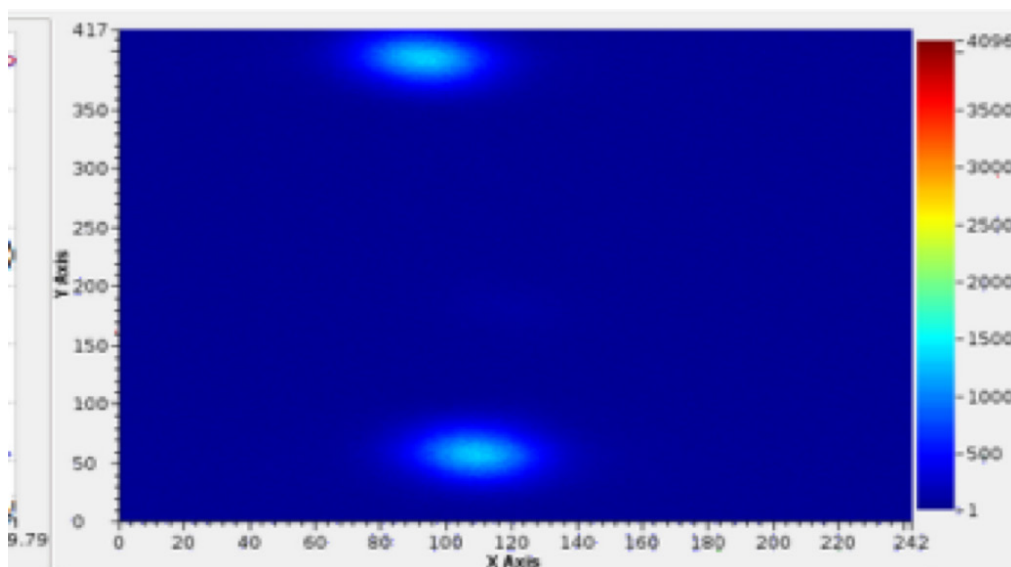


Figure 8: NSLS-II beam stored within the vertical $\frac{1}{2}$ integer resonance stop-band. The beam is shown by the synchrotron light monitor in the two stabilized half integer resonance islands during the crossing.

The horizontal beam emittance of NSLS-II is designed to be $\epsilon_{x0} = 2 \pi \text{ nm rad}$ for the bare lattice. Due to the low field of the bending magnets of 0.4 Tesla , the synchrotron radiation energy loss per electron and turn is only 283 keV . With 20.4 m of damping wigglers (gap is 15 mm , the period is 100 mm and the peak field is 1.85 Tesla ; there are six 3.4 m long units installed in pairs in three equally spaced straight sections) the radiated energy loss increases to 673 keV and so does the radiation damping rate. As the dispersion in the damping wiggler is designed to be zero in lowest order, there is little quantum excitation and the beam emittance almost fully benefits from the increased radiation damping rate $\epsilon_x = \epsilon_{x0} \cdot 286 \text{ keV} / (286 \text{ keV} + 390 \text{ keV}) = 0.9 \pi \text{ nm rad}$. This has been confirmed by measurements (see figure 9). There is some discrepancy between prediction and measured horizontal emittance which is attributed to limited resolution of the pin-hole imaging emittance monitor.

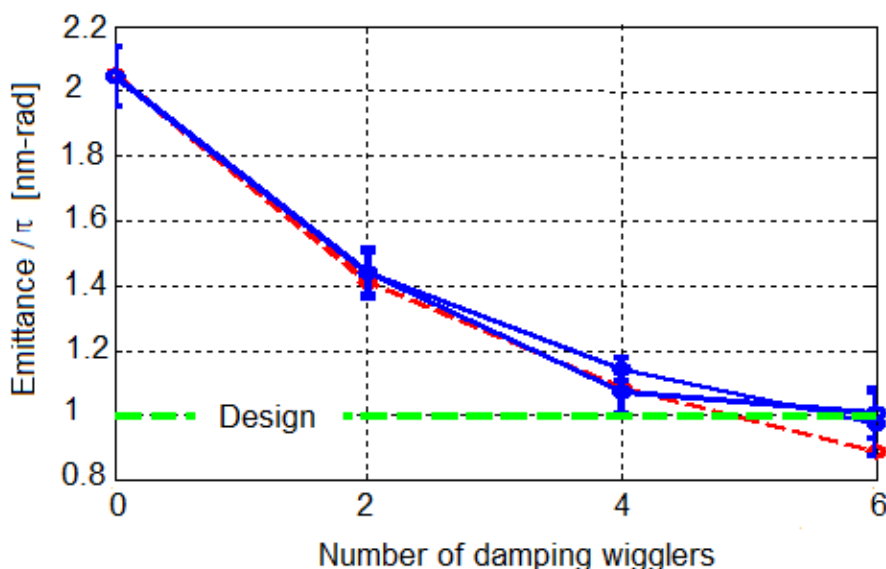


Figure 9: Measurement of horizontal emittance vs. number of damping wigglers with a pin-hole X-ray monitor (blue: measurements, red: calculation)

3.5.7.3 Orbit Stabilization

NSLS-II beam orbits are quite stable even without active stabilization. The magnet support system does not amplify the ground vibrations which are measured at the level of up to 100 nm . Most of the ground motion is attributed to heavy traffic of a nearby highway. All rotating equipment is well isolated from the storage ring tunnel floor. The beam closed orbit varies within an envelope of about $\pm 1\ \mu\text{m}$ (this refers to the 1 m beta points in the center of a short straight section). In the horizontal plane, where the beam size is about $40\ \mu\text{m}$ this level of stability satisfies the requirements of stability to 10% of the beam size. In the vertical plane, where the beam size is only $3\ \mu\text{m}$, active stabilization is required.

A fast orbit feedback system has been implemented. The feedback algorithm is distributed over 30 FPGA based cell controllers which collect the data from all beam position monitors around the ring with a 10 kHz update rate and calculate changes in the 2×6 correctors within their cells respectively. Data are transmitted via the fast deterministic serial data link which supports the 10 kHz BPM data rate. The feedback algorithm was carried over from the well proven NSLS orbit stabilization system [16]. The feedback acts on orbit deviations from a reference orbit using an empirical response matrix in singular value (SVD) decomposition. All 90 eigenvalues of the matrix (per oscillation plane) are used for correction and each eigenvector has individual PID loop parameters. With active stabilization, the residual beam motion is well within the specification of 10% of the beam size (see figure 10). The actively controlled horizontal orbit varies by about 1% of the beam size; the vertical orbit varies by 6%. The feedback suppresses the orbit motion up to 100 Hz by a factor of 2.7. In particular, the 60 Hz component of the orbit motion is fairly well controlled. There is little suppression beyond 200 Hz and slight excitation occurs in the vicinity and beyond the theoretical 3db point of 300 Hz .

Slow thermal drifts in NSLS-II are minimized by a tight temperature control of $0.1\text{ }^\circ\text{C}$ of the tunnel air. The girders are solidly bolted to the tunnel floor at six support points to avoid amplification of ground vibration. In order to avoid significant buckling of the girders due to small temperature changes of the girder, a special plastic polymer layer (3MTM-Viscoelastic[®]) was inserted between two plates in the girder support which allows the girder to thermally expand while still being firmly locked to the support at for faster oscillations. This measure limits the thermal motion of the quadrupole magnets well within the $30\ \mu\text{m}$ alignment tolerance without compromising the suppression of vibrations.

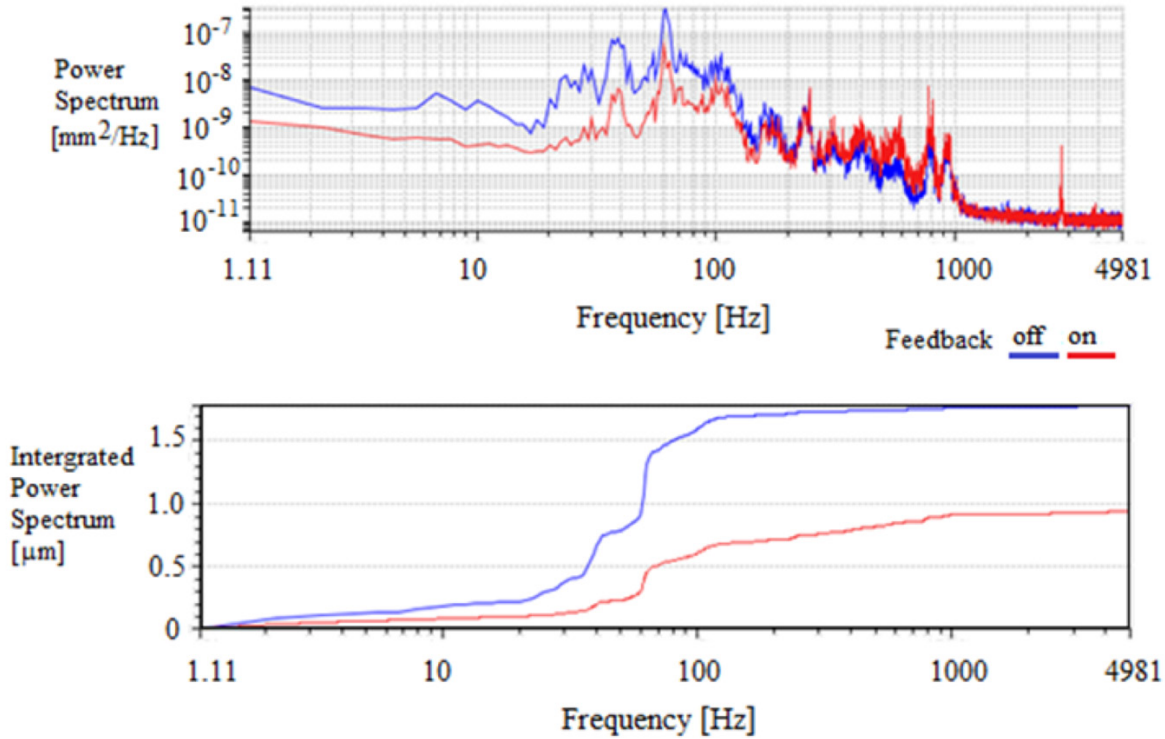


Figure 10: Power spectrum of vertical orbit averaged over 30 BPMs. Note that the average beam size is $14 \mu\text{m}$ at the BPM locations. The spectra and the integrated spectra are shown for feedback off (blue lines) and feedback on (red lines).

3.5.7.4 Dynamic Aperture Commissioning

The dynamic aperture has been verified in the commissioning process. Considerable effort was spent in optimizing the dynamic aperture during the design and construction phase of NSLS-II. The parameters such as tunes and sextupole strengths have been optimized taking into account magnetic field imperfections from magnetic measurements. Relative magnetic multipole errors in quadrupole and dipole magnets were specified and confirmed to be smaller than 10^{-4} at $r = 25 \text{ mm}$ and in the sextupole magnets 10^{-3} .

Like in all low emittance lattices, the dynamic aperture in NSLS-II is compromised by the small dispersion which requires strong sextupoles to compensate the high chromaticity. NSLS-II has three chromatic sextupole families and six families at locations with zero linear dispersion to compensate the nonlinear field effects consisting of higher order chromaticity and tune shift with amplitude as well as driving terms of non-linear resonances. Integrated sextupoles strengths $m = \frac{ec}{E} \int ds \frac{\partial^2 B_y}{\partial x^2}$ are in the range of $(3-7) m^{-2}$. The sextupoles outside the achromat contribute to the compensation of the nonlinear chromaticity. After correction, the contributions to nonlinear chromaticity from variation of the beta functions and the dispersion function with δ , $\frac{\partial \beta}{\partial \delta}$ and $\frac{\partial D_x}{\partial \delta}$ cancel to a large extent which reduces the nonlinear chromaticity significantly. Figure 11 shows the residual chromatic tunes shift versus momentum offset $\delta = \Delta p/p$.

Sextupole strengths are optimized by minimizing simultaneously the linear- and nonlinear chromaticities as well as the driving terms of nonlinear resonances and tune shifts with amplitude up to 2nd order in the strengths of the sextupoles. There are a total of 26 driving terms

characterizing nonlinear chromaticity, non-linear resonances up to order 4, and tune-shift with amplitude taken into the optimization process. The result in simulations is a dynamic aperture which accommodates betatron oscillations of up to 20 mm in the horizontal plane, up to 3 mm in the vertical plane.

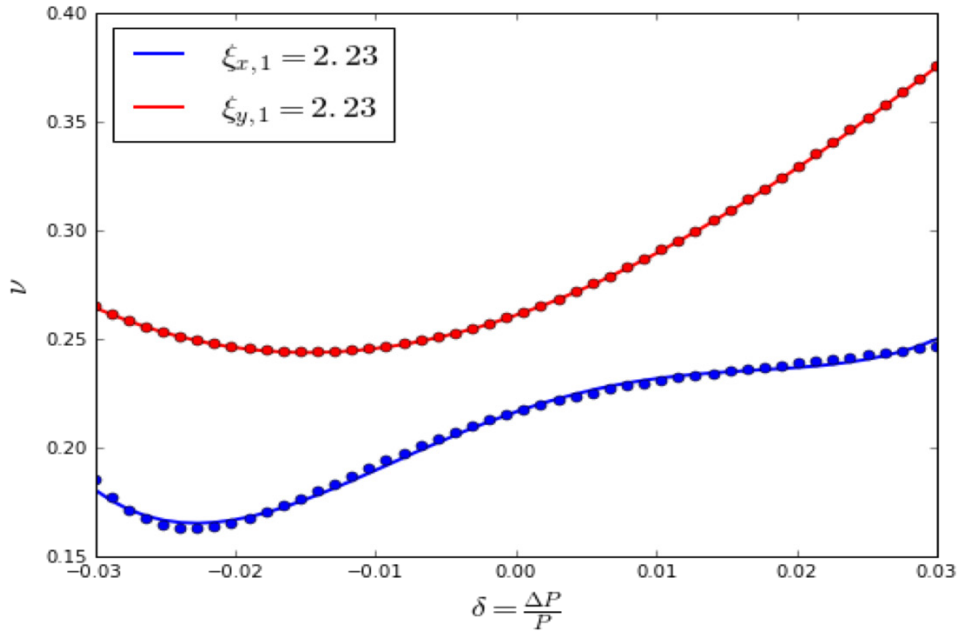


Figure 11: Momentum dependence of the NSLS-II horizontal (blue) and vertical (red) betatron tunes after adjusting the linear chromaticity to $+2.3$ in both planes and after optimization of the third chromatic sextupole circuit as well as additional sextupoles outside the achromat. The dots are obtained by numerical tracking and the lines correspond to a fit to a 4th order polynomial in the momentum deviation $\delta = \Delta p/p$ [17].

Table 2 shows the nonlinear driving terms after optimization of the sextupole strengths.

An alternative method for optimization the dynamic aperture is the so called “Multi-Objective” approach [18] where the entire parameter space of sextupole strengths is varied and the mesh size is successively refined in the vicinity of the most successful parameters point in the scan. This procedure converges quite well and results in similar optimized sextupole strengths than the method of minimizing driving terms.

A well-established method to probe the dynamic aperture by simulation is to generate and inspect a frequency map [19]. Particles are launched into phase space at the injection point tracking over a certain number of turns around the accelerator. The change in betatron tunes average over the first and second half of the tracking run is evaluated for each starting point. The result of this procedure is visualized by plotting the tune changes (from the zero amplitude tunes) in a color code in a phase space diagram. The frequency map as shown in figure 12 allows clearly identifying the

Table 2: Residual Nonlinear Driving terms after Sextupole Optimization [3]. Residual values of resonance driving terms (labelled by the resonance they excite), chromaticity and tune-shift with amplitude are evaluated and normalized using action values $I_x = 1 \text{ nm rad}$, $I_y = 8 \text{ pm rad}$ and $\delta/\bar{p} = 0.34 \cdot 10^{-3}$.

Effect	Residual Value	Effect	Residual Value
$\partial v_x / \partial \delta$	5.4×10^{-7}	$2v_x + 2v_y$	5.1×10^{-8}
$\partial v_y / \partial \delta$	1.5×10^{-6}	$2v_y$	6.0×10^{-7}
$\partial \eta_x / \partial \delta$	2.0×10^{-6}	$2v_y$	3.9×10^{-7}
$\partial \beta_x / \partial \delta$	2.4×10^{-6}	$4v_y$	1.7×10^{-7}
$\partial \beta_y / \partial \delta$	1.7×10^{-6}	$\partial v_x / \partial J_x$	9.0×10^{-7}
v_x	8.6×10^{-7}	$\partial v_{x,y} / \partial J_{y,x}$	3.8×10^{-6}
v_x	9.2×10^{-7}	$\partial v_y / \partial J_y$	7.3×10^{-7}
$3v_x$	7.0×10^{-7}	$\partial^2 v_x / \partial J_x \partial \delta$	3.2×10^{-7}
$v_x - 2v_y$	3.7×10^{-6}	$\partial^2 v_{x,y} / \partial J_{y,x} \partial \delta$	8.1×10^{-7}
$v_x + 2v_y$	9.8×10^{-7}	$\partial^2 v_y / \partial J_y \partial \delta$	4.5×10^{-7}
$2v_x$	3.1×10^{-7}	$\partial^2 v_x / \partial \delta^2$	9.7×10^{-7}
$2v_x$	5.0×10^{-8}	$\partial^2 v_y / \partial \delta^2$	1.9×10^{-7}
$4v_x$	7.3×10^{-7}	$\partial^3 v_x / \partial \delta^3$	1.8×10^{-7}
$2v_x - 2v_y$	1.5×10^{-6}	$\partial^3 v_y / \partial \delta^3$	1.4×10^{-7}

boundary of stability and tuning variations within the aperture. It also shows the presence of strong resonances as connected points of larger tune variation.

The dynamic aperture corresponds to the sextupole strengths obtained and confirmed by these procedures has been verified during commissioning. NSLS-II has fast kicker magnets installed, one for each plane. Firing these kickers launches the beam on trajectories in the entire range of physical aperture. The trajectory with the largest amplitude and no beam loss is interpreted as the border of stability. Figure 12 shows a typical simulation for the NSLS-II bare lattice and the corresponding experimental results are plotted in Figure 13.

The conclusion of the dynamic aperture tests is that the measured dynamic aperture of NSLS-II is fairly close to simulated values. The most important benefit of sufficient dynamic aperture is an injection efficiency of 100%, a Touschek lifetime of more than 3 hours and reasonable margin in dynamic aperture for insertion device operations.

The off-momentum dynamic aperture was determined by simulations to be $\Delta p/p_{max} = \pm(2.5 - 3) \%$. This has been confirmed with the beam in the following way [20]: A bunch with a charge of 1.32 nC (0.5 mA) is stored in NSLS-II and the beam lifetime is measured as a function of RF voltage. The lifetime is limited by the Touschek effect [21] and depends on the energy acceptance. For low RF voltage it is limited by the RF bucket height and the lifetime increases with increasing RF

voltage. If a level is reached where the momentum aperture is limited dynamically, the lifetime should not increase further with increasing RF voltage. This, however, could not be observed for available RF voltages up to 1.9 MV which corresponds to a bucket height of $\Delta p/p_{rf\text{-bucket}} = 2.3\%$. This allows the conclusion that the momentum acceptance is larger than 2.3%.

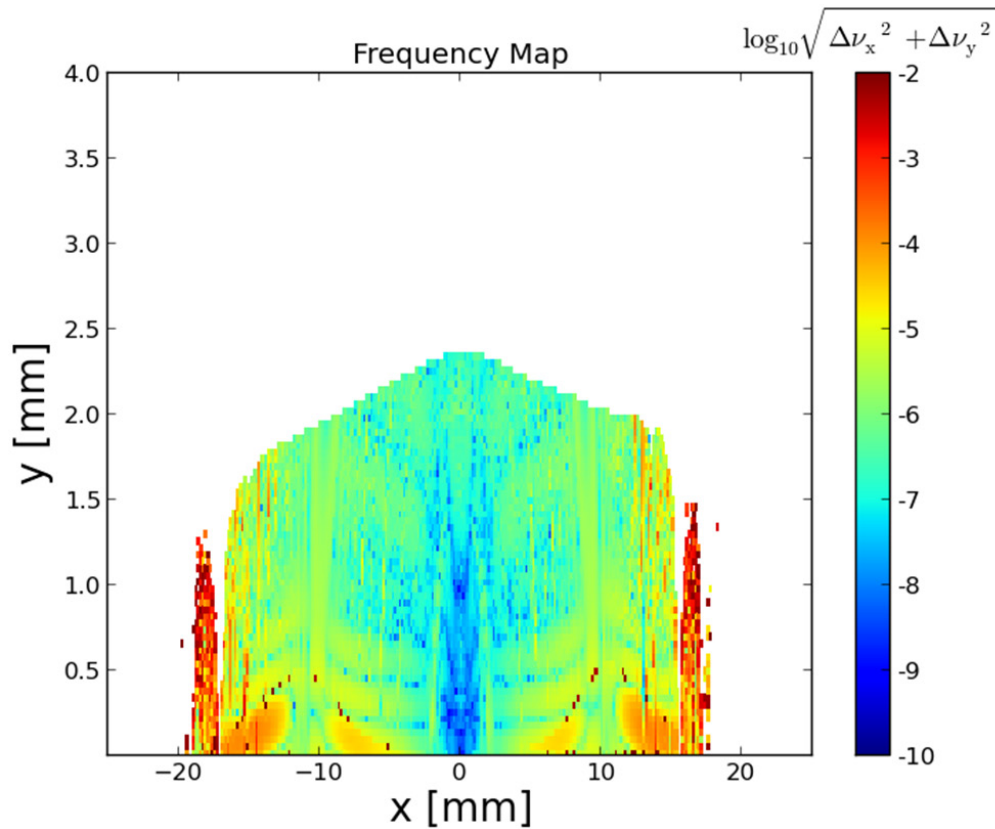


Figure 12: Frequency map of NSLS-II Dynamic Aperture (DA) in the x-y plane at the injection point. Magnetic field errors and orbit distortions (corrected) are included in the model as well as 6 damping wigglers. The color scheme ranges from tune changes of 10^{-7} (blue) which is stable to 10^{-2} (red) which is unstable on a short time scale. $\Delta\nu = 10^{-4}$ (orange) is close to the border of stability. If the particles were lost before reaching the full number of turns, the corresponding starting point is left white.

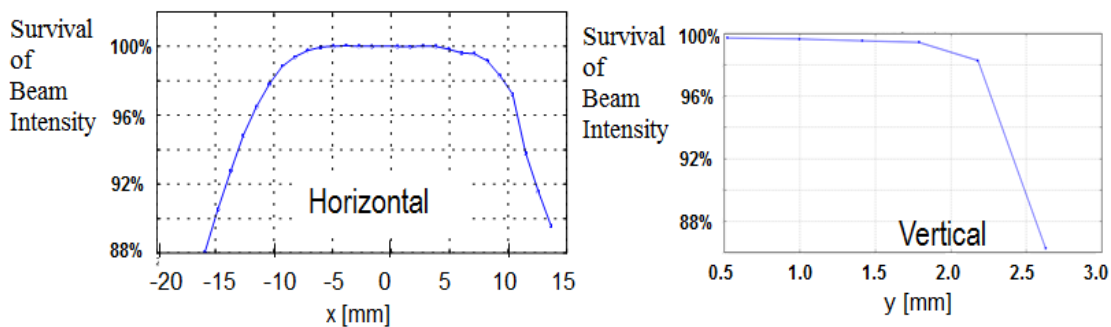


Figure 13: Probing the NSLS-II DA by kicking the beam with a fast kicker (same reference point as above). The kicker strength is varied and the ratio of beam intensities before and after the kicks is plotted versus the oscillation amplitudes corresponding to each kick.

3.5.7.5 *High Intensity Commissioning*

A large effort has been spent during the design of NSLS-II in optimizing the impedance of vacuum chambers and devices seen by the beam [22]. During accelerator studies [23], the single bunch intensity in NSLS-II is limited by transverse mode coupling instability in the vertical plane at $I_b = 0.95 \text{ mA}$ (bare lattice, $\xi_{x,y} = 0$, $I_b = 3 \text{ mA}$) which can be concluded from the significant tune change as a function of bunch intensity and the fact that the bunch becomes unstable if the tune shift reaches half the synchrotron tune. The estimates based on calculated impedance and with an RF voltage of 3.9 MV predict a threshold of 1.5 mA (ten in-vacuum undulators were assumed to be in the lattice). Present state of RF conditioning limits the voltage to about 2 MV . Thus the calculation doesn't contradict the experimental value if the values are scaled to the same voltage. The threshold for the micro-bunch instability is calculated to be 9 mA [24]. Longitudinal bunch stability is demonstrated up to 6 mA .

The NSLS-II design beam current is 500 mA which is close to the expected multi-bunch instability limit due to resistive wall impedance in the 5 mm gap insertion devices. A broad band (250 MHz) transverse damper system has been installed to actively stabilize the beam. However we observe that at nominal values of the chromaticity of $\xi_{x,y} = +2$, the onset of transverse instability is observed at currents above 20 mA . The observed multi-bunch modes of unstable beam cluster around $m = 0$. Head tail damping from chromaticities > 2 can stabilize the beam up to 150 mA . The reason for the discrepancy between estimated and measured multi-bunch threshold is not fully understood. It is observed that the onset of stability can be shifted to larger beam intensity if the bunch train is split in up to six sub-trains. This indicates the presence of fast ion instability [25]. Thus for beam currents above 150 mA , the beam needs to be kept stable by active damping. No further beam dynamics reason was found which limits the intensity. At this point a maximum beam intensity of up to 400 mA has been stored with no beam stability issues. Cooling of the ceramic injection kicker chambers needs to be improved to reach 500 mA .

The vacuum performance as a function of beam current parameterized by the dynamic pressure rise $\Delta P/I_{beam}$ is improving steadily but more slowly so than in other electron accelerators. This is explained by the fact that the vacuum chambers are not exposed to direct synchrotron radiation but only see radiation scattered off the masks and absorbers. After about 360 Ah of beam dose, the average pressure is $(1-5) 10^{-9} \text{ mbar}$ at 350 mA of beam current. However, the average pressure is dominated by a short section of beam pipe near the photon exit ports which did not have any pumping due to lack of space. NEG coated chambers were installed recently to improve the local vacuum. Figure 14 [26] summarizes the current vacuum performance of the NSLS-II storage ring.

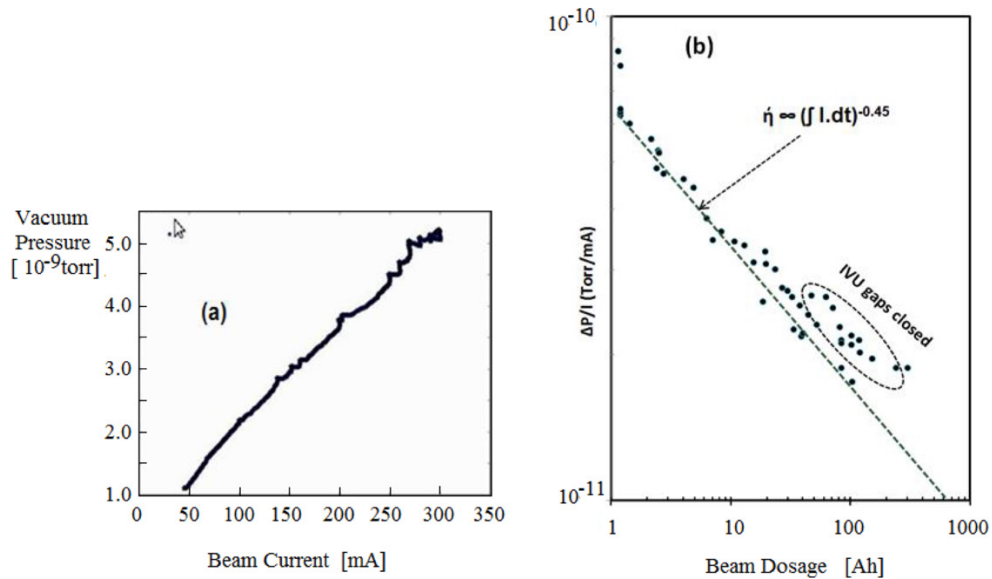


Figure 14: Vacuum performance with high beam current in NSLS-II (a) and improvement dynamic pressure rise $\Delta P/I$ with beam dosage (b). Note the double logarithmic scale in figure 14 (b).

3.5.8 Insertion Devices and Integration in Accelerator Operations

State of the art insertion devices are installed in the storage ring in order to fully exploit the NSLS-II beam parameters. They provide high brightness photon beams for the beam lines. The first suite of NSLS-II insertion devices includes the six damping wigglers with a period length of 100 mm and a peak field of *1.85 Tesla* with a gap opening of *15 mm* for which the field quality is optimized. These wigglers have Vanadium Permادur poles (Hybrid design). The damping wigglers which were initially planned to serve as damping wigglers are also sources of X-rays up to photon energies of *100 keV* for three beamlines.

The insertion device workhorses of NSLS-II are in vacuum undulators which allow closing the gap to *5 mm*. There are two *3 m* long in vacuum undulators (IVU) with period of $\lambda = 20 \text{ mm}$, a gap height of $g = 5.2 \text{ mm}$, and a peak field of *1.0 Tesla* ($k = ecB_{peak}\lambda / (2\pi m_0 c^2) = 1.8$) called IVU20. This is also a hybrid device with Vanadium-Permادure poles. There are a number of similar devices with slightly modified period and different lengths, a *3 m* long, wide pole IVU with $\lambda = 22 \text{ mm}$ called IVU22, and $g = 7.4 \text{ mm}$ which is installed in a high-beta long straight section, a *1.5 m* long, $\lambda = 21 \text{ mm}$, $g = 6.4 \text{ mm}$ called IVU21. The initial suite of devices constructed as part of the NSLS-II project also include a pair of *2 m* long APPLE-II type elliptical polarizing undulators (EPU) with a period length of $\lambda = 49 \text{ mm}$, called EPU49.

The next suite of nine beamlines (the projects are called ABBIX, three beamlines which are funded by NIH and NEXT, five beamlines which are funded as a DOE major item of equipment (MIE) project) which are being completed at this point have two further IVU21 and three IVU23 devices with a modified length $l = 2.8 \text{ m}$ and a period length of *23 mm*. These beamlines also need four further EPUs, two with a period lengths of $\lambda = 57 \text{ mm}$ and *105 mm*.

The next suite of beamlines to be built is completed or nearing completion. One project, called ABBIX, is funded by NIH to build three beamlines. A DOE major item of equipment (MIE) project called NEXT is constructing five. These beamlines have two more IVU21 and three IVU23 devices with a modified length $l = 2.8 \text{ m}$ and a period length of *23 mm*. These beamlines also require four

more EPUs, two with a period length of $\lambda = 57 \text{ mm}$ and two with $\lambda = 105 \text{ mm}$. There is a suite of beamlines built in collaborations with other science institutions (Partner) which use undulators carried over from other facilities (X25 undulator from NSLS, U42 planar undulator from ESRF and an EPU60 from ALADIN). Eight beamlines are presently under construction. They use radiation from bending magnets or from a wavelength shifter installed next to the dipole. This is a wiggler magnet with three poles (TPW). The central pole is short (3 cm) and strong (1.14 Tesla). The field integral is zero.

Table 3 lists all 25 devices which are presently (May 2016) installed or are being prepared for installation in 2016.

Table 3: Insertion Devices installed/built as of 02/03/16.

Beam	Project	Type	Design	Beampost	Location	Length	Period	Peak	K_{\max}	Mag	Canting	Vac	FE	Fundamental photon Energy	Total
Line						[m]	[mm]	Field [T]		Gap [mm]	Angle [mrad]	Aper [mm]	Aper	[eV]	Power [kW]
CSX1/CSX2	NSLS-II	EPU49	PPM	Low- β_x	23-ID	4 (2x2)	49	0.57 (heli)	2.6 (heli)	11.5	0.16	8	0.6 x 0.6	230 (heli)	7.3 (heli)
								0.94 (Lin)	4.3 (Lin)					180 (Lin)	9.9 (Lin)
								0.72 (vlin)	3.2 (vlin)					285 (vlin)	5.5 (vlin)
								0.41 (45d)	1.8 (45d)					400 (45d)	1.7 (45d)
IXS	NSLS-II	IVU22	Hybrid	High- β_x	10-ID	6 (2x3) center	22	1.52	1.52	7.4	0	7.2	0.5 x 0.3	1802	4.7x2
HXN	NSLS-II	IVU20	Hybrid	Low- β_x	3-ID	3	20	1.03	1.83	5.2	0	5	0.5 x 0.3	1620	8
CHX	NSLS-II	IVU20	Hybrid	Low- β_x	11-ID	3	20	1.03	1.83	5.2	0	5	0.5 x 0.3	1620	8
SRX/XFN	NSLS-II	IVU21	Hybrid	Low- β_x	5-ID	1.5 downstream	21	0.9	1.79	6.4	2.0	6.2	0.5 x 0.3	1570	3.6
XPDP/PDF	NSLS-II	DW100	Hybrid	High- β_x	28-ID	6.8 (2x3.4)	100	1.8	~16.5	15		11.5	1.1 x 0.15		64.5
ESM*	NEXT	EPU105/	PPM	High- β_x	21-ID	2.7(downstream)	105/49	0.74/0.57 (heli)	7.23/3.55 (heli)	16	2.0		0.7 x 0.7		4.22/1.2 (heli)
		/1.4 (upstream)				0.90 (vlin)		7.23/3.06(vlin)	4.22/0.86 (vlin)						
						1.14/0.83 (Lin)		11.2/4.4 (Lin)	10.1/2.0 (Lin)						
SIX*	NEXT	EPU57	PPM	High- β_x	2-ID	7.0 (2x3.5)	57	0.57 (heli)	3.55 (heli)	16	0		0.3 x 0.3		4.4 (heli) x2
								0.83 (Lin)	4.41 (Lin)						6.8 (Lin) x2
ISR	NEXT	IVU23	Hybrid	High- β_x	4-ID	2.8	23	0.95	2.05	6.2	2	6	0.5 x 0.3		
SMI	NEXT	IVU23	Hybrid	High- β_x	12-ID	2.8	23	0.95	2.05	6.2	2	6	0.5 x 0.3		
ISS+XFP	NEXT	DW100	Hybrid	High- β_x	18-ID	6.8 (2x3.4)	100		~16.5	15		11.5	1.1 x 0.15		64.5
FXI	NEXT	DW100	Hybrid	High- β_x	8-ID	6.8 (2x3.4)	100		~16.5	15		11.5	0.8 x 0.3		64.5
LIX	ABBIX	IVU23	Hybrid	High- β_x	16-ID	2.8	23	1.02	2.2	5.7	0	5.5	0.5 x 0.3		
FMX/AMX	ABBIX	IVU21	Hybrid	Low- β_x	17-ID	1.5	21	0.9	1.79	6.4	2.0	6.2	0.5 x 0.3		3.6
SST*	Partner	U42	Hybrid	Low- β_x	7-ID	1.6 (upstream)	42	0.82	3.27	11.5	2	8			3.2
		EPU60	PPM	Low- β_x	7-ID	0.89 (downstream)	60	0.73 (heli)	4.1 (heli)	11.5		8			1.8 (heli)
								1.02 (Lin)	5.7 (Lin)						2.7 (Lin)
NYX*	Partner	IVU18	Hybrid	Low- β_x	19-ID	1.0 (upstream)	18	0.95	1.55	5.6	0	5.4			2.5
HEX*	Partner	SCW55	EM	Low- β_x	27-ID	1	80	4.5	21.6	13	0	10			49.7

The field quality requirements for all undulators are very demanding but all have been met by careful shimming. The first integrals are lower than 50 gauss cm , the second integrals are less than $10,000 \text{ gauss cm}^2$. Integrated multipole errors are comparable to errors found acceptable in the dipole magnets.

The damping wigglers require local optics correction and global tune correction. The residual effects after corrections are small.

Experience with the devices which are installed so far is quite good. The beam orbit and the tunes change only little if the undulator gaps are closed. After optimization of the correction coils, the residual effects on the beam are negligible. The dynamic aperture is only slightly affected by the

insertion devices provided that the beam orbit is carefully centered in the small gap undulators [27]. As a result the injection efficiency can still be tuned close to 100% efficiency.

The long bending magnet of NSLS-II which has many advantages does not provide satisfactory bending magnet radiation. For this reason, a short wavelength shifter in form of a three-pole wiggler (3PW) with 1.2 T field in the center is foreseen to be placed upstream of the downstream dipole. Three of these devices have been installed for bending magnet beamlines.

With these insertion devices NSLS-II will provide photon beam with a brightness of

$$B = (2-3) \cdot 10^{21} s^{-1} mm^{-2} mrad^{-2} (0.1\% BW)^{-1}$$

in the photon energy range of 4-9 keV. Figure 15 shows the brightness versus photon energy for the NSLS-II devices but also includes results for possible future devices such as a cryogenically cooled IVU based on PrFeB (CPMU17) and a 14mm period superconducting undulator (SCU14), and superconducting wiggler with a 4 Tesla peak field.

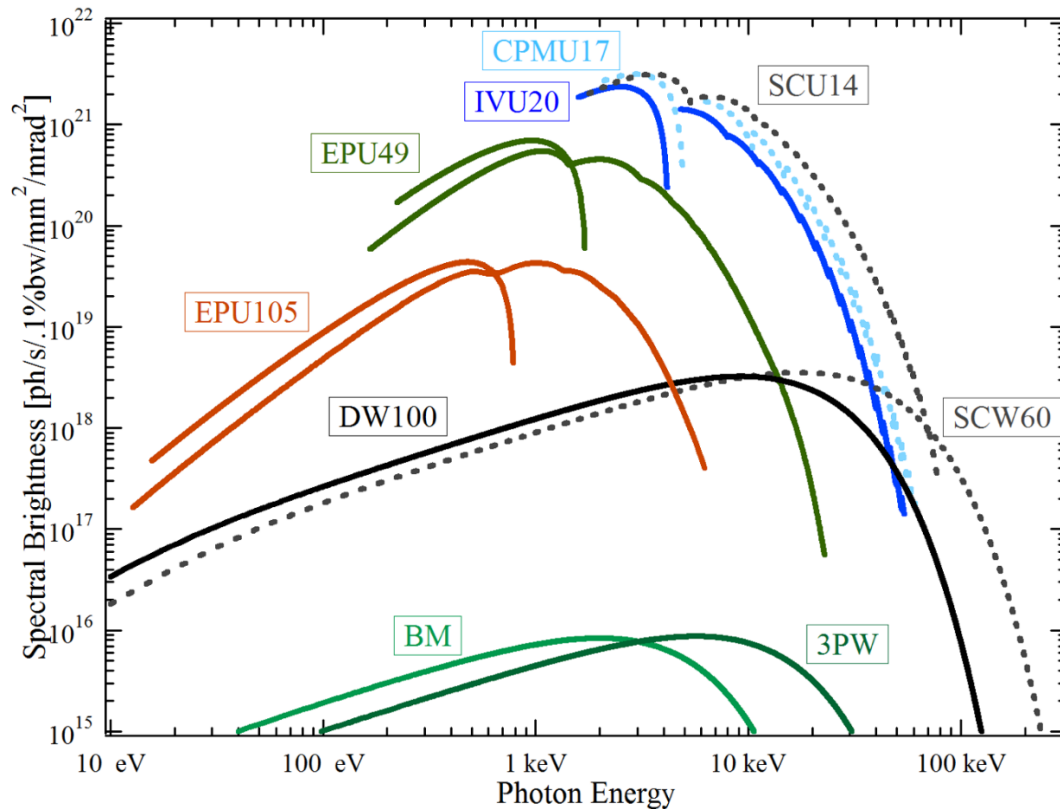


Figure 15: Brightness of NSLS-II photon beam versus photon energy for various radiation devices [28]

3.5.9 Present Performance

During the first year of operation from February 2015 to April 2016, NSLS-II has achieved all its design goals except for full beam intensity. The small horizontal emittance has been confirmed by measurements and the vertical emittance was shown to be as small as $6 \pi pm rad$. The required beam orbit stability was achieved in the in the horizontal plane without any active stabilisation. In

the vertical plane, where the requirement is 300 nm, active fast orbit feedback is used to stabilize the orbit to this level. The injection efficiency is close to 100%.

Since October 2015, NSLS-II is operated in top-off mode after adding a number of interlocks to ensure that beam cannot enter the photon extraction channel. The uniformity of the fill is about 5% and the beam intensity is kept constant within 0.2 %. Time between subsequent injections is ≈ 2 min.

The beam lifetime will be eventually limited by Touscheck scattering. With 250 mA, half the design current, a beam lifetime of 8 hours is achieved typically, which indicates that the Touscheck lifetime is increased by bunch lengthening.

The beam intensity is limited at this point by the RF voltage, as the recently installed 2nd RF cavity has not yet been fully conditioned. There was also heating of one of the ceramic injection kicker chambers due to damaged Ti-N coating. As this has been repaired, it is expected that 500 mA can be reached during the upcoming user run. At present (May 2016), the maximum beam current is 400 mA.

The insertion devices which have been installed in NSLS-II (6 damping wigglers DW100, in vacuum devices: 2 IVU20, 3 IVU21, 1 IVU22, 3 IVU23, elliptically polarizing undulators: 2 EPU49, 1 EPU57) are fully integrated in operations. Their impact on beam orbit and tune is small (beam survives closing of the gaps without corrections) and residual changes after corrections are negligibly small. Injection efficiency is usually tuned to values above 90% with all gaps closed.

While a considerable amount of time was spent on the commissioning of new beamlines, their insertion devices and frontends, 2100 hours for user operations have been scheduled during the 2nd half of FY15 and 3800 hours in FY16. Operational reliability (the time beam is available for beamlines within the scheduled period divided by the time scheduled for beamline operations) was 84.7% in the 6 months of running in 2015, the first year of operations. In the fiscal year 2016, the 2nd year of operations, reliability of 90% or above is expected. While the reliability of the hardware system is excellent in general, frequent trips of the RF system are associated with an aggressive program to raise the beam current and insufficient time spent on RF conditioning.

Table 4 summarizes the present state of NSLS-II performance. All design parameters (except the beam intensity) have already been achieved or have been exceeded.

Table 4: NSLS-II Design and Mid-2016 Parameters

<i>Parameter</i>	<i>Design Value</i>	<i>Current Value</i>
Beam Energy [GeV]	3	3
Beam Current [A]	0.5	0.4
Beam Emittance h [nm rad]	0.9	0.9
Beam Emittance h [pm rad]	8	6
Orbit stability [beam size]	10%	<10%
Relative Energy Spread	0.04%	0.04%
Dynamic Aperture h, v [mm]	>15, >2.5	15, 2.5

3.5.10 Conclusion

Construction of NSLS-II, the ultimate 3 GeV 3rd Generation Light Source has been successfully completed and commissioning of the facility went very smoothly. All design parameters have been achieved or exceeded except for the peak intensity which is planned to be stored during the summer of 2016. Accelerator development work is concentrating now on making the accelerator more reproducible, improving the operating system, and consolidating the computer software for operating the machine. Efforts to understand collective effects and to achieve the required stability and reproducibility in routine operations have been successful and the facility has transitioned from start-up to routine user operations. The performance of the machine is very stable and mature and recovery from shutdowns is remarkably quick and uneventful. NSLS-II is now a fully functioning synchrotron radiation light source facility with world record performance parameters.

3.5.11 Acknowledgments

The successful construction and commissioning of NSLS-II is the result of the hard work of the entire very committed, high-skilled NSLS-II staff. The author is indebted to Satoshi Ozaki for advice and support during construction of NSLS-II.

3.5.12 References

1. Nobel Prize (1/2) for Roderick McKinnon in Chemistry 2003
http://www.nobelprize.org/nobel_prizes/chemistry/laureates/2003/
2. Nobel Prize (1/3) for Thomas A. Steitz in Chemistry 2009
http://www.nobelprize.org/nobel_prizes/chemistry/laureates/2009/.
3. NSLS-II Preliminary Design Report PDR, Brookhaven National Laboratory, (2007), unpublished
4. M. Sands, SLAC Publication 121 UC28 ACC (1970), unpublished, <http://inspirehep.net/record/60854/files/slac-r-121.pdf>
5. F. Willeke, Proceedings of the Particle Accelerator Conference, New York, 2011
6. Alexander Temnykh, Vibrating wire field-measuring technique, NIMA, Volume 399, Issues 2-3, 11 November
7. H. Padamsee, Proceedings of the Particle Accelerator Conference, San Francisco (1991), pp786-788
8. Sergey Gurov et al, Proceedings of the International Particle Accelerator Conference, Dresden, (2014), MOPRO088
9. E. Blum et al, Proceedings of the International Particle Accelerator Conference, IPAC2015, 2015, Richmond
10. T. Shaftan, Proceedings of the International Particle Accelerator Conference IPAC13, Shanghai (2013)
11. NSLS-II Commissioning Report, Brookhaven National Laboratory (2015), BNL Techn. Note 168, unpublished
12. J. Safranek, Nucl. Inst. and Meth. A388, 27 (1997).
13. G. Ripken, F. Willeke, AIP Conf. Proc. 184(1989)
14. V. Lebedev, A. Bogazc, arXiv:1207.5526
15. Li, Yongjun, Proceedings of the International Particle Accelerator Conference, IPAC2015,

- 2015, Richmond,
16. L.H. Yu et al, Nucl. Instr. Meth. A 284,(1989)
 17. Yongjun Li, unpublished data, private communication (2016).
 18. Linyun Yang, Weiming Guo, Samuel Krinsky, Proceedings of the Particle Accelerator Conference (2011), New York City, BNL94896-2011-CP, PAC 2011
 19. J. Laskar, Physica D: Nonlinear Phenomena, 1993
 20. B. Podobedov et al Proceedings of the IPAC 2015, Richmond (2015) MOPJE053
 21. Henri Brook, Circular Particle Accelerators, Los Alamos Scientific Laboratory, 1972
 22. A. Blednykh, Proceedings of the Particle Accelerator Conference, Vancouver, (2009) FR5RFP031, pp 4595-4557
 23. A. Blednykh, Proc. Of the Internat. Particle Accelerator Conference, Richmond, (2015), TUABL, pp 1332-1334
 24. Li Hu Yu et al, Proc. of the Particle Accelerator Conference , Vancouver, (2009) FR5RFP033, pp 4601-4603
 25. T.Raubenheimer, F.Zimmermann, SLACPUB95-6740
 26. H. C. Hseuh et al, Journal of Vacuum Science & Techn. A 34 031603 (2016), [HTTP://DX.DOI.ORG/10.116/1.4945406](http://dx.doi.org/10.116/1.4945406)
 27. G. M. Wang, Proceedings of the International Accelerator Conference, Richmond (2015), TUPHA006
 28. Calculations performed by O. Tchoubar (2010), unpublished

4 Workshop and Conference Reports

4.1 EuCARD2 workshop on “Status of Accelerator Driven Systems Research and Technology Development”

Giulia Bellodi, CERN
Mail to: giulia.bellodi@cern.ch
CERN, Geneva, Switzerland

Megawatt power range, high intensity accelerator beams can potentially find an application as drivers for nuclear waste transmutation and energy production. The typical assembly consists of a high power accelerator, a spallation target for neutron production, and a subcritical core that is neutronicly coupled to the target. Such Accelerator Driven Systems (ADS) would offer new prospects and advantages for the transmutation of spent fuel by converting highly-radioactive material to lower toxicity material with a shorter half-life. In addition, these hybrid systems could generate electricity during the conversion of transuranic waste. R&D towards an ADS demonstration facility started well into the 1990’s but no complete demonstration facility has yet been built to date.

In the framework of the EuCARD2 WP4 networking package on Accelerator Applications, a couple of workshops were organised on ADS in 2014 and 2015, focusing respectively on the accelerator technology choice and beam requirements (<https://indico.cern.ch/event/300409/>), and on the accelerator reliability issue (<https://indico.cern.ch/event/384686/>). To conclude the EuCARD2 mandate, a third workshop in this series was organised at CERN on 7-9 February 2017, focusing on the “Status of Accelerator Driven Systems Research and Technology Development” (<https://indico.cern.ch/event/564485/>). Objective of this workshop was to review the current state of the art of ADS technology by presenting the different activities and initiatives carried out at national and international levels and to highlight in conclusion the most critical areas of study where further R&D is needed before proving the feasibility of a demonstration facility.

There were 72 registered participants to the workshop and 28 presentations from laboratories and research centres worldwide.

The workshop was organised around four separate sessions, identified by the Scientific Advisory Committee: 1) ADS national programs, 2) Critical aspects of accelerators, 3) Targets and coupling experiments and 4) Innovative ideas and new R&D.

A range of present national and international ADS programmes was presented in the first session, covering Europe (MYRRHA project), China, India, Japan, Ukraine and the United

States. The presentations put in evidence the impressive effort which is ongoing worldwide on ADS technologies developments. Common timescales are unfortunately quite far in the future, with planned applications being only scheduled after 2030. The accent was put on global cooperation at international level as a progress keystone for ADS, which will require efforts of convergence in goals and utilization purposes.

The second session focused on the critical aspects of accelerator technology for ADS systems and showed how the separation between the linac and cyclotron schools is still well in place. The different technologies were compared in terms of i) their capability to meet beam quality and reliability requirements, ii) their suitability to upgrade to industrial scale, iii) costs of construction and operation and iv) licensing issues.

Thanks to the progress done in superconducting RF, existing high power linacs have demonstrated that it is already possible to meet beam energy and intensity targets. The cyclotron option is preferred by some as a more compact and economic design solution, although there are less concrete benchmarks available concerning costs and operation. Reliability goals are not yet within reach, irrespective of the accelerator technology chosen: two to three orders of magnitude are still missing today for both types of machines. A realistic way-forward towards the realisation of an ADS project would most likely rely on the use of established technologies, allowing for an efficient prototyping of different parts and investing on scalability of the design.

Another critical component of an ADS is the spallation target, which is designed to generate the maximum amount of neutrons while ensuring the safe removal of the heat released in the spallation process (at power densities of several hundreds of kW per litre occurring in the structure). The target structure material has to withstand the mechanical stresses induced by protons and neutrons interactions, radiation-induced degradation of its mechanical properties as well as chemical corrosion/erosion due to the coolant material. Beam trips can also result in cyclic thermal stresses, which produce thermal fatigue and limit the target lifetime. Promising results were shown from the post-irradiation analysis of the MEGAPIE experiment, to be published this year.

After proof of all the singular ADS assembly components in a standalone way, a second phase of validation to be pursued will need to focus on the coupling between accelerator, target and nuclear core. Here is where zero- (or low) power reactors are of interest, for the opportunity given to gather validation and parametric measurements on neutron cross-sections, power distribution and nuclear physics data in a safe and flexible way. A review of past and current projects worldwide was presented at the workshop and detailed talks were given on existing European, Chinese and Japanese activities.

Finally, the last session focused on more recent R&D initiatives and developments. A particular mention was given to CYCLADS, a recently submitted EU FET-OPEN project (not-yet approved) whose consortium, coordinated by CERN, includes major industrial and academic European partners such as iTheC, PSI, AIMA-Dev, HNI, ENEA, N-21, ASG. The aim of the project is to establish the conceptual design of an innovative high-power, compact and cost-effective cyclotron to be used for transmutation of nuclear waste.

The workshop closed with summary reports from the Session Chairpersons highlighting the current status and future challenges of ADS around the world. The detailed programme and specific presentations are all available on the workshop website (<https://indico.cern.ch/event/564485/>).

4.2 The Compact Linear Collider (CLIC) workshop 2017

Rickard Stroem, CERN
Mail to: rickard.stroem@cern.ch

The annual Compact Linear Collider (CLIC) workshop took place at CERN on 6-10 March, gathering 220 collaborators from 26 countries to discuss the latest status of the CLIC accelerator and detector studies (figure 1). The CLIC accelerator is based on a novel concept for linear acceleration up to multi-TeV energies and remains the only mature option for multi-TeV electron-positron collisions for the era beyond the High-Luminosity LHC.

During the workshop, particular focus was directed towards the recently published updated staging scenario for the CLIC accelerator [1], where construction and operation is pursued in three energy stages with collision energies of 380 GeV, 1.5 TeV and 3 TeV respectively. This staging scenario is crucial to exploit the full physics landscape. At its initial energy CLIC is optimised for Higgs and top measurements and further enables a scan at the top quark pair production threshold. The higher energy stages provide the best sensitivity to new physics through direct and indirect searches. High-energy operation also gives access to rare processes such as double Higgs production which is sensitive to the important Higgs self-coupling. First beams could be foreseen in 2035; the starting point of a 20-25 years long physics programme.

CLIC Week 2017 hosted a variety of sessions with 150 speakers, covering the activities of both the accelerator and detector-and-physics studies. During the open plenary session on Wednesday March 8, several talks were given to provide an overview of the CLIC accelerator and detector-and-physics programme, placed in the context of LHC results. This session also addressed the use of CLIC-related developments in other applications. The spokesperson for the CLIC accelerator collaboration, Philip Burrows, presented the current status of the machine design and the pathway towards the European strategy for 2019 and beyond. The latter was also the focus in meetings among the CLIC accelerator institutes and the detector-and-physics institutes. Particular priority is given to the studies where cost and power can be reduced, presenting the initial CLIC project as a realistic option compatible with the resources needed to realize earlier projects at CERN [2].

A summary talk on the CLIC Test Facility at CERN (CTF3) was given by its coordinator Roberto Corsini, reporting on the successful demonstration of key technological concepts allowing a CLIC-style accelerator to be built. With the completion of the CTF3 experimental programme the facility has now been approved for conversion into an electron accelerator facility, CLEAR (CERN Linear Electron Accelerator for Research). The future CLEAR program will include CLIC high-gradient and instrumentation studies. A status and outlook report of the CLEAR facility was presented on Wednesday afternoon by Erik Adli.

With the adoption of a single detector concept based around the interaction point, a new unified detector model has been developed for CLIC [3]. The detector features all-silicon vertex and tracking detectors, for which a wide range of detector R&D is currently

underway. Many of the technologies under study for the CLIC detector are also of interest to the High Luminosity LHC upgrade, as well as for the HEP community at large, where the high granularity and time-resolution needed for CLIC are equally crucial.

The successful operation of high-gradient accelerating structures and experience with advanced beam-dynamics techniques, developed for the small dimensions of these structures, have inspired a growing number of application outside of particle physics. Application of high-gradient and X-band technology include compact linacs and advanced diagnostics for photon sources, as well as medical applications [4].

The CLIC Week 2017 (clicw2017.web.cern.ch) took place on March 6-10 at CERN. The Indico pages are open and video recordings exist for the public session on Wednesday March 8.

4.2.1 References:

1. "Updated baseline for a staged Compact Linear Collider", CERN Yellow Report, CERN-2016-004
2. "CLIC cost and power studies",
<https://indico.cern.ch/event/577810/contributions/2452078/attachments/1425401/2186459/clic-cost-power-CLICWS.pptx>
3. "CLICdet: The post-CDR CLIC detector model", CLICdp-Note-2017-001
4. "X-band applications",
https://indico.cern.ch/event/577810/contributions/2452093/attachments/1425370/2186373/X_applications_final.pptx



Figure 1: Participants of the CLIC Workshop 2017.

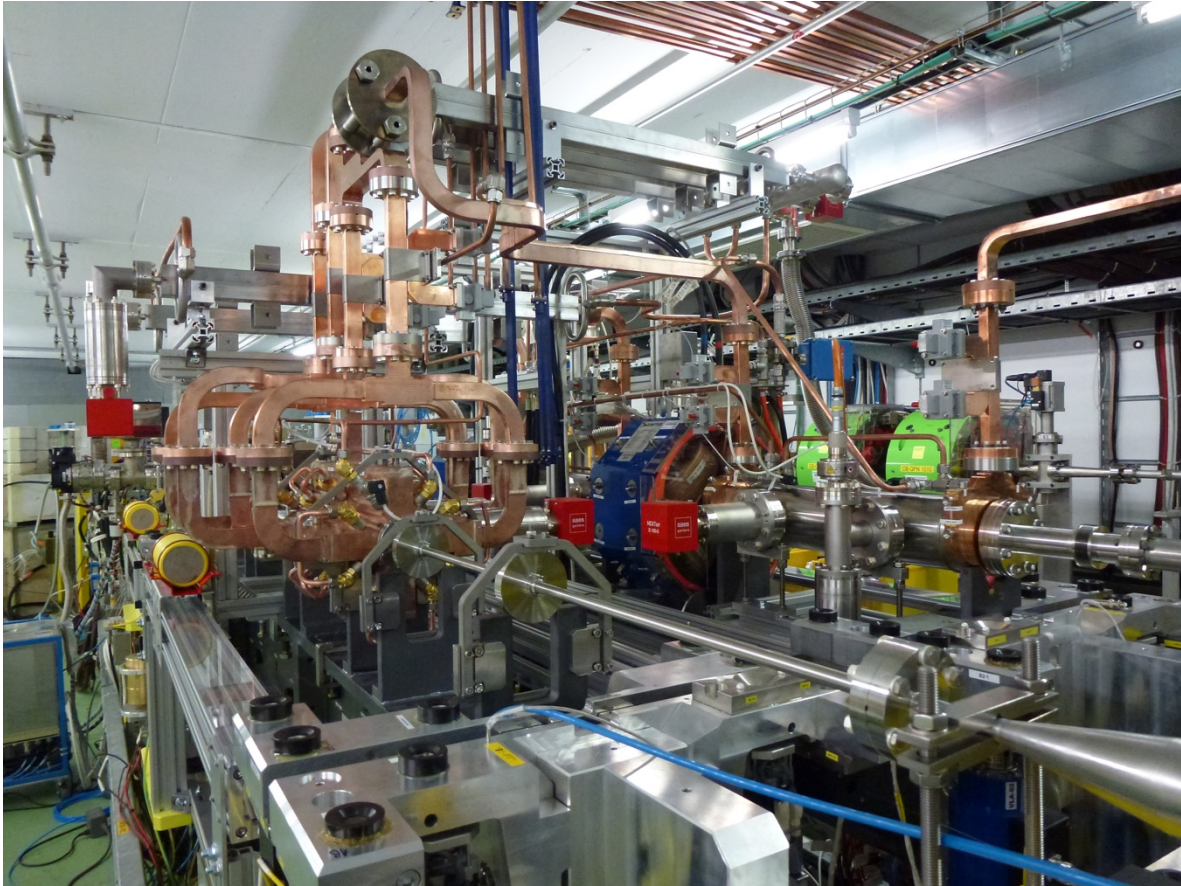


Figure 2: Acceleration in the two-beam module at the CLIC Test Facility at CERN (CTF3) was thoroughly tested in 2015-2016; RF power production from the drive beam and beam energy gain of the probe beam were verified at CLIC operational conditions (100 MV/m accelerating gradient and 240 ns pulse duration).

4.3 The ICFA miniworkshop Beam Dynamics meets Vacuum, Collimation, and Surfaces

Cristina Bellachioma, Sara Casalbuoni*, Giuliano Franchetti
GSI Helmholtzzentrum für Schwerionenforschung GmbH

*Karlsruhe Institute of Technology (KIT)

Mail to: g.franchetti@gsi.de

The workshop "Beam Dynamics meets Vacuum, Collimations and Surfaces" ("[BeVa2017](#)"), took place at the Karlsruhe Institute of Technology (KIT) from 8 to 10 March 2017 (poster in Figure 1). At the event the state of the art of these disciplines was addressed and revealed significant synergies. The event brought together experts from the various interrelated research areas in order to reach a common understanding of the challenges waiting ahead and to better define the interfaces and common points. The interplay of Beam Dynamics, Vacuum, and Surfaces, therefore, is an important pillar underpinning the FAIR, LHC, FCC, and other present and future projects. Mastering this interplay requires a close coordination of competences in diverse fields of science. The BeVa2017 workshop was organized jointly by the Institute of Beam Physics and Technology of KIT and EuCARD-2 XRING. "Extreme Rings" (XRING) is a networking task of the XBEAM package of EuCARD-2, focused on enhancing communication and mutual understanding between different accelerator communities so as to advance accelerator R&D at the forefront of global research. BeVa2017, held under the auspices of ICFA, DVG, and AIV, and sponsored by several industrial partners (Agilent, SAES, BNG, and Edwards) was the last in a four-year series of exciting and successful EuCARD-2 XRING events, inspired by the same underlying approach.

The workshop was attended by 66 international participants (Europe, America, Asia) from more than 20 different institutions (Figure 2). The overall atmosphere of the meeting profited from the interdisciplinary attitude of the attendees, which catalyzed lively discussions, new levels of future collaboration, and improved sharing of information. The scientific program of the workshop was set up by the International Organizing Committee of 20 members. The workshop was hosted by Karlsruhe Institute of Technology (KIT), and administrative organization was carried out by Margit Costarelli KIT and Paola Lindenberg GSI.

33 talks were presented during the 2.5 days of the meeting. Giovanni Ruomlo CERN and Oleg Malychev STFC Daresbury set the tone of the meeting introducing the basic issues of beam dynamics and vacuum. A session dedicated to present and future machine has brought to the audience the significant challenges: Ryutaro Nagaoka has discussed the beam dynamics & vacuum challenges in present light sources and future low emittance ring; Collider issues for LHC were addressed by Vincent Baglin, but studies on future colliders were presented for the e-p collider by Christoph Montag, and for FCC by Frank Zimmermann. The present status of FAIR was reviewed by Carsten Omet. Many discussions took place on issues of impedances, vacuum instabilities, and electron cloud. Details on physics of surfaces and vacuum emerged from Mauro Taborelli.

Unconventionally the meeting has given space for talks from participants from industry which covered aspects of NEG coating with Paolo Mannini SAES, Ion pumps with new design from Mauro Audi AGILENT, and the vacuum chamber for superconducting undulators C. Boffo BNG.

The detail program and talks are available via the workshop website.
<https://indico.gsi.de/conferenceDisplay.py?confId=5393>

<https://indico.gsi.de/conferenceDisplay.py?confId=5393>

Beam Dynamics *meets* Vacuum, Collimations, and Surfaces

Chairs: C. Bellachioma, S. Casalbuoni, G. Franchetti

Secretariat
 Margit Costarelli, KIT Tel.: +49 (0)721 608 26288 Fax: +49 (0)721 608 26789 margit.costarelli@kit.edu
 Paola Lindenberg, GSI Tel.: +49 (0)8159 71 1550 p.lindenberg@gsi.de

International Advisory Committee

Eshraq Al Dmour	MaxIV	Mei Bai	FZJ
Paolo Chiggiato	CERN	Riccardo Bartolini	Diamond
Roberto Cimino	INFN Frascati	Wolfram Fischer	BNL
Michael Hahn	ESRF	Ubaldo Iriso	Alba
Hseuh Hsiao-Chaun	BNL	Edgar Mahner	CERN / FAIR
Alexander Krasnov	BINP	Anke-Susanne Müller	KIT
Paolo Manini	SAES	Kazuhiro Ohmi	KEK
Oleg Malyshev	ASTeC	Giovanni Rumolo	CERN
Hartmut Reich-Sprenger	GSI	Jens Stadlmann	GSI
Mauro Taborelli	CERN	Frank Zimmermann	CERN

Karlsruhe, Germany
 March 8-10th, 2017

Logos at the bottom: saes group, DVG, Agilent Technologies, EUCARD² EXTREME, BEAM RING, KIT Karlsruhe Institute of Technology, ICFA, EDWARDS, BILFINGER Babcock Noell GmbH.

Figure 1: Beam Dynamics meets Vacuum, Collimations, and Surfaces: Workshop poster.



Figure 2: Participants of the workshop in KIT.

5 Recent Doctorial Theses

5.1 Study on the Key Physics Problems of SPPC/CEPC Accelerator Design

Feng Su
IHEP, CAS, 100049, Beijing, China
Mail to: sufeng@ihep.ac.cn

Graduation date: 9 May 2017
Institutions: Institute of High Energy Physics, CAS, China
Supervisors: Prof. Jie Gao (IHEP)

Abstract

The development and history of particle physics is a magnificent poem of the verification of the Standard Model. With the discovery of the Higgs boson at LHC, people found all the particles predicted by Standard Model in laboratory. But due to some imperfection of theory, the physicists believe that Standard Model is just the low energy part of a larger basic theory. To explore the new physics beyond Standard Model will be the key point of the whole physics world. This is also the goal to design a new collider. The particle accelerators have been widely used for fundamental physics research for more than 60 years. Many important discoveries of particle physics were based on the development of accelerator. After the discovery of Higgs boson at LHC in 2012, the world high energy physics community is investigating the feasibility of a Higgs Factory as a complement to the LHC for studying the Higgs and pushing the high energy frontier. CERN physicists are busy planning the LHC upgrade program, including HL-LHC and HE-LHC. They also plan a more inspiring program called FCC, including FCC-ee and FCC-hh, aiming to explore the high energy frontier and expecting to new physics. Chinese accelerator physicists also came up an idea to build an ambitious machine called CEPC-SPPC (Circular Electron Positron Collider-Super Proton Proton Collider) during a workshop in Beijing on September 13, 2012. The CEPC-SPPC program contains two stages. The first stage is an electron-positron collider with center of mass energy 240 GeV to study the Higgs properties carefully. The second stage is a proton-proton collider at center-of-mass energy of more than 70 TeV. This thesis focuses on the key physics problems of SPPC/CEPC accelerator design. The first part is about the parameter choice, lattice design and the beam dynamic study of SPPC main ring. The second part is about the lattice design of CEPC, including partial double ring scheme, advanced partial double ring scheme and double ring scheme. We developed a systematic method of how to make an appropriate parameter choice for a circular proton-proton collider by using an analytical expression of beam-beam tune shift limit, starting from the required luminosity goal, beam energy, physical constraints at the interaction point and some technical limitations. We calculated and designed a set of SPPC parameter list including 61 km-70 TeV, 100 km-100 TeV, 100 km-128 TeV, 82 km-100 TeV and 100 km-75 TeV. Then we start the lattice design according to the parameter choice and focused on the 61 km-70 TeV and 100 km-100 TeV scheme. We designed the first version lattice and showed the result of the dynamic

aperture. For CEPC design, there were several schemes developed after the publication of the Preliminary Conceptual Design Report(Pre-CDR) of CEPC-SPPC in March 2015, including single ring scheme with pretzel, partial double ring scheme, advanced partial double ring scheme and double ring scheme. For CEPC partial double ring scheme, we gave the layout according to SPPC layout and the possibility of installation in the same tunnel and running at the same time. Then we designed lattice of the partial double ring part according the appropriate parameter choice for the electro-static separators. We also studied the dynamic aperture of this scheme. For CEPC advanced partial double ring scheme and double ring scheme, we also gave the layout, designed the lattice and studied the beam dynamics.

6 Forthcoming Beam Dynamics Events

6.1 International workshop on Nonlinear dynamics and Collective Effects in particle beam physics (NOCE 2017).

Arcidosso, a medieval town in Southern Tuscany in Italy, hosted four successful international workshops on nonlinear beam dynamics and collective effects in the last decade of the past century. Tens of experts on beam dynamics in particle accelerators and mathematicians of nonlinear dynamics participated. A new edition of the Arcidosso workshop is now organized as an ideal continuation of the work that, 20 years ago, helped the establishment of theories, techniques and accelerator designs of current operational colliders, synchrotron light sources and linear accelerators-driven light sources.

The workshop will review the advances made in the past two decades on the manipulation, in linear and circular accelerators, of high brightness particle charged beams. While still in the framework of nonlinear beam dynamics and collective effects, the workshop will update its content on the basis of state-of-the-art technologies and scientific results obtained at existing accelerator facilities. Challenges and solutions, proposed or implemented, for the operation of circular colliders, third and fourth generation light sources, will be reviewed and discussed. Constructive interaction between communities of linear and circular accelerators will be encouraged, such as, for instance, in the investigation of a complementarity between single-pass and recirculating light sources in energy, timing and spectral operational modes.

The program will focus on the following topics:

- linear and nonlinear particle dynamics in storage rings for colliders and light sources,
- collective effects in storage rings and in linacs for free electron lasers
- design concepts and design tools for synchrotron light sources, free electron lasers and Compton/Thomson light sources,
- complementarity of synchrotron light sources and free electron lasers: timing, energy and spectral operational modes.
-

Many talks will be plenary, in order to allow different groups in the accelerators community to share their work and ideas, and possibly find synergy of intents. Some room will be given to working groups, and the groups will eventually report in plenary session.

The event is an "ICFA mini-workshop" organized by Elettra-Sincrotrone Trieste S.C.p.A. and by Comune of Arcidosso, with the sponsorship of INFN-Bologna, "Scuola Normale Superiore" of Pisa, and ICFA. The workshop website:

<https://www.elettra.eu/Conferences/2017/NOCE/>

will be regularly updated to include the latest information as it becomes available.

Simone Di Mitri, Conference Chair NOCE 2017.

6.2 The 13th International Topical Meeting on the Applications of Accelerators

AccApp'17 is the thirteenth international topical meeting on the applications of accelerators; it is being organized by the [Accelerator Applications Division](#) of the American Nuclear Society (ANS) and the Canadian Nuclear Society ([CNS](#)). **AccApp'17 will be held at the Hilton Québec Hotel, in Québec City, Québec, Canada July 31-August 4, 2017.**

The purpose of these topical AccApp meetings is to provide an international forum for discussing the various applications of particle accelerators. Meetings are focused on the production and utilization of accelerator-produced neutrons, photons, electrons and other particles for scientific and industrial purposes; production or destruction of radionuclides significant for energy, medicine, defense, or other endeavors; safety and security applications; medical imaging, diagnostics, and therapeutic treatment. One of the great strengths of the AccApp meetings is the dissemination of knowledge on the diverse applications of accelerators.

The conference provides an opportunity for nuclear physicists, accelerator physicists, nuclear engineers, and other experts in the international community to meet and discuss their research face-to-face. These interactions can help establish good working relationships and collaborations to solve common problems across multiple disciplines. Also, old friendships can be cultivated and new ones established. You are cordially invited to participate in AccApp'17 by submitting an abstract, making an oral or poster presentation, and submitting a full paper for publication in our conference proceedings.

The deadline for abstract submission (200 word limit) is April 24, 2017. Full papers (10 pages or less) are due on September 10, 2017. Given the timing of this announcement just prior to the due date, please inform Philip Cole colephil@isu.edu should you wish to submit an abstract past this deadline. The templates for both the abstract and the full paper can be found on www.accapp17.org/call-for-papers.

We are looking forward to seeing you in la belle ville de Québec!

<http://accapp17.org/>

Philip Cole, Conference General Chair AccApp'17
Adriaan Buijs, Conference General Co-Chair AccApp'17

6.3 International Workshop on Beam-Beam Effects in Circular Colliders

The 5th workshop on Beam-Beam Effects in Circular Colliders will take place from September 27 to 29, 2017 at the Lawrence Berkeley National Laboratory, Berkeley, USA. This workshop is a successor and follows up to similar workshops held at CERN in April 1999, at Fermilab in June 2001, in Montauk 2003, and at CERN in March 2013.

A lot of progress has been made since the last workshop at CERN in the study of the beam-beam effects in colliders such as the LHC. Meanwhile, there are also beam-beam challenges in future colliders such as the next generation nuclear physics electron ion collider (EIC). The purpose of this workshop is to bring experts in this field to review progress in beam-beam studies of the current and past colliders and to discuss potential beam-beam issues and solutions in the future colliders. The workshop website:

<https://indico.physics.lbl.gov/indico/event/431/>

Ji Qiang and Jean-Luc Vay, IOC Chairs BeamBeam2017

6.4 Prof. Roger M. Jones, Conference Chair for VHEE17 Mini ICFA Beam Dynamics Workshop

We will have a mini-ICFA beam dynamics VHEE17 workshop in July 2017 in the United Kingdom. This workshop, *Very High Energy Electron Radiotherapy: Medical & Accelerator Physics Aspects Towards Machine Realisation Radiotherapy* (<https://www.cockcroft.ac.uk/events/VHEE17/>) will be held at the Cockcroft Institute of Accelerator Science and Technology in the UK from Monday the 24th of July 2017 until lunchtime of Wednesday the July 26th. The purpose of this workshop, referred to as VHEE17, is to explore a range of medical, RF and beam dynamics issues associated with the realisation of a machine for radiotherapy treatment. This machine is intended to deliver high dose, rapidly and precisely.

In order to achieve high gradient, room temperature X-band structures are a natural choice. CLIC for example, is now aiming at an accelerating gradient of 100MV/m at 12 GHz and has successfully fabricated and tested a host of such structures –and in this sense the technology is relatively mature. Other accelerators are already in use commercially at X-band for medical cancer treatment and for cargo scanning. It is natural to exploit synergies in these areas. This workshop will bring together researchers working on these issues in order to pool common areas of interest. Both fundamental medical physics, radiological physics and technological aspects of linacs and drive beams will be explored. There will be the opportunity to discuss with international experts both experimental and theoretical/simulation issues.

A preliminary list of topics includes:

- Contrasting salient potential benefits and potential pitfalls of VHEE radiotherapy, to those of extant modalities (X-ray, proton, carbon ion, etc).
CLIC, GLC/NLC, and other optimization schemes based on copper structures to provide acceleration to facilitate high gradient linac operation for medical linacs.
- Novel acceleration techniques (laser plasma, hybrid mode, photonic band gap, THz etc)
- Integration of a complete set of components with a view to machine realisation
 - Overall machine design including gantry, linac, beam focussing, beam collimation and beam scanning
 - Patient imaging (with a view to allowing for rapid implementation and rapid dose delivery)
 - Beam dynamics featuring a start-to-end simulation of tracking beam from gun to patient (or sections thereof)
 - Approximate costing of a VHEE machine.
- Exploitation of existing facilities (national labs, university labs with capability of demonstrating acceleration, and being used for radiological dose and biological

studies).

- Fundamental medical and radiobiological physics issues associated with VHEE studies.
 - Cell survival fraction and amendment to LQ model, TCP/NTCP
 - Geant4/TOPAS/GATE studies of sensitivity to heterogeneities
 - Single and double strand breaks to DNA, RBE studies

A series of invited plenary talks will be given in addition to contributed working group papers. This will be a unique opportunity for accelerator physicists working on beam dynamics and structure design to interact with medical physicists and oncologists to explore the potential for a new paradigm in cancer treatment. Early registration is advised: <https://eventbooking.stfc.ac.uk/news-events/very-high-energy-electron-radiotherapy-vhee-372>



6.5 A Summary of Upcoming Workshops and Conferences

FCC Week 2017	Future Circular Collider Week 2017, May 29 - June 2 in Berlin, Germany. http://fccw2017.web.cern.ch
SLHiPP Meeting	SLHiPP (Superconducting High Power Proton linacs) meeting, June 8-9, 2017 at IPN Orsay, France.
ERL17	59 th ICFA Advanced Beam Dynamics workshop on Energy Recovery Linacs, June 18-23, 2017 at CERN (Geneva). http://indico.cern.ch/event/470407/
SRF2017	International Conference on RF Superconductivity, July 17 – 21, 2017 in Lanzhou, China. http://srf2017.csp.escience.cn
VHEE'17	ICFA Mini-Workshop on Very High Energy Electron (VHEE) Radiotherapy: Medical and Accelerator Physics Aspects Towards Machine Realisation, July 24-26, 2017, at Cockcroft Institute, Daresbury, UK. https://eventbooking.stfc.ac.uk/news-events/very-high-energy-electron-radiotherapy-vhee-372
ACCAPP17	Accelerator Applications Workshop (ACCAPP17), July 31-August 4, 2017 in Quebec City, Canada. http://accapp17.org/
IBIC 17	International Beam Instrumentation Conference, August 20-24, 2017 in Grand Rapids, Michigan. http://indico.fnal.gov/event/ibic2017
	Topical Workshop on Injection and Injection System (TWIIS), August 28-30, 2017 at HZB / BESSY II, Berlin. https://indico.cern.ch/event/635514
FFAG'17	2017 International Workshop on FFAG Accelerators, September 6-12, 2017, at Cornell University, USA. https://www.bnl.gov/ffag17/
	ICFA Mini-Workshop on Impedances and Beam Instabilities in Particle Accelerators, September 19-22, 2017 in Benevento, Italy. http://prewww.unisannio.it/workshopwakefields2017/
	ICFA Mini-Workshop on Non-linear Dynamics and Collective Effects, September 19-22, 2017 in Arcidosso, Italy. https://www.elettra.eu/Conferences/2017/NOCE/
	ICFA Mini-Workshop on Beam-Beam Effects in Circular Colliders, September 27-29, 2017 in Berkeley, CA, USA. https://indico.physics.lbl.gov/indico/event/431/
Space Charge 2017	ICFA Mini-Workshop, "Space Charge 2017", October 4-6, 2017, at TU Darmstadt, Germany. https://indico.gsi.de/conferenceDisplay.py?confId=5600
ICALEPCS2017	International Conference on Accelerators and Large Experimental Physics Control Systems, October 8-13, 2017 at the Palau de Congressos de Catalunya in Barcelona, Spain. http://icalepcs2017.org
	ICFA Mini-Workshop on Slow Extraction, November 9-10, 2017, at CERN.

7 Announcements of the Beam Dynamics Panel

7.1 ICFA Beam Dynamics Newsletter

7.1.1 Aim of the Newsletter

The ICFA Beam Dynamics Newsletter is intended as a channel for describing unsolved problems and highlighting important ongoing works, and not as a substitute for journal articles and conference proceedings that usually describe completed work. It is published by the ICFA Beam Dynamics Panel, one of whose missions is to encourage international collaboration in beam dynamics.

Normally it is published every April, August and December. The deadlines are 15 March, 15 July and 15 November, respectively.

7.1.2 Categories of Articles

The categories of articles in the newsletter are the following:

1. Announcements from the panel.
2. Reports of beam dynamics activity of a group.
3. Reports on workshops, meetings and other events related to beam dynamics.
4. Announcements of future beam dynamics-related international workshops and meetings.
5. Those who want to use newsletter to announce their workshops are welcome to do so. Articles should typically fit within half a page and include descriptions of the subject, date, place, Web site and other contact information.
6. Review of beam dynamics problems: This is a place to bring attention to unsolved problems and should not be used to report completed work. Clear and short highlights on the problem are encouraged.
7. Letters to the editor: a forum open to everyone. Anybody can express his/her opinion on the beam dynamics and related activities, by sending it to one of the editors. The editors reserve the right to reject contributions they judge to be inappropriate, although they have rarely had cause to do so.

The editors may request an article following a recommendation by panel members. However anyone who wishes to submit an article is strongly encouraged to contact any Beam Dynamics Panel member before starting to write.

7.1.3 How to Prepare a Manuscript

Before starting to write, authors should download the template in Microsoft Word format from the Beam Dynamics Panel web site:

<http://icfa-bd.kek.jp/icfabd/news.html>

It will be much easier to guarantee acceptance of the article if the template is used and the instructions included in it are respected. The template and instructions are expected to evolve with time so please make sure always to use the latest versions.

The final Microsoft Word file should be sent to one of the editors, preferably the issue editor, by email.

The editors regret that LaTeX files can no longer be accepted: a majority of contributors now prefer Word and we simply do not have the resources to make the conversions that would be needed. Contributions received in LaTeX will now be returned to the authors for re-formatting.

In cases where an article is composed entirely of straightforward prose (no equations, figures, tables, special symbols, etc.) contributions received in the form of plain text files may be accepted at the discretion of the issue editor.

Each article should include the title, authors' names, affiliations and e-mail addresses.

7.1.4 Distribution

A complete archive of issues of this newsletter from 1995 to the latest issue is available at

<http://icfa-usa.jlab.org/archive/newsletter.shtml>.

Readers are encouraged to sign-up for electronic mailing list to ensure that they will hear immediately when a new issue is published.

The Panel's Web site provides access to the Newsletters, information about future and past workshops, and other information useful to accelerator physicists. There are links to pages of information of local interest for each of the three ICFA areas.

Printed copies of the ICFA Beam Dynamics Newsletters are also distributed (generally some time after the Web edition appears) through the following distributors:

John Byrd	jmbyrd@lbl.gov	North and South Americas
Rainer Wanzenberg	rainer.wanzenberg@desy.de	Europe++ and Africa
Toshiyuki Okugi	toshiyuki.okugi@kek.jp	Asia**and Pacific

++ Including former Soviet Union.

** For Mainland China, Jiu-Qing Wang (wangjq@mail.ihep.ac.cn) takes care of the distribution with Ms. Su Ping, Secretariat of PASC, P.O. Box 918, Beijing 100039, China.

To keep costs down (remember that the Panel has no budget of its own) readers are encouraged to use the Web as much as possible. In particular, if you receive a paper copy that you no longer require, please inform the appropriate distributor.

7.1.5 Regular Correspondents

The Beam Dynamics Newsletter particularly encourages contributions from smaller institutions and countries where the accelerator physics community is small. Since it is

impossible for the editors and panel members to survey all beam dynamics activity worldwide, we have some Regular Correspondents. They are expected to find interesting activities and appropriate persons to report them and/or report them by themselves. We hope that we will have a “compact and complete” list covering all over the world eventually. The present Regular Correspondents are as follows:

Liu Lin

Sameen Ahmed Khan

Liu@ns.inls.br

Rohelakan@yahoo.com

LNLS Brazil

SCOT, Middle East and Africa

We are calling for more volunteers as Regular Correspondents.

7.2 ICFA Beam Dynamics Panel Members

Name	eMail	Institution
Rick Baartman	baartman@lin12.triumf.ca	TRIUMF, 4004 Wesbrook Mall, Vancouver, BC, V6T 2A3, Canada
Marica Biagini	marica.biagini@lnf.infn.it	INFN-LNF, Via E. Fermi 40, C.P. 13, Frascati, Italy
John Byrd	jmbyrd@lbl.gov	Center for Beam Physics, LBL, 1 Cyclotron Road, Berkeley, CA 94720-8211, U.S.A.
Yunhai Cai	yunhai@slac.stanford.edu	SLAC, 2575 Sand Hill Road, MS 26 Menlo Park, CA 94025, U.S.A.
Swapan Chattopadhyay	swapan@fnal.gov	Northern Illinois University, Dept. of Physics, DeKalb, Illinois, 60115, U.S.A.
Yong Ho Chin	yongho.chin@kek.jp	KEK, 1-1 Oho, Tsukuba-shi, Ibaraki-ken, 305-0801, Japan
Jie Gao	gaoj@ihep.ac.cn	Institute for High Energy Physics, P.O. Box 918, Beijing 100039, China
Ajay Ghodke	ghodke@cat.ernet.in	RRCAT, ADL Bldg. Indore, Madhya Pradesh, 452 013, India
Ingo Hofmann	i.hofmann@gsi.de	High Current Beam Physics, GSI Darmstadt, Planckstr. 1, 64291 Darmstadt, Germany
Sergei Ivanov	sergey.ivanov@ihep.ru	Institute for High Energy Physics, Protvino, Moscow Region, 142281 Russia
In Soo Ko	isko@postech.ac.kr	Pohang Accelerator Lab, San 31, Hyoja-Dong, Pohang 790-784, South Korea
Elias Metral	elias.metral@cern.ch	CERN, CH-1211, Geneva 23, Switzerland
George Neil	neil@jlab.org	TJNAF, 12000 Jefferson Ave., Suite 21, Newport News, VA 23606, U.S.A.
Toshiyuki Okugi	toshiyuki.okugi@kek.jp	KEK, 1-1 Oho, Tsukuba-shi, Ibaraki-ken, 305-0801, Japan
Peter Ostroumov	Ostroumov@frib.msu.edu	FRIB, National Superconducting Cyclotron Laboratory, Michigan State University, 640 S. Shaw Lane East Lansing, Michigan 48824, U.S.A.
Mark Palmer	mpalmer@bnl.gov	Brookhaven National Lab, Upton, NY 11973, U.S.A.
Chris Prior	chris.prior@stfc.ac.uk	ASTeC Intense Beams Group, STFC RAL, Chilton, Didcot, Oxon OX11 0QX, U.K.
Yuri Shatunov	Yu.M.Shatunov@inp.nsk.su	Acad. Lavrentiev, Prospect 11, 630090 Novosibirsk, Russia
Jiu-Qing Wang	wangjq@ihep.ac.cn	Institute for High Energy Physics, P.O. Box 918, 9-1, Beijing 100039, China
Rainer Wanzenberg	rainer.wanzenberg@desy.de	DESY, Notkestrasse 85, 22603 Hamburg, Germany
Zhentang Zhao	zhaozhentang@sinap.ac.cn	SINAP, Jiading campus: 2019 Jia Luo Road, Jiading district, Shanghai 201800, P. R. China Zhangjiang campus: 239 Zhang Heng Road, Pudong New District, Shanghai 201203, P. R. China

*The views expressed in this newsletter do not necessarily coincide with those of the editors.
The individual authors are responsible for their text.*